3-2015

Assessment of Multi-Story Building Seismic Design Factors with Structural Irregularity

El Sayed Abdel Naby Abdel Aziz Abou Khalifa

UAEU

جامعة الإمارات العربية المتحدة
United Arab Emirates University

United Arab Emirates University

College of Engineering

Department of Civil and Environmental Engineering

ASSESSMENT OF MULTI-STORY BUILDING SEISMIC DESIGN FACTORS WITH STRUCTURAL IRREGULARITY

El Sayed Abdel Naby Abdel Aziz Abou Khalifa

This thesis is submitted in partial fulfillment of the requirements for the degree of Master of Science in Civil Engineering

Under the Supervision of Dr. Aman Mwafy

March 2015

Declaration of Original Work

I, El Sayed Abdel Naby Abdel Aziz Abou Khalifa, the undersigned, a graduate student at the United Arab Emirates University (UAEU), and the author of the thesis entitled "*Assessment of Multi-Story Building Seismic Design Factors with Structural Irregularity*", hereby, solemnly declare that this thesis is an original research work that has been done and prepared by me under the supervision of Dr. Aman Mwafy, in the College of Engineering at UAEU. This work has not been previously formed as the basis for the award of any academic degree, diploma or similar title at this or any other university. The materials borrowed from other sources and included in my thesis have been properly cited and acknowledged.

Student's Signature ..... Date 1/6/2015

This Master Thesis is approved by the following Examining Committee Members:

1) Advisor (Committee Chair): Dr. Aman Mwafy

Title: Associate Professor

Department of Civil and Environmental Engineering

College of Engineering

Signature _____ Date 26/4/2015

2) Member: Dr. Amr Sweedan

Title: Associate Professor

Department of Civil and Environmental Engineering

College of Engineering

Signature _____ Date April 26th, 2015

3) Member (External Examiner): Prof. Michael N. Fardis

Title: Professor and Director of Structures Laboratory

Civil Engineering Department

Institution: University of Patras, Greece

Signature _____ Date 21-April-2015

This Master Thesis is accepted by:

Dean of the College of Engineering: Prof. Mohs Sherif

Signature Mohsen Sherif Date May 31st, 2015

Dean of the College of Graduate Studies: Prof. N

Signature Nagi Wahba Date 1/6/2015

Copy 13 of 13

Abstract

Many high-rise buildings are practically irregular as a result of the architectural and service requirements in the design process, errors and modifications during the construction phase, and changes of the building use throughout its service life. Structural irregularities could increase the uncertainties related to the ability of the building to meet the design objectives. This study is thus devoted to assess the safety margins and calibrate the seismic design response factors of modern high-rise buildings with different vertical irregularity features. A brief survey of the most common vertical irregularities in reinforced concrete multi-story buildings is conducted to select reference structures. Five 50-story high-rise buildings are then selected and fully designed using international building codes to represent well-designed tall buildings with principal vertical irregularity types. Fiber-based simulation models are developed to assess the seismic response of the five benchmark buildings under the effect of forty earthquake records representing far-field and near-field seismic scenarios. The comprehensive results obtained from inelastic pushover and incremental dynamic analyses are employed to provide insights into the local and global seismic response of the reference structures. The probabilistic vulnerability assessment of the five high-rise buildings is conducted at different limit states using fragility relationships.

The study concluded that the seismic performance of well-designed regular and vertically irregular high-rise buildings is satisfactory under the design earthquake. Under severe earthquakes, the seismic response of tall buildings with extreme soft story and geometric irregularity is not inferior to that of the regular

counterpart at different seismic performance levels. Despite the overstrength factor adopted in the design of buildings with discontinuities in the lateral-force-resisting system and extreme weak story, the observed negative impacts of these irregularity categories on increasing the vulnerability of high-rise buildings are substantial. This confirms the pressing need for mitigation strategies to reduce the expected seismic losses of the latter classes of building. The calibration of seismic design response factors of the reference high-rise buildings also confirms that, although the code coefficients are adequately conservative, they can be revised to arrive at a more efficient and cost-effective design of regular and irregular high-rise buildings.

Keywords: Multi-story buildings, vertical irregularity, seismic design coefficients, seismic vulnerability, dynamic response, design provisions

Title and Abstract (in Arabic)

تقييم معاملات تصميم المباني متعددة الطوابق لمقاومة الزلازل مع عدم الانتظام الإنشائي

الملخص

تعتبر كثير من المباني المرتفعة من الناحية العملية غير منتظمة انشائيا وذلك نظرا للمتطلبات المعمارية والخدمية اثناء عمليه التصميم، والاخطاء والتعديلات خلال مرحله التنفيذ، والتغييرات في استعمال المنشأ اثناء فترة الاستخدام. وتتزايد الشكوك حول امكانيه الوصول للأهداف التصميمية المرجوة عند وجود عدم الانتظام الانشائي بالمباني. ومن ثم خصصت هذه الدراسة لتقييم هوامش الامان ومعايرة عوامل تصميم السلوك الزلزالي للمباني الحديثة المتعددة الطوابق الغير منتظمة إنشائيا في الاتجاه الرأسي. تم اجراء مسح موجز للأنواع الشائعة من عدم الانتظام الانشائي في المباني الخرسانية متعددة الطوابق لتحديد نماذج مرجعيه للمباني. تم اختيار خمسه مباني بارتفاع 50 طابق وتم تصميمها بشكل كامل باستخدام مواصفات التصميم الدولية لتمثل المباني المرتفعة الحديثة التي تحتوي على الانواع الرئيسية لعدم الانتظام الانشائي في الاتجاه الرأسي. تم تطوير نماذج محاكاه تم التحقق من دقتها لتقيم السلوك الزلزالي للمنشآت الخمسة المرجعية، حيث تم تعريض هذه النماذج لأربعين سجلا لزلزال طبيعية تمثل سيناريوهين زلزاليين وهما الزلازل الشديدة المتولدة في مناطق بعيده وكذلك المتوسطة المسجلة في مناطق قريبه. تم استخدام النتائج التي تم الحصول عليها من التحليلات الاستاتيكية متزايدة الشدة الغير مرنة (inelastic pushover analysis) وكذلك التحليلات الديناميكية متزايدة الشدة (incremental dynamic analysis) وذلك لتقييم السلوك الزلزالي لنماذج المنشآت المرجعية على مستويي العناصر الإنشائية والنظام الانشائي الكامل. تم تقييم السلوك الزلزالي المحتمل لنماذج المنشآت المرجعية عند حالات الحدود المختلفة باستخدام منحنيات الهشاشة (fragility curves).

خلصت الدراسة إلى أن سلوك المباني المرتفعة المنتظمة والغير منتظمة رأسيا والمصممة تصميما جيدا يعتبر مرضيا تحت تأثير مستوى الزلزال التصميمي، كما انه تحت تأثير الزلازل الشديدة فان السلوك الزلزالي للمباني المرتفعة التي تحتوي علي طابق شديد الليونة (extreme soft story) او عدم انتظام هندسي (geometric irregularity) ليست أقل شأنا من نظيرهما المنتظم عند مستويات الزلازل المختلفة. وعلى الرغم من استخدام معامل زيادة المقاومة (overstrength factor) في تصميم المباني المرتفعة التي تحتوي

على عدم اتصال في نظام مقاومة الاحمال الجانبية (discontinuities in the lateral-force-resisting system) او التي تحتوي علي طابق شديد الضعف (extreme weak story irregularity) فقد لوحظ ان عدم الانتظام الانشائي قد تسبب في آثار سلبية جوهرية لهذه الفئات من المباني. وقد اكدت نتائج هذه الدراسة على الحاجة الملحة لاستراتيجيات للحد من الخسائر الزلزالية المتوقعة لفئات المباني الغير منتظمة سابقه الذكر. كما اظهرت معايرة عوامل تصميم السلوك الزلزالي لنماذج المباني المرجعية إلى أنه على الرغم من أن المعاملات المستخدمة في تصميم المباني المرتفعة هي متحفظة على نحو كاف، الا انه يمكن تعديل تلك المعاملات للوصول الي تصميمات إنشائية أكثر كفاءة وفعالية من حيث التكلفة.

Acknowledgements

I wish to deeply thank my enthusiastic supervisor, Dr. Aman Mwafy, Associate Professor of Structural Engineering, for his technical and moral support provided to me throughout this study. The encouragement and enthusiasm given by him were the spine to get this thesis done.

Profound gratitude goes to all those who have supported me in the UAE University. In particular, I would like to thank Dr. Bilal El-Ariss, Associate Professor of Structural Engineering, for helping me in my post-graduate study. I also appreciate the support of all faculty members of the Civil and Environmental Engineering Department during my academic study at the UAE University. Special appreciation goes to my research group, including Eng. Abdel Rahman Ashri, Eng. Wael Al Waeli and Eng. Anas Issa for their cooperation and the successful coordination throughout different phases of this MSc thesis.

I would like to express my infinite love and thanks to all my family members for their love and support during this long period. I deeply appreciate the encouragement given to me by my wife, Dr. Soheir Abdel Hamied, who made innumerable sacrifices in order to help me concentrate on my study. The last but not the least, the highest appreciation goes to my parents, my brothers Abdel Aziz and Mohamed and sisters without whom this success would have not been possible. All what I have accomplished in life is the result of their love and years of sacrifices.

Dedication

To my beloved family and the spirit of my father

Table of Contents

List of Tables

List of Figures

Abbreviations

1d: Design earthquake

2d: Twice the design earthquake

2D: Two-dimensional

3D: Three-dimensional

$(a_g)_y$: Peak ground acceleration at first indication of yield

$(a_g)_c$: Peak ground acceleration at collapse

a/v: Ratio of peak ground acceleration to peak ground velocity

C_d: Deflection amplification factor

CP: Collapse prevention limit state

D/C: Demand over capacity ratio

DOF: Degrees of freedom

ELFP: Equivalent lateral force procedure

ESA: Equivalent static analysis

EVA: Eigenvalue analysis

f_{cu}: Concrete cube strength

f_c': Concrete cylinder strength

f_y: Steel yield strength

g: Gravitational acceleration

IO: Immediate occupancy limit state

IDA: Incremental dynamic analysis

IDA_L: Local response from IDA

IDA_G: Global response from IDA

IDR: Inter-story drift ratio

IPOA: Inelastic pushover analysis

LFRS: Lateral force-resisting-system

LS: Life safety limit state

MRSA: Modal response spectrum analysis

OP: Operational limit state

PGA: Peak ground acceleration

PSHA: Probabilistic seismic hazard analysis

PT: Inverted triangular load distribution

PU: Uniform lateral load distribution

R: Force reduction factor

R_{code}: Force reduction factor of the design code

R_{μ}: Ductility reduction factor

S_1: Spectral response acceleration at 1.0 sec.

S_a: Spectral acceleration

S_{D1}: Design spectral response acceleration at 1.0 sec

SDC: Seismic design category

S_{DS}: Design spectral response acceleration at 0.2 sec

S_s: Spectral response acceleration at 0.2 sec.

T: Period

THA: Time-history analysis

T_L: Long-period transition period

V: Design lateral strength of the building

V_E: Elastic base shear under the design earthquake

V_{gy}: Lateral strength of the building at global yielding

V_{max}: Base shear at ultimate strength

V_u: Ultimate lateral strength

V_y: Lateral strength of the building at the first yielding

$\beta_{D|GMI}$: Demand uncertainty

β_{CL}: Capacity uncertainty

β_M: Modeling uncertainty

Δ: Displacement

Δ_y: Displacement at first yield

Δ_{max}: Maximum deformation

δ: Roof drift at the ultimate capacity

δ_E: Elastic roof drift at the ultimate capacity under the design earthquake

Φ: Standard normal cumulative distribution function

λ_{CL}: Ln (median of drift capacity for a particular limit state)

$\lambda_{D|GMI}$: Ln (calculated median demand drift given the ground motion intensity)

Ω: Overstrength factor

Ω_o: Design overstrength factor

Ω_{1ph}: Overstrength factor at the first plastic hinge (first indication of yielding)

Ω_{1php}: Overstrength factor at the first indication of yielding from IPOAs

Ω_{1phd}: Overstrength factor at the first indication of yielding from IDAs

Ω_{gy}: Overstrength factor at global yielding

Ω_u: Overstrength factor at ultimate capacity

Chapter 1: Introduction

1.1 Introduction

Many tall buildings are practically irregular, as a perfect regular high-rise building rarely exists. The architectural design concepts of modern high-rise buildings have become more complex, and hence impose special requirements for seismic design. Modern seismic design codes distinguish between plan and vertical irregularity (CEN, 2004; ASCE-7, 2010). The tendency to separate irregularity in plan and in elevation also characterizes the scientific literature (e.g. Shahrooz and Moehle, 1990b; Aziminejad and Moghadam, 2005; Athanassiadou, 2008; De Stefano and Pintucchi, 2008). The growing interest in investigating the seismic behavior of building irregularity has been shown in the literature, particularly for vertical irregularity (Das and Nau, 2003; Chintanapakdee and Chopra, 2004; Varadharajan et al., 2013; Heidari et al., 2014). However, the impacts of different types of vertical irregularity have not been thoroughly covered in the literature, particularly the extreme irregularity of tall buildings.

The seismic hazard is a key component in the seismic vulnerability assessment studies. The seismicity of the Arabian Gulf region, particularly the United Arab Emirates, was investigated in a number of previous studies. This region is exposed to two main earthquake scenarios: (i) local earthquakes, and (ii) regional events. Some of the previous studies considered all local seismic sources reported in the scientific literature (e.g Mwafy et al., 2006; Sigbjornsson and Elnashai, 2006). Other studies disregarded certain local earthquake faults (e.g. Aldama-Bustos et al., 2009; Khan et al., 2013), which influenced the seismicity of the studied area. For

Dubai, previous studies recommended a wide range of design PGA, ranging from 0.047g to 0.32g for 10% probability of exceedance in 50 years. Hence, the seismic vulnerability assessment of the regular and irregular building stock under different earthquake scenarios and mitigation plans are highly needed in this region for reducing earthquake losses.

Fragility curves represent another crucial component for the estimation of seismic losses (e.g. Moehle, 1984; Jeong et al., 2012). To develop the fragility relationships, different sources of uncertainty such as the ground motion variability should be accounted for. A wide range of earthquake records conforming to the latest understanding of the seismo-tectonic characteristics of the study region should be considered in fragility analysis to account for the input ground motion uncertainty. Moreover, the selection of suitable performance criteria for the investigated structures is of high importance. Despite the important role played by fragility relationships in seismic loss estimation, few previous studies were directed towards the fragility assessment of irregular structures. There is a pressing need for developing fragility functions for irregular tall buildings with different irregularity categories.

The seismic design response factors are employed to account for the inelastic seismic response during the design process (Shahrooz and Moehle, 1990a; Elnashai and Di Sarno, 2008; FEMA-P750, 2009). A number of previous studies investigated the seismic design response factors of multi-story buildings (e.g. Mwafy and Elnashai, 2002; Kim and Choi, 2005; Mwafy, 2011). However, the systematic assessment of these important design factors for tall buildings with substantial

vertical irregularity features was not fully addressed in the literature. The recommended seismic design factors by building codes should be thoroughly assessed for irregular tall buildings to verify their relative safety margins at different limit states.

1.2 Study objectives

The main objectives of the current study are as follows:

- Review of the current state of knowledge related to the seismic response of irregular multi-story RC buildings and the seismicity of the UAE.
- Select rational performance criteria for tall buildings depending on their irregularity category.
- Assess the seismic vulnerability of high-rise buildings with various irregularity features and their relative margin of safety at different performance limit states using systematic vulnerability assessment methodologies.
- Provide recommendations regarding the impacts of irregularity on seismic response factors for the design of high-rise RC buildings.

1.3 Thesis organization

This MSc thesis is organized into seven chapters. This introductory chapter outlines the motives and objectives of the study.

Chapter 2 covers a general literature review of the tall buildings development, construction material and structural systems. This chapter also covers

the background related to the UAE seismicity, structural irregularity, vulnerability assessment, fragility relationships, and seismic design response factors.

Chapter 3 focuses on the selection and structural design approach of the benchmark high-rise buildings investigated in the present study. The selection of a regular and four irregular structures with various irregularities is addressed. The design process of different structural members using modern design tools and design provisions is discussed in detail. Finally, the design outcomes of the selected buildings are summarized in tables and structural drawings.

Chapter 4 introduces the fiber-based modeling approach of the reference tall buildings. Additionally, the selection of input ground motions to represent the seismicity of the study region is discussed in detail.

Chapter 5 describes the conducted analyses in the current study. Eigenvalue analysis is used to evaluate the dynamic characteristics and to verify the fiber-based models of the selected buildings. Inelastic static pushover analysis is employed to estimate the lateral capacity, while time-history and incremental dynamic analyses are carried out for the vulnerability assessment of the reference structures.

Chapter 6 discusses in detail the seismic performance assessment of the regular and irregular benchmark high-rise buildings. The results of the inelastic pushover and incremental dynamic analyses, which are used to evaluate seismic design response factors and assess the vulnerability of the reference buildings, are presented. Additionally, the selection of the performance criteria for fragility analysis

is discussed. Finally, the assessment results of the seismic design factors of the reference structures are presented.

Chapter 7 summarizes the main tasks and findings of the current study. Conclusions related to the seismic design response factors and vulnerability assessment of tall buildings with different irregularities are drawn. Finally, recommendations for future research studies are provided.

Chapter 2: Literature Review

2.1 Development of tall buildings

In the last few decades, many urban areas have been developed as a result of rapid population growth. These urban developments and the great numbers of inhabitants led to the emergence of high-rise buildings (Cohen, 2006). The tall building developments have been rapidly increased worldwide. Tall buildings have several uses such as commercial, residential and hospitality or could be a mix of several uses. Figure 2.1 shows the distribution of the tall building uses worldwide during the period between 1910 to 2006. This figure shows the significant increase in the numbers of tall buildings during the past fifty years.

High-rise buildings have been widely constructed in the United Arab Emirates, particularly in the cities of Dubai and Abu Dhabi. According to Moon et al. (2007), the height range of the most commonly constructed tall buildings is 50 - 70 stories, as per the survey for the 200 tallest buildings in the world shown in Figure 2.2. Based on the above-mentioned survey, which is in line with the modern high-rise buildings inventory in the UAE, five 50-story buildings are selected for the purpose of the current study to investigate the impact of building irregularity on the seismic response of tall buildings, as discussed in Chapter 3.

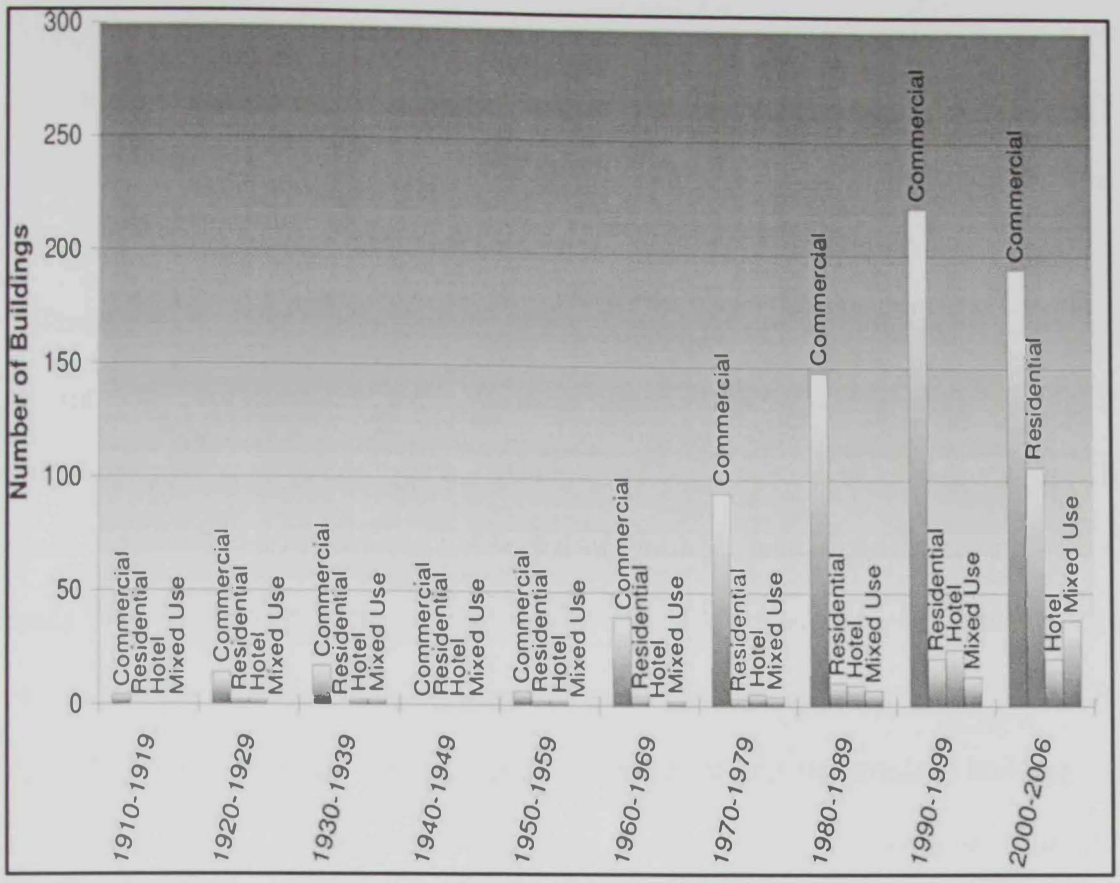

Figure 2.1: Distribution of tall building uses during the period of 1910 to 2006 (Ali and Moon, 2007)

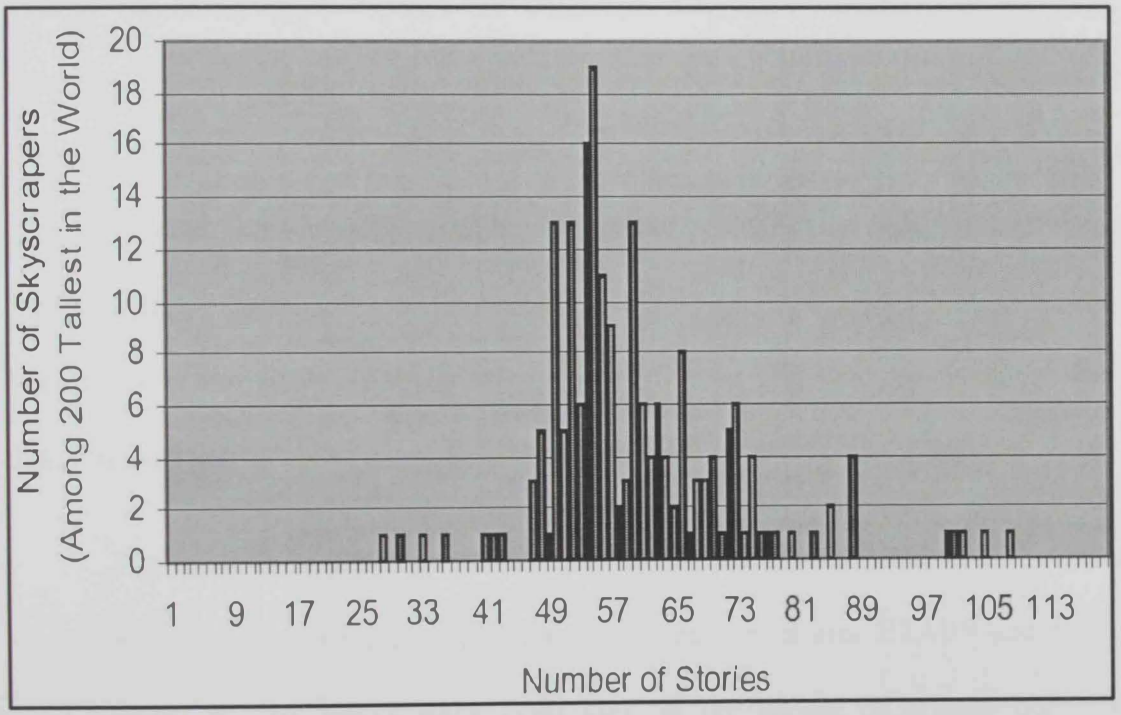

Figure 2.2: Result of survey for the 200 tallest buildings in the world (Moon et al., 2007)

The efficient design of high-rise buildings depends on several parameters such as the structural system, construction material and analysis tool (e.g. fib, 2014). The structural systems of high-rise buildings were reviewed in several previous studies. Halis and Emre (2007) reviewed the structural systems of buildings with different heights. The study concluded that for a fifty-story building, shear walls are recommended for the lateral force-resisting-system (LFRS). This structural system is one of the most appropriate systems for high-rise buildings since the high stiffness of shear walls effectively controls the lateral deformation under earthquake and wind loads. The shear wall structural system is also recommended in seismic design provisions for unlimited building height in seismic design category "C" (e.g. ASCE-7, 2010). This seismic design category is recommended for the standard buildings in the case study area considered in this study (Dubai, UAE), as shown in Table 2.1 (ASCE-7, 2010).

High-strength material, particularly high performance concrete, is mainly used in the construction of high-rise buildings. The main advantage of the high-strength concrete is its ability to sustain the high compression stresses. In the last few decades, the concrete technology has notably advanced and several high-strength concrete models have been developed to accurately predict its response under the cyclic loading. Several concrete strength values are used in the design of the benchmark high-rise buildings investigated in the present study, as explained in detail in Chapter 4.

The analysis and design of the reference buildings assessed in the current study are carried out using the widely used software packages ETABS and SAFE (CSI, 2011a, 2011b), which have been used in the design of several high-rise

structures such as Burj Khalifa (Baker et al., 2007). Three-dimensional (3D) simulation models can be easily developed for the high-rise buildings using the structural analysis software ETABS in order to analyze and design their LFRS, while floor slabs can be exported from ETABS to SAFE with their load combinations for the design of horizontal structural members. The details of the design process carried out in the present study are discussed in Chapter 3.

Table 2.1: Limitations of bearing walls according to different seismic design categories (ASCE-7, 2010)

Seismic Force-Resisting System	ASCE 7 Section Where Detailing Requirements Are Specified	Response Modification Coefficient, R	Overstrength Factor, Ω_o	Deflection Amplification Factor, C_d	Structural System Limitations Including Structural Height, h_n (ft) Limits[c]				
					Seismic Design Category				
					B	C	D	E	F
A. BEARING WALL SYSTEMS									
1. Special reinforced concrete shear walls	14.2	5	2½	5	NL	NL	160	160	100
2. Ordinary reinforced concrete shear walls	14.2	4	2½	4	NL	NL	NP	NP	NP
3. Detailed plain concrete shear walls	14.2	2	2½	2	NL	NP	NP	NP	NP
4. Ordinary plain concrete shear walls	14.2	1½	2½	1½	NL	NP	NP	NP	NP
5. Intermediate precast shear walls	14.2	4	2½	4	NL	NL	40	40	40
6. Ordinary precast shear walls	14.2	3	2½	3	NL	NP	NP	NP	NP
7. Special reinforced masonry shear walls	14.4	5	2½	3½	NL	NL	160	160	100
8. Intermediate reinforced masonry shear walls	14.4	3½	2½	2¾	NL	NL	NP	NP	NP
9. Ordinary reinforced masonry shear walls	14.4	2	2½	1¾	NL	160	NP	NP	NP
10. Detailed plain masonry shear walls	14.4	2	2½	1¾	NL	NP	NP	NP	NP
11. Ordinary plain masonry shear walls	14.4	1½	2½	1¼	NL	NP	NP	NP	NP
12. Prestressed masonry shear walls	14.4	1½	2½	1¾	NL	NP	NP	NP	NP
13. Ordinary reinforced AAC masonry shear walls	14.4	2	2½	2	NL	35	NP	NP	NP
14. Ordinary plain AAC masonry shear walls	14.4	1½	2½	1½	NL	NP	NP	NP	NP
15. Light-frame (wood) walls sheathed with wood structural panels rated for shear resistance or steel sheets	14.1 and 14.5	6½	3	4	NL	NL	65	65	65
16. Light-frame (cold-formed steel) walls sheathed with wood structural panels rated for shear resistance or steel sheets	14.1	6½	3	4	NL	NL	65	65	65
17. Light-frame walls with shear panels of all other materials	14.1 and 14.5	2	2½	2	NL	NL	35	NP	NP
18. Light-frame (cold-formed steel) wall systems using flat strap bracing	14.1	4	2	3½	NL	NL	65	65	65

NP: Not permitted
NL: Not limited
R: Response modification factor
Cd: Deflection amplification factor
Ωo: Overstrength factor

2.2 Seismic hazard

Assessment of seismic hazard is a key input for the structural design and performance assessment of structures in seismic region. Seismic hazard (seismicity) refers to the geographic and historical distribution of earthquakes in a certain region. The seismicity of an area depends on several parameters such as earthquake sources (faults); seismic events in term of numbers, durations and magnitudes; and the tectonic settings of the study region. The seismic hazard of the UAE is briefly reviewed in the subsequent section.

2.2.1 UAE seismicity

The UAE is located in the South-Eastern part of the Arabian plate. This plate is the home to the countries of Kuwait, Bahrain, Qatar, UAE, Oman, Yemen, Saudi Arabia, Syria, Jordan and Iraq, as shown in Figure 2.3. The Arabian plate separated from the African plate and shifted to north and northeast (Konert et al., 2001). The Arabian plate collided with the Eurasian plate, and hence Zagros and Makran thrusts were formed in northeast and east of the Arabian plate, respectively. The Zagros fault, as shown in Figure 2.4 and Figure 2.5, is very active and represents the major source of earthquakes in the eastern region of the Arabian plate (Kaviani et al., 2007). Another main source of earthquakes in the Arabian plate is the Makrane subduction zone (Rajendran et al., 2013). The above-mentioned fault formations constitute the main seismic hazard of the case study area (UAE), as shown in Figure 2.3 to Figure 2.5.

Figure 2.3 shows the moderate to large seismic events at the Arabian plate boundaries during the period between 1900 to 2012 (USGS, 2014). Recent earthquake records extracted from the website of the European-Mediterranean seismological center (EMSC) for the UAE and the surrounding area are also shown

in Table 2.2 and Table 2.3 (EMSC, 2014). It is shown from Figure 2.3, Table 2.2, and Table 2.3 that the events at the southern part of Iran, which is close to the northern Emirates, are significant and have high magnitudes.

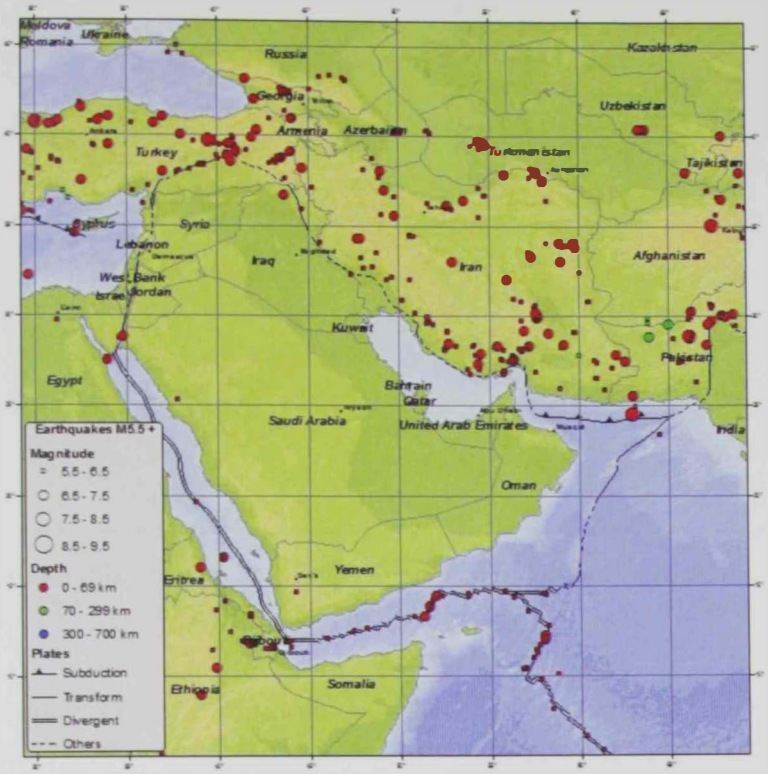

Figure 2.3: Seismicity map of the Arabian peninsula from 1900 to 2012 (USGS, 2014)

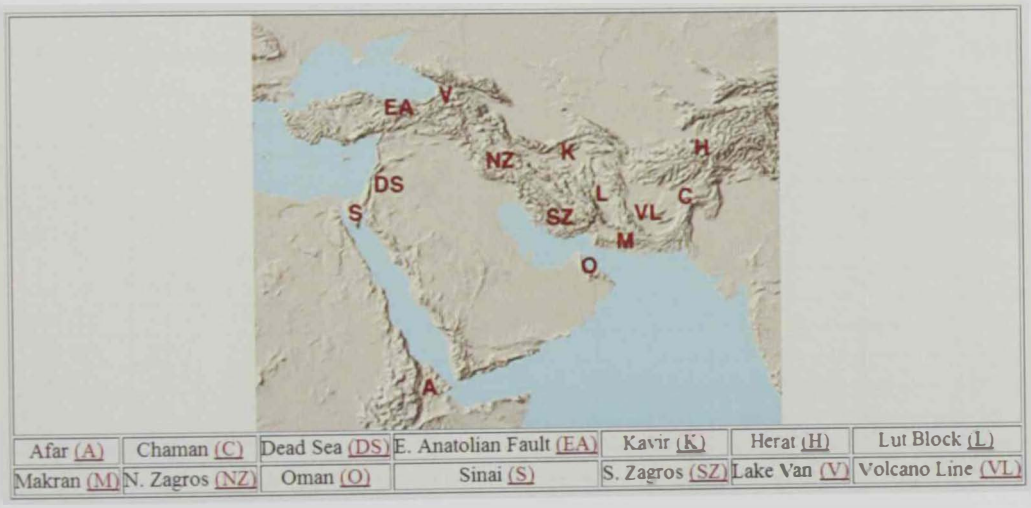

Figure 2.4: Faults layout at the Arabian plat boundaries (NASA, 2014)

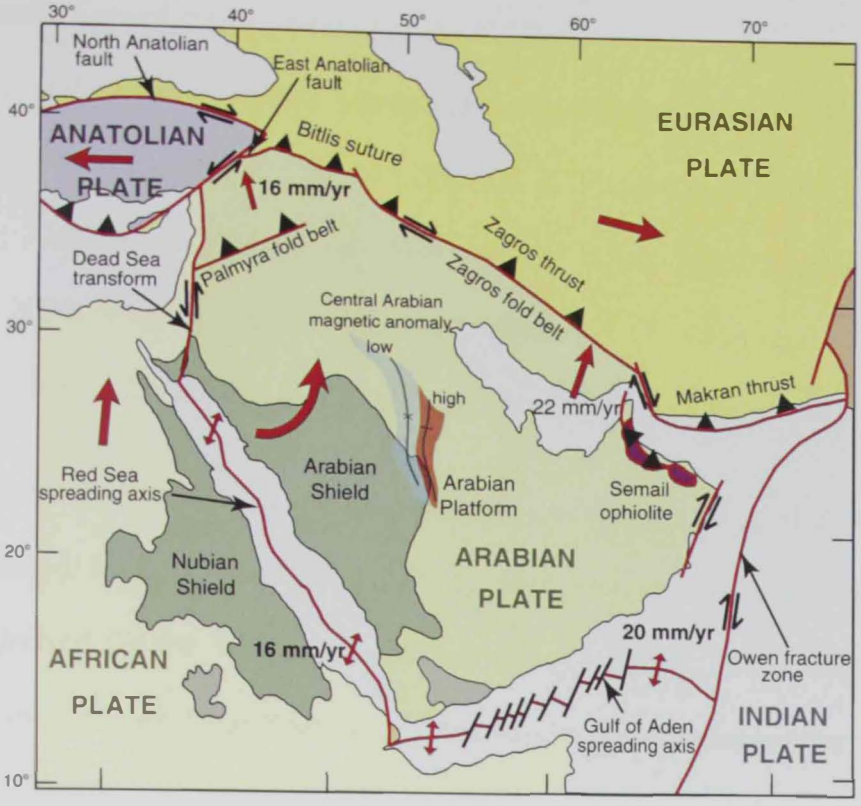

Figure 2.5: The Arabian plate with plate boundaries and faults layout (Stern and Johnson, 2010)

Table 2.2: Sample of recent earthquakes recorded in Oman and the UAE (EMSC, 2014)

Date	Time	Latitude degrees		Longitude degrees		Depth (km)	Magnitude (MW)
2009-06-08	18:14:01.2	25.90	N	56.39	E	14	3.8
2009-03-31	05:35:44.3	25.56	N	56.43	E	4	2.8
2009-03-31	02:21:26.5	25.56	N	56.42	E	3	2.2
2007-09-13	15:47:08.7	25.50	N	56.13	E	20	4.6

Table 2.3: Sample of recent earthquakes recorded in southeastern Iran (EMSC, 2014)

Date	Time	Latitude degrees		Longitude degrees		Depth km	Magnitude
2014-01-27	02:46:33.0	28.93	N	60.18	E	2	4.9
2013-09-30	03:44:51.0	26.96	N	60.37	E	10	4.8
2012-04-18	17:40:38.0	27.88	N	58.12	E	60	5.2
2012-03-26	00:06:19.0	27.69	N	58.85	E	74	4.8
2011-07-21	03:09:26.0	26.60	N	59.60	E	20	4.8
2011-01-28	05:06:44.0	28.20	N	59.17	E	2	4.8
2011-01-28	04:20:37.0	28.15	N	59.10	E	10	5.1
2011-01-27	09:07:55.0	28.40	N	59.15	E	2	4.8
2011-01-27	08:43:30.2	28.31	N	59.14	E	5	4.8
2011-01-27	08:38:29.0	28.26	N	59.01	E	12	6.0
2011-01-27	07:02:03.0	28.21	N	59.03	E	12	4.9
2010-12-20	22:13:00.0	28.29	N	59.27	E	14	4.8
2010-12-20	18:41:59.0	28.49	N	59.25	E	4	6.5
2010-11-03	19:56:11.3	29.17	N	59.84	E	40	4.8
2009-04-30	10:04:28.0	27.85	N	61.55	E	100	5.5
2007-03-26	06:36:50.6	29.05	N	58.30	E	30	5.0
2007-03-17	14:20:22.6	26.63	N	58.31	E	50	4.9

2.2.2 Seismic hazard studies related to the UAE

Several previous studies conducted probabilistic seismic hazard analysis (PSHA) and hazard assessment for the UAE (e.g. Al-Haddad et al., 1994; Grünthal et al., 1999; Abdallh and Al-homoud, 2004; Mwafy et al., 2006; Sigbjornsson and Elnashai, 2006; Aldama-Bustos et al., 2009; Shama, 2011; Khan et al., 2013). The most important studies related to the UAE are briefly presented below.

A probabilistic seismic hazard assessment of the Kingdom of Saudi Arabia was conducted by Al-Haddad et al. (1994) using the ground motion prediction equation derived for the Western North America (Campbell, 1985). Although the study mainly considered the KSA region, the results were presented for the entire Arabian Peninsula. The study employed the earthquake catalogue shown in Figure 2.6. The maximum record magnitude considered in this study in the vicinity of the UAE on Richter scale was 7.5, and the shortest distance between the source and Dubai was 125 km. The considered earthquake sources near the UAE were Zagros and Makran. This study concluded that the PGA value for 10% probability of exceedance in 50 years corresponding to a return period of 475 years for Dubai is less than 0.05g. Accordingly, the UAE was considered a low seismicity region (zone 0 as per UBC 1997).

The above-mentioned conclusion is consistent with the recommendation of Aldama-Bustos et al. (2009). The latter study presented PSHA based on ground motions at bedrock. The results of the Aldama-Bustos et al. (2009) study indicated that Dubai, Abu Dhabi and Ras al Khaimah have low seismicity. It is important to note that Aldama-Bustos et al. (2009) did not consider the effect of the surface soil

strata, which could significantly magnify the acceleration of the long distance earthquake scenario generated in Zagros and Makran faults.

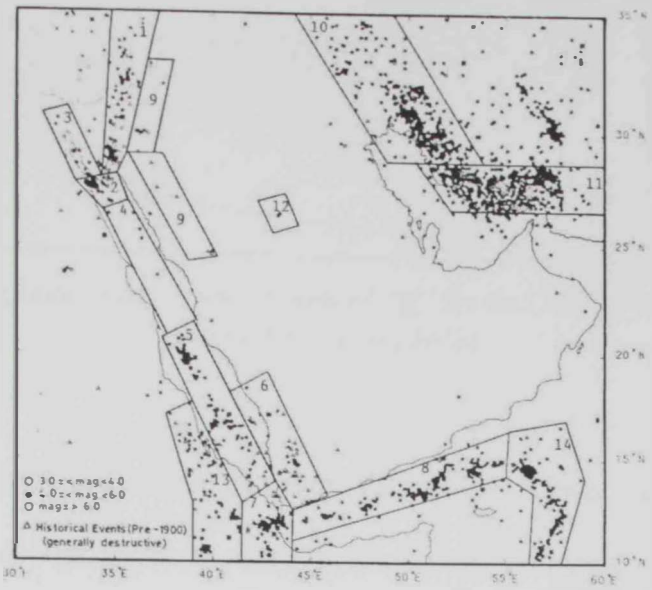

Figure 2.6: Records map for the Arabian Peninsula (Al-Haddad et al., 1994)

Another PSHA for the UAE was performed by Khan et al. (2013). Different databases were used to assemble the earthquake records around the UAE for 110 years (from 1900 to 2010), including historical and instrumental events. PGA contour lines as well as spectral accelerations at periods of 0.2 second (S_s) and 1.0 second (S_1) were derived for the UAE, as shown in Figure 2.7. The earthquake records originated from the local faults of the west coast were not included in this study, which explains the recommended low seismicity for the UAE. A PGA of 0.047 for 10% probability of exceedance in 50 years was assigned to Dubai. The conclusions of the latter study were in line with those of Aldama-Bustos et al. (2009) and Al-Haddad et al. (1994).

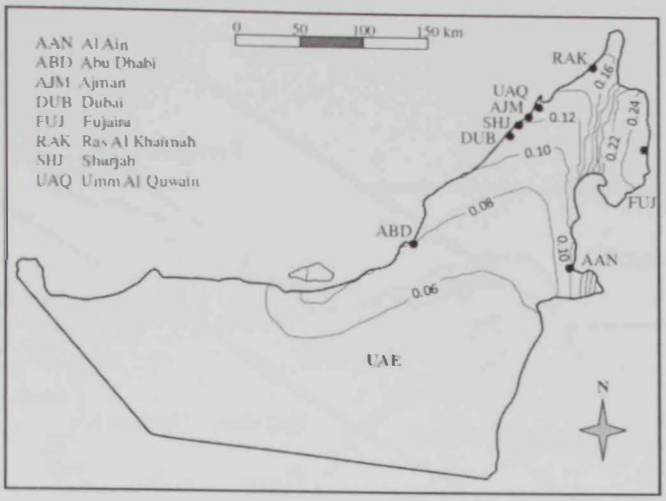

Figure 2.7: Peak ground accelerations in units of "g" for the UAE for 2,475 years return period (Khan et al., 2013)

A seismic hazard map was generated for Europe, Africa, and the Middle East by the global seismic hazard assessment program (Grünthal et al., 1999). According to the results of this study, a high PGA of 0.32g for 10% probability of exceedance in 50 years was assigned to Dubai. However, the study did not consider any specific site in the UAE. The developed seismic map in this study was reviewed by Kossobokov and Nekrasova (2012) and obvious contradictions were reported. The latter study concluded that the developed map in the study of Grünthal et al. (1999) is not accurate for the understudy region.

A probabilistic seismic hazard assessment for the UAE and its surroundings was performed by Abdallh and Al-homoud (2004). Seven seismic zones were considered in this study: (I) main Zagros thrust region, (II) north east Arabian Gulf region, (III) northern Emirates region, (IV) Lut region, (V) central Iran region, (VI) Makran region, and (VII) south east Arabian Gulf region, as shown in Figure 2.8. A PGA of 0.15g for 10% probability of exceedance in 50 years is assigned to Dubai. Additionally, seismic maps for the region were developed, as shown in Figure 2.9.

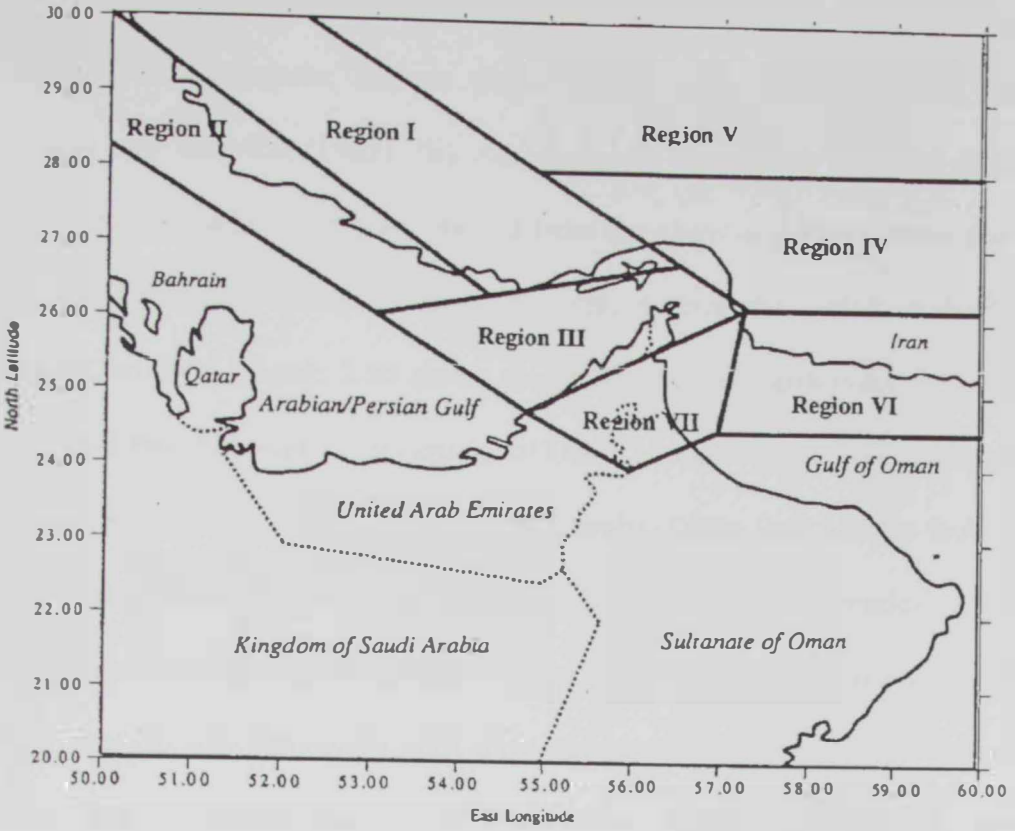

Figure 2.8: Seismic zones of the UAE (Abdallh and Al-homoud, 2004)

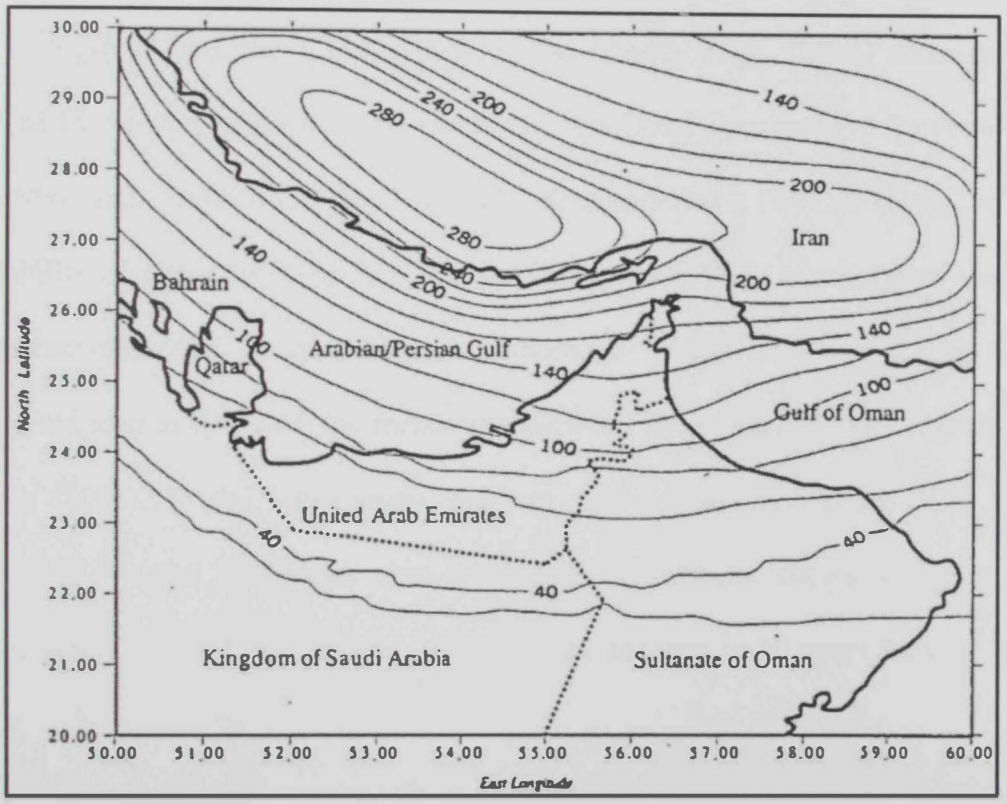

Figure 2.9: PGA (cm/sec^2) with a 10% probability of exceedance in a 50 years timespan for the UAE (Abdallh and Al-homoud, 2004)

Mwafy et al. (2006) and Sigbjornsson and Elnashai (2006) carried out PSHA for Dubai. The earthquake sources used in this study were published in: (i) Ambraseys and Melville (1982), (ii) Ambraseys et al. (1994), and (iii) GSHAP (2004). The earthquake catalogue obtained from the above-mentioned three studies, including the historical and instrumental records, covered the period of the fourth century BC to 2004. Figure 2.10 shows the distribution of earthquake data for the period 734–1996. Although the seismicity of Dubai is dominated by the south of Iran earthquake records, the seismic hazard of local faults (Dibba fault and the fault along the west coast of the UAE) were included in these studies. Two scenarios of records were recommended: (i) high magnitude with far distance from the epicenter (far-field records), and (ii) low magnitude with short distance from the epicenter (near-field records). The near-field and far-field scenarios represent earthquake records generated from the local and regional faults, respectively.

Sigbjornsson and Elnashai (2006) and Mwafy et al. (2006) estimated the PGA of Dubai using the strong motion estimation model developed by Ambraseys et al. (1996) and Simpson (1996). The study recommended a PGA of 0.16g for 10% probability of exceedance in 50 years for Dubai. This PGA is consistent with the value recommended by Abdallh and Al-homoud (2004), which is 0.15g. These values are also in line with the recommended PGA by another PSHA conducted by Shama (2011). In the latter study, uniform seismic hazard spectra using return periods of 475 and 2475 years were developed for Dubai, as shown in Figure 2.11. The recommend PGA for 10% probability of exceedance in 50 years for Dubai was 0.17g.

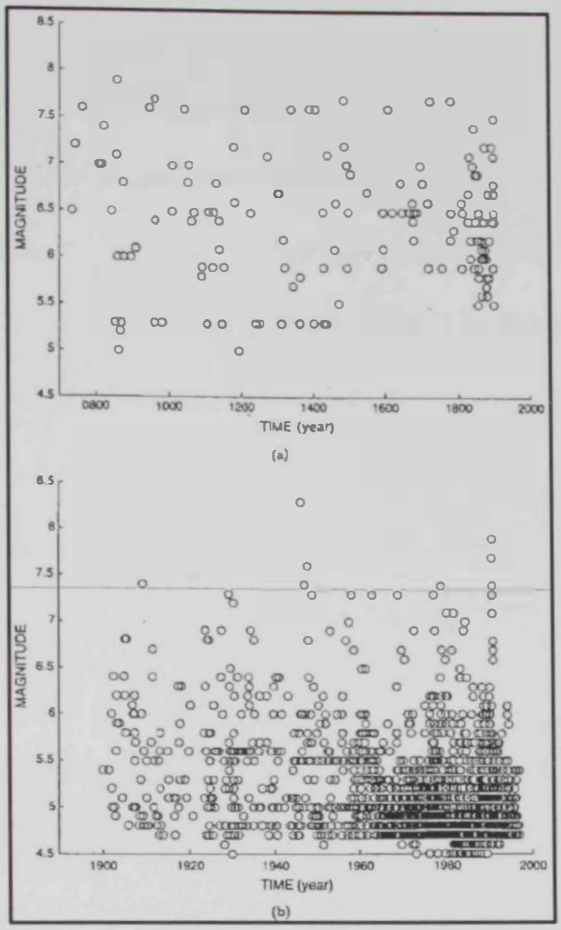

Figure 2.10: Distribution of earthquake data for the period 734–1996: (a) historical (b) instrumental (Sigbjornsson and Elnashai, 2006)

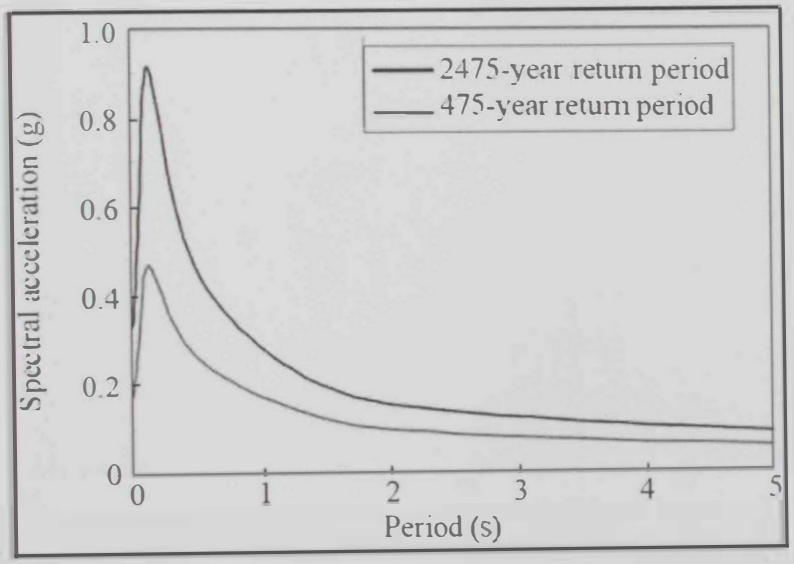

Figure 2.11: Uniform hazard spectra for return periods of 475 and 2,475 years (Shama, 2011)

Al Khatibi et al. (2014) discussed the improvement provided by the Dubai municipality seismic network (DSN) on the seismic characteristics and earthquake recording in the UAE. This seismic network was established in 2006, as shown in Figure 2.12 (Al Khatibi et al., 2014). Small earthquakes that could not be felt by global networks were detected and recorded by DSN. The study of Al Khatibi et al. (2014) divided the UAE local events to three main clusters: (i) East of Masafi, (ii) Wadi Nazwa, and (iii) Northern Huwaylat, as shown in Figure 2.13. Although the study did not specify a specific PGA for Dubai, the detected earthquakes reflected the low to moderate seismicity of the UAE from 2006 to 2013.

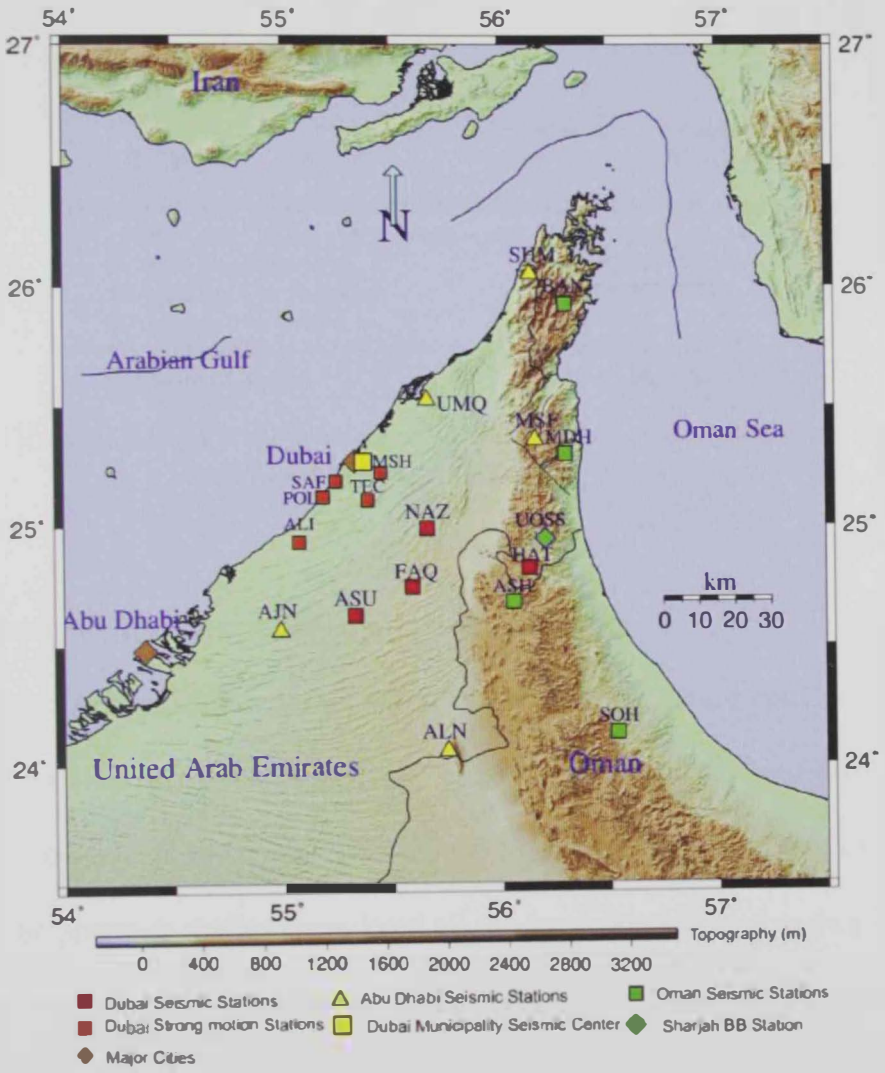

Figure 2.12: Permanent local seismic stations connected to the Dubai municipality seismic center (Al Khatibi et al., 2014)

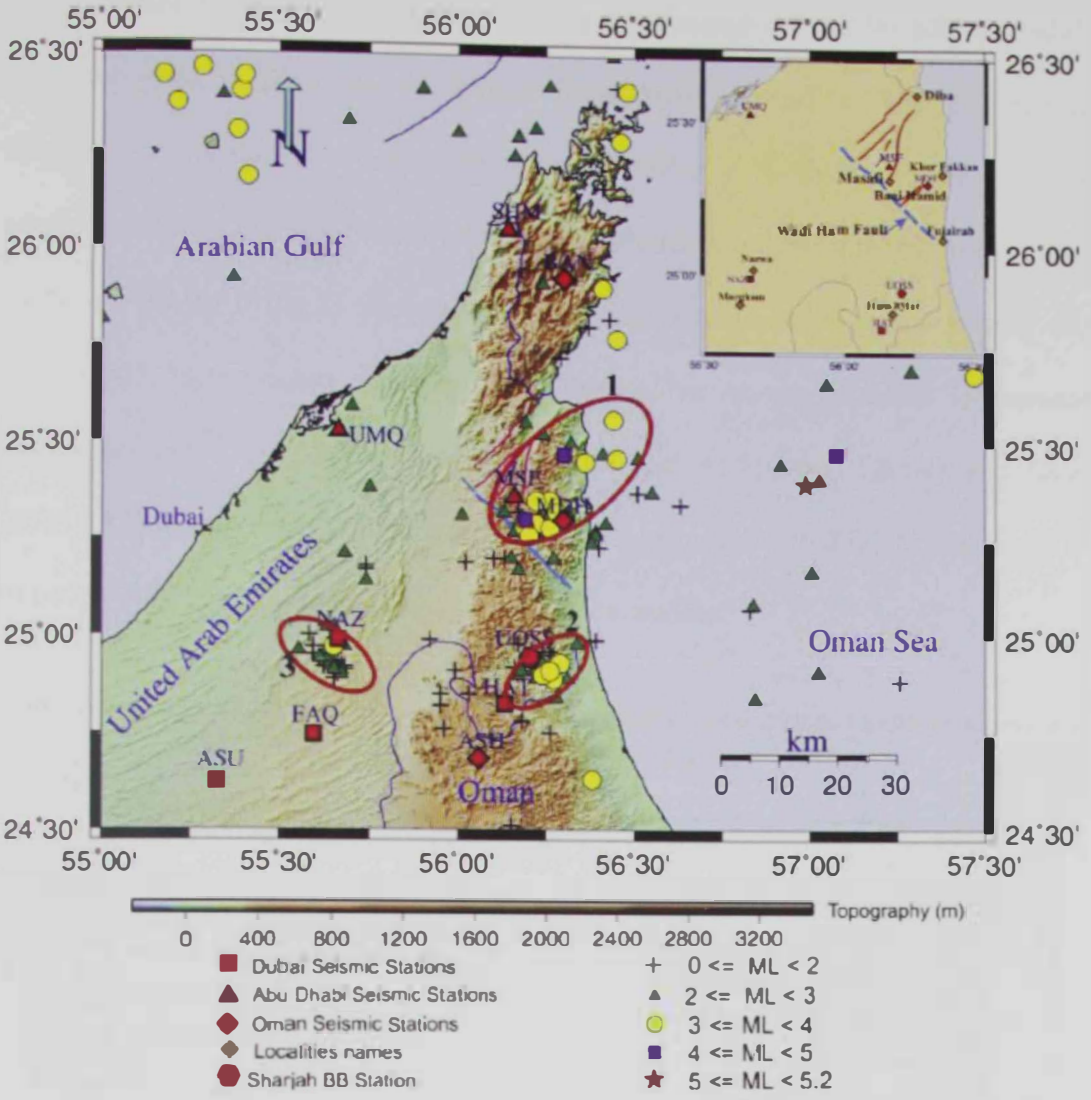

Figure 2.13: Local seismic activity recorded by the Dubai seismic network from April 2006 to June 2013 (Al Khatibi et al., 2014)

2.2.3 Seismic design criteria based on the UAE seismicity

The previous studies presented in the preceding section concluded that the main sources of the earthquakes in the UAE are: (i) local and (ii) regional faults. The main local sources are the Dibba fault and the fault along the west coast of the UAE. Some of the previous studies considered all the local seismic sources (e.g Mwafy et al., 2006; Sigbjornsson and Elnashai, 2006), while other studies disregarded some local sources (e.g. Khan et al., 2013), which notably influenced the seismic hazard of the studied area.

Table 2.4 shows a comparison of the recommended PGA for 10% probability of exceedance in 50 years for Dubai from previous studies. The discrepancies between the results of previous studies are attributed to the adoption of various seismic source zones and the use of different attenuation relationships. In the current study, a PGA of 0.16g is adopted following the recommendations of Mwafy et al. (2006) and Sigbjornsson and Elnashai (2006). This recommendation is consistent with other previous studies such as Abdallh and Al-homoud (2004) and Shama (2011). The adopted PGA is between the over-conservative (0.32g) and the very low (0.047g) PGAs recommended in other previous studies.

Table 2.4: Peak ground acceleration for 10% probability of exceedance in 50 years assigned to Dubai from previous studies

No.	previous studies	PGA
1	Grünthal et al. (1999)	0.32g
2	Shama (2011)	0.17g
3	Sigbjornsson and Elnashai (2006) and Mwafy et al. (2006)	0.16g
4	Abdallh and Al-homoud (2004)	0.15g
5	Al-Haddad et al. (1994)	<0.05g
6	Aldama-Bustos et al. (2009)	<0.05g
7	Khan et al. (2013)	0.047g

2.3 Seismic design provisions related to vertical irregularity

The structural irregularity is widely used in buildings due to the complexity of the architectural design and service requirements, particularly in high-rise buildings. The structural irregularity is classified to two main categories: (i) plan, and (ii) vertical irregularity. The plan (horizontal) irregularity occurs as a result of several reasons such as when the structure is significantly influenced by torsion or a discontinuity in LFRS out of its plane. The vertical irregularity could be occurred when significant changes in the stiffness, strength, mass, dimensions, or a discontinuity in the plane of LFRS. In the current study, the impact of vertical

irregularities on the seismic response of high-rise buildings is assessed. The definitions of different types of vertical irregularity according to modern seismic design provisions are reviewed in subsequent sections, (CEN, 2004; NBCC, 2005; ASCE-7, 2010).

2.3.1 American codes

According to the latest American design guidelines and design codes (FEMA-P750, 2009; ASCE-7, 2010; ICC, 2012), a building exhibits extreme - soft story irregularity when a story lateral stiffness (K_i) is less than 60% of the stiffness of the story above (K_{i+1}), or less than 70% of the average stiffness of the three stories above, as explained in Figure 2.14-1 (FEMA-P750, 2009). The mass irregularity occurs when the mass of a story (M_i) is more than 150% of the mass of adjacent story (M_{i+1} or M_{i-1}), as shown in Figure 2.14-2. The vertical geometric irregularity exists when the horizontal dimension of the LFRS in any story (L_i) is more than 130% of that in an adjacent story (L_{i+1}), as shown in Figure 2.14-3. In-plane discontinuity exists when an in-plane offset of a vertical seismic force resisting element of more than the dimension of the seismic force resisting element below (L_{below}) is introduced, as depicted in Figure 2.14-4. The extreme weak story irregularity is identified when a story lateral strength (Str_i) is less than 65% of the lateral strength for the story above (Str_{i+1}), as shown in Figure 2.14-5.

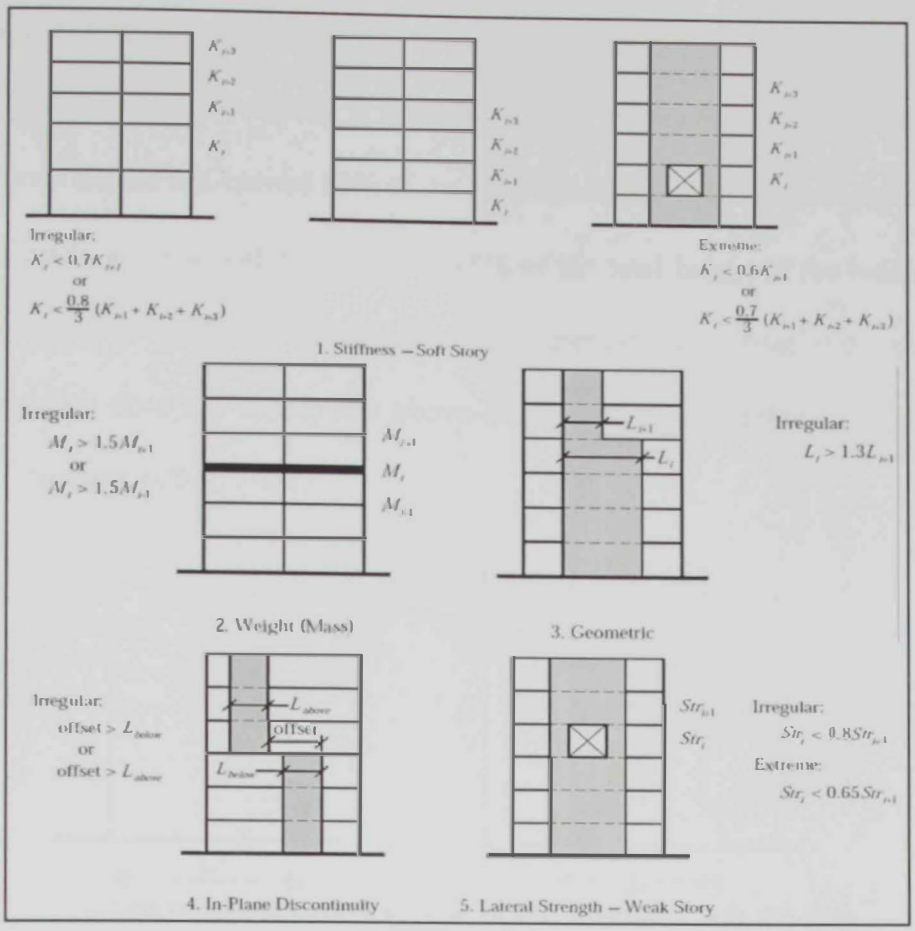

Figure 2.14: Definition of structural vertical irregularity according to FEMA-P750 (2009)

2.3.2 European standards

Eurocode-8 (CEN, 2004; fib, 2014) categorizes structures into regular and non-regular. The building is to be vertically regular if the following conditions are valid:

- All LFRSs run without any interruption from their base up to the top of the structure.
- The lateral stiffness and the mass of all stories shall remain constant or reduce gradually, without sudden changes, from the base up to the top of a building.
- In framed buildings, the ratio of the actual story resistance to the resistance required by the analysis should not vary disproportionately between adjacent stories.

- Individual setbacks of each side of the building do not exceed 10% of the parallel dimension of the story below. If setbacks are not symmetric, the total setbacks at all stories should not exceed 30% of the plan dimension at the ground floor.
- For a single setback within the lowest 15% of the total height of the building, the setback shall not exceed 50% of the parallel dimension at the base of the building.

If the building does not satisfy the above conditions, it is considered a vertically irregular structure (CEN, 2004).

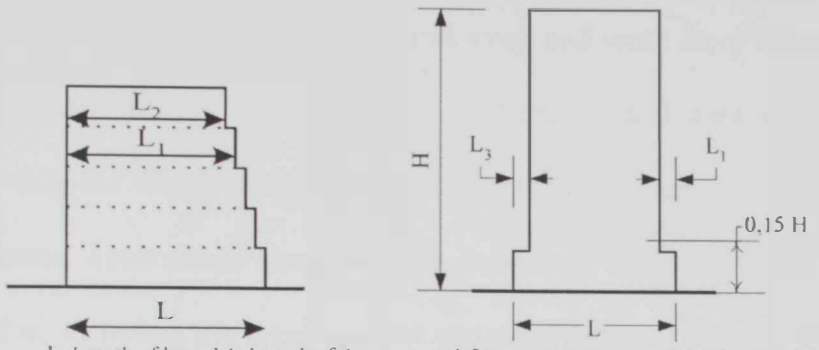

L: Length of base, L1: Length of the concerned floor, and L2: Length of the floor above

Figure 2.15 Definition of setback irregularity (CEN, 2004)

2.3.3 Canadian code

The definition of the vertical irregularities in the national building code of Canada (NBCC, 2005) is consistent with that of the international building code (ICC, 2012). The vertical stiffness irregularity is to be considered when the stiffness of the LFRS in any story is less than 70% of the adjacent story or 80% of the average stiffness of three stories below or above. The vertical geometrical irregularity exists when the horizontal dimension of the LFRS is more than 130% of the adjacent story. The irregularity due to the in-plane discontinuity in LFRS is when an in-plane offset in the LFRS is introduced. Finally, a weak story irregularity occurs when the story shear strength is less than that in the story above.

2.3.4 Comparison of the vertical irregularity definitions in design provisions

According to the above discussion, the design codes have different descriptions for the various types of irregularity. Table 2.5 summarizes the code definitions for different type of vertical irregularity. Basically, all codes categorize the vertical irregularity to five types: (i) stiffness, (ii) mass, (iii) geometric, (iv) in-plane discontinuity in LFRS, and (v) discontinuity in the LFRS strength.

Unlike the Canadian code (NBCC, 2005) and Eurocode-8 (CEN, 2004), ICC (2012) has two levels of severity for the soft story and weak story irregularities. In the latter code, the stiffness irregularity is divided into: (i) soft story, and (ii) extreme soft story, while the discontinuity of lateral strength is divided into: (i) weak story, and (ii) extreme weak story. These detailed definitions of the soft story and weak story irregularities reflect the importance of assigning different penalties according to the severity of these two types of irregularities. The ICC (2012) design provision are employed in the current study since they are adopted in the study region (UAE).

Table 2.5 Classification of vertical irregularity according to various seismic design codes

Type of irregularity	Design code		
	International building code (ASCE-7, 2010; ICC, 2012)	Eurocode-8 (CEN, 2004)	National Building Code of Canada (NBCC, 2005)
Stiffness/ soft story	$K_i < 70\% K_{i+1}$	$K_i < K_{i+1}$	$K_i < 70\% K_{i+1}$
Stiffness/extreme soft story	$K_i < 60\% K_{i+1}$	N/A	N/A
Geometric	$L_i > 130\% L_{i+1}$	$L_i > 120\text{-}150\% L_{i+1}$	$L_i > 130\% L_{i+1}$
In-plane Discontinuity	$L_o > L_{below}$	when L_o exists	when L_o exists
discontinuity in lateral strength/ weak story	$Str_i < 80\% Str_{i+1}$	$Str_i < Str_{i+1}$	$Str_i < Str_{i+1}$
discontinuity in lateral strength/extreme weak story	$Str_i < 65\% Str_{i+1}$	N/A	N/A

K_i: Stiffness of the soft story
K_{i+1}: Stiffness of the floor above the soft story
L_i: Length of irregular floor
L_{i+1}: Length of the floor adjacent to the irregular floor
L_o: Vertical element offset
L_b: Vertical element length in the story below the irregular story
Str_i: Lateral strength of weak story
Str_{i+1}: Lateral strength of the floor above the weak story
N/A: not applicable

2.4 Previous studies related to the assessment of irregular structures

Although several real buildings are practically irregular, the published research related to the seismic assessment of irregular structures is fewer than those of regular buildings, particularly the research concerned with the vertical irregularity of high-rise buildings (e.g. De Stefano and Pintucchi, 2008). Previous studies concluded that the seismic response of irregular structures is significantly different compared with that of regular buildings. Each of the plan and vertical irregularities were divided to subcategories, as shown in Figure 2.16. The plan irregularity was reviewed in several previous studies (e.g. De Stefano and Pintucchi, 2002; Almazán and de la Llera, 2003; De-la-Colina, 2003; Aziminejad and Moghadam, 2005; De la Llera et al., 2005). A detailed review of the studies related to irregular structures in plan was conducted by De Stefano and Pintucchi (2008). Therefore, the presented review below covers only the previous studies related to vertical irregularity, which is the focus of the present study. The following literature review also covers both experimental and analytical studies. Due to the significant research conducted on setback structures, two phases of review are conducted to cover previous studies related to vertical structural irregularity, as shown in Figure 2.16. The first phase is related to the setback (geometric) irregularity, while the second phase is concerned with the rest of vertical irregularity types.

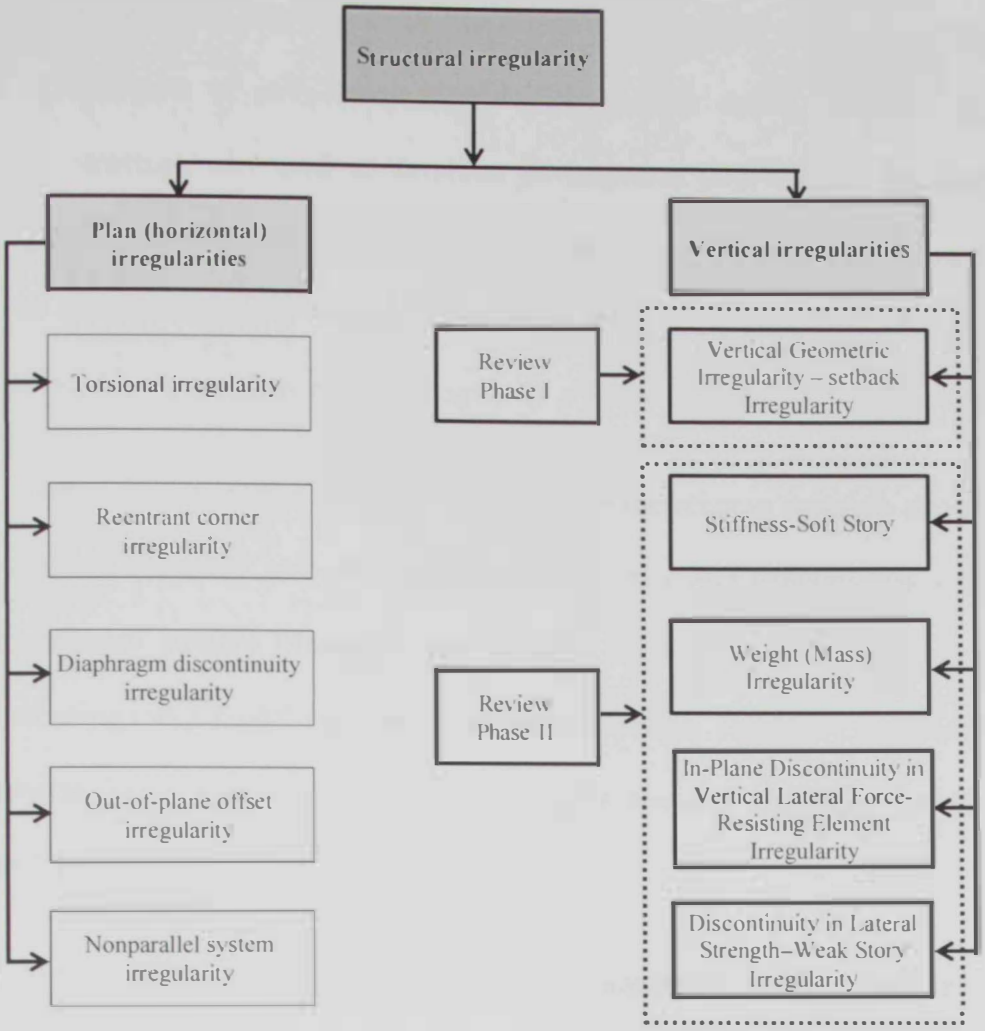

Figure 2.16: Classification of structural irregularities

2.4.1 Setback in LFRS (geometric) irregularity

An experimental assessment study was conducted for a six-story 3D moment resisting frame structure having setback irregularity by Shahrooz and Moehle (1990a). The acceleration histories of the 1940 El Centro record were used to simulate the earthquake shaking. The study concluded the following:

- The measured inter-story drift is more than the design results (UBC 1997).
- The bulding have more overstrength than that required by the design code.
- The measured inter-story reached 3% without any indications of collapse.

It is noted that only one earthquake record was used in the above-mentioned study. The impact of irregularity was not covered in detail, while no regular reference structure was used to correlate its response with that of the irregular building. In addition, the local seismic response was not investigated in detail, which could be substantial in the seismic assessment of irregular structures. Finally, the study only focused on a low rise buildings with a single irregularity type.

The influence of the setback irregularity on the seismic response and design of multi-story buildings was also assessed analytically and experimentally by the abovementioned authors (Shahrooz and Moehle, 1990b). Several buildings were designed using multi-modal and static analysis procedures. The study was conducted for low-rise frame buildings with few earthquake records. The main conclusions were as follows:

- With the exception of torsion, the dynamic characteristics of the tested irregular structure were similar to those expected for a regular structure. However, a concentration of inelastic behavior was observed at the setback level.
- There were no major differences between the seismic performance of the frames that were designed using static or modal-spectral design methods.
- A static analysis method with a design force amplification at the setback was proposed in the study.

Athanassiadou (2008) conducted an assessment for a regular and two irregular buildings with setback. Each reference building had ten stories and three bays with different setback configurations, as shown in Figure 2.17. The reference structures were designed according to Eurocode-8 for the high and medium ductility classes (CEN, 2004). The analytical assessment was conducted using the inelastic

static pushover and inelastic time-history analyses. Only eight records representing the short distance earthquake scenario were employed in this study. This scenario may not be the most significant seismic scenario for high-rise buildings, as recommended in a number of previous studies (e.g. Mwafy et al., 2006). The considered irregularity was in higher stories, while the irregularity in lower stories was not considered although this is a common scenario in buildings with geometric irregularity.

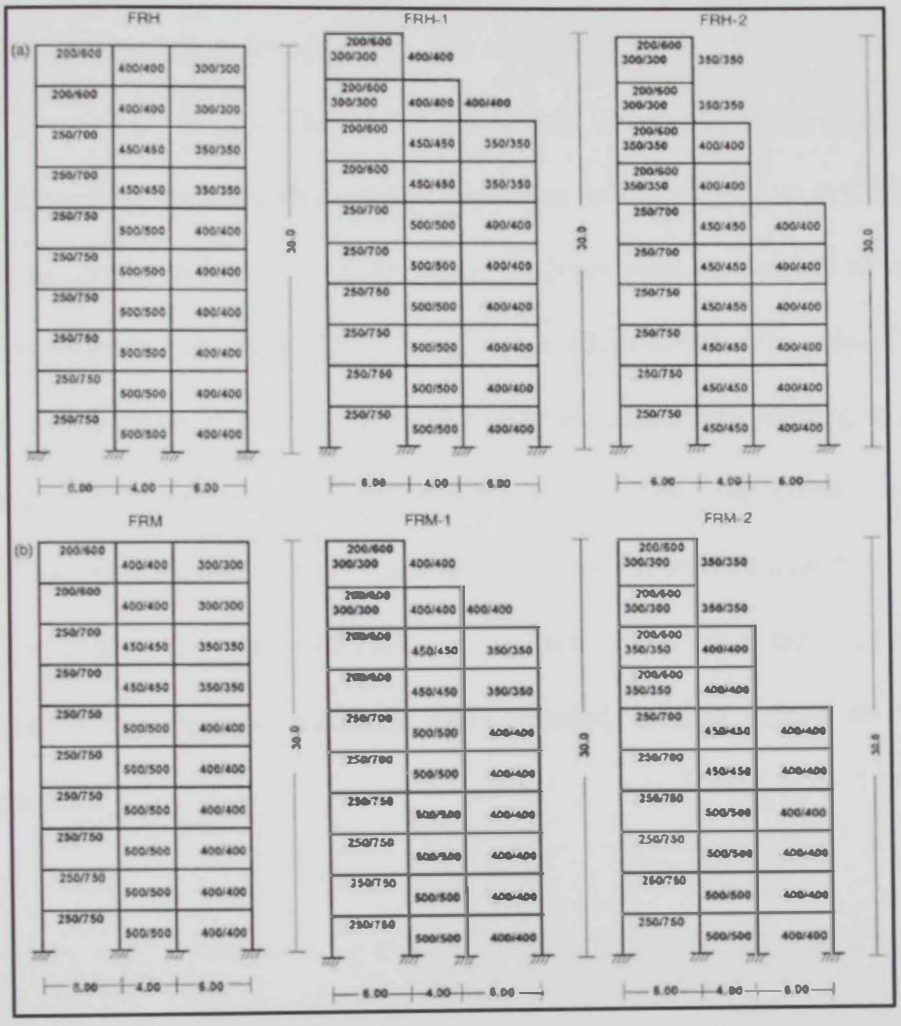

Figure 2.17: Configurations of reference buildings investigated by Athanassiadou (2008): (a) DCH structures and (b) DCM structures

The abovementioned study concluded that the seismic response of geometrically irregular structures was satisfactory. Most plastic hinges in the irregular frames were generated in beams at the design earthquake, which is consistent with the design code approach (i.e. strong columns – weak beams). The overstrength of the irregular building was similar to that of regular structures. The study also concluded that, since higher modes were not accounted for in the inelastic static pushover analysis, this analysis procedure is not recommend for the seismic assessment of high-rise buildings particularly those with vertical irregularity.

Another analytical investigation was conducted for a tall building with 260m high by Lu et al. (2013). The structural system of the building consists of a reinforced concrete frame with a central core. The building had two setbacks in the elevation, as shown in Figure 2.18. Dynamic analyses were carried out to assess the seismic performance of the building using two earthquake records only. The study did not consider other irregularity types or a regular comparable building to correlate its response with the performance of the irregular one. The study concluded that the damage was concentrated at the setback as a result of the sudden change in strength. The limited study did not propose performance limit states, while the vulnerability of the reference building at different input ground motion intensities was not investigated.

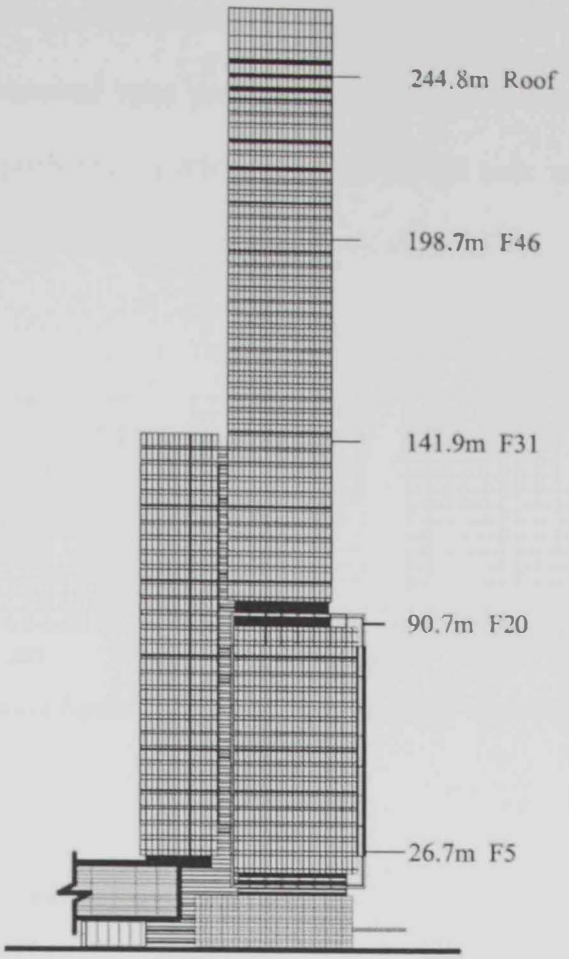

Figure 2.18: Elevation of the reference building studied by Lu et al. (2013)

An extensive study covering the setback structures was conducted by Varadharajan et al. (2013). A large number of frame buildings were assessed using 27 natural earthquake records. Incremental dynamic analyses (IDAs) were conducted to evaluate the impact of the setback irregularity on the dynamic characteristic of the low and medium-rise buildings. Fragility curves were developed for some of the reference buildings. It is noted that the input ground motions used in this study did not represent a specific seismic scenario and exhibit a high variation of PGAs and magnitudes. Additionally high-rise buildings were not investigated in this study.

The study concluded that the fundamental period and IDR were affected by the setback irregularity configuration. The seismic demand of the irregular structures

reflected the high IDRs at the setback regions. Equations for the estimation of the period and seismic demand were proposed to account for the setback irregularity. Comparisons of the proposed equations with the design code relationships indicated that the code approach is conservative.

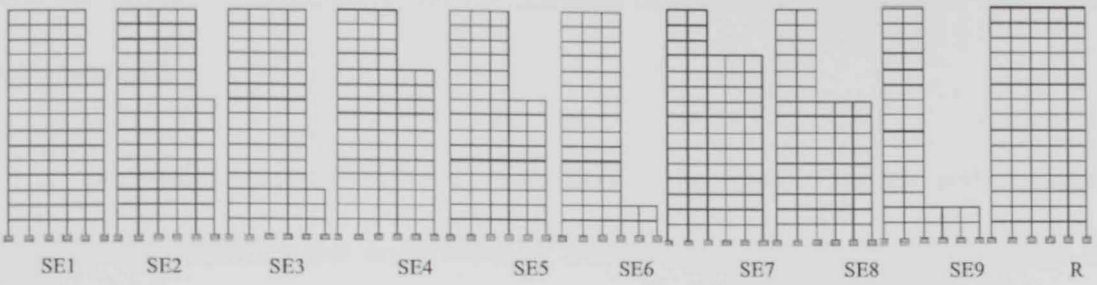

Figure 2.19: Different configurations of a 15-story building model studied by Varadharajan et al. (2013)

2.4.2 Other types of vertical irregularity

Few early study were conducted to assess the seismic response of irregular frame and wall structures (Moehle, 1984; Moehle and Alarcon, 1986). In the study conducted by Moehle (1984), the acceleration history of the 1940 El Centro earthquake was amplified up to 0.4g. The results indicated that the stiffness of the building that had a wall throughout its height was 80% more than that of the structure without wall. The impact of a severe discontinuity in the lateral force resisting system, particularly at the lower stories, was not covered in the abovementioned studies. In addition, the uncertainty in seismic demands was not considered.

Valmundsson and Nau (1997) evaluated the uniform building code (UBC, 1997) boundaries for mass, strength and stiffness for regular buildings. Three frame buildings with five, ten and twenty stories were considered in this study. The response of these three buildings was assessed under four earthquake records. The

study concluded that the mass and stiffness irregularities had a minor impact on the ductility demand compared to the strength irregularity. This study had several shortcomings, particularly related to the structural systems and input ground motions. The investigated frame system is not the most appropriate system for a 20-story building, while few earthquake records were considered in this study. Additionally, only the impacts of irregularity on the ductility demands of the reference structures were assessed.

A detailed parametric study considering the mass, strength and stiffness structural irregularities was undertaken by Das and Nau (2003). The study aimed to check the applicability of the equivalent lateral force procedure (ELFP) in the design of irregular structures. Seventy eight buildings with various interstory stiffness, strength and mass ratios were investigated in this study. The selected buildings included low- to medium-rise structures with five, ten and twenty stories. The LFRS of the investigated buildings was special moment resisting frames (SMRFs), as shown in Figure 2.20. The buildings were designed using ELFP according to UBC (1997). Dynamic time-history analyses were performed using twelve earthquake records matching the UBC-97 response spectrum. The study concluded that although the response of the irregular structures was significantly affected, the seismic demands were still within the UBC limits. Consequently, it was recommended to eliminate the restriction on the use of ELFP in the design of irregular structures. The latter study focused only on the SMRF system and only compared the results of ELFP and time-history analysis. The vulnerability of the reference buildings at different limit states considering the local and global response was not studied. Additionally, tall buildings were not addressed.

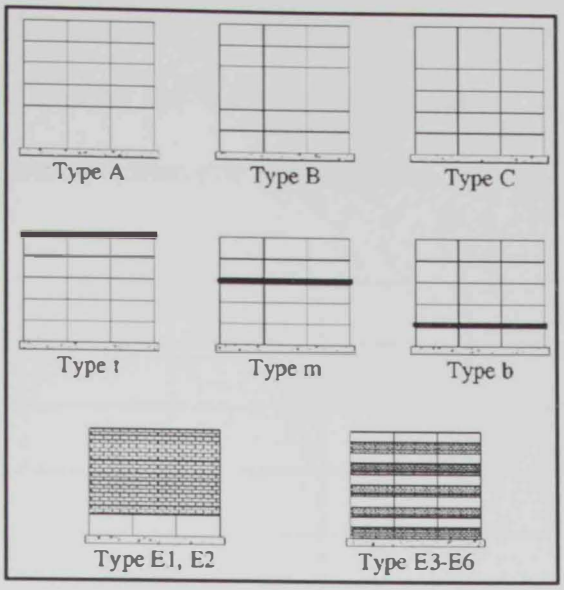

Figure 2.20: Configurations of a five-story building investigated by Das and Nau (2003)

A methodology for comparing the seismic performance of different structural irregularities using IDA was proposed by Michalis et al. (2006). Four types of structural irregularity were studied including stiffness, strength, combined stiffness and strength, and mass irregularities. These irregularities were introduced to a nine story steel frame building. The buildings were modeled using the OpenSees platform, as shown in Figure 2.21. A set of twenty records were selected and scaled at different earthquake intensities to perform IDA. The most important conclusions of this study were as follows:

- Considering the global dynamic instability, the single story irregularities had no impact on the collapse mechanism.
- The impacts of stiffness and mass irregularity were marginal compared with the strength irregularity
- The records selection had an important impact on irregular structures.

In the latter study, the irregular structures were not compared with a regular building. This comparison is essential to evaluate the seismic behavior of different

irregularity features. Also, certain irregularity types (e.g. discontinuity of LFRS) were not considered. Finally, the study only investigated nine-story steel frame structures, which represent medium-rise steel building.

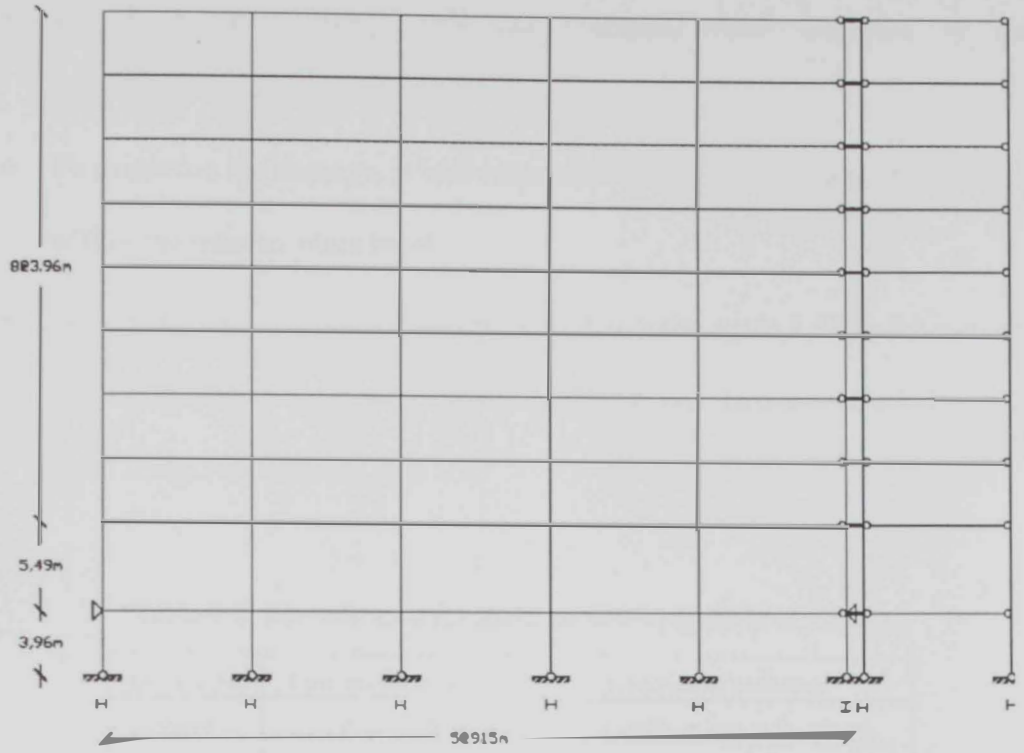

Figure 2.21: OpenSees model of a reference structure studied by Michalis et al. (2006)

A reinforced concrete building with 34 typical stories above a 2.7 m thick transfer slab and three levels of podium was experimentally investigated by Li et al. (2006). The LFRs is a shear wall structural system supported on a transfer slab, which in turn was supported on a wide spaced column system. The model and the structural system of the benchmark building are shown in Figure 2.22 (Li et al., 2006). Shaking table testing was carried out for the aforementioned building using earthquake records representing a moderate seismicity region, as shown in Table 2.6. It is clear that the selected records in this study were limited and did not represent a

specific seismic scenario. Based on the shake table testing, the following conclusions were drawn:

- The majority of the damage and failure occurred above the transfer plate.
- The high-rise buildings will not collapse when subjected to major earthquakes.
- To minimize the damage, it was recommended to reduce the stiffness changes within the transfer plate level.
- For a shear wall structural system with discontinuity in LFRS, the maximum IDRs corresponding to minor, medium and major damage were 0.1%, 0.33% and 1.25%, respectively.

Table 2.6: Records used for shake table testing (Li et al., 2006)

Earthquake	Peak acceleration(g)	Direction of excitation
Minor	0.02–0.06	Unidirectional and bidirectional
Moderate	0.08–0.14	Bidirectional
Major	0.15–0.20	Bidirectional
Super major	0.25–0.34	Bidirectional

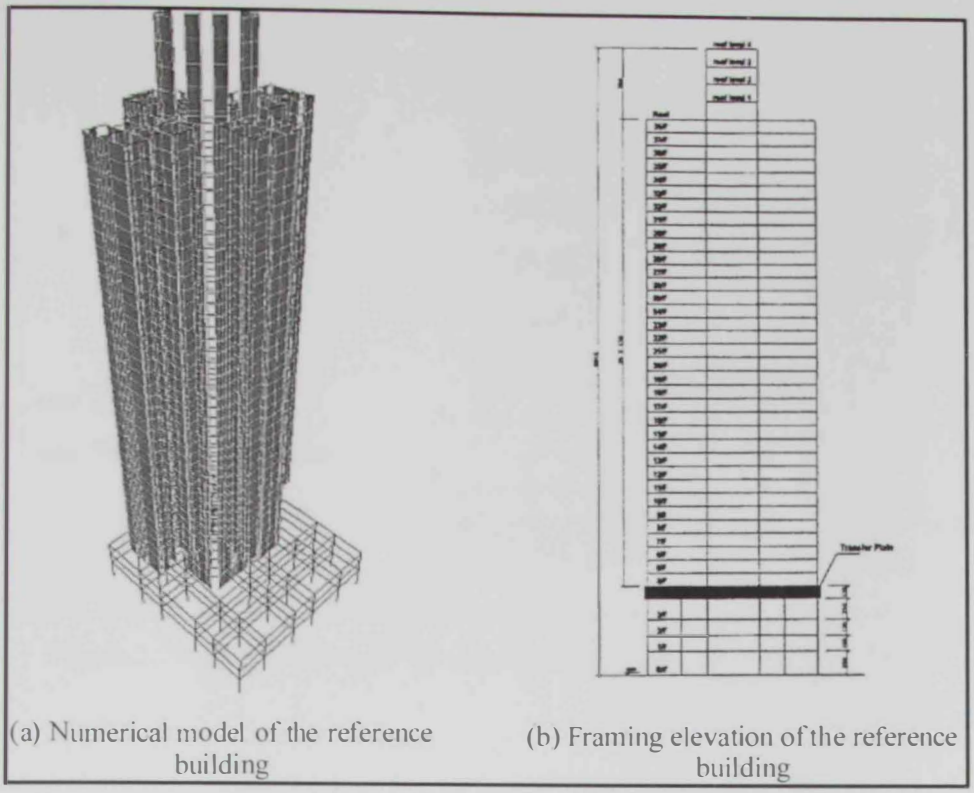

(a) Numerical model of the reference building

(b) Framing elevation of the reference building

Figure 2.22: Reference building configuration (Li et al., 2006)

Three buildings with various irregularities in the lower two stories were experimentally investigated to evaluate their seismic behavior by Lee and Ko (2007). This study was conducted using three specimens representing three 17-story buildings with different irregularity types, as shown in Figure 2.23. The effect of the location of shear wall at the lower stories was also investigated. The most important conclusions were as follows:

- The periods estimated for the studied structural system using UBC-97 equation were consistent with the study results.
- The overstrength factors under the design earthquake were between 2.8 to 3.1, which were consistent with the factor adopted by UBC (1997) and IBC (2000).
- Collapse mechanisms were detected when IDR was 1.57%.

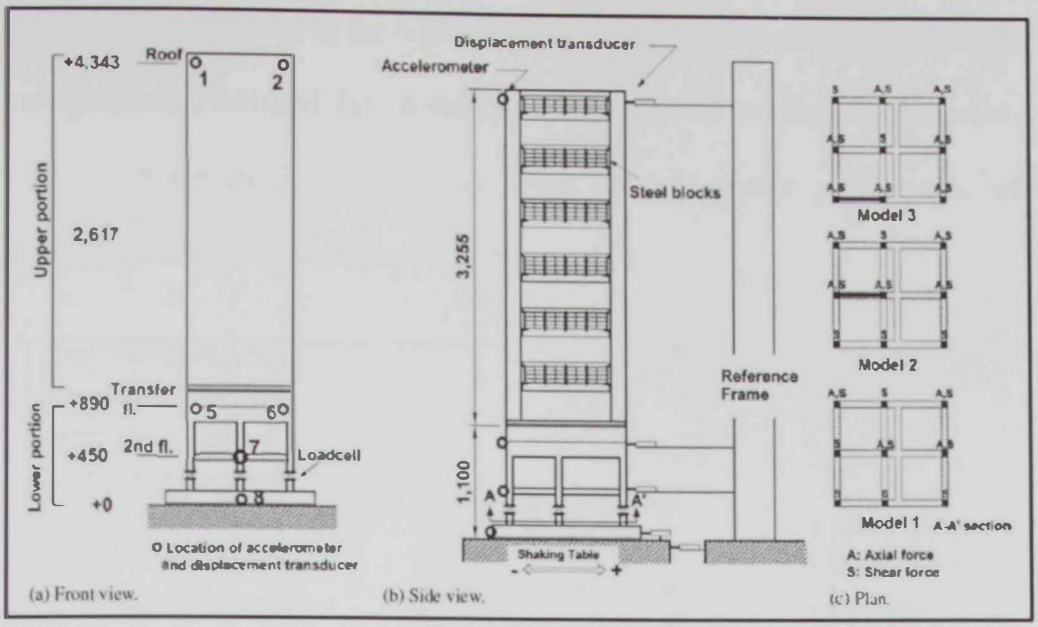

Figure 2.23: Models setup of 17-story buildings, mm, (Lee and Ko, 2007)

Fragility assessment of multi-story reinforced concrete buildings were conducted by Jeong et al. (2012). The buildings were designed using Eurocode-8 to represent modern structures. The reference systems consisted of frame and wall structures as well as regular and irregular buildings, as shown in Figure 2.24. Since the discontinuity of the columns at the ground story was not significant, the effect of irregularity on the seismic performance was not major compared with regular structures. This study focused on evaluating the margin of seismic design safety of buildings. IDAs were conducted using sixty earthquake records to develop the fragility curves of the reference buildings. Three limit states were adopted in this study: (i) immediate occupancy, IO; (ii) life safety, LS; and (iii) collapse prevention, CP. The probability of exceedance different limit states was also identified. The IDRs corresponding to the selected limit states were not affected by irregularity. Only one type of irregularity was considered in medium-rise buildings. The following conclusions related to structural irregularity were drawn:

- The seismic response of the regular and irregular frame buildings designed using modern codes satisfied the life safety limit state under the design earthquake.
- Although the irregularity had an effect on the seismic performance of the irregular structure, this impact was marginal.

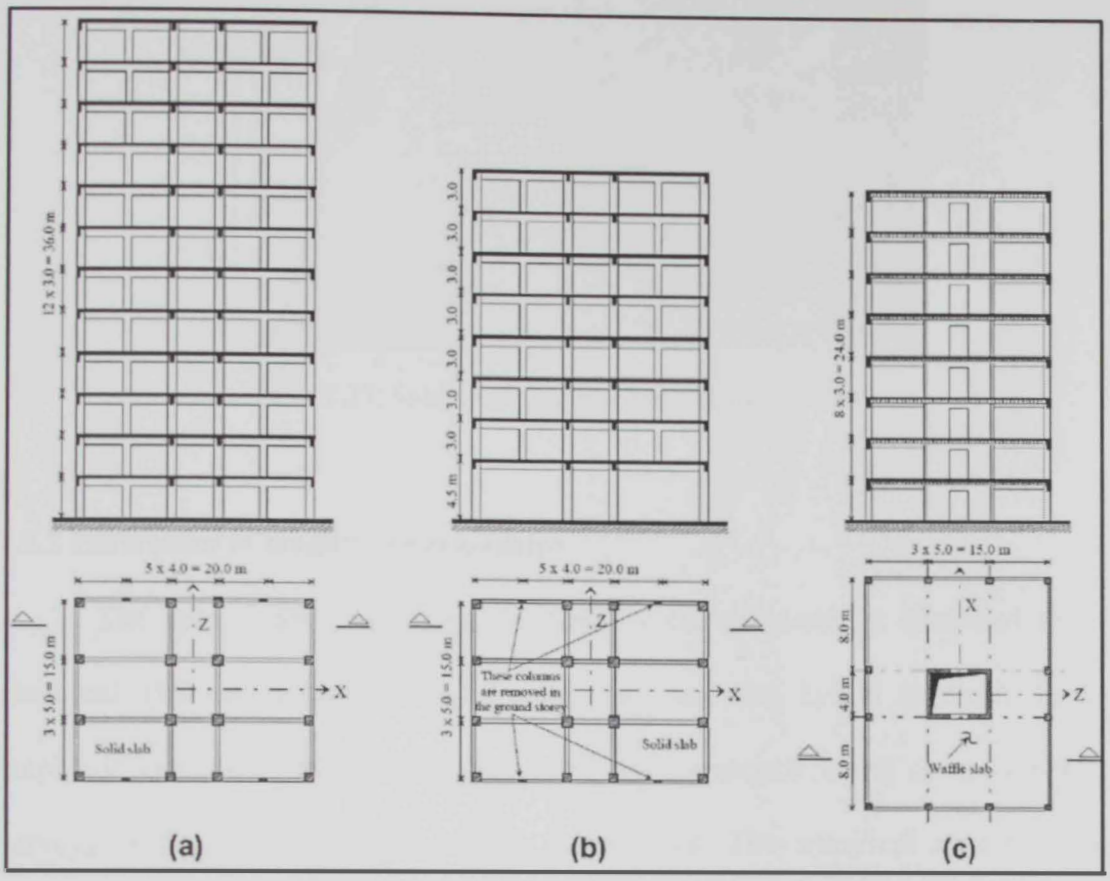

Figure 2.24: Plans and elevations of reference buildings: (a) Regular frame buildings, (b) Irregular frame buildings, and (c) Frame-wall buildings (Jeong et al., 2012)

2.5 Fragility functions

Current loss assessment approaches rely on fragility curves to assess the physical damage. In the last few decades, the development of fragility curves has been the focus of extensive research (e.g. Calvi et al., 2006). A fragility function is defined as the relationship between the earthquake intensities and the probability of exceeding pre-defined limit states, as shown in Figure 2.25. The seismic intensity could be a quantity that represents the severity of the earthquake such as PGA or S_a.

Several response parameters such as maximum displacement, forces or IDRs could be used for the selection of limit states and the development of fragility relationships.

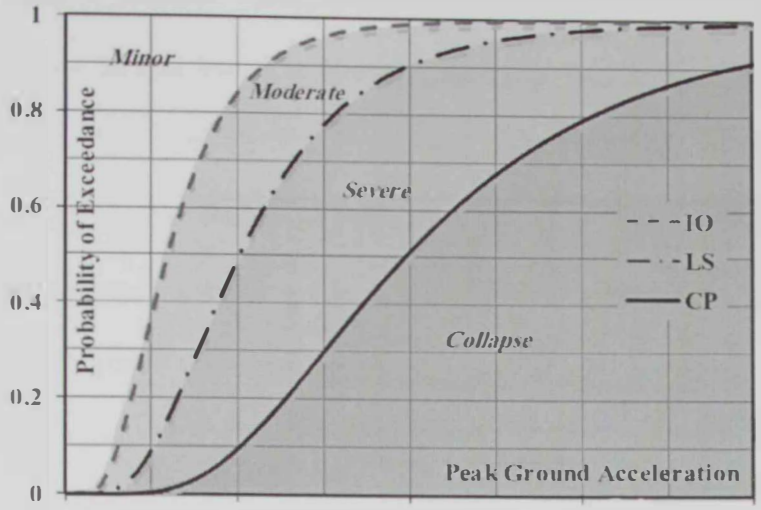

Figure 2.25: Sample of fragility curve (Mwafy, 2010)

2.5.1 Derivation of fragility relationships

The approaches of deriving the fragility curves could be classified to: (i) empirical, (ii) expert judgment, (iii) analytical, and (iv) hybrid methods. In the empirical procedure, the fragility functions are developed based on documented surveys of the damage from previous earthquakes. The empirical approach was adopted in many previous studies (e.g. Rossetto and Elnashai, 2003; Rota et al., 2006). Although this approach has several advantages because it relies on real information related to the earthquake damage, topography, and soil structure interaction, it has several shortcomings such as deriving fragility curves for a specific case of site, record and structures. Additionally, the difficulties of the data collection lead to a high level of uncertainty.

The expert judgment procedure only relies on the opinion of selected experts to derive the fragility curves (ATC-13, 1985). This approach has higher uncertainties than other methods (Kaynia et al., 2013). On the other hand, the analytical approach

is commonly used in modern studies since it has the ability to quantify several sources of uncertainty. The analytical method evaluates the damage based on the results from seismic response simulations. The fragility relationships could be also developed using the simple inelastic pushover analysis (Rossetto and Elnashai, 2005; Borzi et al., 2008). However, the dynamic analysis using multiple earthquake records is widely used to derive the fragility curves since it reduces the uncertainty, particularly due to input ground motions. Finally, the hybrid method for deriving fragility curves integrates two or three of the above-mentioned methods. The latter method could overcome the disadvantages of other approaches such as the lack of information or the high uncertainty (Kappos et al., 2006).

2.5.2 Performance criteria

The fragility curves estimate the probability of exceeding a predefined limit states. To derive the fragility curves for a structure under seismic loads, the performance limit states should be specified. Most previous studies employed the inter-story drift ratio (IDR) to define the performance criteria of structures. There are various approaches to specify the limit states at different performance levels of the structures. For instance, Yun et al. (2002) used two limit states to evaluate the seismic performance of steel moment frames, including the IO and CP limit states. Moreover, three limit states were proposed by Ji et al. (2007b) for high-rise buildings, including serviceability, damage control and CP, which represent minor cracks, first reinforcing steel yielding and ultimate capacity, respectively. Additionally, operational (OP), IO, life safety (LS), and CP are the four limit states proposed by FEMA-450 (2004), as shown in Figure 2.26. Finally, Ghobarah (2004) suggested five different limit states to describe the damage at various performance levels, as shown in Table 2.7.

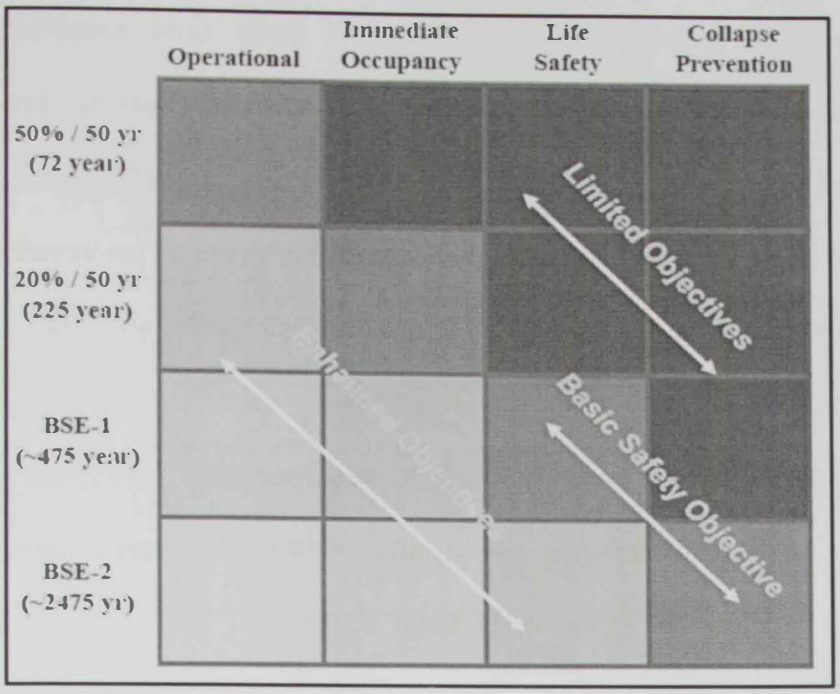

Figure 2.26: Performance criteria (FEMA-450, 2004)

Table 2.7: Inter-story drift ratio corresponding to different limit states (Ghobarah, 2004)

State of damage	Ductile MRF	Nonductile MRF	MRF with infills	Ductile walls	Squat walls
No damage	<0.2	<0.1	<0.1	<0.2	<0.1
Repairable damage (a) Light damage (b) Moderate damage	 0.4 <1.0	 0.2 <0.5	 0.2 <0.4	 0.4 <0.8	 0.2 <0.4
Irreparable damage (>yield point)	>1.0	>0.5	>0.4	>0.8	>0.4
Severe damage - Life safe - Partial collapse	1.8	0.8	0.7	1.5	0.7
Collapse	>3.0	>1.0	>0.8	>2.5	>0.8

ASCE/SEI-41 (2007) proposed three limit state for ductile wall structures: (i) IO, (ii) LS and (iii) CP. The immediate occupancy refers to a minor damage, which corresponds to IDR of 0.5%. The Life safety is related to the extensive damage with IDR of 1%. Finally, the CP is when extensive concrete crushing happens, which corresponds to IDR of 2% (ASCE/SEI-41, 2007). It is noteworthy that the IDR values proposed by seismic provisions such as ASCE/SEI-41 (2007) are usually conservative.

Performance limit states were proposed by Ghobarah (2004) based on analytical and experimental studies. The recommended IDRs for repairable damage i.e. (IO), LS, and CP limit states of ductile shear wall building were 0.4%, 1.5% and >2.5%. Furthermore, an experimental shaking table test was conducted for a seven story wall building by Panagiotou et al. (2010). The IDRs observed corresponding to the IO, LS and CP limit states were 0.35%, 0.89 and 2.36, respectively. Finally, Lehman et al. (2013) used the experimental results of full scale concrete wall structure under seismic loading to estimate the performance criteria. The IDRs corresponding to the IO, LS and CP limit states were 0.5%, 1.0% and 2.27%, respectively.

Previous studies related to the limit states of regular and irregular structures are summarized in Chapter 6. In the current study, three limit states are adopted for regular and irregular wall high-rise building based on extensive inelastic pushover analyses (IPOAs), IDAs as well as the suggested values in previous studies. These limit states are also selected based on two earthquake scenarios, as discussed in details in Chapter 6.

2.5.3 Previous vulnerability assessment studies

There are several sources of uncertainties in fragility analysis such as the seismic demand, system capacity, and modeling approach, as discussed in Chapter 6. Several previous studies were carried out to develop the fragilities of buildings with different heights and structural system. For instance, Ji et al. (2007a) proposed an analytical framework to develop the seismic fragility of RC high-rise buildings, as shown in Figure 2.27. This framework was applied to develop the fragilities of a high-rise building.

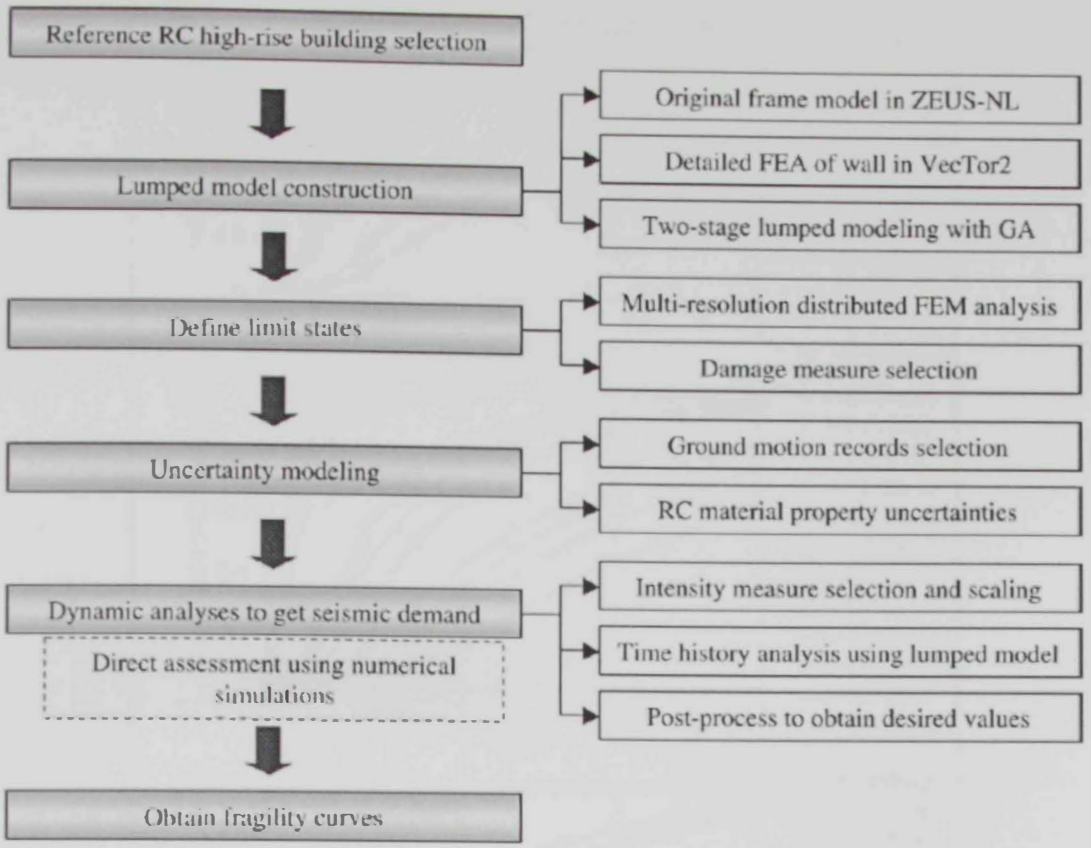

Figure 2.27: Fragility assessment framework proposed by Ji et al. (2007a)

Fragility curves were also developed by Jeong et al. (2012) to esitimate the safety margins of modern high-rise RC buildings using different earthquake scenarios. Twelve buildings with various heights, structural systems, and ductility levels were investigated. Regular and irregular buildings were considered in this study, while sixty natural records were utilized to develop fragilty curves, as shown in Figure 2.28. This study only considerd a single case of minor irregularity, mainly in-plane discontinuty in LFRS. The vulnerability of five sixty-story RC buildings were assessed by Mwafy et al. (2014) to evaluate the impact of increasing the material strength. IPOA and IDA were employed to develop the fragility curves of the reference structures.

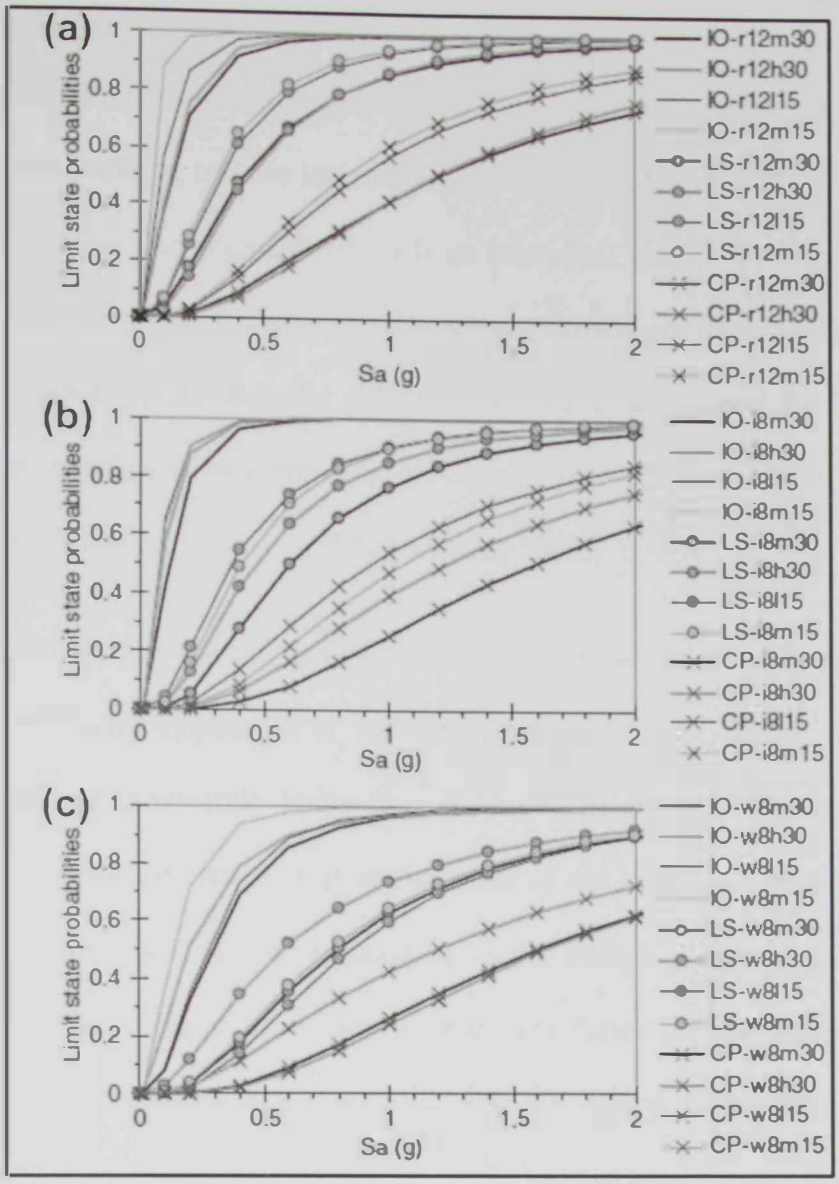

Figure 2.28: Fragility curves of twelve RC buildings (Jeong et al., 2012)

It was shown from this brief literature review that very few studies focused on the fragility assessment of high-rise irregular structures. In the current study, the fragility relationships of the most important vertical irregularity types are developed and compared with those of a regular structure. Additionally the damage probability of the reference structures at different limit states is calculated to assess the relative safety margin of regular and irregular structures.

2.6 Seismic design response factors

A three-dimensional (3D) model of a structure that includes all sources of stiffness, P-delta effects, and the inelastic response is the most accurate approach for the seismic design. Development of such an analytical model is costly and time consuming, and hence 3D inelastic models are not carried out for a typical building design. Alternatively, the inelastic seismic response is accounted for in modern elastic design approaches by employing the response modification factor, R, and the deflection amplification factor, C_d, (FEMA-P750, 2009).

The R factor is the ratio of the base shear that would be developed in the lateral force-resisting-system if it remained entirely elastic under the design earthquake (V_E) to the seismic design base shear (V), as shown in Figure 2.29. The deflection amplification factor (C_d) is the ratio of the roof drift at the ultimate capacity, δ, to the roof drift corresponding to the design ground motions, δ_E/R, (FEMA-450, 2004). Finally the design overstrength factor (Ω_o) is the ratio of the base shear at the ultimate capacity (V_{max}) to the design base shear (V). The definitions of the seismic design factors (i.e. R, C_d and Ω_o) are shown in Figure 2.29.

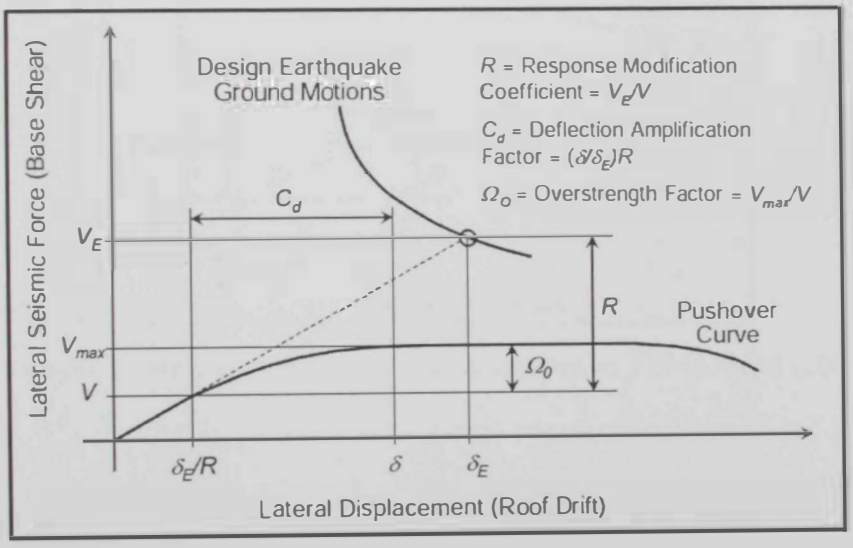

Figure 2.29: Seismic performance factors as defined by FEMA-450 (2004)

FEMA-P695 (2009) proposed an approach to quantify the building seismic design factors, which is consistent with the FEMA-450 (2004) concept, as shown in Figure 2.30. The R, C_d and Ω_o factors are defined as follows:

$$1.5R=\frac{S_{MT}}{C_S} \quad 2.1$$

$$C_d=R \quad 2.2$$

$$\Omega=\frac{S_{max}}{C_s} \quad 2.3$$

where, S_{MT} is the spectral acceleration of the maximum considered earthquake at the period of the structural system (T), S_{max} is the ultimate strength of the structure and C_s is the seismic response coefficient. The approach proposed by FEMA-P695 (2009) was evaluated by NIST (2010) and FEMA-P795 (2011). It was concluded that most code approved systems comply with the FEMA-P695 (2009) method criteria except short period structures.

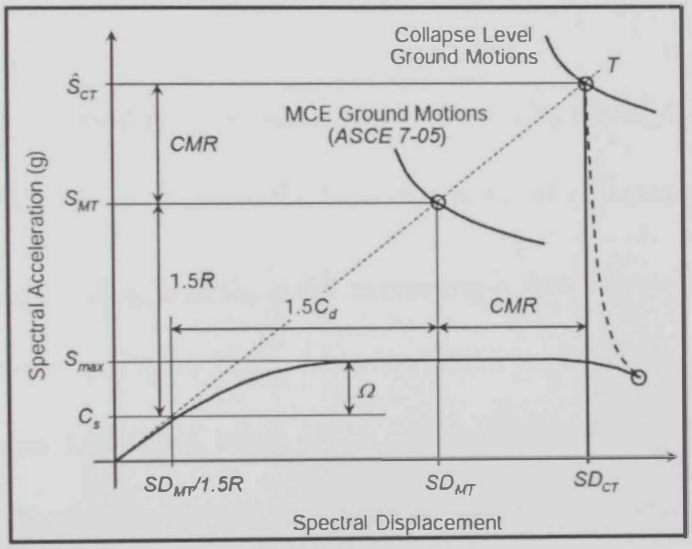

Figure 2.30: Seismic performance factors as defined by FEMA-P695 (2009)

Inelastic pushover analysis (IPOA) and incremental dynamic analysis (IDA) were employed to evaluate the seismic design factors in several previous studies (e.g.

Elnashai and Mwafy, 2002; Mwafy and Elnashai, 2002; Kim and Choi, 2005; Mwafy, 2011). Mwafy (2011) assessed the seismic design response factors of five multi-story buildings with different heights using IPOA and IDA. The selected buildings varied between 20 to 60 stories and were designed using the ACI (2005) code. The study used 20 input ground motions to represent two earthquake scenarios. The first yield overstrength factor was evaluated at the first indication of plastic hinges using two approaches: (i) from IPOA results, and (ii) from IDA. Figure 2.31 summarizes the calculated Ω_{1ph} factors from IPOA and IDA results (Mwafy, 2011).

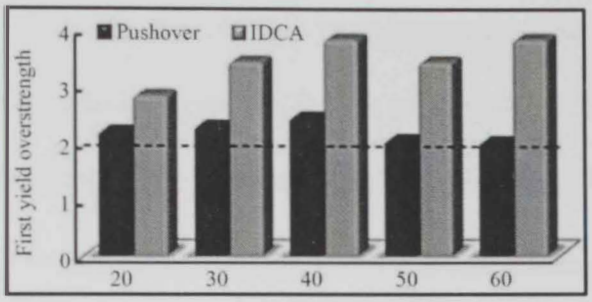

Figure 2.31: First yield overstrength (Ω_{1ph}) of five reference structures from IPOA and IDA results (Mwafy, 2011)

The response modification factor was estimated by Mwafy (2011) as follows: $R=\frac{a_c}{a_y}.\Omega_y$, where a_c is the PGA at the first indication of collapse, a_y is the PGA at first indication of yielding, and Ω_y is the overstrength factor at the first indication of yielding, as shown in Figure 2.32. Mwafy (2011) considered a conservative Ω_y factor, which was calculated using IPOA results, as shown in Figure 2.31. The deflection amplification factor was calculated as follows: $C_d=IDR_c/IDR_y$, where IDR_c is the maximum interstory drift ratio at collapse and IDR_y is the maximum interstory drift ratio at first indication of yielding (Mwafy, 2011).

The calculated R and C_d were compared by Mwafy and Elnashai (2002) and Mwafy (2011) with the code values, which proved that the design coefficient were

conservative for regular structures, as shown in Figure 2.33. It was concluded that the collapse-to yield IDRs were lower than the collapse-to-yield PGA ratios. This confirmed a satisfactory safety margin when equating the C_d and R factors, as shown in Eqn. 2.2 (FEMA-P695, 2009). It was also concluded that the higher the building height, the higher the PGA at collapse, which reflected the lower seismic risk of high-rise structures compared with the medium-rise building.

It is shown from this brief review that the assessment of seismic design response factors for structures representing different irregularity types was not fully covered in the literature. In the current study, a systematic procedure for the assessment of the seismic design response factors of irregular structures is carried out following the approach proposed by Mwafy (2011), as discussed in Chapter 6.

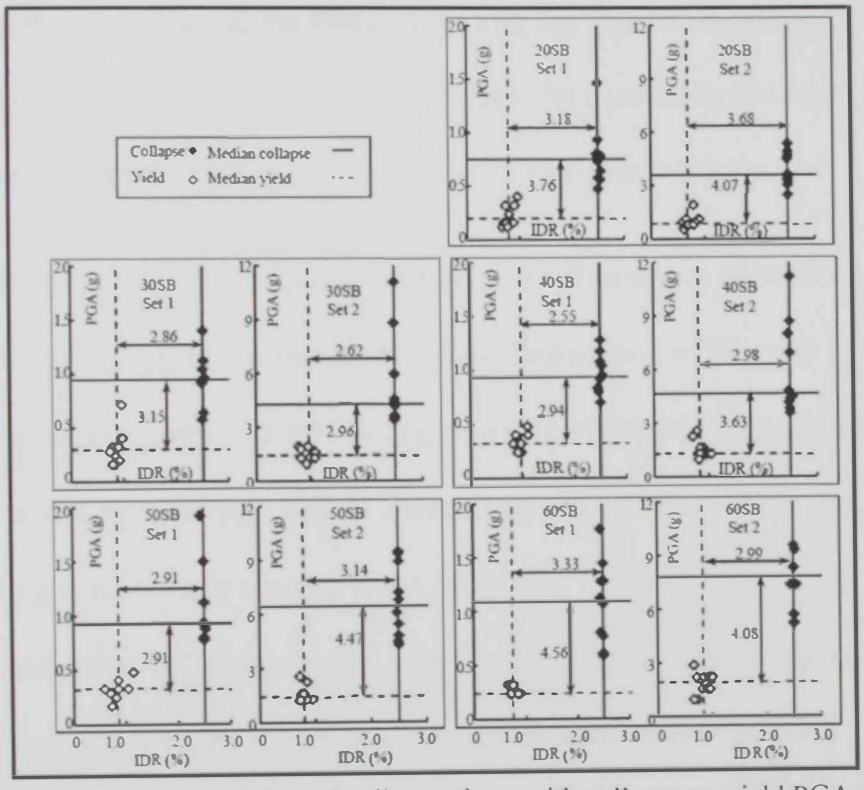

Figure 2.32: IDA results at yield and collapse along with collapse-to-yield PGA ratios and IDR ratios (Mwafy, 2011)

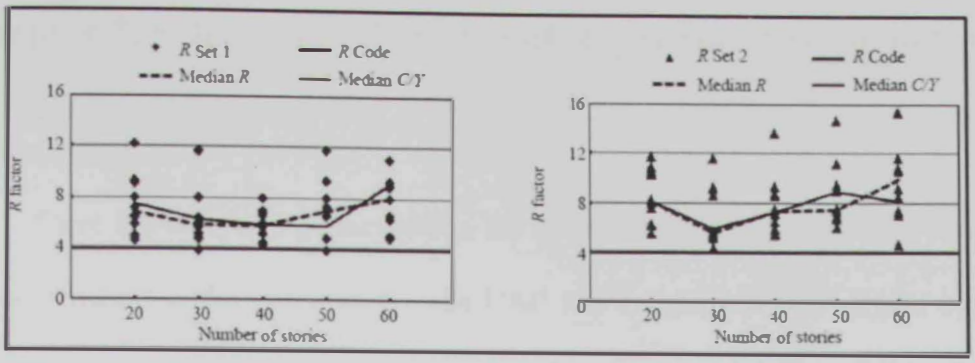

Figure 2.33: Seismic design response factors of five reference buildings obtained from long (set 1) and short (set 2) earthquake scenarios (Mwafy, 2011)

2.7 Concluding remakes

Previous hazard assessment studies concluded that the main sources of earthquakes in the UAE are: (i) local and (ii) regional faults. The discrepancies between the results of previous studies are attributed to the adoption of various seismic source zones and attenuation relationships. A design PGA of 0.16g is adopted in the current study for Dubai following the recommendations of a number of previous studies. The selected PGA is between the over-conservative PGA (0.32g) and the very low value (0.047g) recommended in previous studies.

The following observations summarize the limitations observed in previous studies and research needs related to the seismic assessment of irregular structures:

- Different irregularities of tall buildings was not systematically investigated.
- The assessment of the seismic design response factors of irregular high-rise building was not fully covered in the literature.
- The selection of performance criteria for regular and irregular high-rise buildings under different earthquake scenarios was not fully covered.

The literature review conducted in this chapter greatly emphasizes the importance of the current study.

Chapter 3: Selection and Design of Representative Structures

3.1 Introduction

There has been a large increase in the number of high-rise buildings that have been constructed in the last century. The UAE has a rapid rate of high-rise building construction. Multiuse buildings such as parking facilities, offices, residential and commercial buildings are widely constructed in the UAE. Due to the shortage of buildable land space, it is a common practice for the construction authorities to permit extensions at basement stories to increase the parking areas. Abrupt changes in the stiffness, mass, geometric dimensions, and/or strength of the lateral force-resisting-system (LFRS) along the building height due to architectural and services requirements introduce vertical irregularities. Consequently, irregular structures are more prevalent in this region, particularly buildings with vertical irregularities.

One of the important tasks of the current study is to select reference buildings. One regular and four irregular structures are therefore selected and fully designed for the purpose of this study. The buildings are selected based on a brief survey of the common types of irregular structures, as explained hereafter. This chapter also discusses the characteristics, structural systems, design methodology and results of the five reference structures.

3.2 Irregular high-rise buildings survey

The selection of representative structures is a major aspect in the seismic vulnerability assessment of buildings. Due to the rapid changes and development in the UAE building stock, conducting a reliable survey of the irregular high-rise building stock is a challenging task. A concise survey for irregular high-rise

buildings is conducted to select reference structures based on several structural drawings collected from consulting firms and other sources (e.g. Wong, 2013).

Table 3.1 summarizes the characteristic and main irregularity of the surveyed buildings in the UAE. The structural system layouts and observed irregularities for a sample of the surveyed buildings are shown in Figure 3.1. The building is located in the UAE and consists of two basement stories, a ground story, 16 typical stories, and a roof. Figure A.1 to Figure A.7 in Appendix A show additional structural drawings for the surveyed irregular buildings in the UAE. Moreover, additional irregular buildings collected from other sources are shown in Appendix A, Figure A.8 to Figure A.16 (Moehle et al., 2011; Wong, 2013). In most of surveyed buildings, the irregularities related to geometry and discontinuity in LFRS are frequently observed.

Table 3.1: Characteristic of the surveyed buildings in the UAE

Ref.	Total number of stories	Number of basement stories	Ground story height (m)	Height of building (m)	Type of irregularity
1	31	3	3.7	104	1,3
2	25	3	5.1	99.2	1,2,3
3	23	4	5.0	86	1,2,3
4	20	-	3.6	78.1	1,3
5	12	2	4	42.6	1,3
6	12	3	3.85	43.2	1,3
7	10	-	3.95	34.8	1,3
8	10	-	3.95	35.8	1,3

Irregularity1: Discontinuity in the lateral force-resisting-system
Irregularity2: Soft story
Irregularity3: Geometric

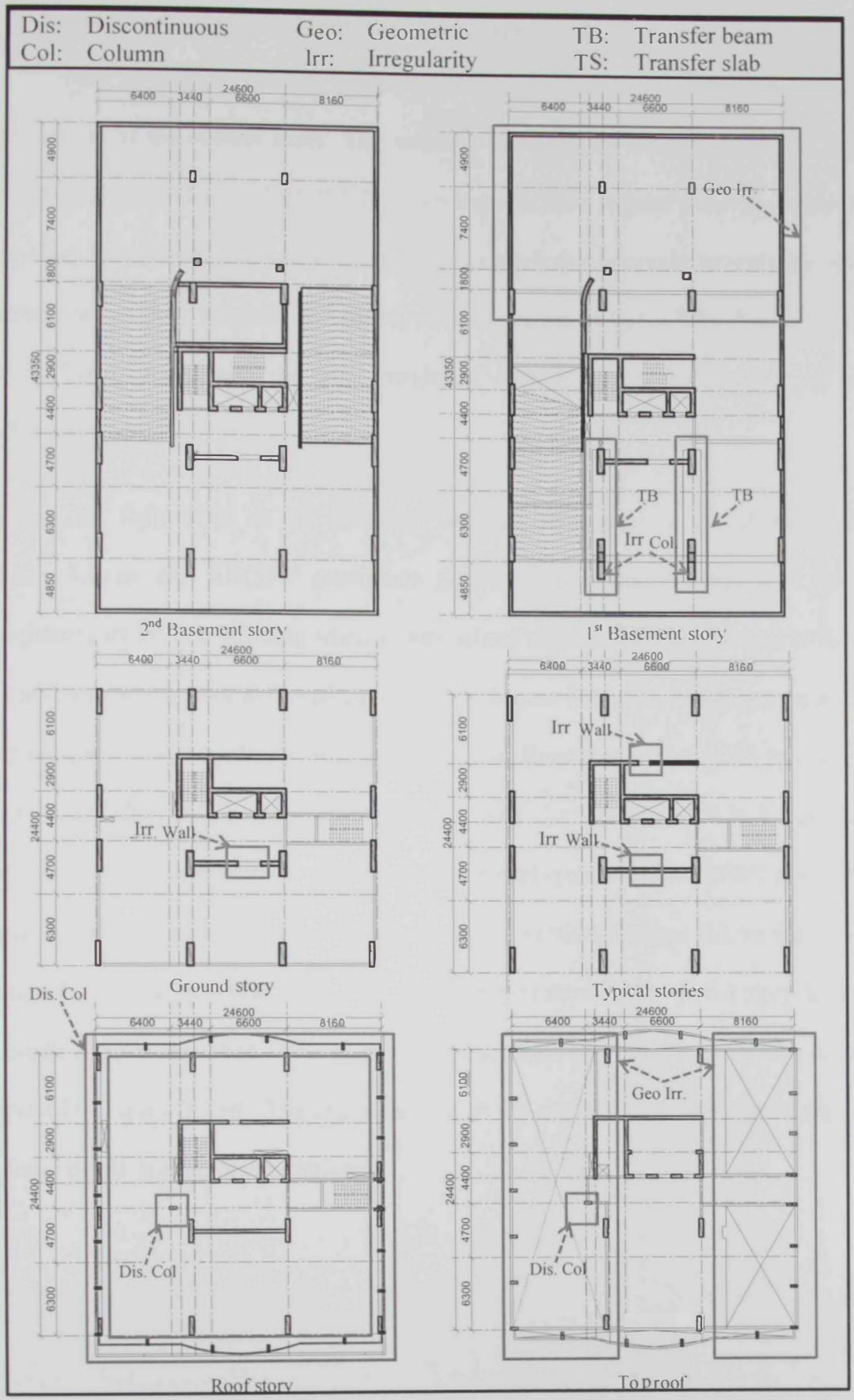

Figure 3.1: Sample of surveyed buildings – layouts of building 1 showing its irregularity features

3.3 Characteristic of selected buildings for present study

Five 50-story reinforced concrete (RC) high-rise buildings are selected for the purpose of the current study. The selected buildings are denoted B1-REG, B2-SST, B3-GEO, B4-DIS and B5-WST, which characterize a regular structure, extreme soft story irregularity, geometric irregularity, in-plane discontinuity irregularity, and extreme weak story irregularity, respectively, as shown in Table 3.2. The height of the different stories and the total height of each building are summarized in Table 3.2.

The definitions of the selected building irregularities are depicted in Figure 3.2 as per ASCE-7 provisions (2010). A stiffness/extreme soft story irregularity exists in a building when a story lateral stiffness (S_1) is less than 60% of the stiffness of the story above (S), as shown in Figure 3.2 (a). A building exhibits a vertical geometric irregularity when the horizontal dimension of the LFRS in a story (Li) is more than 130% of that in an adjacent story (Ls), as presented in Figure 3.2 (b). The in-plane discontinuity exists when a vertical element of the LFRS is shifted by a distance (L_1), which exceeds the length of the vertical element (L), as shown in Figure 3.2 (c). The extreme weak story irregularity is introduced when a story lateral strength (St_1) is less than 65% of the lateral strength (St) for the story above, as depicted in Figure 3.2 (d). The characteristics of the selected buildings are described in more detail in subsequent sections.

Table 3.2: Characteristics of reference structures

Building reference	Building irregularity type	Typical story height (m)	Ground story height (m)	First basement height (m)	Total height (m)
B1-REG	Regular building	3.2	3.2	3.2	160
B2-SST	Stiffness/ extreme soft story irregularity	3.2	6.5	3.2	163.2
B3-GEO	Geometric irregularity	3.2	3.2	3.2	160
B4-DIS	In-Plane Discontinuity irregularity	3.2	4.7	4.7	163
B5-WST	Discontinuity in lateral strength/weak story irregularity	3.2	3.2	3.2	160

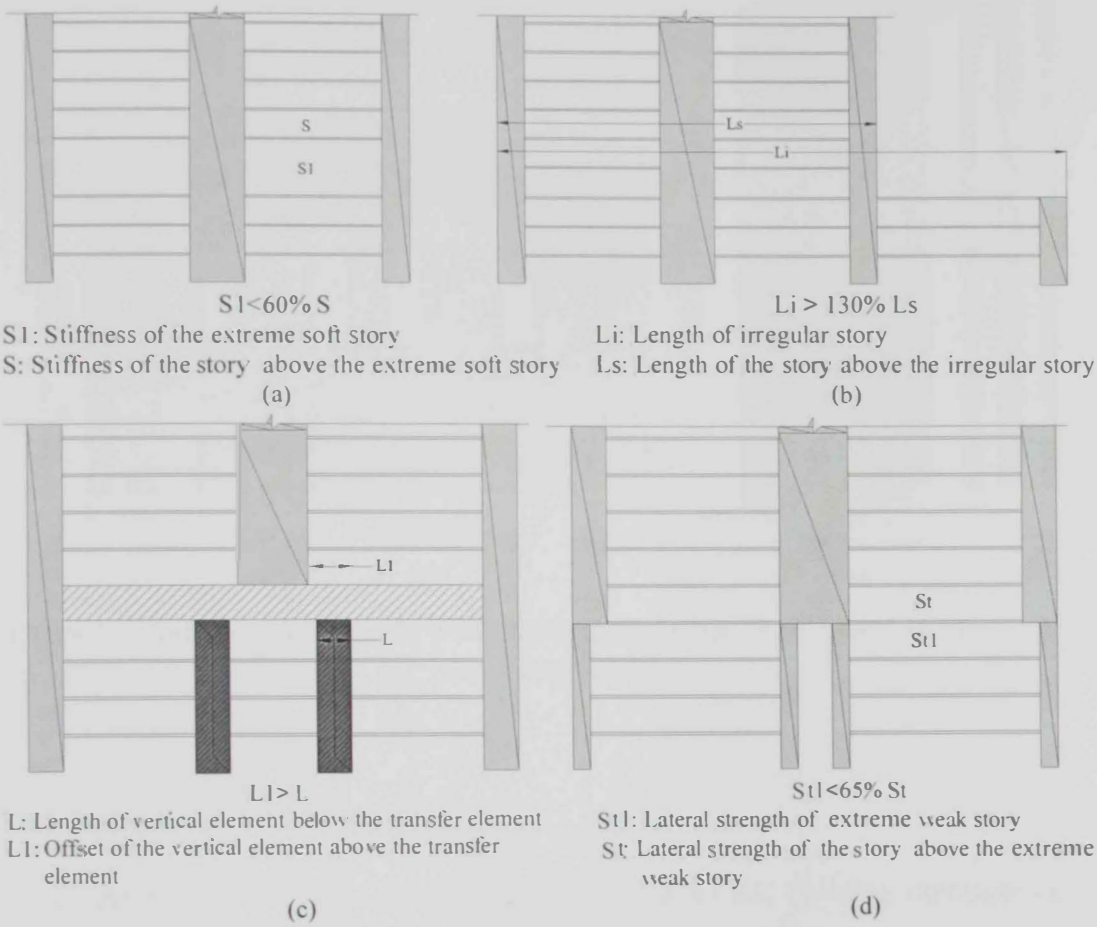

S1<60% S

S1: Stiffness of the extreme soft story
S: Stiffness of the story above the extreme soft story

(a)

Li > 130% Ls

Li: Length of irregular story
Ls: Length of the story above the irregular story

(b)

L1> L

L: Length of vertical element below the transfer element
L1: Offset of the vertical element above the transfer element

(c)

St1<65% St

St1: Lateral strength of extreme weak story
St: Lateral strength of the story above the extreme weak story

(d)

Figure 3.2: Definition of vertical structural irregularities: (a) extreme soft story, (b) geometric irregularity, (c) in-plane discontinuity, and (d) extreme weak story

3.3.1 Reference building B1-REG

B1-REG is a 50-story RC building representing regular high-rise structures. The building consists of three basement stories, a ground story, and 46 typical stories. The height of each story is 3.2m and the total height of the building is 160m.

The plan layout (42.0m x 29.20m) represents a common structural layout for high-rise buildings. The LFRS extends from the foundation throughout the building height without any interruption. The seismic response of this regular building is used as a benchmark for comparison with that of other irregular structures. Figure 3.3 shows different structural elements of the B1-REG building.

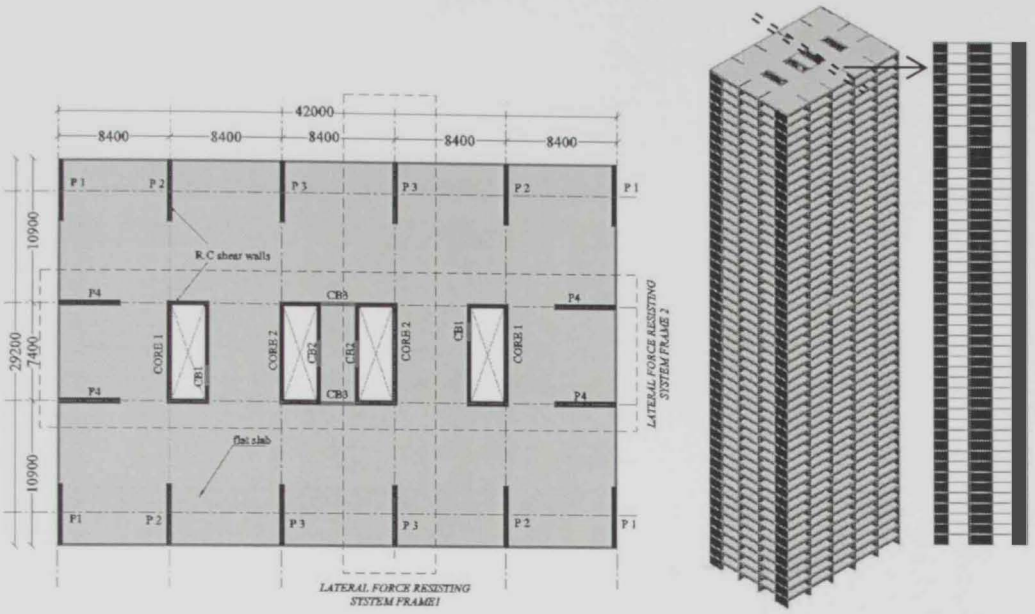

Figure 3.3: Reference structure B1-REG, (a) building layout, (b) 3D view, and (c) LFRS in transverse direction

3.3.2 Reference building B2-SST

As shown in Figure 3.4, B2-SST is a 50-story RC building representing the extreme soft story irregularity. The building consists of three basement stories, a ground story, and 46 typical stories. The height of typical and basement stories is 3.2m, while the total height of the building is 163.3m. The increased height of the ground story (6.5m), which is more than double the height of the story above, causes significant reduction in stiffness. This irregularity is practically shown in most multi-story buildings. Figure 3.5 shows the applied load and boundary conditions used to

calculate the stiffness of the ground and first stories of building B2-SST. The ETABS software (CSI, 2011a) is used to calculate the stiffness of the ground and first stories. The ratio between the calculated initial stiffness of the ground story to that of the first story is 45%. The stiffness of the ground story is therefore less than 60% of the story above, which results in an extreme soft story (ASCE-7, 2010).

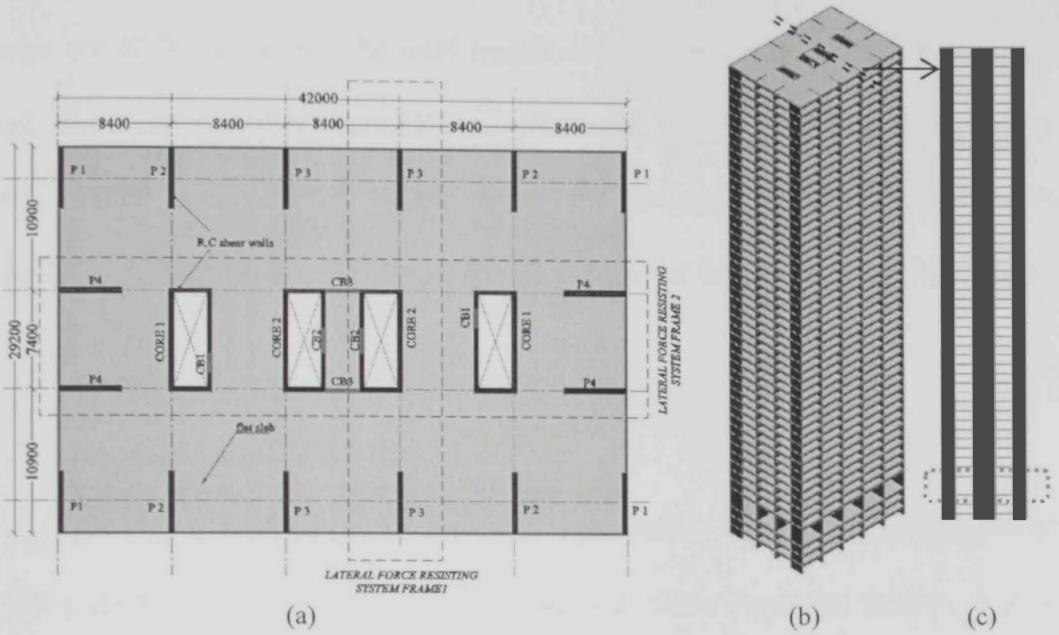

Figure 3.4: Reference structure B2-SST, (a) building layout, (b) 3D view, and (c) LFRS in transversal direction

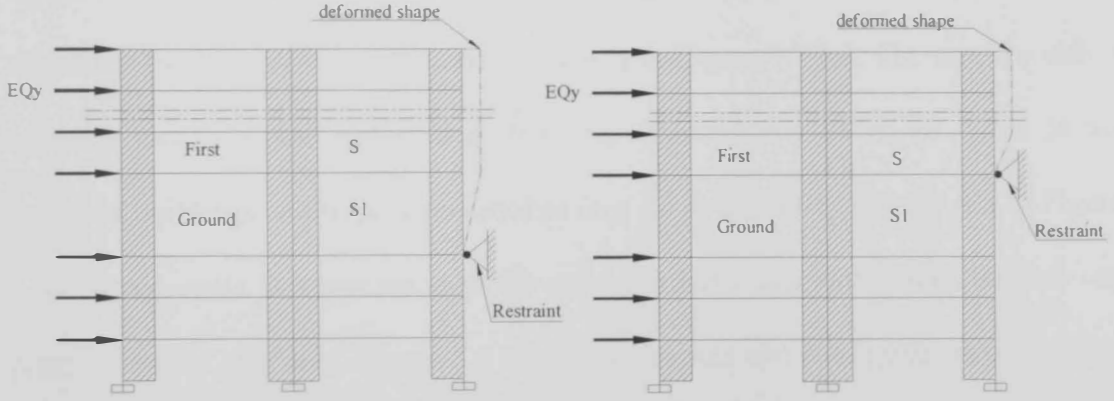

Figure 3.5: Approach of stiffness estimation for: (a) ground story and (b) first story

3.3.3 Reference building B3-GEO

B3-GEO is a 50-story RC building that exemplifies the vertical geometric irregularity according to ASCE-7 (2010). The building consists of three basement stories, a ground story, and 46 typical stories. The height of each story is 3.2m and the total height of the building is 160m. The footprint dimensions of the basement stories are 42.0m x 45.5m, while the layout dimensions of the ground and typical stories are 42.0m x 29.2m. The total length of the LFRS is decreased at the ground level. The ratio between the LFRS length at the basement and ground stories is 156%, which is more than 130%. Hence the building has a vertical geometric irregularity (ASCE-7, 2010). Figure 3.6 illustrates the layouts and configurations of building B3-GEO.

3.3.4 Reference building B4-DIS

B4-DIS is a 50-story RC building representing an in-plane discontinuity of LFRS (ASCE-7, 2010). The building consists of three basement stories, a ground story and 46 typical stories. The height of each story is 3.2m. The plan dimensions of all stories are 42.0m x 29.2 m. A transfer slab at the first story level is introduced to support the planted central core walls of typical stories. This transfer slab is supported by RC cores and columns, as shown in Figure 3.7 (a). The transfer slab is typically much thicker and heavier than the typical story slabs, as noted in the surveyed buildings and in previous studies (e.g. Li et al., 2006). Figure A.8 to Figure A.12 in Appendix A show some of the surveyed buildings with a transfer slab and planted vertical elements. Figure 3.7 shows the layouts and configuration of building B4-DIS.

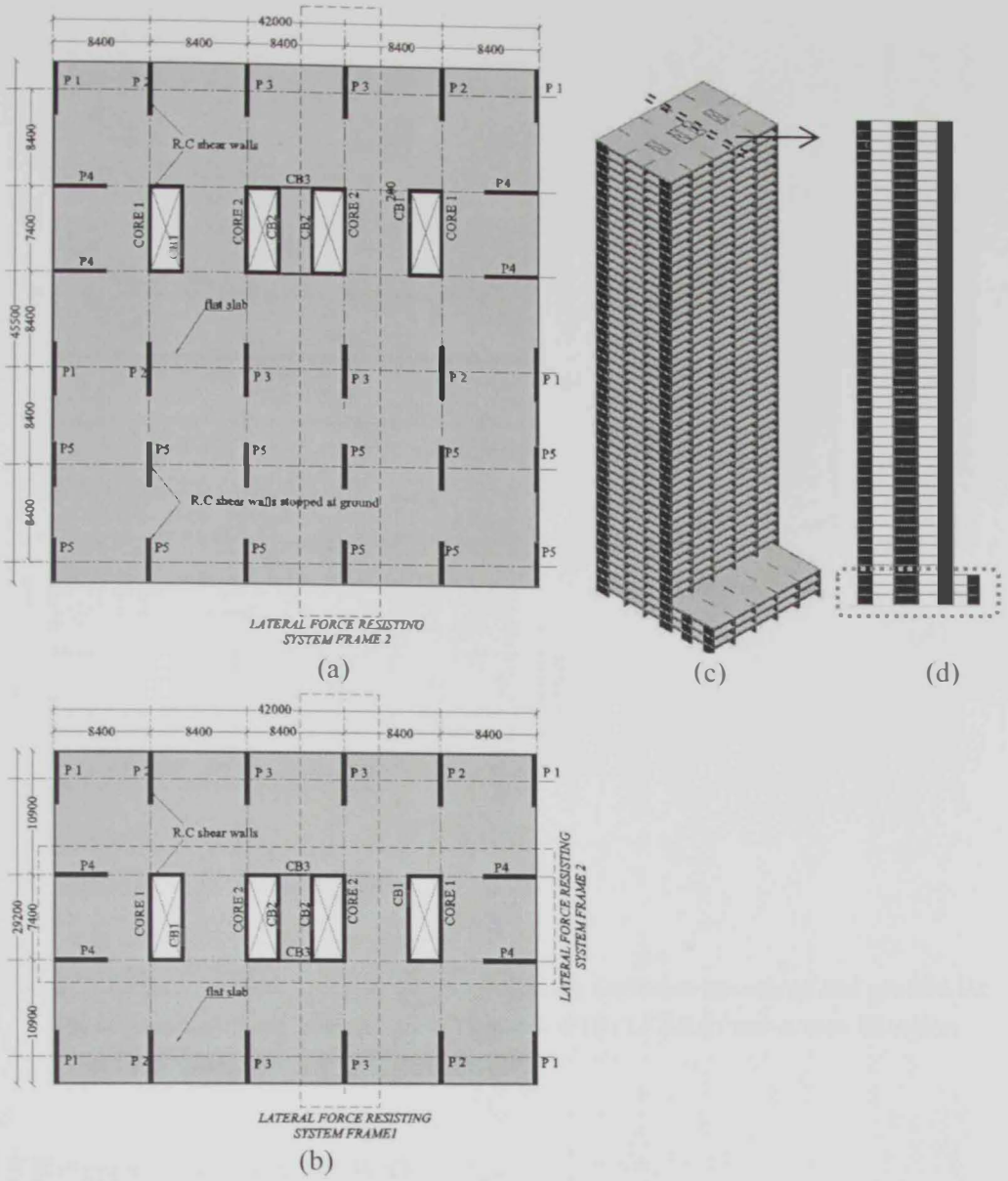

Figure 3.6: Reference structure B3-GEO, (a) building layout at basement stories, (b) layout at ground and typical stories, (c) 3D view and (d) LFRS in transversal direction

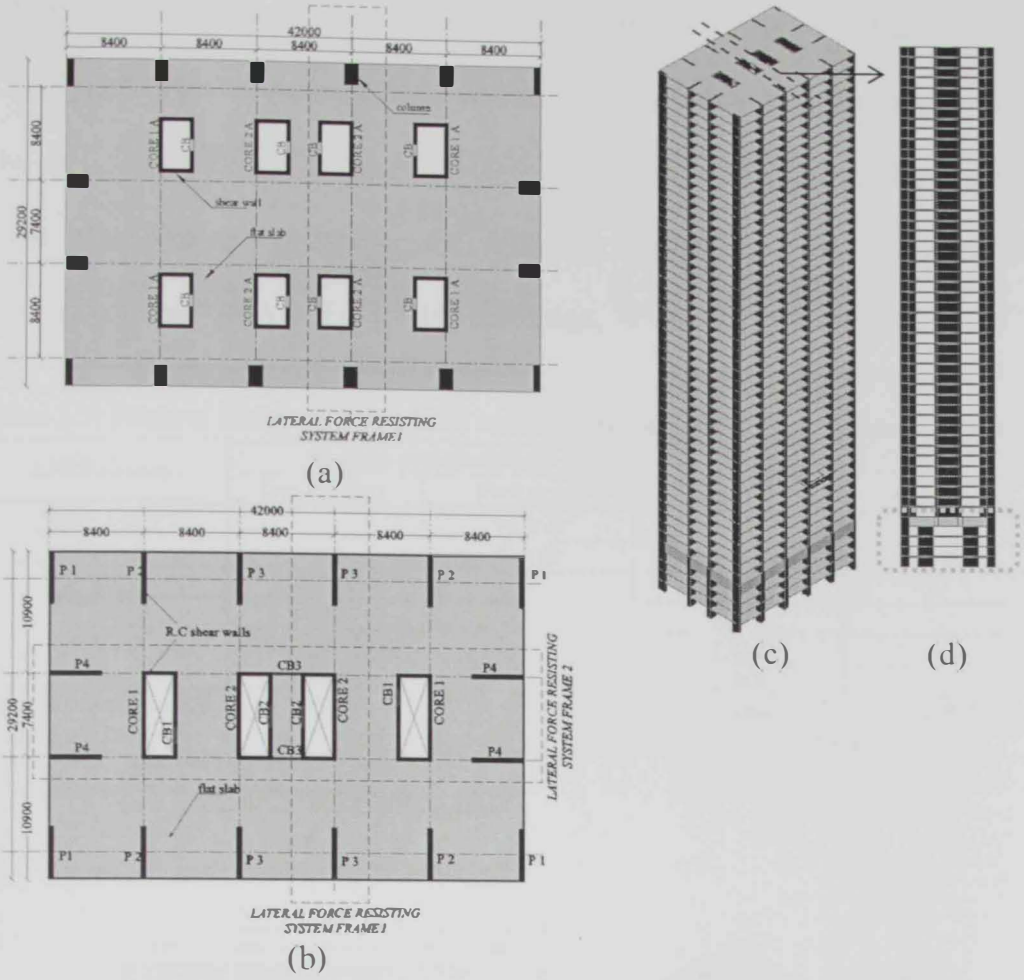

Figure 3.7: Reference structure B4-DIS, (a) building layout at basement and ground stories, (b) layout at typical stories (c), 3D view and (d) LFRS in transverse direction

3.3.5 Reference building B5-WST

As shown in Figure 3.8, B5-WST is a 50-story RC building representing the extreme weak story irregularity. The building consists of three basement stories, a ground story, and 46 typical stories. The height of each story is 3.2m, while the total height of the building is 160 m. Due to the major changes of the LFRS at the basement and ground stories (i.e. replacing shear walls with columns), the lateral strength of the lower stories significantly decreases. The lateral flexural and shear strength values are calculated for different vertical structural members at the ground and first stories using the design code approach (ACI-318, 2011), as shown in

Table 3.3. It is clear that the ratio of the flexural strength at the ground story to that at the first story is 38%, while the ratio of the shear strength at the ground story to that at the first story is 58%. The lateral strength of the ground story is thus less than 65% of the story above. Therefore, the building exhibits an extreme weak story irregularity, as per the ASCE-7 (2010) definition.

Table 3.3: Flexural and shear strength of vertical members for the ground and first stories

LFRS elements	Flexural strength (kN.m)		Shear strength (kN.m)	
	Ground story	First story	Ground story	First story
Shear wall P3	-	94,418	-	18,792
Core 2	-	50,163	-	22,496
C1	8,718	-	7,032	-
C2	10,135	-	6,054	-
C3	12,287	-	5,638	-
C4	23,820	-	5,340	-
Total flexural strength	54,960	144,581	24,064	41,288
Ratio of GSS to FSS	38%		58%	

GSS: strength of the vertical elements at ground story
FSS: strength of the vertical elements at first story

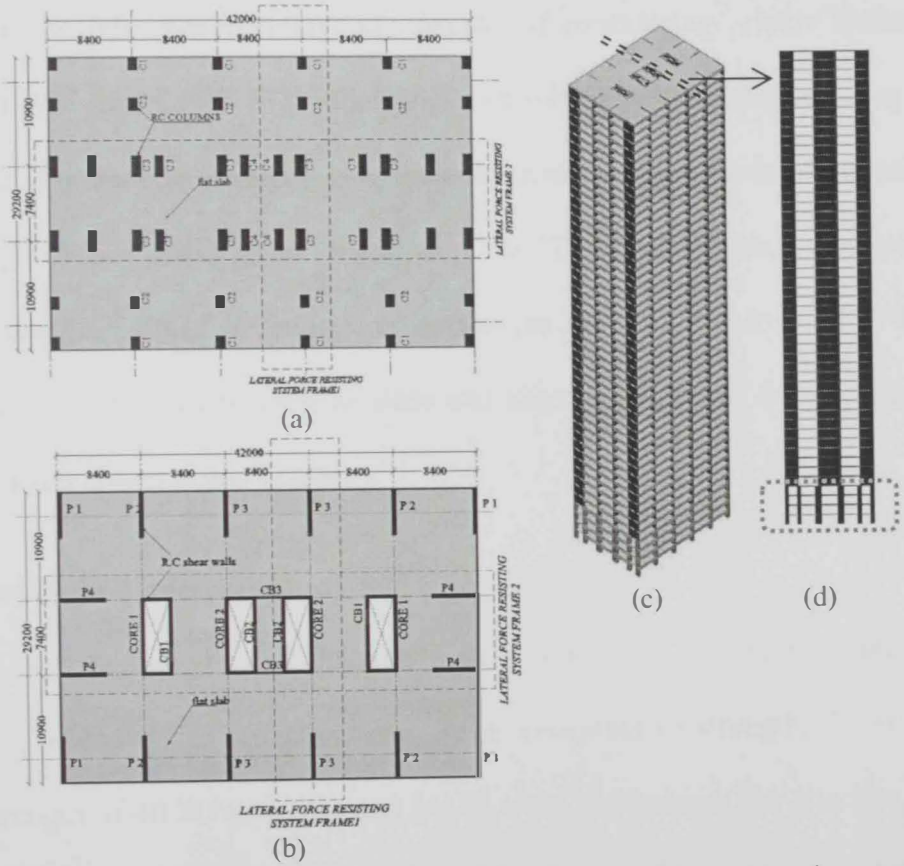

Figure 3.8: Reference structure B5-WST, (a) building layout at basement and ground stories, (b) building layout at typical stories (c), 3D view and (d) LFRS in transverse direction

3.4 Structural system and design approach

Shear and core walls are mainly used for the LFRS of the reference structures. Flat slabs with marginal beams are employed as a horizontal diaphragm to transfer the gravity loads to vertical elements. The shear wall LFRS is more efficient than moment resisting frame in controlling the lateral deformations developed by wind or earthquake loads (Ali and Moon, 2007; Halis and Emre, 2007). In buildings B4-DIS and B5-WST, columns are used at the basement stories as result of their irregularity.

The five reference structures are fully designed for the purpose of this study. Three-dimensional (3D) simulation models are developed using the Extended Three-dimensional Analysis of Building Systems ETABS (CSI, 2011a). This platform is widely used for the analysis and design of the multi-story buildings. 3D ETABS models of the reference buildings are developed considering gravity loads, lateral loads and P-Δ effects. The 3D models are used for: (i) determining straining actions of structural members, (ii) estimating the deformations and periods of vibration, and (iii) design of vertical structural members. The 3D ETABS models account for the stiffness and strength of structural elements as per the design code (ACI-318, 2011). Shell elements are used to idealize slabs and shear walls, while frame elements are used to model columns and beams.

3.4.1 Material characteristics

Concrete strength with different values is used for the design of the selected buildings, as shown in Table 3.4. A cylinder compressive strength, f'_c, of 32 MPa (cube strength of 40 MPa, f_{cu}) is used for all slabs and beams. The concrete strength varies throughout the height of vertical element starting from f'_c of 48 MPa (cube strength of 60 MPa, f_{cu}) at the foundation to 32 MPa (f_{cu} of 40 MPa) at the roof. The

modulus of elasticity of concrete (E_c) is as per ACI-318 (2011). The specific weight of reinforced concrete is 25 kN/m^3. The yield strength (f_y) of reinforcing steel bars is 460 MPa for flexural design and 420 MPa for shear design (ACI-318, 2011). The steel modulus of elasticity (E_s) is 200,000 MPa.

Table 3.4: Material characteristics used in the ETABS design models

Material	Characteristics			
	f_{cu} (MPa)	f_c' (MPa)	f_y (MPa)	E_c , E_s (MPa)
Steel- flexural	N/A	N/A	460	200,000
Steel-Shear	N/A	N/A	420	200,000
Concrete1	40	32	N/A	26,587
Concrete2	50	40	N/A	29,725
Concrete3	60	48	N/A	32,562

N/A: not applicable

3.4.2 Design loads

Permanent loads include the self-weight of structural members with a concrete density of 25 kN/m^3. Superimposed dead load is 4.0 kN/m^2, which includes other permanent loads such as partitions. Live loads are adopted according to ASCE-7 (2010) as follows:

- 2.0 kN/m^2 for the residential areas,
- 4.8 kN/m^2 for corridors and staircases, and
- 3.0 kN/m^2 for basement stories (parking areas)

Two cases of lateral loads (wind and earthquake) are adopted for the design of the reference structures according to ASCE-7 (2010). Seismic loads are calculated using the design response spectrum recommended by ASCE-7 (2010), as shown in Figure 3.9.

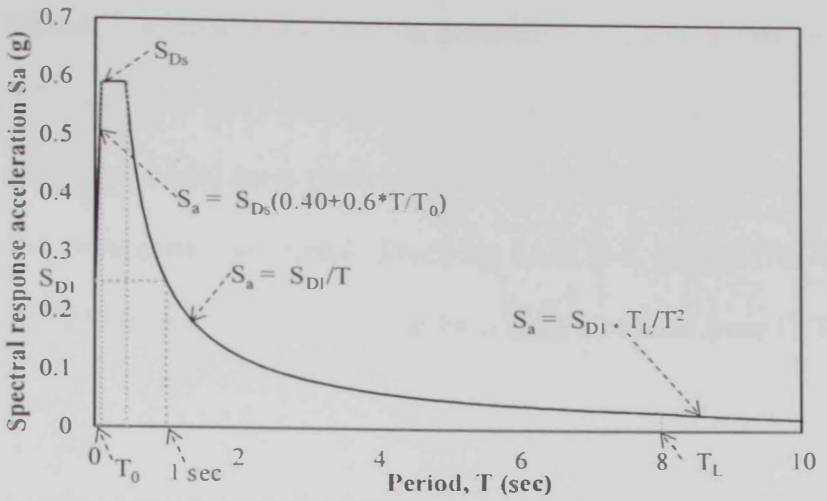

Figure 3.9: Design response spectrum for a site class "C" and a seismic design category "C" (ASCE-7, 2010)

The reference buildings are considered to be located in Dubai, UAE, which represent a medium seismicity region. The seismic parameters are defined according to the design code (ASCE-7, 2010; AD-IBC, 2013). The seismic parameters are considered as follows:

- Site class: C
- Spectral response acceleration at 0.2 sec: $S_s = 0.83$ for site class B (rock)
- Spectral response acceleration at 1.0 sec: $S_1 = 0.24$ for site class B (rock)
- Long-period transition period: $T_L = 8$
- Site coefficient F_a is 1.068 for site class C
- Site coefficient F_v is 1.56 for site class C
- Response modification coefficient, R = 4
- Overstrength factor, $\Omega_o = 2.5$

The equivalent lateral force procedure (ELFP) and modal response spectrum analysis (MRSA) are employed to estimate the lateral seismic forces (ASCE-7, 2010). The base shear, calculated using ELFP, is only considered to verify the base

shear from MRSA. The approximate period parameters, C_t, and, x, are considered as 0.0488 and 0.75, respectively. The analysis is conducted with 20 modes of vibration to obtain a combined modal mass participation of more than 90% of the actual mass in each of the orthogonal horizontal directions (ASCE-7, 2010). The base shear obtained from MRSA is at least 85% of the base shear obtained from ELFP (ASCE-7, 2010).

3.4.3 Design code requirements for irregular structures

Some of the irregularity types require special analysis and load conditions as per the design code (ASCE-7, 2010). The in-plane discontinuity of the LFRS and the discontinuity in lateral strength of the LFRS (weak story irregularity) should be designed using special cases of loading. Table 3.5 shows the code recommended analysis procedure and special loads for the seismic design category "C" (ASCE-7, 2010). The special seismic load combinations are discussed hereafter.

Table 3.5: Recommended analysis procedures and special loads for different irregularity types in seismic design category "C"

Type of irregularities	Provisions				
	H	ELFP	MRSA	SRHP	SSL
Stiffness/extreme soft story irregularity	NL	P	P	P	NR
Geometric irregularity	NL	P	P	P	NR
In-plane discontinuity irregularity	NL	P	P	P	R
Discontinuity in lateral strength / extreme weak story irregularity	NL	P	P	P	R

ELFP: equivalent lateral force procedure
SRHP: seismic response history procedures
NL: not limited
R: required

H: building height
MRSA: modal response spectrum analysis
SSL : special seismic load
NR: not required
P: permitted

3.4.4 Load combinations

Both serviceability and ultimate limit state load combinations are considered in the design process. Service load combinations are employed to verify the vertical and lateral deformations, while the structural elements are designed using the

ultimate load combinations (ASCE-7, 2010). The design load combinations of the regular structure are as follows.

$1.4D$ 3.1

$1.2D + 1.6L + 0.5L_r$ 3.2

$1.2D + 1.6L_r + L$ 3.3

$1.2D + 1.6L_r + 0.5W$ 3.4

$1.2D + 1.0W + L + 0.5L_r$ 3.5

$1.2D + 1.0E + L$ 3.6

$0.9D + 1.0W$ 3.7

$0.9D + 1.0E$ 3.8

Where: D is the dead load, E is the earthquake load, L is the live load, L_r is the roof live load, and W is the wind load

The dead load in the above-mentioned combinations includes the self-weight, partitions, services and any other superimposed dead loads. The seismic load case "E" represents both the horizontal and vertical component of ground motion. Hence, for the load combination in Eqn. 3.6, the seismic load, E, shall be calculated as $E_h + E_v$, where E_h and E_v are the horizontal and vertical components of earthquake load, respectively. For the load combination in Eqn. 3.8, the seismic load shall be considered as $E_h - E_v$. The horizontal seismic load effect is estimated by multiplying the redundancy factor (ρ) times the effect of horizontal seismic forces (Q_E). The redundancy factor (ρ) is 1.0 for SDC "C". The vertical seismic load component (E_v) is $0.2S_{DS}$ times D, where S_{DS} is the design spectral response acceleration at 0.2 sec (ASCE-7, 2010). From this discussion, the ultimate load combinations, including the seismic vertical and horizontal effects, are presented as per Eqns. 3.9 and 3.10, as follows (ASCE-7, 2010):

$(1.2+0.2S_{DS})\ D + \rho\ Q_E + L$ 3.9

$(0.9-0.2S_{DS})\ D + \rho\ Q_E$ 3.10

The above combinations are adopted for the design of the regular structure as well as the buildings with stiffness irregularity and geometric irregularity. The overstrength factor Ω_o is utilized for the design of the irregularity introduced in buildings B4-DIS and B5-WSST (ASCE-7, 2010). The load combinations including the overstrength factor are as follows:

$(1.2 + 0.2S_{DS})\ D + \Omega_o\ \rho\ Q_E + L$ 3.11

$(0.9 - 0.2S_{DS})\ D + \Omega_o\ \rho\ Q_E$ 3.12

3.5 Design results

The serviceability limit state of the reference buildings is verified according to the design code. The maximum inter-story drift ratios (IDRs) according to ASCE-7 (2010) is 2% for the shear wall structural system located in risk category II. Figure 3.10 shows a comparison between the periods of the first three modes of the five reference buildings. Figure 3.11 shows the vibration periods of the first two modes in the transverse direction, while Figure 3.12 shows the vibration periods of the first two modes in the longitudinal direction. The comparison shows that, with the exception of building B3-GEO, which has slightly shorter periods, the fundamental vibration periods of the irregular buildings in the transverse direction are greater than the regular counterpart (B1-REG). The differences in the vibration periods of the reference buildings are attributed to the changes in the dimensions, stiffness and strength of their LFRS.

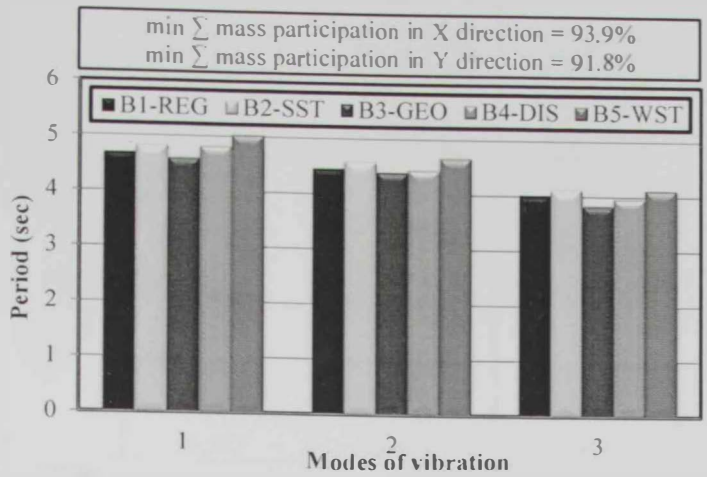

Figure 3.10: First three periods of vibration of the five reference buildings

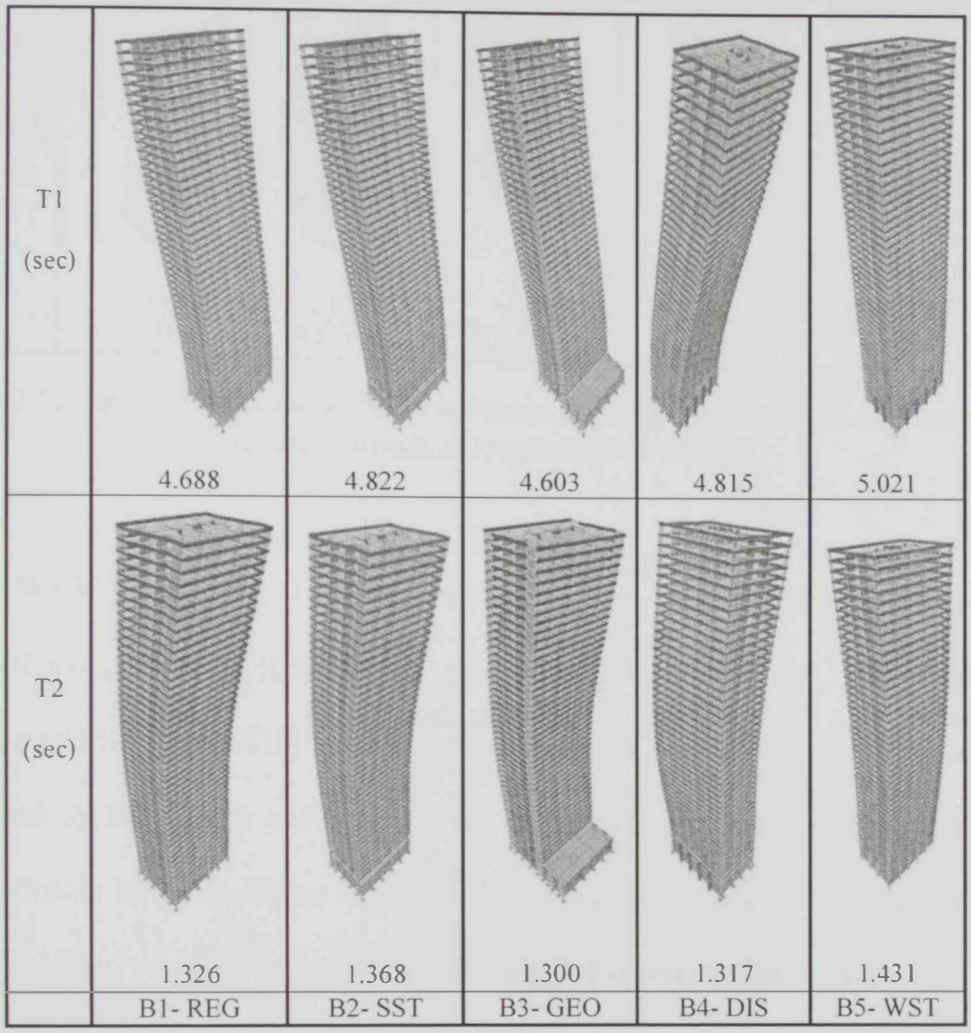

Figure 3.11: First two mode shapes of the reference structures along with the corresponding vibration periods in transverse direction

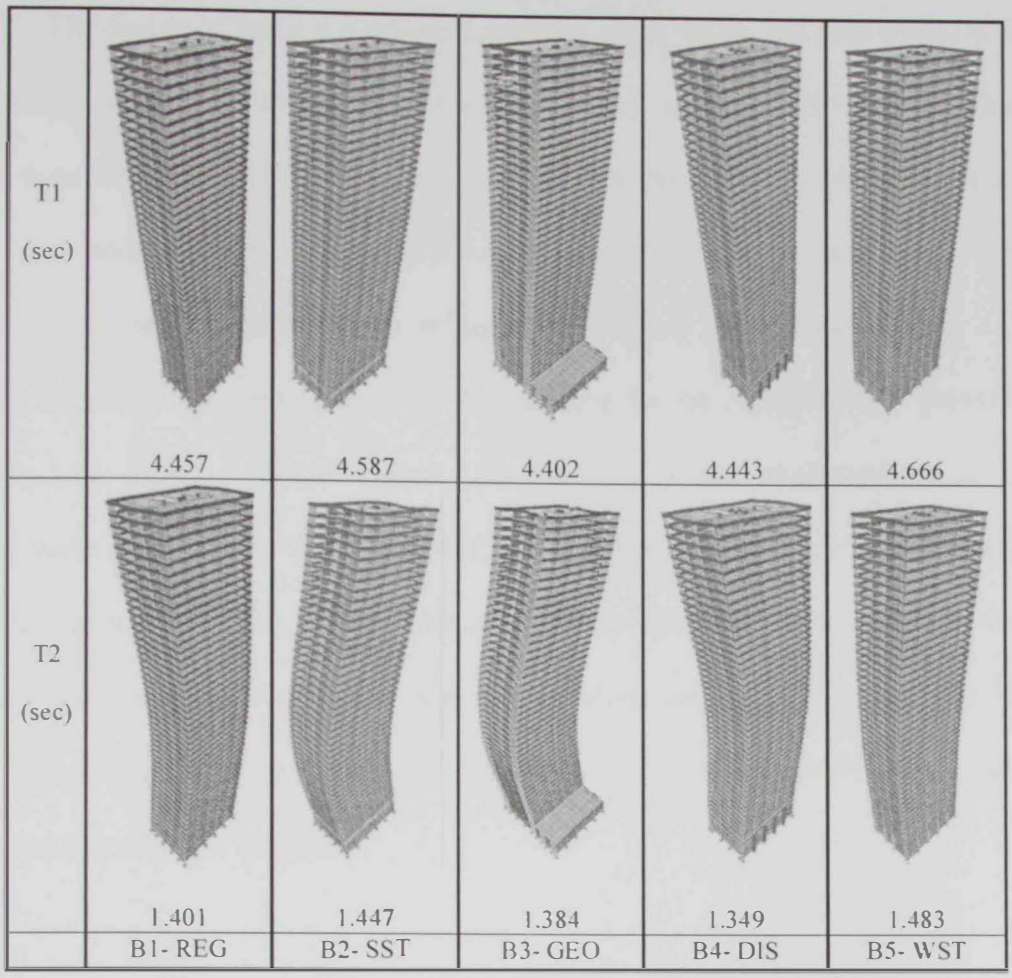

Figure 3.12: First two mode shapes of the reference structures along with the corresponding vibration periods in longitudinal direction

While the vertical structural elements of the five reference buildings are designed using ETABS (CSI, 2011a), the Slab Analysis by the Finite Element software SAFE (CSI, 2011b) is used for the design of floor slabs. Straining actions developed by the gravity and lateral loads are considered in the slab design. The seismic forces have significant influence on the slab reinforcement, particularly at the connections between the slabs and the vertical elements (shear walls, columns and core walls). Figure 3.13 to Figure 3.21 show the slab layout and reinforcement details, while Table 3.6 to Table 3.9 show the additional reinforcement of the floor slabs for the five reference buildings.

The design of vertical elements (columns, shear walls, and core walls) is fully automated using ETABS. The ACI-318 (2011) and ASCE-7 (2010) design provisions are considered in the design. Although the boundary elements of shear and cores walls are not required by the design code for SDC "C" (ACI-318, 2011), they are utilized in the design to enhance the seismic performance of the LFRS. These boundary elements are detailed according to the ACI318-2011 provisions. Figure 3.22, Figure 3.23 and Figure 3.24 show the typical reinforcement detail of shear walls according to the ACI-318 (2011). Table 3.10 to Table 3.14 summarize the design results of the vertical elements for the reference buildings. The design results are used to develop the nonlinear analysis models using the fiber-based platform Zeus-NL (Elnashai et al., 2012). The nonlinear modeling approach is discussed in detail in Chapter 4.

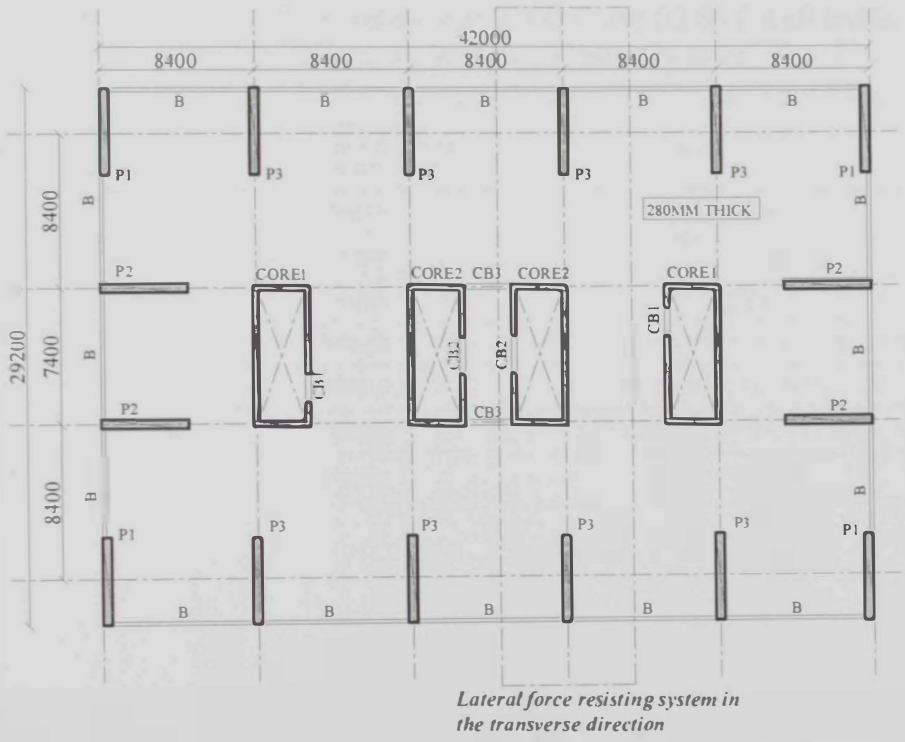

Figure 3.13: Slab layout of B1-REG and B2-SST at all levels, and B3-GEO, B4-DIS and B5-WST at typical story levels

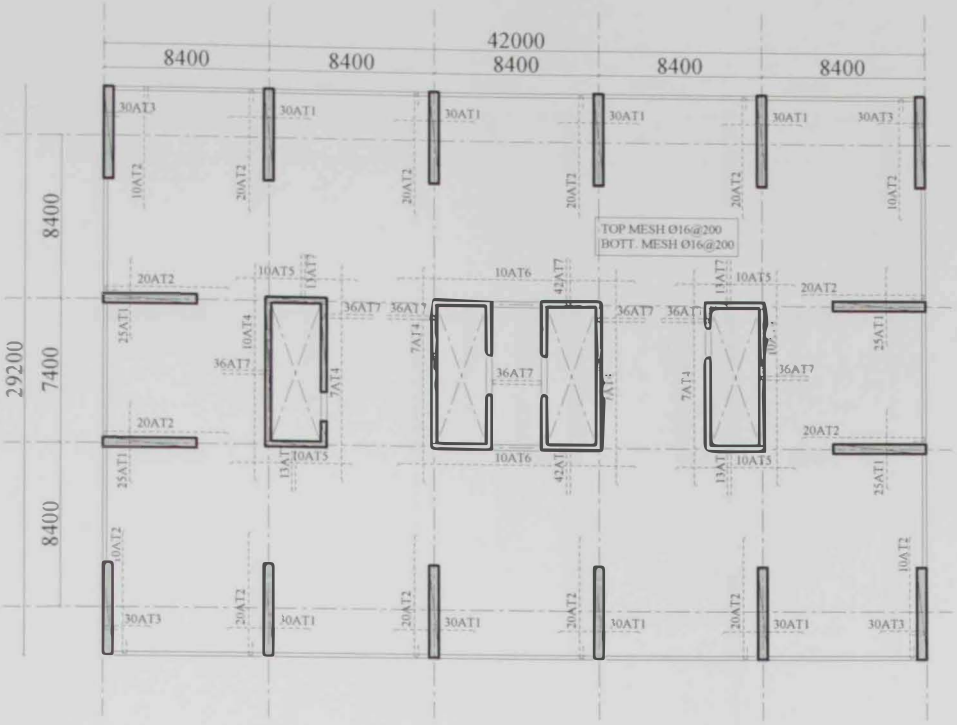

Figure 3.14: Slab reinforcement details of B1-REG and B2-SST at all levels, and B3-GEO, B4-DIS and B5-WST at typical story levels

Table 3.6: Slabs additional top reinforcement of B1-REG and B2-SST at all levels, and B3-GEO, B4-DIS and B5-WST at typical story levels

BAR MARK	ADDITIONAL TOP REBARS FOR FLOORS FROM BASE TO 19 TH	ADDITIONAL TOP REBARS FOR FLOORS FROM 20 TO ROOF	SHAPE
AT1	T20@200	T16@200	
AT2	T20@200	T16@200	
AT3	T20@200	T16@200	
AT4	T25@200	T20@200	
AT5	T25@200	T20@200	
AT6	T25@200	T20@200	
AT7	T25@200	T20@200	

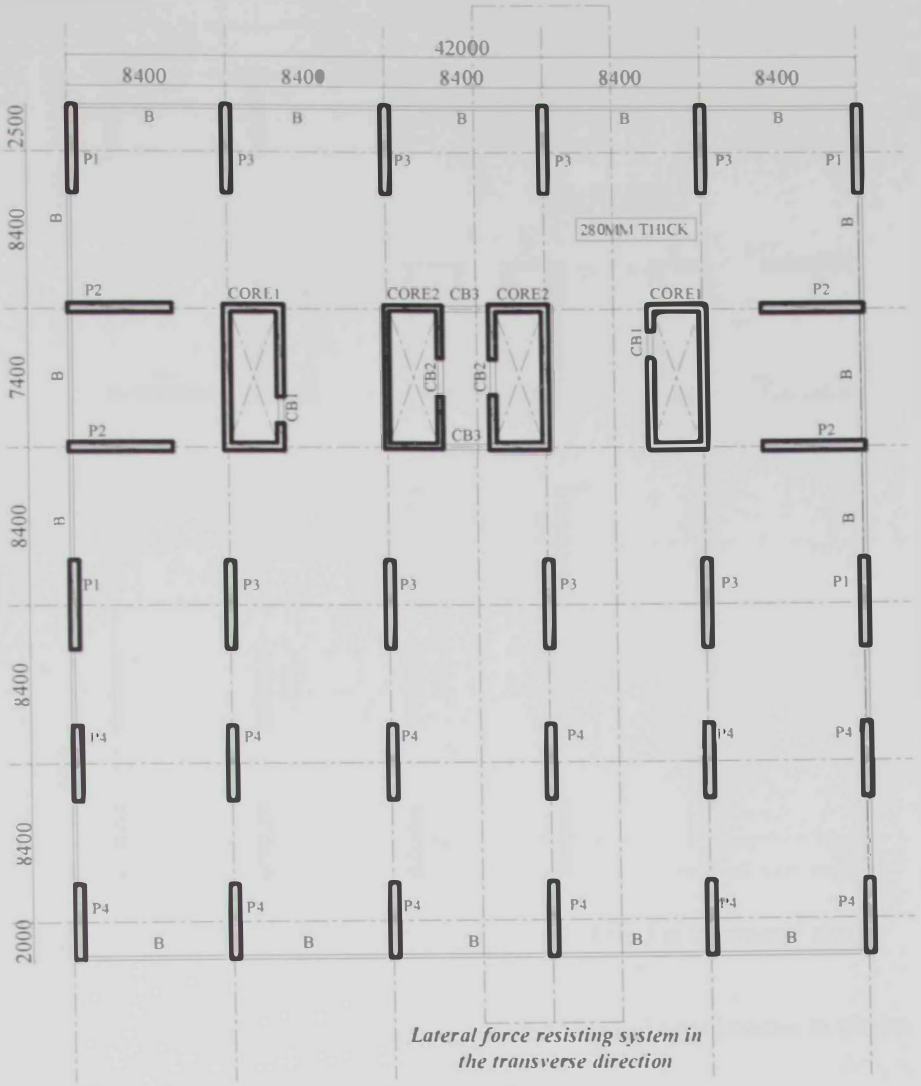

Figure 3.15: Structural elements of B3-GEO at basement stories

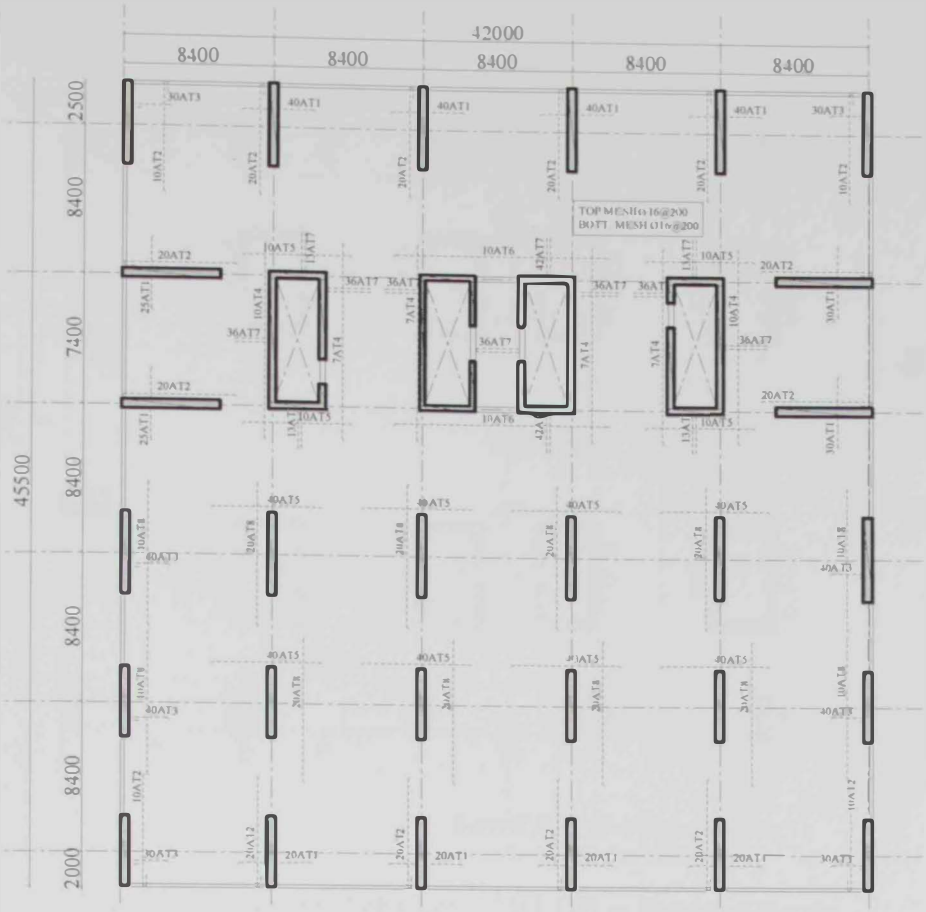

Figure 3.16: Slabs reinforcement details of B3-GEO at basement stories

Table 3.7: Slab additional top reinforcement of B3-GEO at basement stories

BAR MARK	ADDITIONAL TOP REBARS	SHAPE
AT1	T20@200	4000
AT2	T20@200	6200, 600, 200
AT3	T20@200	2200, 600, 200
AT4	T25@200	11000
AT5	T25@200	6000
AT6	T25@200	12000
AT7	T25@200	2400, 2400, 200
AT8	T25@200	8000

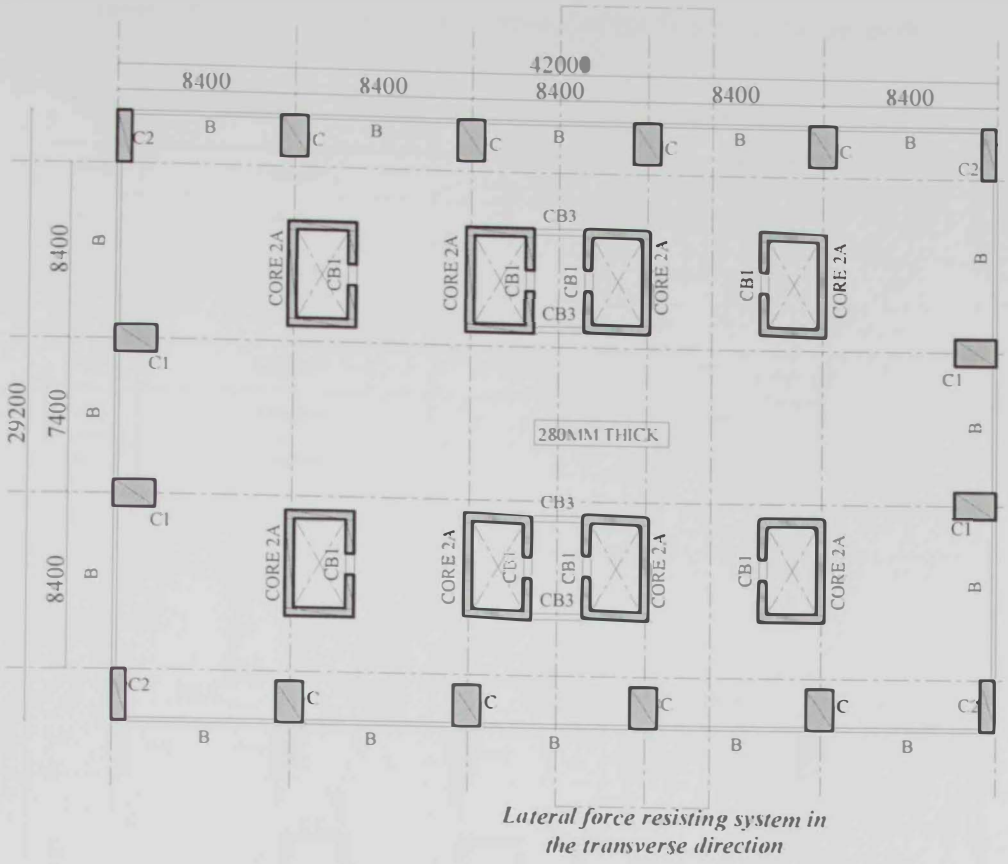

Figure 3.17: Structural elements of B4-DIS at basement stories

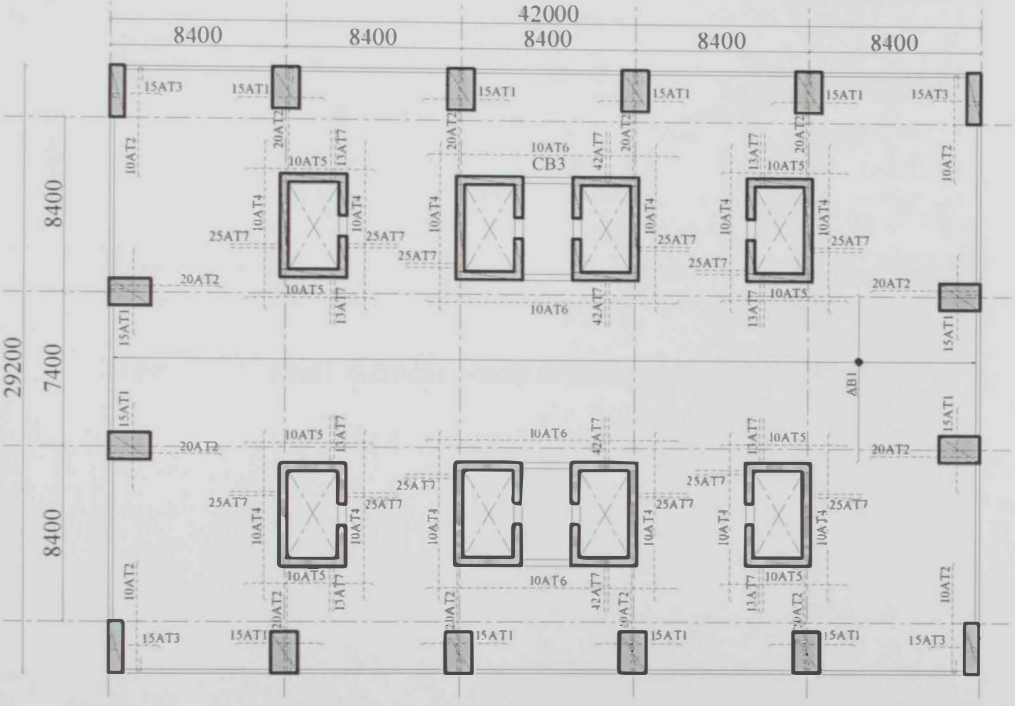

Figure 3.18: Slabs reinforcement details of B4-DIS at basement stories

Table 3.8: Slab additional reinforcement of B4-DIS at basement stories

BAR MARK	ADDITIONAL TOP REBARS	SHAPE
AT1	T20@200	
AT2	T20@200	
AT3	T20@200	
AT4	T25@200	
AT5	T25@200	
AT6	T25@200	
AT7	T25@200	
AB1	T20@200	

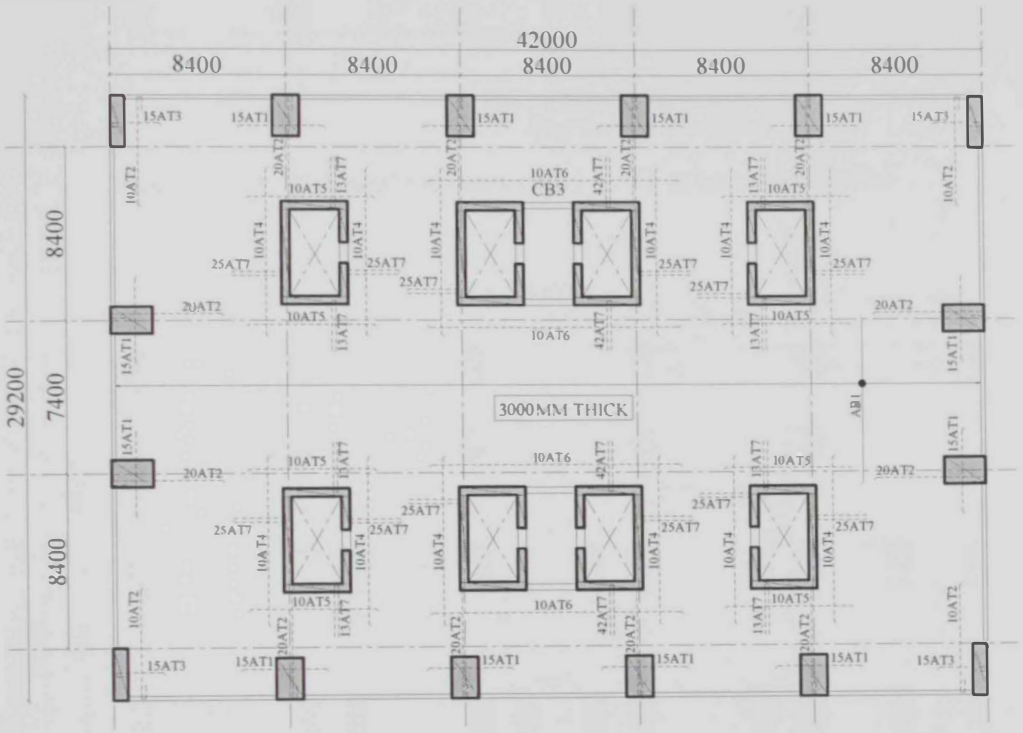

Figure 3.19: Reinforcement details of the transfer slab of B4-DIS

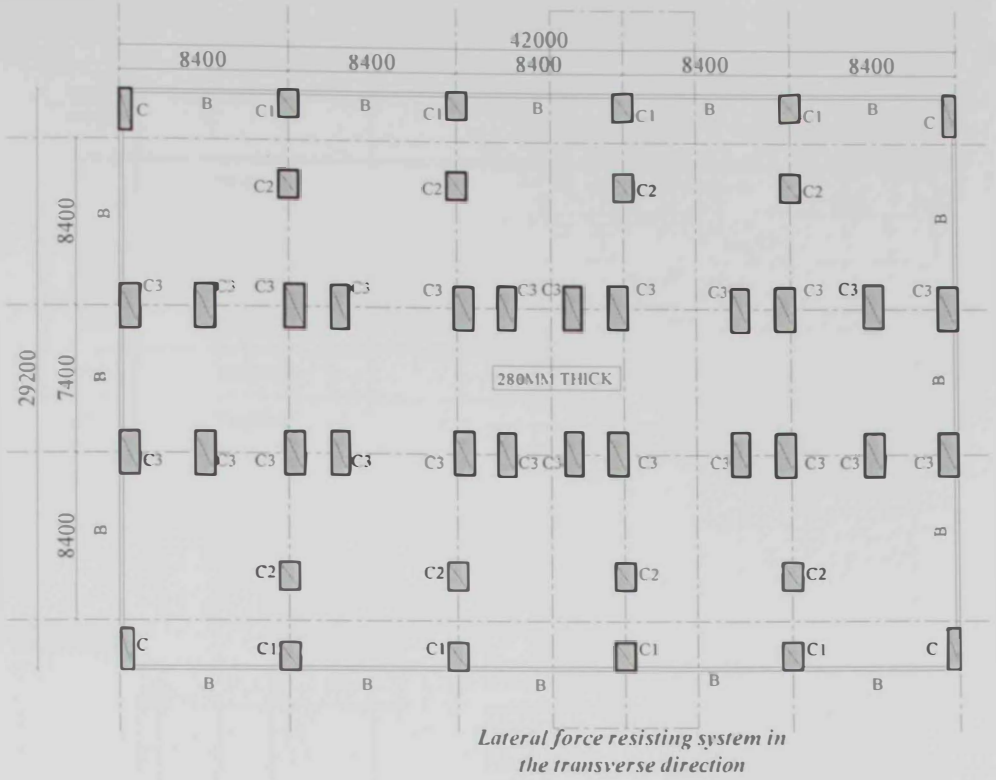

Figure 3.20: Structural elements of B5-WST at basement stories

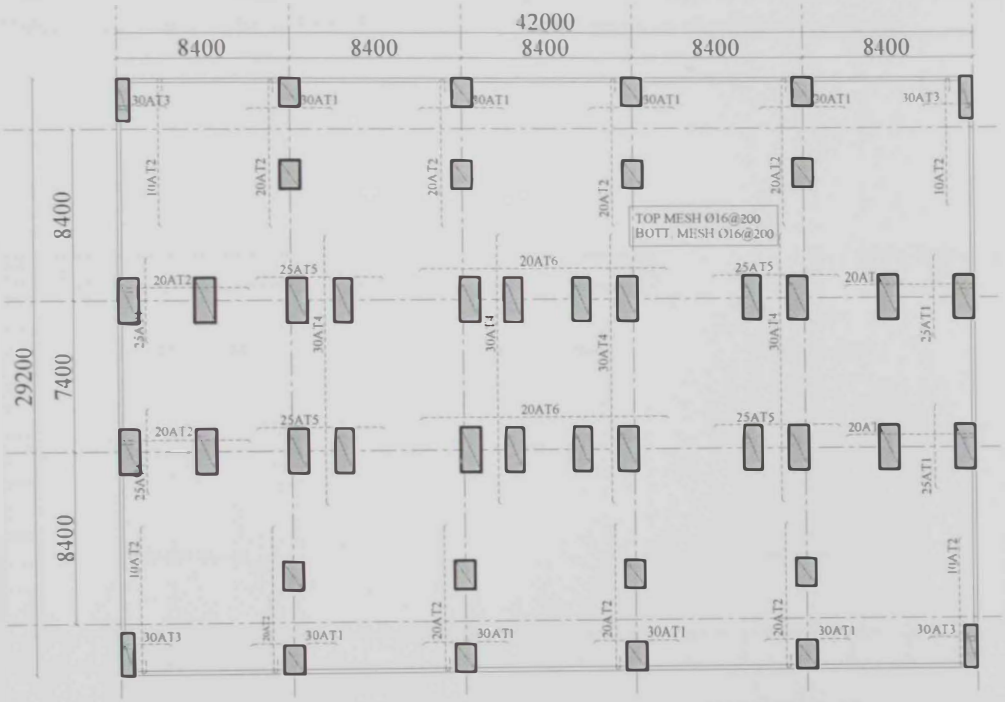

Figure 3.21: Slab reinforcement details of B5-WST at basement stories

Table 3.9: Slab additional top reinforcement of B5-WST at basement stories

BAR MARK	ADDITIONAL TOP	SHAPE
AT1	T20@200	
AT2	T20@200	
AT3	T20@200	
AT4	T25@200	
AT5	T25@200	
AT6	T25@200	

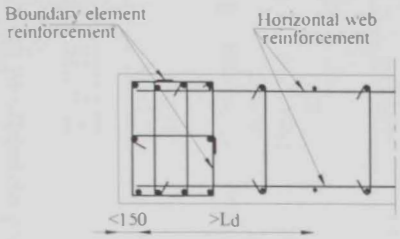

Figure 3.22: Boundary element for special shear wall (ACI-318, 2011)

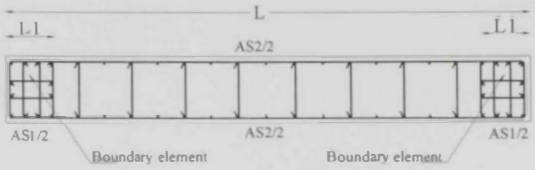

Figure 3.23: Typical reinforcement details used in the design of walls

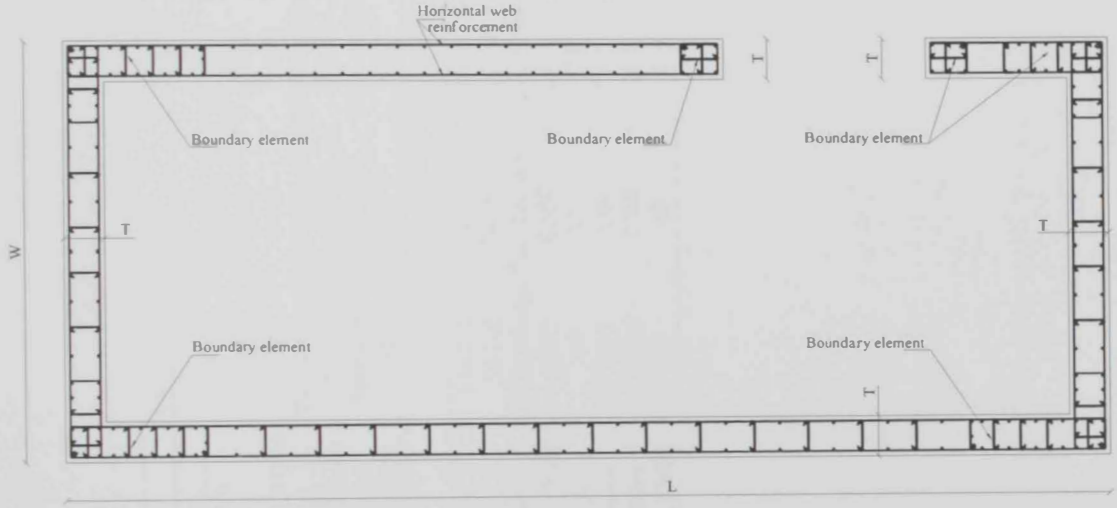

Figure 3.24: Typical reinforcement detail of core walls

Table 3.10: Design results for the vertical structural members of building B1-REG

Location of section	Base	Story no.1	Story no 6	Story no 11	Story no.16	Story no 21	Story no 26	Story no.31	Story no.36	Story no.41
Shear wall P3										
VL. Reinforcement (AS1+AS2)*	36T40+ 44T40	36T40+ 40T40	36T40+ 40T40	32T40+ 36T40	32T40+ 36T40	32T40+ 36T32	32T32+ 36T14	32T20+ 36T14	16T16+ 34T16	16T14+ 34T14
Boundary elements length (mm)	1.0m	1.0m	1.0m	1.0m	1.0m	1.0m	1.0m	1.0m	1.0m	1.0m
HL. reinforcement	T12-200mm	T12-200mm	T12-200mm	T12-200mm	T12-200mm	T12-200mm	T12-200mm	T12-200mm	T12-200mm	T12-200mm
Design/Capacity (D/C) Ratio	0.968	0.971	0.973	0.952	0.935	0.926	0.966	0.966	0.681	0.505
Pier section mm x mm	500x4750	450x4750	450x4750	400x4750	400x4750	350x4750	350x4750	300x4750	300x4750	200x4750
Concrete strength (f_c') MPa	48	48	40	40	32	32	32	32	32	32
Core 2										
VL. Reinforcement (AS1+AS2)	146T12+ 96T40	146T12+ 96T40	146T12+ 96T40	146T16+ 96T32	146T16+ 96T32	146T16+ 96T20		146T12+ 50T12		
HL. reinforcement	T12-200mm	T12-200mm	T12-200mm	T12-200mm	T12-200mm	T12-200mm		T12-200mm		
Design/Capacity (D/C) Ratio	0.993	0.987	0.946	0.987	0.981	0.976		0.946		
Core thickness "T" (mm)	300	250	250	200	200	200		200		
Core width "W" (mm)	3200	3200	3200	3200	3200	3200		3200		
Core length "L" (mm)	7700	7700	7700	7700	7700	7700		7700		
Concrete strength (f_c') MPa	48	48	40	40	32	32		32		

* refer to Figure 3.23

Table 3.11: Design results for the vertical structural members of building B2- SST

Location of section	Base	Story no.1	Story no.6	Story no.11	Story no.16	Story no.21	Story no.26	Story no.31	Story no.36	Story no.41
Shear wall P3										
VL. Reinforcement (AS1+AS2)	36T40+ 44T40	36T40+ 40T40	36T40+ 40T40	32T40+ 36T40	32T40+ 36T40	32T40+ 36T32	32T32+ 36T14	32T20+ 36T14	16T16+ 34T16	16T14+ 34T14
Boundary elements length	1.0m	1.0m	1.0m	1.0m	1.0m	1.0m	1.0m	1.0m	1.0m	1.0m
HL. reinforcement	T12-200mm	T12-200mm	T12-200mm	T12-200mm	T12-200mm	T12-200mm	T12-200mm	T12-200mm	T12-200mm	T12-200mm
Design/Capacity (D/C) Ratio	0.972	0.971	0.972	0.951	0.934	0.925	0.966	0.966	0.681	0.505
Pier section mm x mm	500x4750	450x4750	450x4750	400x4750	400x4750	350x4750	350x4750	300x4750	300x4750	200x4750
Concrete strength (f_c') MPa	48	48	40	40	32	32	32	32	32	32
Core 2										
VL. Reinforcement (AS1+AS2)	146T12+ 96T40	146T12+ 96T40	146T12+ 96T40	146T16+ 96T32	146T16+ 96T32	146T16 +96T20		146T12+ 50T12		
HL. reinforcement	T12-200mm	T12-200mm	T12-200mm	T12-200mm	T12-200mm	T12-200mm		T12-200mm		
Design/Capacity (D/C) Ratio	0.993	0.987	0.946	0.987	0.981	0.976		0.946		
Core thickness (mm)	300	250	250	200	200	200		200		
Core width (mm)	3200	3200	3200	3200	3200	3200		3200		
Core length (mm)	7700	7700	7700	7700	7700	7700		7700		
Concrete strength (f_c') MPa	48	48	40	40	32	32		32		

Table 3.12: Design results for the vertical structural members of building B3- GEO

Location of section	Base	Story no.1	Story no.6	Story no.11	Story no.16	Story no.21	Story no.26	Story no.31	Story no.36	Story no.41
				Shear wall P3						
VL. Reinforcement	36T40+	36T40+	36T40+	32T40+	32T40+	32T40+	32T32+	32T20+	16T16+	16T14+
(AS1+AS2)	44T40	40T40	40T40	36T40	36T40	36T32	36T14	36T14	34T16	34T14
Boundary elements length	1.0m	1.0m	1.0m	1.0m	1.0m	1.0m	1.0m	1.0m	1.0m	1.0m
HL. reinforcement	T12-200mm	T12-200mm	T12-200mm	T12-200mm	T12-200mm	T12-200mm	T12-200mm	T12-200mm	T12-200mm	T12-200mm
Design/Capacity (D/C) Ratio	0.971	0.956	0.973	0.973	0.936	0.968	0.965	0.969	0.685	0.493
Pier section mm x mm	500x4750	450x4750	450x4750	400x4750	400x4750	350x4750	350x4750	300x4750	300x4750	250x4750
Concrete strength (f_c') MPa	48	48	40	40	32	32	32	32	32	32
				Core 2						
VL. Reinforcement	146T12+	146T12+	146T12+	146T16+	146T16+	146T16+	146T12+			
(AS1+AS2)	96T40	96T40	96T40	96T32	96T32	96T20	50T12			
HL. reinforcement	T12-200mm	T12-200mm	T12-200mm	T12-200mm	T12-200mm	T12-200mm	T12-200mm			
Design/Capacity (D/C) Ratio	0.981	0.963	0.931	0.975	0.970	0.949	0.937			
Core thickness (mm)	300	250	250	200	200	200	200			
Core width (mm)	3200	3200	3200	3200	3200	3200	3200			
Core length (mm)	7700	7700	7700	7700	7700	7700	7700			
Concrete strength (f_c') MPa	48	48	40	40	32	32	32			
				Shear wall P5						
VL. Reinforcement	24T20+									
(AS1+AS2)	30T12									
Boundary elements length	1.0m									
HL. reinforcement	T12-200mm									
Design/Capacity (D/C) Ratio	0.97									
Pier section mm x mm	300x4000									
Concrete strength (f_c') MPa	48									

Table 3.13: Design results for the vertical structural members of building B4- DIS

Location of section	Base	Story no.1	Story no.6	Story no.11	Story no.16	Story no.21	Story no.26	Story no.31	Story no.36	Story no.41
					Shear wall P3					
VL. Reinforcement (AS1+AS2)		56T25+ 36T12	52T32+ 36T12	52T25+ 36T12	40T16+ 36T12	36T25+ 36T12	40T14+ 36T12	32T12+ 36T12	28T12+ 36T12	50T14
Boundary elements length		1.0m	1.0m	1.0m	1.0m	1.0m	1.0m	1.0m	1.0m	1.0m
HL. reinforcement		T12-200mm	T12-200mm	T12-200mm	T12-200mm	T12-200mm	T12-200mm	T12-200mm	T12-200mm	T12-200mm
Design/Capacity (D/C) Ratio		0.952	0.919	0.909	0.907	0.962	0.908	0.778	0.702	0.621
Pier section mm x mm		700x4750	650x4750	600x4750	550x4750	500x4750	450x4750	400x4750	300x4750	250x4750
Concrete strength (f_c') MPa		48	40	40	40	32	32	32	32	32
					Core 2					
VL. Reinforcement		194T40+ 176T40	144T12+ 136T32	144T12+ 136T16	144T12+ 124T14	144T12+ 124T12	148T12+ 124T12	202T12	202T12	202T12
HL. reinforcement		T12-200mm	T12-200mm	T12-200mm	T12-200mm	T12-200mm	T12-200mm	T12-200mm	T12-200mm	T12-200mm
Design/Capacity (D/C) Ratio		0.630	0.880	0.850	0.817	0.858	0.822	0.836	0.635	0.407
Core thickness (mm)		400	350	350	300	300	250	200	200	200
Core width (mm)		3200	3200	3200	3200	3200	3200	3200	3200	3200
Core length (mm)		7700	7700	7700	7700	7700	7700	7700	7700	7700
Concrete strength (f_c') MPa		48	40	40	40	32	32	32	32	32
					Core 2A					
VL. Reinforcement (AS1+AS2)	212T32									
HL. reinforcement	T12-200mm									
Design/Capacity (D/C) Ratio	0.89									
Core thickness (mm)	400									
Core width (mm)	3600									
Core length (mm)	5500									
Concrete strength (f_c') MPa	48									
					Column C					
VL. Reinforcement	28T25									
HL. reinforcement	T12-200mm									
Design/Capacity (D/C) Ratio	0.974									
Section width	1300									
Section length	2000									
Concrete strength (f_c') MPa	48									

Table 3.14: Design results for the vertical structural members of building B5-WST

Location of section	Base	Story no 1	Story no 6	Story no.11	Story no 16	Story no 21	Story no 26	Story no.31	Story no.36	Story no 41
Shear wall P3										
VL Reinforcement (AS1+AS2)		56T25+36T12	52T32+36T12	52T25+36T12	40T16+36T12	36T25+36T12	40T14+36T12	32T12+36T12	28T12+36T12	50T14
Boundary elements length		1 0m	1 0m	1 0m	1 0m	1 0m	1 0m	1 0m	1 0m	1 0m
HL. reinforcement		T14-200mm	T12-200mm	T12-200mm	T12-200mm	T12-200mm	T12-200mm	T12-200mm	T12-200mm	T12-200mm
Design/Capacity (D/C) Ratio		0.952	0.919	0.909	0.907	0.962	0.908	0.778	0.702	0 621
Pier section mm x mm		700x4750	650x4750	600x4750	550x4750	500x4750	450x4750	400x4750	300x4750	250x4750
Concrete strength (f_c') MPa		48	40	40	40	32	32	32	32	32
Core 2										
VL. Reinforcement		194T40+176T40	144T12+13632	144T12+136T16	144T12+124T14	144T12+124T12	148T12+124T12	202T12	202T12	202T12
HL. reinforcement		T14-200mm	T12-200mm	T12-200mm	T12-200mm	T12-200mm	T12-200mm	T12-200mm	T12-200mm	T12-200mm
Design/Capacity (D/C) Ratio		0.630	0.880	0.850	0.817	0.858	0.822	0.836	0.635	0.407
Core thickness (mm)		400	350	350	300	300	250	200	200	200
Core width (mm)		3200	3200	3200	3200	3200	3200			
Core length (mm)		7700	7700	7700	7700	7700	7700			
Concrete strength (f_c') MPa		48	40	40	40	32	32	32	32	32
Column C1										
VL. Reinforcement	80T40	72T40								
HL. reinforcement	T12-200mm	T12-200mm								
Design/Capacity (D/C) Ratio	0 882	0 925								
Section width	1000	1000								
Section length	1600	1400								
Concrete strength (f_c') MPa	48	48								
Column C2										
VL. Reinforcement	70T40	62T40								
HL reinforcement	T12-200mm	T12-200mm								
Design/Capacity (D/C) Ratio	0 835	0 834								
Section width	1000	1000								
Section length	1400	1300								
Concrete strength (f_c') MPa	48	48								
Column C3										
VL. Reinforcement	118T40	100T40								
HL reinforcement	T12-200mm	T12-200mm								
Design/Capacity (D/C) Ratio	0.994	0.991								
Section width	1300	1000								
Section length	2200	2200								
Concrete strength (f_c') MPa	48	48								

3.6 Concluding remarks

Based on a concise survey, five RC buildings were selected to represent the common regular and vertically irregular high-rise structures in the UAE. The selected buildings, which were denoted B1-REG, B2-SST, B3-GEO, B4-DIS and B5-WST, represented a regular structure and four irregular high-rise buildings with extreme soft story, geometric irregularity, LFRS in-plane discontinuity, and extreme weak story, respectively. The five reference buildings were fully designed for the purpose of this study using the international building codes adopted in the case study region. Three-dimensional finite element models were developed for the design of the five reference buildings using the finite element computer package ETABS. Gravity, wind and earthquake loads were applied to the 3D building models according to the design codes. The design results were tabulated and presented in this chapter. The design results were utilized to develop the fiber-based analytical models used for inelastic analysis, as discussed in Chapter 4.

Chapter 4: Analytical Modeling for Inelastic Analysis and Selection of Earthquake Records

4.1 Introduction

Structures behave in a nonlinear manner during strong earthquakes. Therefore linear analysis procedures cannot capture the actual structural behavior under the effect of seismic excitations (FEMA-P695, 2009; NEHRP, 2010a). Consequently, the seismic assessment of buildings should be performed using inelastic dynamic time-history analysis (THA). The selection of an inelastic analysis platform and realizing its capabilities and limitations are essential in the seismic assessment of a structure. For the purpose of the current study, the nonlinear platform Zeus-NL is employed to conduct the required inelastic analysis (Elnashai et al., 2012). In this chapter, the modeling approach and capabilities of the inelastic analysis platform along with the selection of the input ground motion are discussed.

4.2 Inelastic analysis platform Zeus-NL

The analytical models of the reference structures are developed using Zeus-NL (Elnashai et al., 2012). Zeus-NL is a nonlinear analysis system employing the fiber modeling approach. It was developed at Imperial College London and at the University of Illinois at Urbana-Champaign. Several verifications of the program were conducted on the member and structure levels. These verifications were undertaken against full scale tests carried out in Europe and the U.S. (e.g. Jeong and Elnashai, 2005; Kwon and Elnashai, 2006).

Jeong and Elnashai (2005) developed a 3D analytical model using Zeus-NL for a three story RC irregular frame building. The layout and configurations of the building are shown in Figure 4.1. An experimental 3D test was conducted for the

same building at the Joint Research Centre, Ispra, Italy. Test results and those obtained from Zeus-NL analysis were compared to verify the analytical model. The study concluded that Zeus-NL accurately predicted the seismic response of the irregular multi-story building. Moreover a shake table test was carried out by Bracci et al. (1992) for a three-story RC frame building using one-third scale model. Nonlinear analysis for the latter building was also conducted using Zeus-NL (Kwon and Elnashai, 2006). Building periods and global deformations from THA were compared with experimental results. The Kwon and Elnashai (2006) study provided additional verification for Zeus-NL. Figure 4.2 shows the plan and sectional elevation of the prototype building used in the studies of Bracci et al. (1992) and Kwon and Elnashai (2006) .

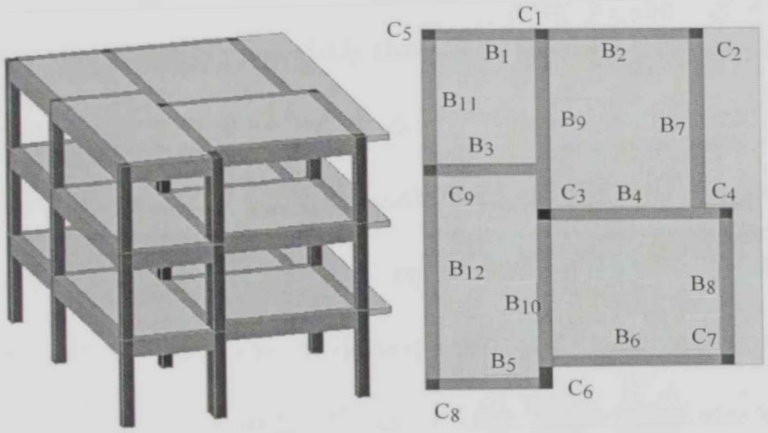

(a) 3D view of the test structure (b) Plan of the test structure

Figure 4.1: Configuration and plan of three-story structure (Jeong and Elnashai, 2005)

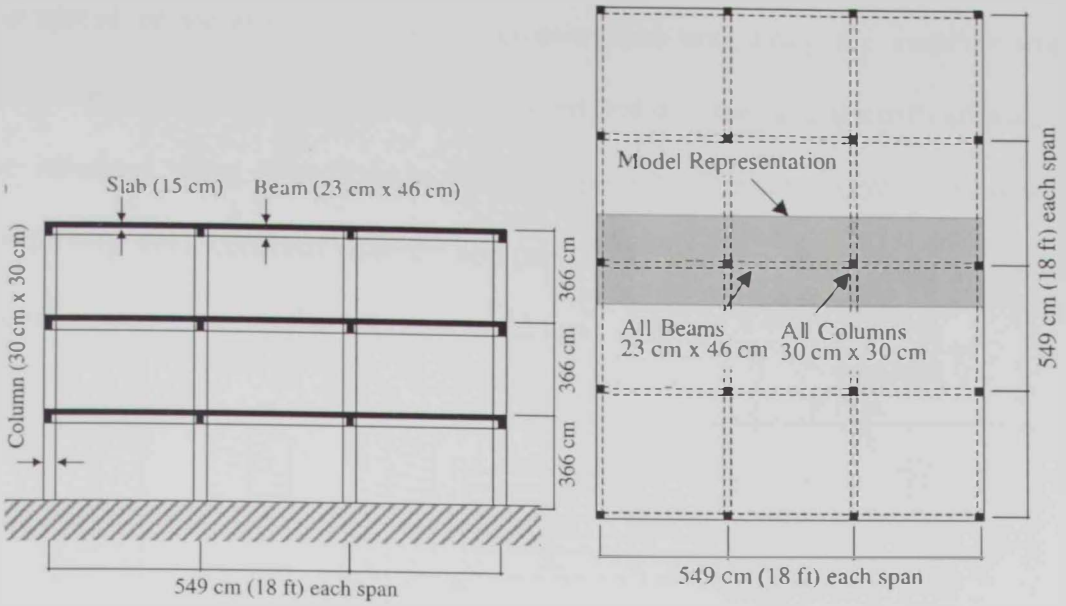

Figure 4.2: Sectional elevation and plan of the prototype structure used for the Zeus-NL verification (Bracci et al., 1992; Kwon and Elnashai, 2006)

4.3 Geometric modeling of reference buildings

It is assumed in the present study that each reference building consists of four lateral force-resisting-systems (LFRSs) in the transverse direction, as shown in Figure 4.3. Two dimensional (2D) simulation models are developed for the five reference buildings using Zeus-NL to represent the LFRSs in the transversal direction. The rigid arm length is the distance between the centerline and the face of the vertical elements, as presented in Figure 4.4 (b). Three cubic elasto-plastic frame elements are used to idealize each horizontal and vertical structural member (slabs, columns, shear walls and core walls). This allows utilizing three different cross-sections for each structural member, one at each member edge and one at the mid-span. These three sections help to accurately model different reinforcement profiles of structural members according to the design. Figure 4.4 (c) shows the Zeus-NL cubic elasto-plastic element, which include two Gauss section, as well as the concrete and reinforcing steel fibers. This modeling approach effectively represents

the spread of inelasticity within the cross-section and along the member length (Elnashai et al., 2012). Reinforcing steel, confined concrete and unconfined concrete are idealized using this fiber modeling approach. The strain-stress response of reinforcing steel, confined concrete and partially confined concrete is used to assess the seismic response of the reference buildings.

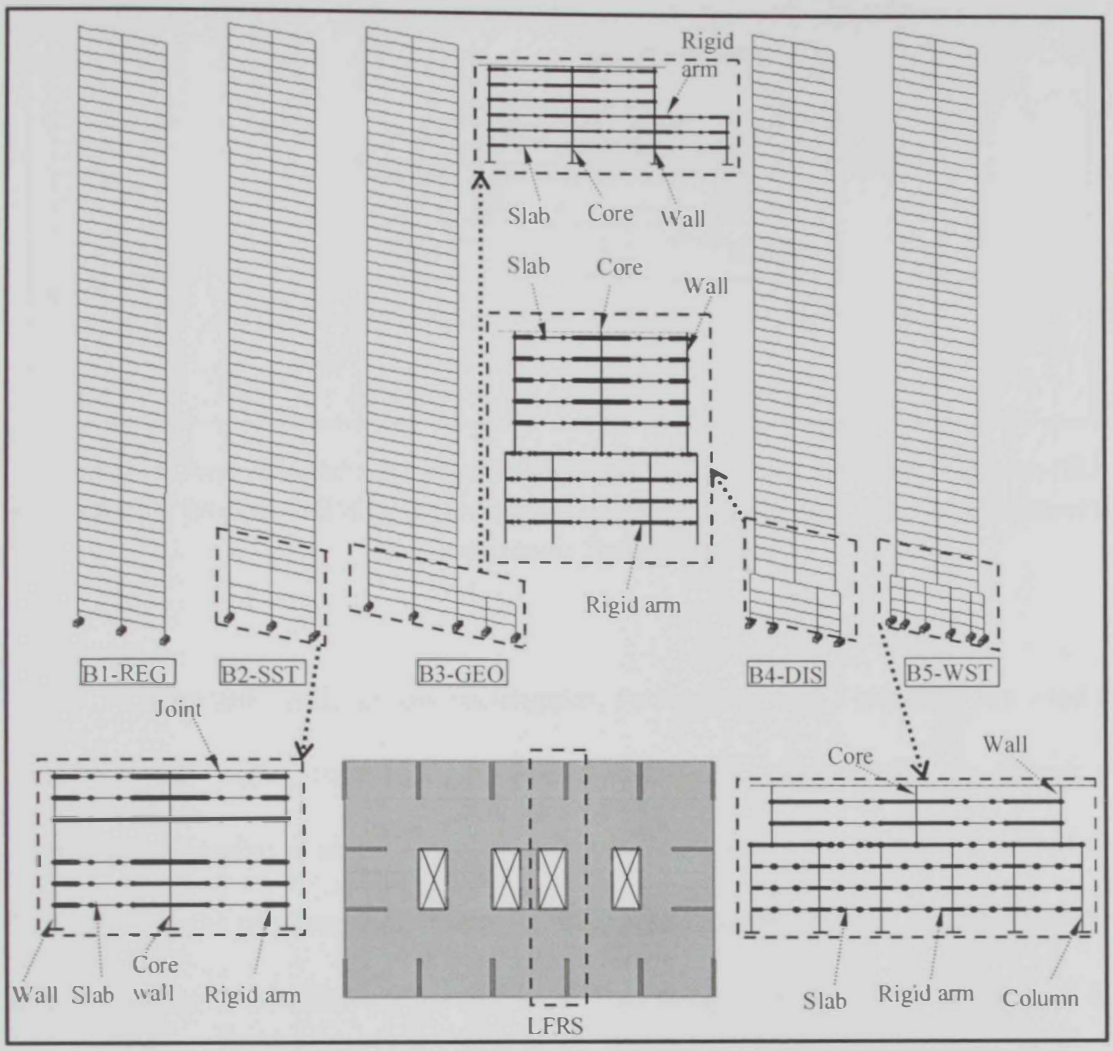

Figure 4.3: Modeling approach for inelastic analysis showing the typical layout of reference buildings with lateral force-resisting systems

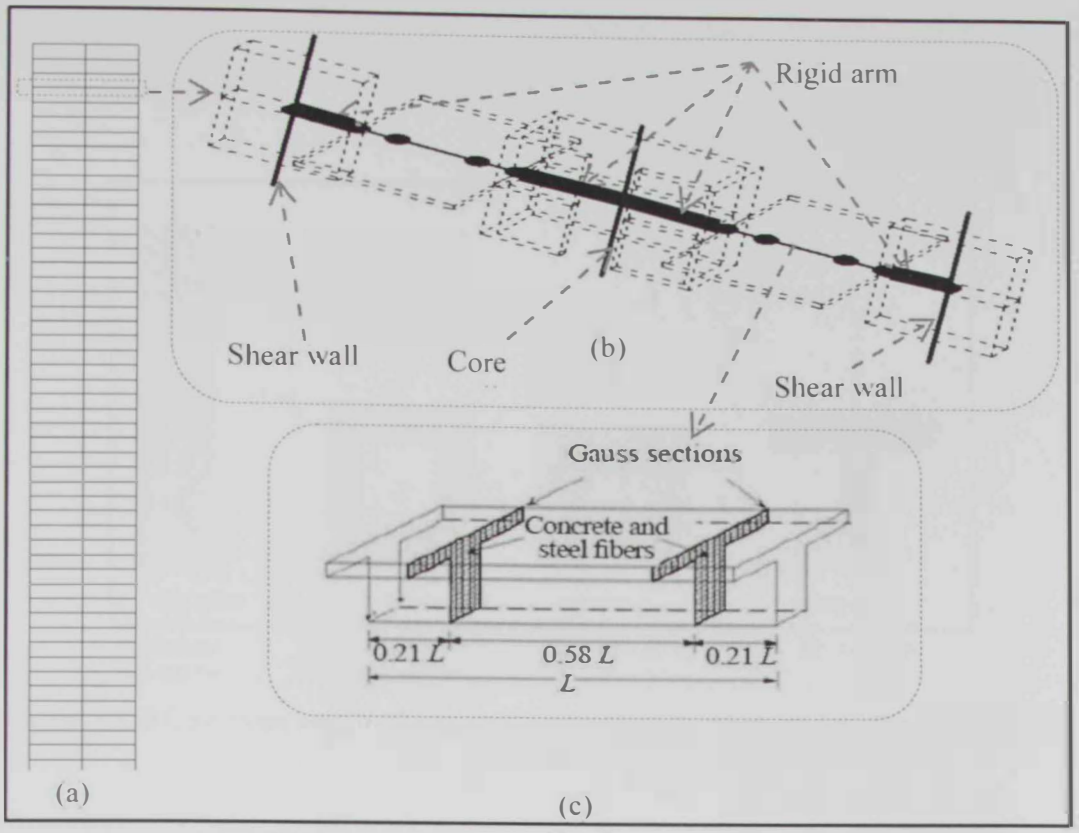

Figure 4.4: Geometric and fiber-based modeling of the reference structures: (a) Zeus-NL model for the B1-REG building (b) Geometric modeling of horizontal and vertical elements (c) Elasto-plastic frame element

RC flexural wall, hollow rectangular, rectangular and T-sections are used to idealize shear walls, core walls, columns and slabs, respectively, as shown in Figure 4.5 (Elnashai et al., 2012). The nonlinear analysis is conducted for one of the four LFRS in the transverse direction. The idealized framing system resists the lateral seismic forces in addition to gravity loads including 25% of the total mass of the building. It is assumed in the present study that the exterior structural system only support gravity load, and hence the seismic lateral forces are entirely resisted by the internal LFRSs. In the longitudinal direction, only one frame resists the seismic lateral loads and the whole building mass, while other structural members only support gravity loads. It is noted that, the transverse direction of the reference buildings is more vulnerable than the longitudinal direction. Therefore the nonlinear

analysis is conducted only for the LFRSs in the transversal direction to save time and computer resources.

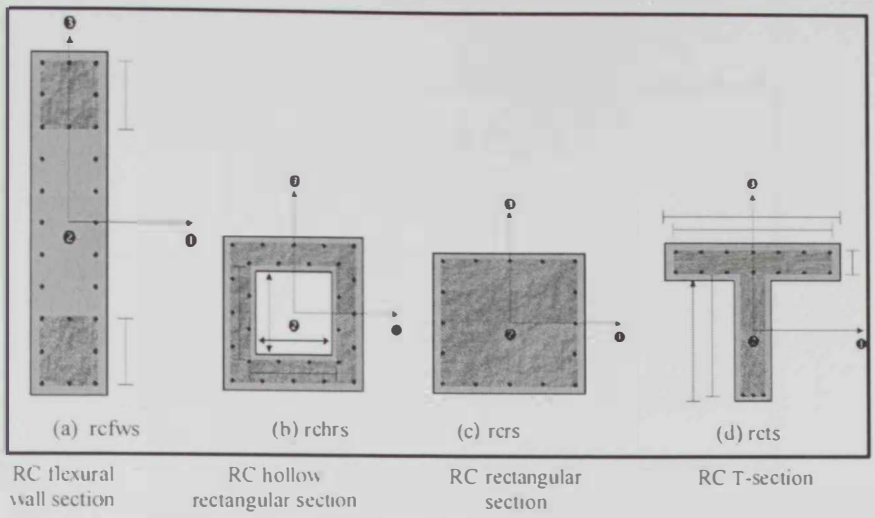

Figure 4.5: RC sections used in the Zeus-NL modeling of reference buildings (Elnashai et al., 2012)

4.4 Material modeling

A uniaxial constant confinement concrete model and a bilinear elasto-plastic reinforcing steel model with kinematic strain-hardening are used in the Zeus-NL models, as shown in Figure 4.6. The actual material strength is used in the current study to assess the seismic response of the reference structures. The concrete confinement is investigated in order to utilize an accurate value for the analysis. Mander et al. (1988) developed a stress-strain model for the confined concrete subjected to uniaxial compressive loading, as shown in Figure 4.7. Madas and Elnashai (1992) concluded that the model is not only simple, but also has adequate accuracy. Martínez-Rueda and Elnashai (1997) developed an enhanced concrete model for confined concrete under cyclic loads based on the Mander et al. (1988) model and implemented in Zeus-NL. This concrete model is adopted in the present study. Fully confined concrete is used in columns and in the boundary elements of

shear walls and core walls. Partially confined concrete is used in the web of shear walls and core walls, while the unconfined concrete is used to model the concrete cover.

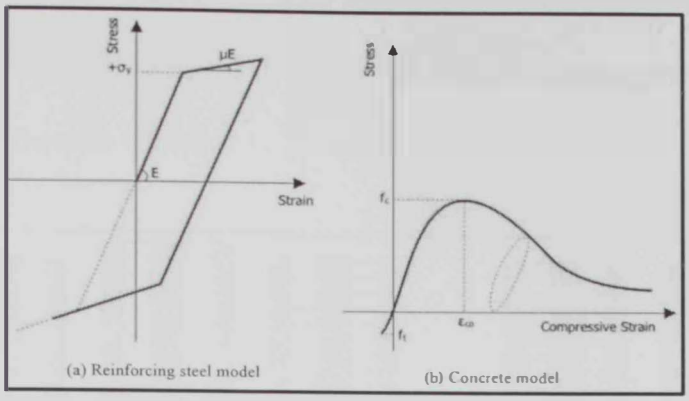

Figure 4.6: Material models (Elnashai et al., 2012)

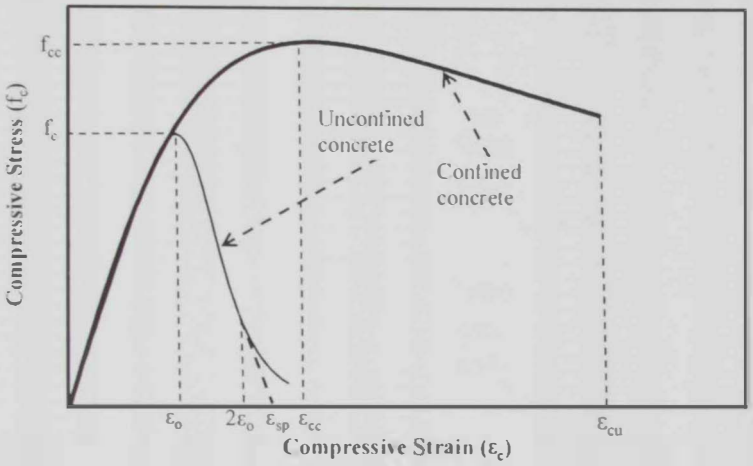

Figure 4.7: Stress-strain model of confined and unconfined concrete developed by Mander et al. (1988)

4.5 Mass and damping modeling

Five analytical models were idealized using the Structural Analysis Program, SAP2000 (CSI, 2011c) to calculate the lamped masses of the reference buildings, as shown in Figure 4.8. Masses calculated from the SAP2000 models are used in the eigenvalue analysis and THA, while gravity loads are used in IPOA and THA. Each LFRS of the reference buildings in the transverse direction is subjected to 25% of the total dead load. Three types of analyses are finally conducted using Zeus-NL. Firstly,

eigenvalue analysis is used to verify the vibration periods and deformed shapes of the reference buildings. Secondly, inelastic static pushover analysis (IPOA) is employed to obtain the capacity curves of the reference buildings. The development of plastic hinges and crushing in concrete are also traced in structural members using IPOA. Lastly, THA is conducted to assess the local and overall seismic performance under a wide range of earthquake records.

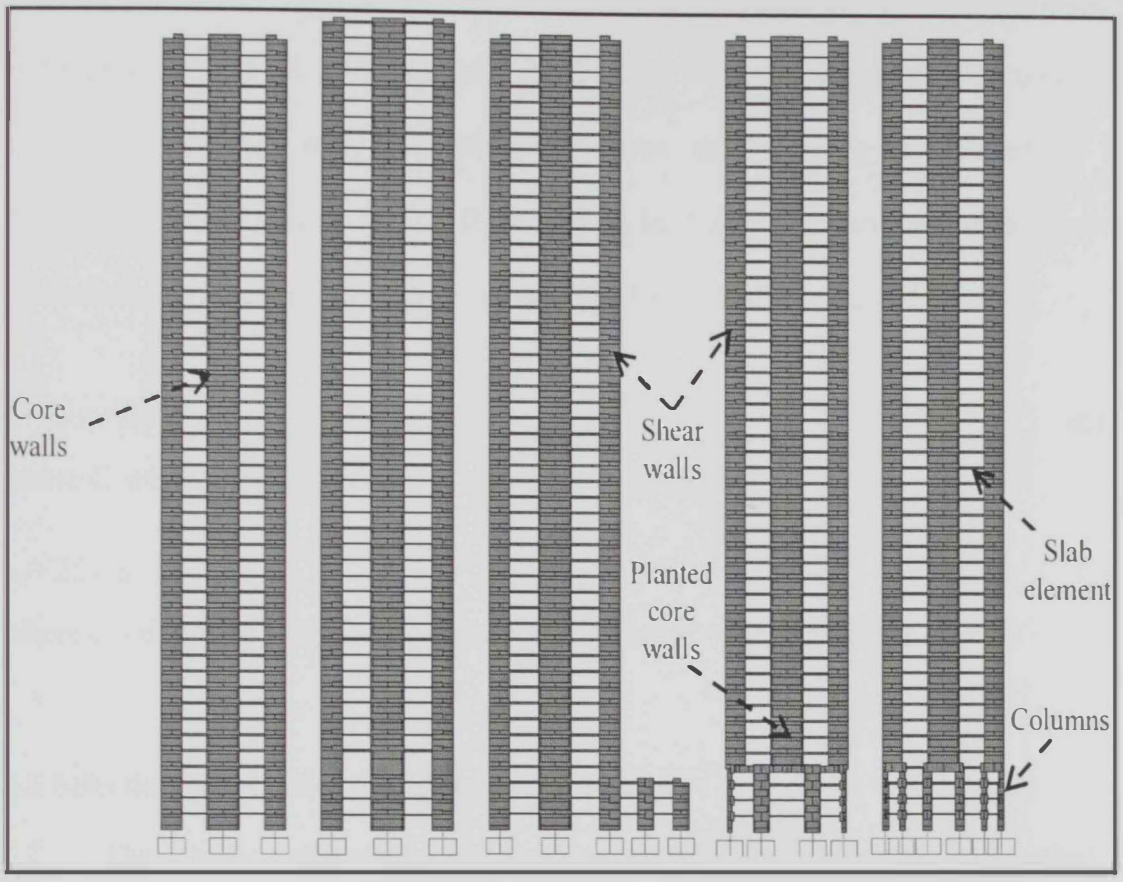

Figure 4.8: Idealized SAP2000 models for the reference buildings for mass calculations

Although the damping is a critical parameter that affects the nonlinear analysis, its precise estimation is hard. Damping could be classified to two categories, hysteretic and non-hysteretic damping. The hysteretic damping sources, such as the inelastic deformations of structural elements under dynamic loading, are included in the elasto-plastic fiber element modeling. The non-hysteretic damping is

caused by many sources such as the internal friction of structural elements and the friction between structural elements and nonstructural components. The latter type of damping is considered by utilizing Rayleigh damping (e.g. Priestley and Grant, 2005; Chopra, 2012; Izzuddin, 2012; Spence and Kareem, 2013). The Rayleigh damping has two components namely the mass proportional and stiffness proportional damping, as shown in Eqn. 4.1 (Chopra, 2012). The mass proportional damping in building assessment gives a spurious damping and it should be neglected (Priestley and Grant, 2005; TBI, 2010; Chopra, 2012). The stiffness proportional damping is calculated for each reference building, where the damping coefficient a_1 is determined using Eqn. 4.2. The frequency ω in Eqn. 4.2 is calculated using the equivalent period of each structure as proposed by (Alwaile et al., 2014).

$$C=a_0 m + a_1 k \quad (4.1)$$

where C is the damping ratio, m is mass, and k is stiffness

$$a_1 = 2\zeta / \omega \quad (4.2)$$

where ζ is damping ratio and ω is circular frequency, which is 2π /period

4.6 Selection and scaling of input ground motions

The selection of input ground motions for the seismic assessment of high-rise buildings is a critical task due to the wide range of vibration periods of significance. Despite the conclusion of few previous studies regarding the marginal effect of magnitude and distance on the dynamic analysis results (e.g. Iervolino and Cornell, 2005), other studies concluded that these seismological parameters affect the dynamic analysis of buildings (e.g. Naeim et al., 2004; Kwon and Elnashai, 2006; Mwafy et al., 2006; Haselton et al., 2012). In the current study, seismological and site parameters, such as record magnitude, epicenteral distance, soil class, ratio of

peak ground acceleration to peak ground velocity (a/v), and peak ground acceleration (PGA) are considered in the selection of earthquake records to represent the common seismic scenarios expected in the case study region.

According to NEHRP (2011), three types of seismic performance assessment of buildings are recommended; intensity-based assessment, scenario-based assessment, and risk-based assessment. The selection of the seismic records depends on the implemented type of assessment. In the current study, a scenario-based assessment is implemented as per the recommendation of several previous studies for the case study region (Sigbjornsson and Elnashai, 2005; Mwafy et al., 2006; Sigbjornsson and Elnashai, 2006; Aldama-Bustos et al., 2009; Shama, 2011). The employed scenarios represent: (i) severe events with a long distance from the epicenter, and (ii) moderate earthquakes with a short distance from the epicenter. For far-field events, a magnitude (M_w) range of 6.93 to 7.64, epicenteral distance range of 91 to 161 km, stiff and very dense soil classes, low a/v ratio (<0·8 g/m s^{-1}), and a PGA range of 0.9 to 2.39 m/s^2 are considered in the record selection, as shown in Table 4.1. Furthermore, for the near-field records, a magnitude (M_w) range of 5.14 to 6.04, epicenteral distance range of 2.86 to 29.9 km, stiff and very dense soil classes, high a/v ratio (>1·2 g/m s^{-1}), and a PGA range of 0.85 to 4.96 m/s^2 are considered in the selection of earthquake records, as shown in Table 4.2.

Two databases are used to select the input ground motions, which are the Pacific Earthquake Engineering Research center database (PEER, 2012) and the internet site for European Strong-motion Database (ESD, 2012). From the selected databases, 20 far-field and 20 near-field natural records are selected to represent the earthquake scenarios in the study region. The near-field earthquake records represent

the local seismic events, while the far-field scenario is for the earthquakes originated from long distance sources. The far-field records match the ASCE-7 (2010) response spectrum in the long period range, as shown in Figure 4.9, while the near-field seismic events match the design response spectrum in the short period range, as shown Figure 4.10. Figure 4.11 shows all spectra of near-field and far-field earthquake records.

The above-mentioned two seismic scenarios account for the uncertainty of input ground motions. The selected records are scaled to a design PGA of 0.16g before applying to the reference building models, as per the recommendation of previous studies for 10% probability of exceedance in 50 years (e.g. Mwafy et al., 2006; Sigbjornsson and Elnashai, 2006). Figure 4.12 and Figure 4.13 show the acceleration histories of the scaled far-field records, while Figure 4.14 and Figure 4.15 depict those of near-field records.

Table 4.1: Characteristics of far-field input ground motions

Ref	Earthquake	Station	Comp.	Date	Mag (M_w)	Site class	Ep Dist (km)	Duration (sec)	PGA (m/s^2)	a/v g/ms^{-1}	a/v clas.
RL1	Bucharest	Building res Institute	EW	04-03-1977	7 53	stiff	161	18	1 73	0 60	
RL2	Chi-Chi	CWB 99999 II.A013	EW	20-09-1999	7 62	v dense	135	117	1.36	0 52	
RL3	Loma Prieta	Emeryville	260	18-10-1989	6 93	v dense	96 5	39	2 45	0 57	
RL4	Loma Prieta	Golden Gate Bridge	270	18-10-1989	6 93	v dense	100	38	2 29	0 61	
RL5	Hector Mine	Indio - Coachella Canal	0	16-10-1999	7 13	stiff	99	60	0 90	0 70	
RL6	Izmit	Ambarli-Termik	EW	17-08-1999	7 64	stiff	113	150	1 80	0 60	
RL7	Izmit	Istanbul-Zeytinburnu	NS	17-08-1999	7 64	stiff	96	129 24	1 08	0 77	
RL8	Kocaeli	Bursa Tofas	E	17-08-1999	7 51	stiff	95	139	1 06	0 49	
RL9	Kocaeli	Hava Alani	90	17-08-1999	7 51	v dense	102	106 615	0 92	0 46	
RL10	Loma Prieta	Alameda Naval Air Stn Hanger	270	18-10-1989	6 93	stiff	91	29	2 39	0 73	low
RL11	Loma Prieta	Berkeley LBL	90	18-10-1989	6 93	v dense	98	39	1 15	0 65	
RL12	Loma Prieta	Oakland-Outer Harbor Wharf	0	18-10-1989	6 93	stiff	94	40	2 75	0 67	
RL13	Manjil	Abhar	N57E	20-06-1990	7 42	stiff	91	29 49	1 30	0 62	
RL14	Manjil	Tonekabun	N132	20-06-1990	7 42	v dense	131	40	1 22	0 76	
RL15	Chi-Chi	TAP005	E	20-09-1999	7 62	stiff	156	134	1 34	0 49	
RL16	Chi-Chi	TAP010	E	20-09-1999	7 62	stiff	151	144	1 19	0 50	
RL17	Chi-Chi	TAP021	E	20-09-1999	7 62	stiff	151	125	1 15	0 47	
RL18	Chi-Chi	TAP032	N	20-09-1999	7 62	v dense	144	90	1 13	0 64	
RL19	Chi-Chi	TAP090	E	20-09-1999	7 62	stiff	156	125	1 28	0 41	
RL20	Chi-Chi	TAP095	N	20-09-1999	7 62	stiff	158	123	0.96	0 52	

a/v: PGA/PGV, a/v classification (<0.8 Low & >1.2 high), Vs_{30} of very dense soil = 360-760 m/s, and for stiff soil = 180-360 m/s

Table 4.2: Characteristics of near field input ground motions

Ref	Earthquake	Station	Comp	Date	Mag (M_w)	Site class	Ep Dist (km)	Duration (sec)	PGA (m/s^2)	a/v g/ms^{-1}	a/v class.
RS1	Coyote Lake	San Juan Bautista, 24 polk St	213	8/6/1979	5 74	v. dense	19 7	15	0 991	1 424	
RS2	Livermore-02	Livermore-Morgan Terr Park	355	1/27/1980	5 42	v dense	14 1	14	2 235	2 581	
RS3	Hollister-04	City Hall	271	28/11974	5 14	v dense	9 8	21	1 651	1 480	
RS4	Whittier Narrows-01	Brea Dam (L Abut)	130	10/1/1987	5 99	v dense	24 0	26	1 299	1 460	
RS5	Whittier Narrows-01	LA-Centry City CC North	90	10/1/1987	5 99	stiff	29 9	9 9	0 851	1 788	
RS6	Whittier Narrows-01	LB-Orange Ave	2280	10/1/1987	5 99	stiff	24 5	20	2 111	1 468	
RS7	Northridge-06	Panorama City-Roscoe	90	3/20/1994	5 28	stiff	11 8	30	1 141	1 916	
RS8	Montenegro (aftershock)	Petrovac-Hotel Oliva	Y	4/15/1979	5 80	v dense	24 0	15	0 873	1 426	
RS9	Umbria Ma.	Castelnuovo-Assisi	NE	26/09/1997	6.04	v dense	16 0	12	1 600	1 254	
RS10	Lazio Abr Y	Cassino-Sant Elia	EW	7/5/1984	5 93	v dense	16	11	1 123	1 590	
RS11	Mammoth Lakes-02	Mammoth Lakes H S	344	5/251980	5 69	v dense	3 49	28	4 064	1 957	
RS12	Mammoth Lakes-06	Fish & Game (FIS)	0	5/271980	5 94	stiff	12 02	7 2	3 979	2 753	high
RS13	Coalinga-04	Anticline Ridge Free-Field	270	7/9/1983	5 18	v dense	6 34	45	3 220	2 048	
RS14	Coalinga-04	Anticline Ridge Pad	270	7/9/1983	5 18	v dense	6 34	20	3 246	2 350	
RS15	Coalinga-05	Burnett Construction	360	7/22/1983	5 77	stiff	12.38	30	2 915	1 988	
RS16	Whittier Narrows-01	Alhambra - Fremont School	180	10/1/1987	5.99	v dense	6 77	21	3 806	1 514	
RS17	Whittier Narrows-01	Garvey Res - Control Bldg	60	10/1/1987	5.99	v dense	2 86	26	3 775	2 432	
RS18	Whittier Narrows-01	LA - 116th St School	360	10/1/1987	5 99	stiff	21 26	38	3 343	1 888	
RS19	Whittier Narrows-01	LA - Obregon Park	360	10/1/1987	5 99	stiff	9 05	25	4 161	1 748	
RS20	Friuli (aftershock)	Bregmj-Fabrika IGLI	Y	15/9/1976	6	v dense	21	30	4 956	2 333	

a/v, PGA/PGV, a/v classification (<0.8 Low & >1 2 high), $V's_{30}$ of very dense soil = 360-760 m/s, and for stiff soil = 180-360 m/s

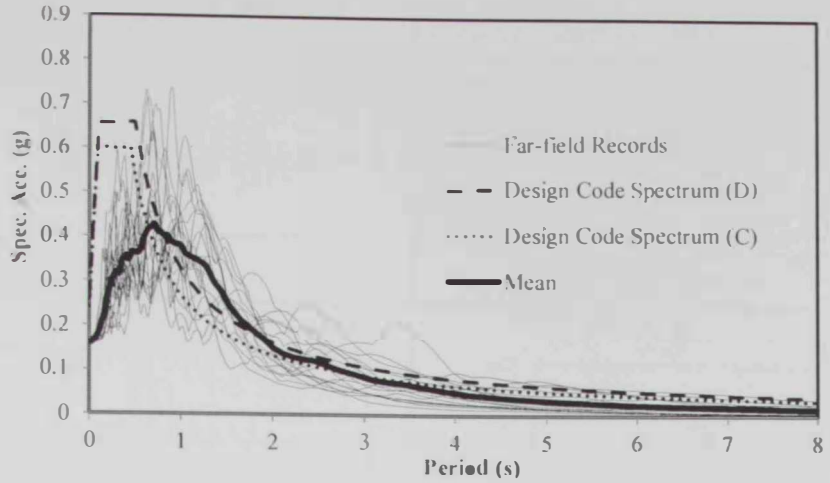

Figure 4.9: Response spectra of 20 far-field earthquake records along with the design response spectra of site class "C" and "D"

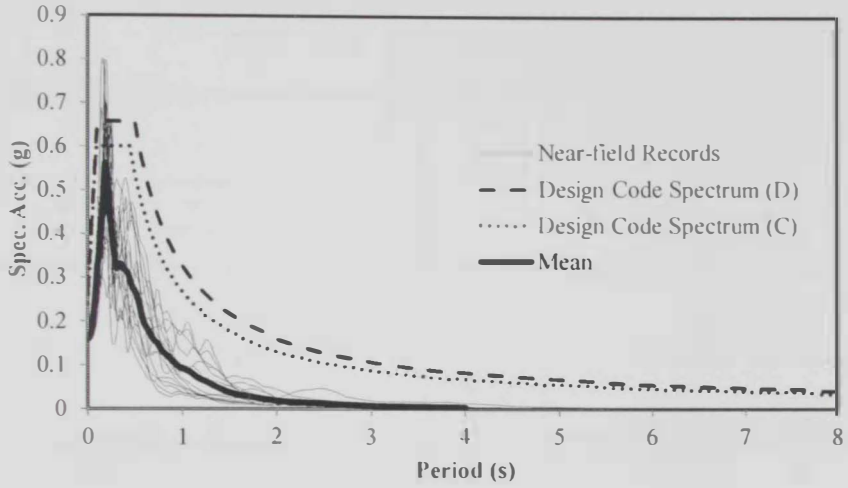

Figure 4.10: Response spectra of 20 near-field earthquake records along with the design response spectra of site class "C" and "D"

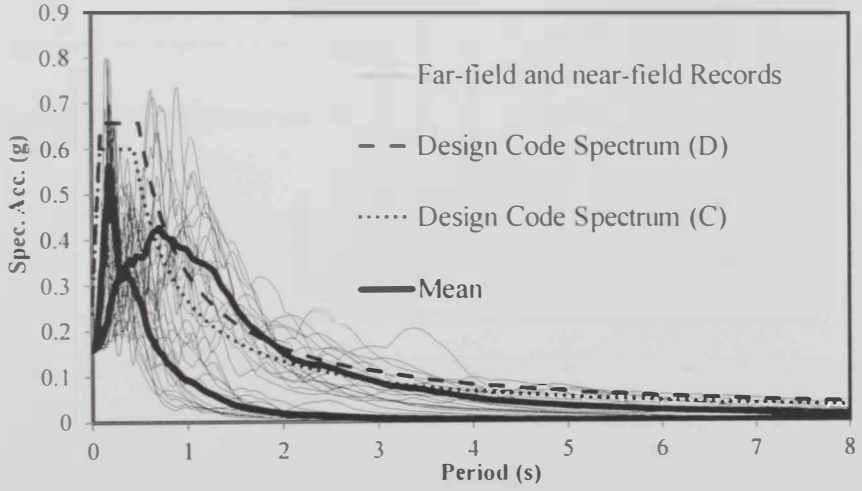

Figure 4.11: Response spectra of 40 earthquake records representing far-field and near-field events along with the design response spectra of site class "C" and "D"

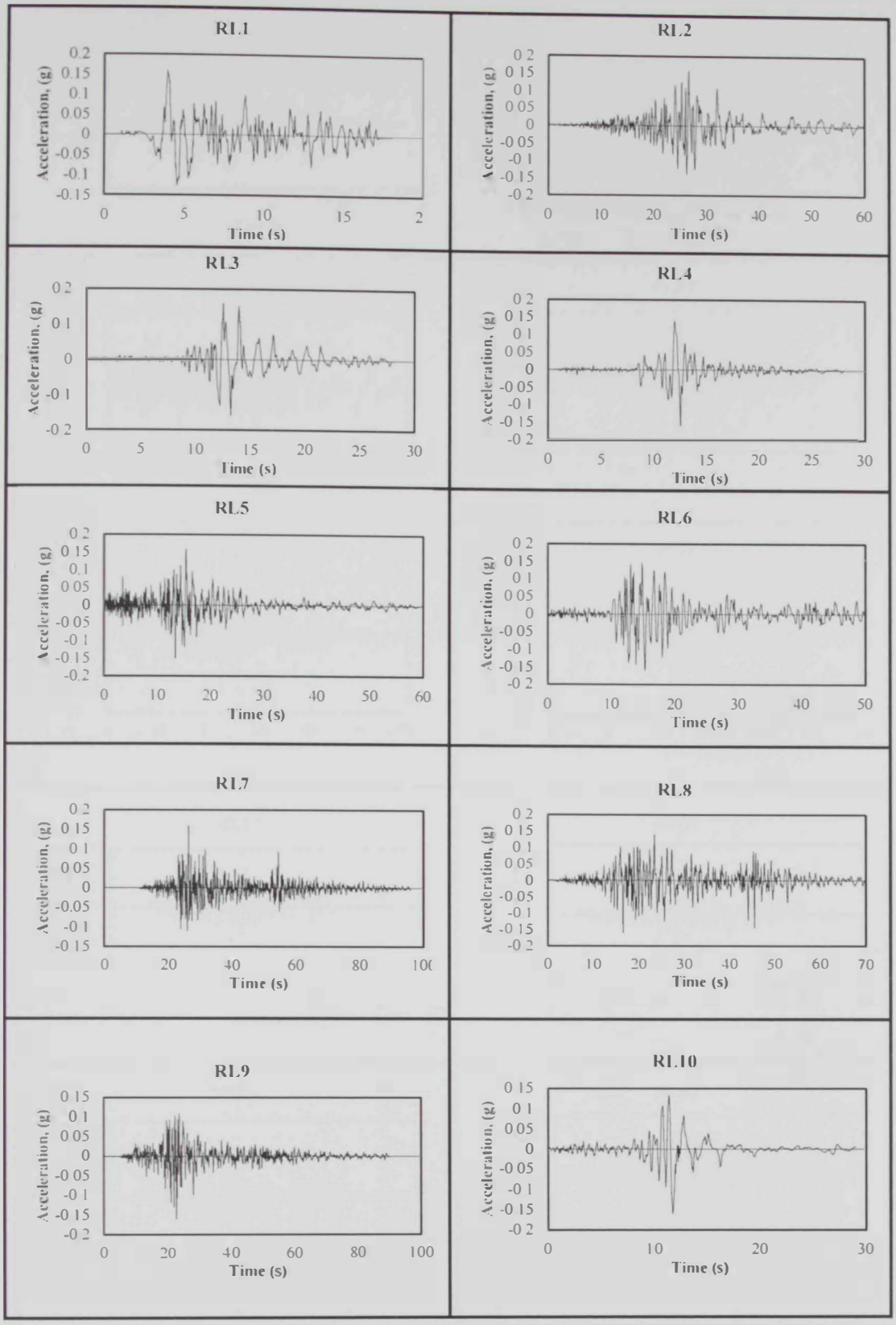

Figure 4.12: Ten selected records representing far-field earthquakes (RL1 to RL10)

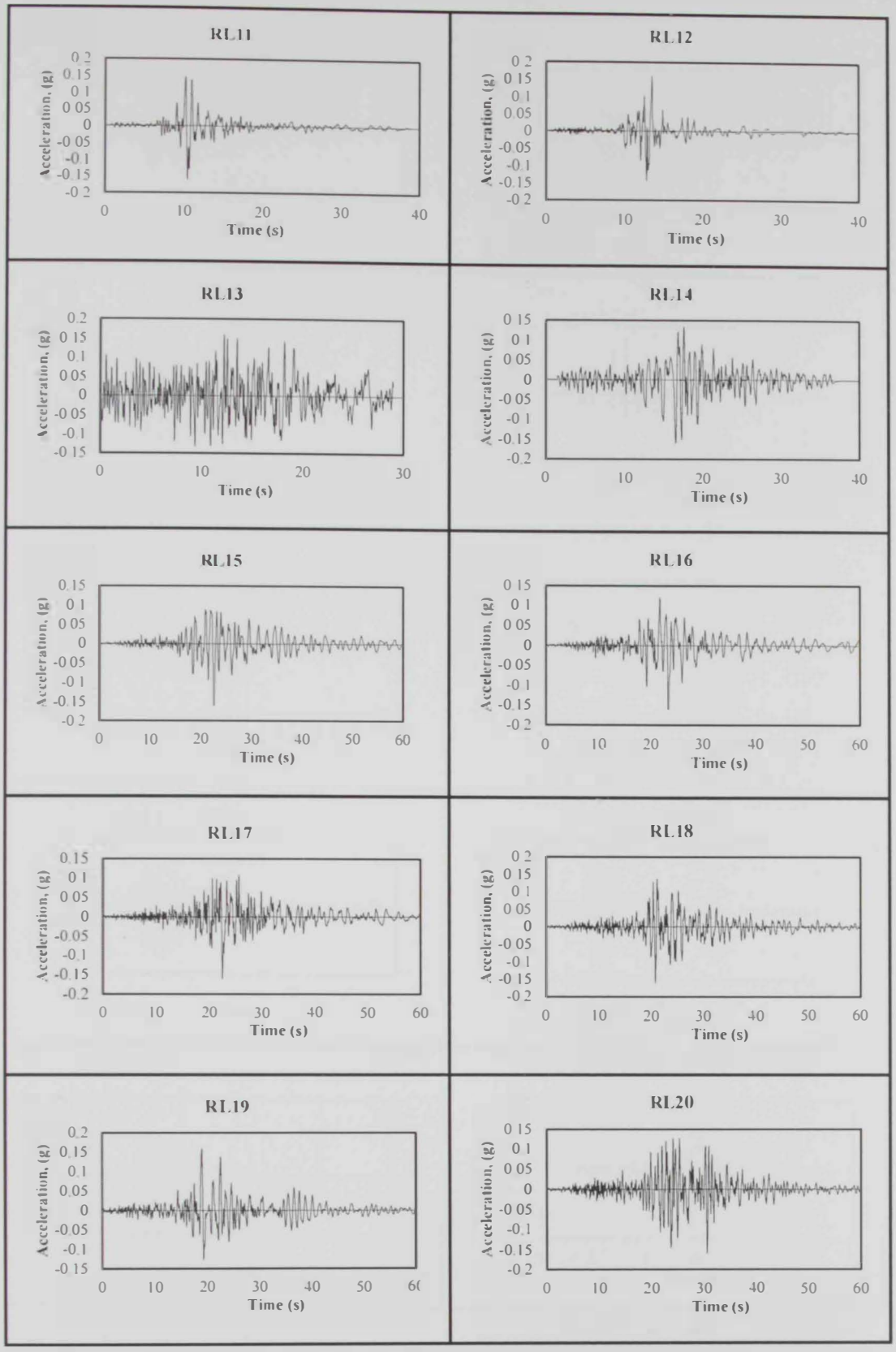

Figure 4.13: Ten selected records representing far-field earthquakes (RL11 to RL20)

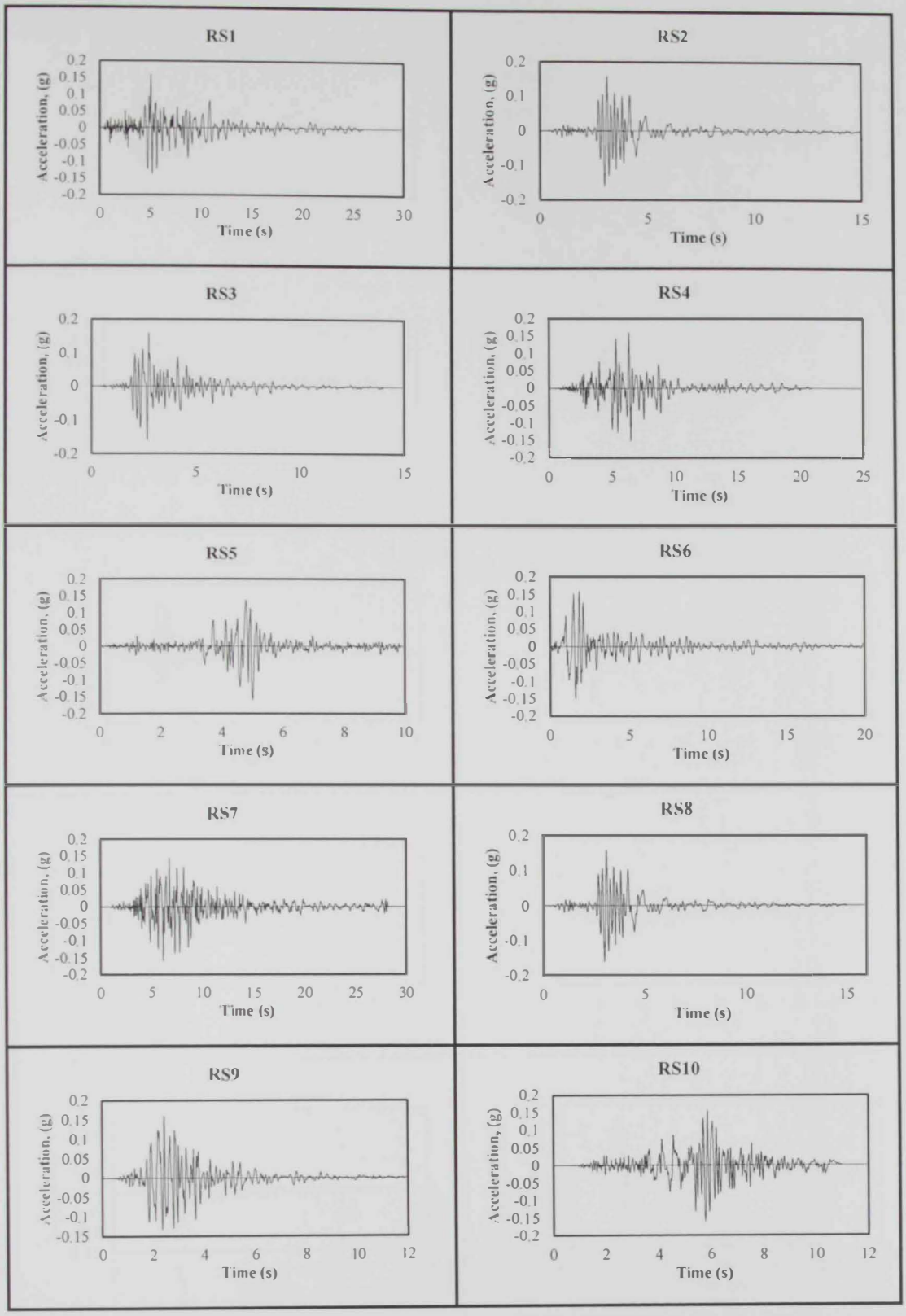

Figure 4.14: Ten selected records representing near-field earthquakes (RS1 to RS10)

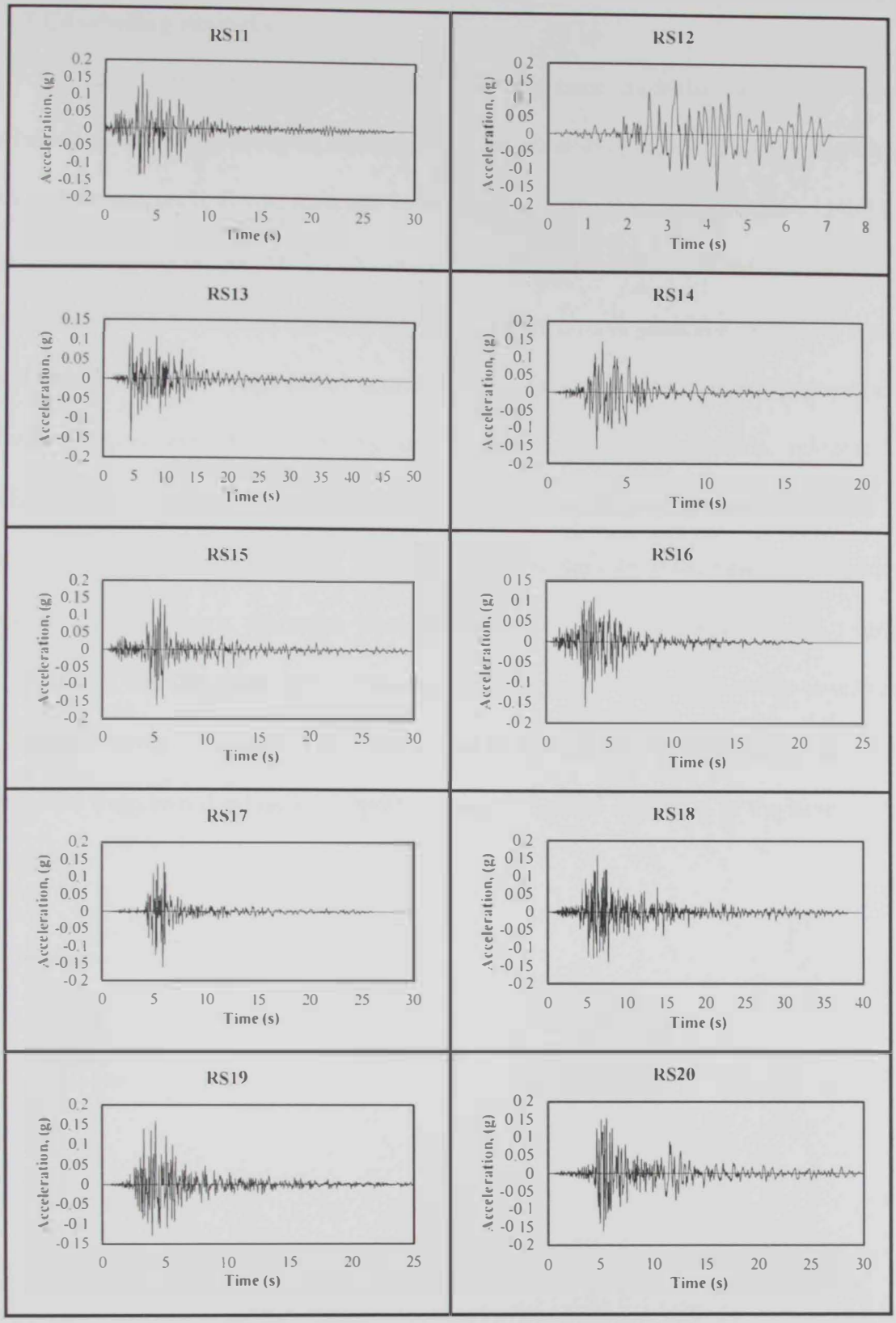

Figure 4.15: Ten selected records representing near-field earthquakes (RS11 to RS20)

4.7 Concluding remarks

The analytical models of the five reference high-rise structures were developed using the inelastic analysis platform Zeus-NL, which employs the fiber modeling approach. It was assumed in the present study that each reference building consists of four comparable LFRSs in the transverse direction. The inelastic analysis was conducted for one of the four LFRS in the transverse direction, which is more vulnerable than the longitudinal counterpart, to save time and computer resources. Seismological and site parameters such as the earthquake magnitude, epicenteral distance, soil class, and peak ground acceleration-to-velocity ratio were considered in the earthquake records selection. To represent the seismicity of the case study region, the following seismic scenarios were accounted for: (i) severe events with a long distance to the epicenter; and (ii) moderate earthquakes with a short site-to-source distance. Twenty far-field and twenty near-field natural earthquake records were selected from two databases to represent the earthquake scenarios in the case study region.

Chapter 5: Model Verifications and Conducted Analyses

5.1 Introduction

In this chapter the details of the conducted analyses to assess the seismic performance of the reference buildings are discussed. The fiber-based modeling verification is also presented. For the purpose of this study, three types of analyses are conducted. Firstly, free vibration analysis (FVA) using the eigenvalue procedure is employed to determine the dynamic characteristic of the reference buildings. This simple analysis is also used to verify the modeling approach, as discussed hereafter. Secondly, inelastic pushover analysis (IPOA) is used to preliminary evaluate the lateral capacity and inelastic response of the reference buildings. The capacity curves are traced and local structural response is monitored during this multi-step analysis. Lastly, incremental dynamic analysis (IDA) is performed using the selected 40 earthquake records in this study to assess the dynamic behavior of the reference structures. The above-mentioned analyses are undertaken using the fiber-based platform Zeus-NL, as discussed in Chapter 4 (Elnashai et al., 2012).

5.2 Free vibration analysis and model verification

When it is oscillated without any external dynamic excitation, the building is under a free vibration state (Chopra, 2012). There are two procedures to identify the dynamic response parameters of structures namely; experimental methods and analytical analyses. The experimental methods such as the forced vibration test are used to assess the dynamic characteristics of existing structures. Several previous studies evaluated this experimental method (e.g. Yu et al., 2005; Shabbir and Omenzetter, 2008). Analytical methods such as the eigenvalue analysis is used to determine the dynamic characteristics of structures (e.g. Li et al., 2000; Chopra,

2012; Heidari et al., 2014). The dynamic characteristics of structures such as natural period, circular frequency, mode shapes and cyclic frequency are determined using the free vibration analysis procedures.

In the current study, the Zeus-NL fiber based models of the five buildings investigated in the current study are employed to conduct FVAs (Elnashai et al., 2012). Lumped masses are only applied to the Zeus-NL models, while gravity and dynamic loads are not needed for this analysis, as discussed in Chapter 4. Mode shapes and periods of vibration are obtained from the eigenvalue analysis results. Figure 5.1 and Figure 5.2 depict the first three mode shapes along with the corresponding periods obtained from Zeus-NL fiber-based models.

It is noted from the results shown in Figures 5.1 and 5.2 that unlike B3-GEO, the fundamental period of the B2-SST, B4-DIS and B5-WST are higher compared with that of the B1-REG building. This is attributed to the reduced stiffness of the lower stories in buildings B2-SST, B4-DIS and B5-WST. On the other hand, the footprint of the lower stories of building B3-GEO is larger than those of the regular structure, and hence the stiffness increases and period decreases.

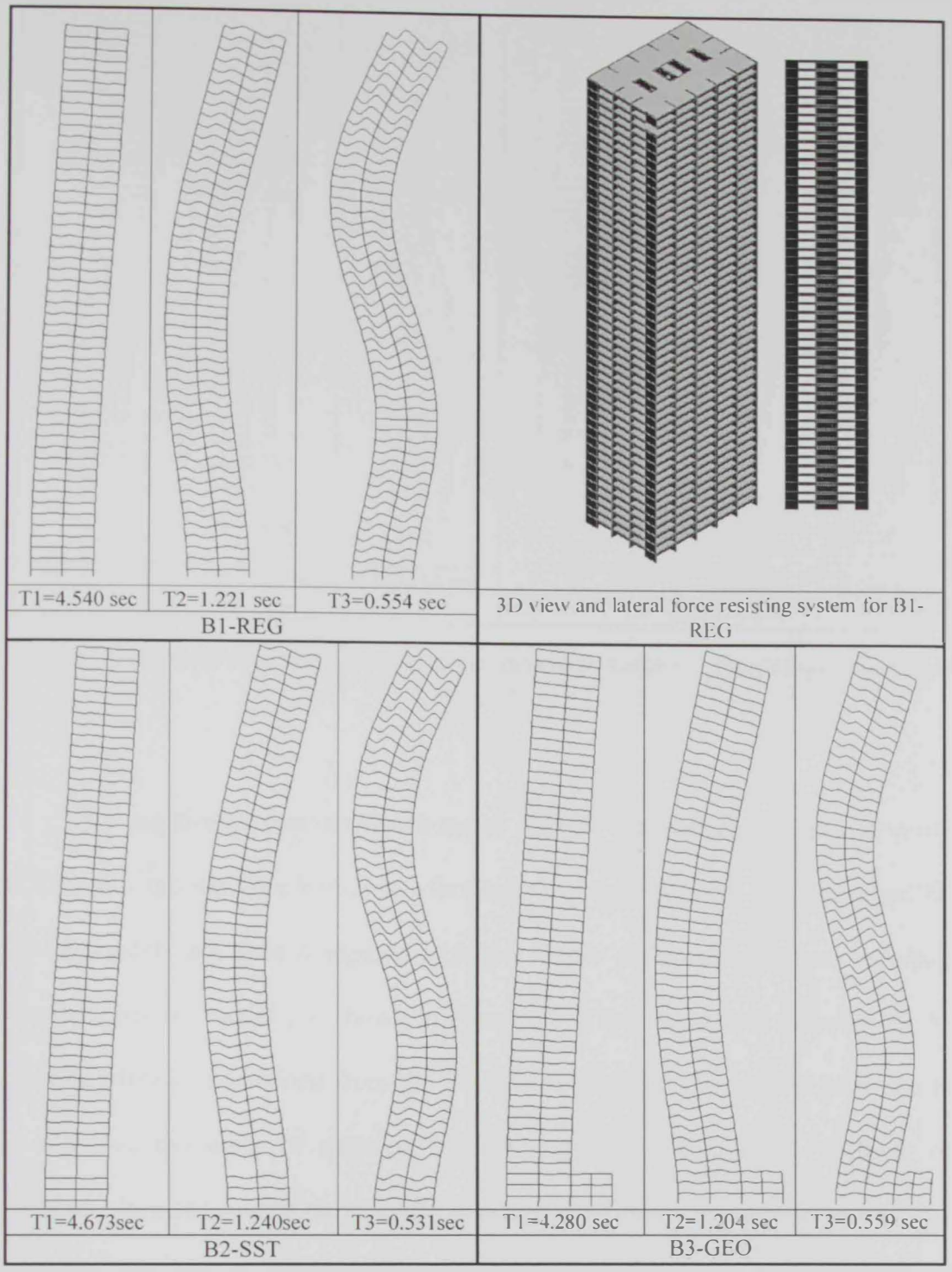

Figure 5.1: First three modes of vibration in the transverse direction of buildings B1-REG, B2-SST and B3-GEO

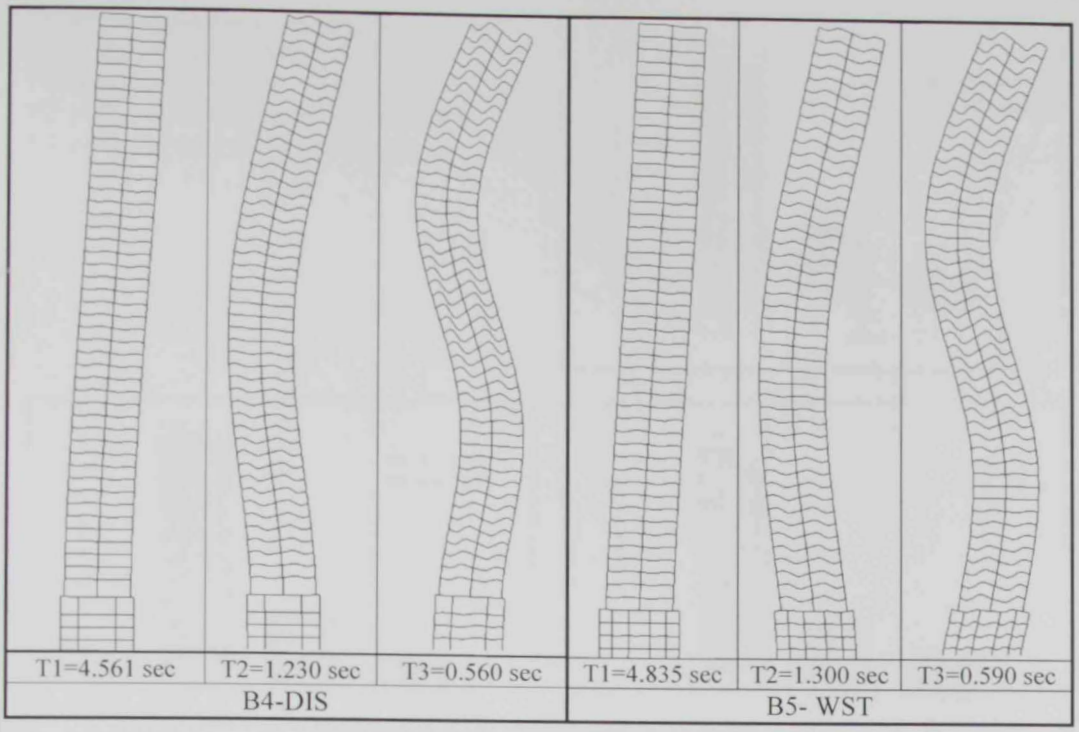

Figure 5.2: First three modes of vibration in the transverse direction of buildings B4-DIS and B5-SST

The eigenvalue analysis is conducted prior to the inelastic analysis to verify the Zeus-NL models. The period of vibrations are obtained from the uncracked 3D ETABS models and then compared with the elastic period of vibrations obtained from the Zeus-NL models, as shown in Figure 5.3. There is a minor reduction in the period of vibrations obtained from the fiber-based models. This reduction is due to the effective modeling of rebar in Zeus-NL, which increases the stiffness of structural elements unlike the ETABS models. The above-mentioned results and discussion lend weight and validate the Zeus-NL models used for the assessment of the seismic response of the reference buildings using IPOA and IDA.

FEM: finite element modelling
FBM: fiber based modelling
T1: period of first mode of vibration
T2: period of second mode of vibration
T3: period of third mode of vibration

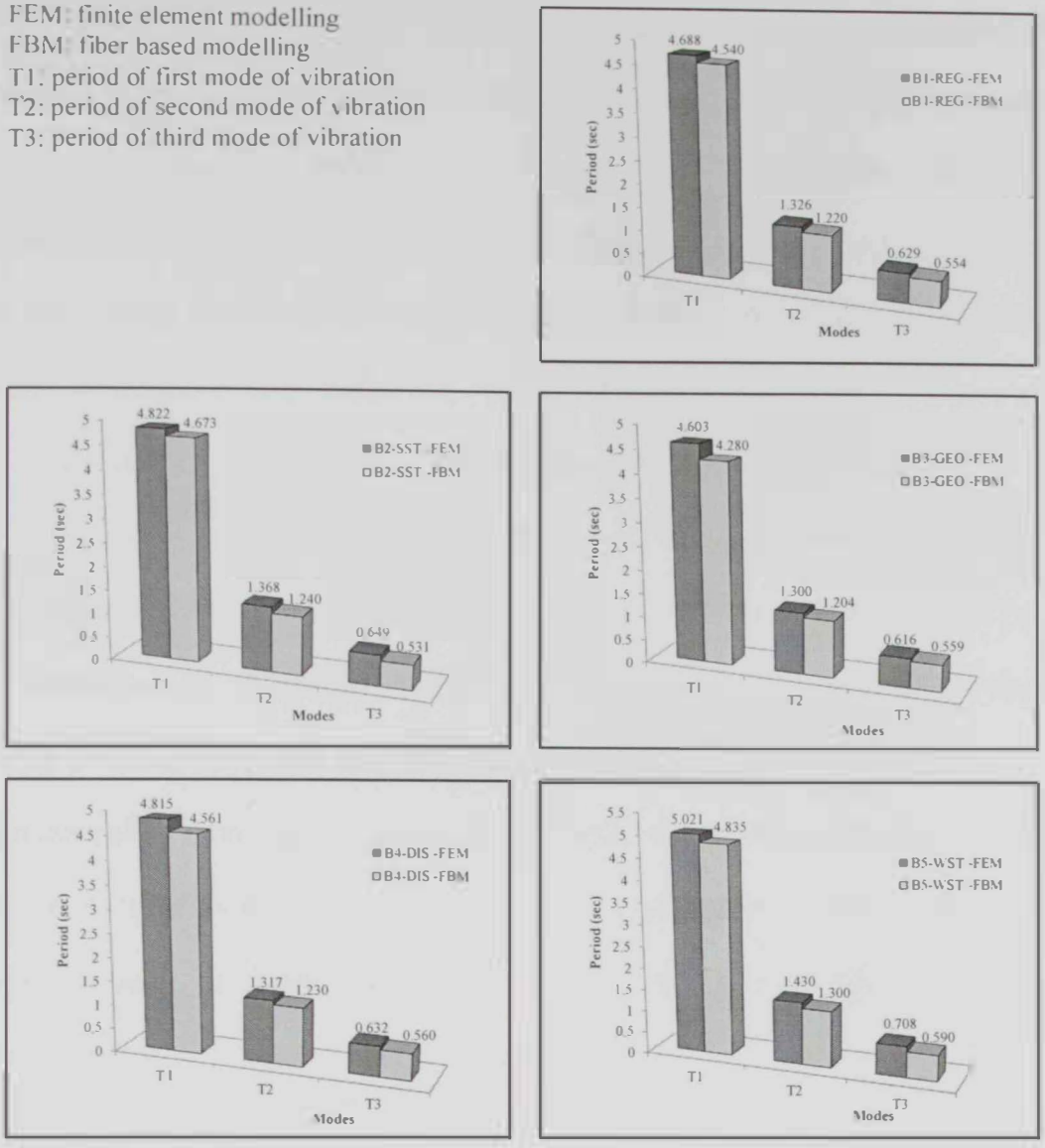

Figure 5.3: Comparison of the first three modes of vibration of the reference buildings obtained from finite element and fiber-based models

5.3 Inelastic pushover analysis

The capacity of structural systems in terms of displacements and forces is usually evaluated using static approaches such as the equivalent static analysis (ESA) and inelastic pushover analysis (IPOA). The ESA is the simplest method, which is used to assess the elastic seismic performance of structures. In this method, the equivalent static lateral forces are used to represent earthquake loads. The obtained results from ESA are approximate since important factors such as damping and stiffness degradation are ignored.

In IPOA, static forces or displacement patterns are applied throughout the structure height and combined with gravity loads. When these patterns are constant during the analysis, it is referred to the conventional IPOA. In the adaptive IPOA, the lateral load patterns change depending on several factors such as the vibration modes and story shear. IPOA was developed and studied during the last three decades by several investigators (e.g. Saiidi and Sozen, 1981; Bracci et al., 1997; Krawinkler and Seneviratna, 1998; Mwafy and Elnashai, 2001; Chopra and Goel, 2002; Chintanapakdee and Chopra, 2003; Kalkan and Kunnath, 2006). Some of the previous studies have not recommend the IPOA for the seismic assessment of high-rise buildings (e.g. TBI, 2010). On the other hand, some previous studies concluded that the IPOA accuracy was not significantly depreciated even for irregular structures (Chintanapakdee and Chopra, 2004). Additionally, other previous studies concluded that the uniform lateral load distribution can be conservatively used to estimate the initial stiffness and lateral capacity of high-rise buildings (Mwafy et al., 2006; Mwafy, 2011).

In the current study, IPOA is deployed to carry out the following (i) estimate the capacity curves of the five reference structures, (ii) determine the inter-story drift and the global response parameters, and (iii) assess the local response of different structural elements. Inverted triangular (PT) and uniform (PU) lateral load distributions are used in the IPOA procedure, as shown in Figure 5.4. The lateral loads are applied throughout the building height and monotonically increased until the ultimate building capacity is reached. The PU load pattern, which represents the mass distribution throughout the building height, is adopted to trace the strain of concrete and reinforcing steel, as shown in Figure 5.5. The inter-story drift is also monitored and mapped with the local response of structural members on the capacity

curves, as shown in Figure 5.5 and Figure 5.6. The IPOA results are discussed in detail in Chapter 6.

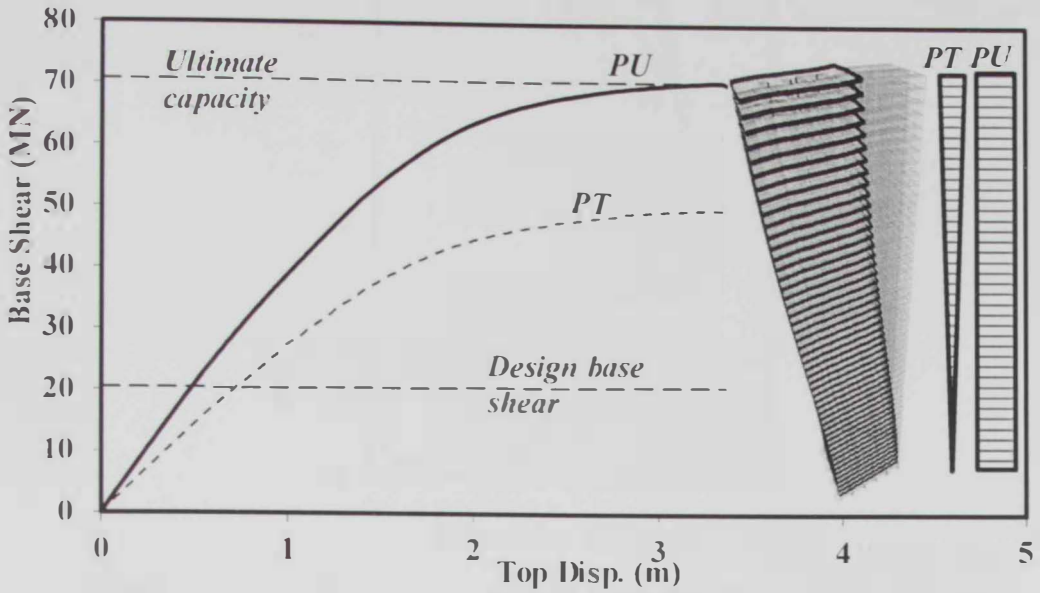

Figure 5.4: Lateral capacity of the B1-REG building in the transverse direction using PU and PT loading scenarios

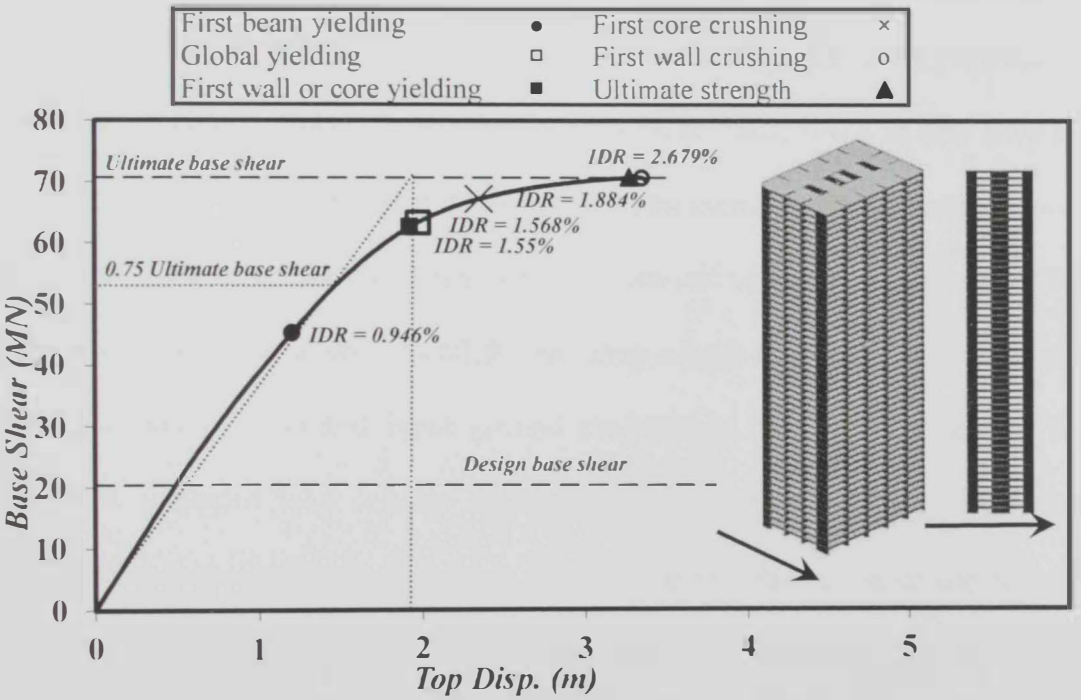

Figure 5.5: Lateral capacity of the B1-REG building in the transverse direction along with the inter-story drift ratios at the first indication of member yielding and crushing

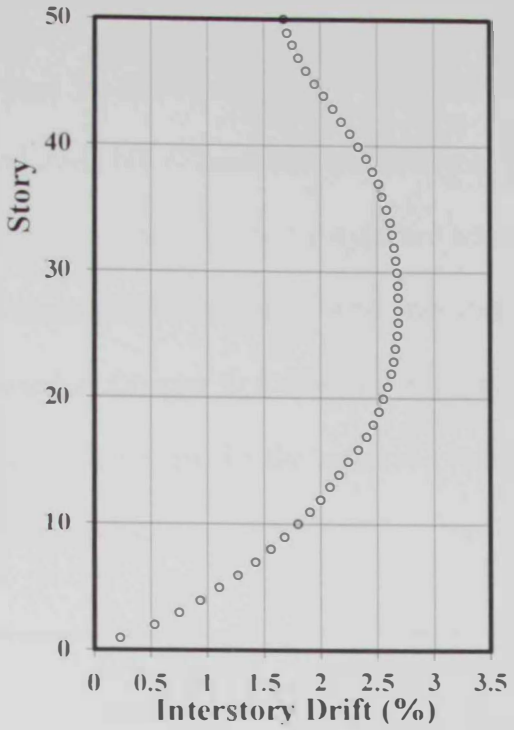

Figure 5.6: Distribution of inter-story drift ratios of the B1-REG building

5.4 Inelastic time-history analysis

The inelastic static analysis procedure has limited capabilities to accurately capture the dynamic performance of structures under earthquake loads, particularly for high-rise buildings (NEHRP, 2010b). In the present study, IPOA is only used for the verification of the analytical models and the assessment of lateral capacity and limit states of the reference buildings, while the seismic response assessment of the regular and irregular structures is undertaken using a large number of inelastic time-history analyses (THAs) and input ground motions. In the THA procedure, the structure is subjected to a seismic acceleration with predefined time steps. The response of the structure in this analysis depends on the interaction of the seismic loads with the dynamic characteristics of the structure. Therefore, the closer the interval of time steps, the more accurate the analysis results are.

It is noteworthy that 40 natural input ground motions representing two seismic scenarios are used in the current study to conduct the THA of the five reference buildings using Zeus-NL (Elnashai et al., 2012), as discussed in Chapter 4. The most significant parameters that affect the dynamic analysis results such as the structural damping and material characteristics were investigated and suitable values were selected, as discussed in Chapter 4. Figure 5.7 and Figure 5.8 show sample of THA results. Additional THA results for the reference buildings are presented and discussed in Chapter 6 and Appendix B.

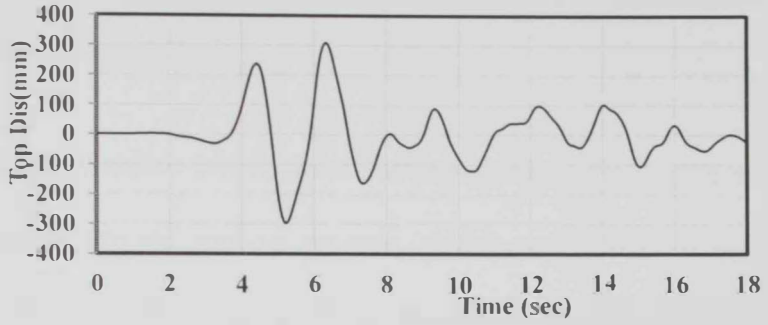

Figure 5.7: Top displacement response history of the B1-REG building under a long period earthquake record (RL1) scaled to twice the design earthquake level (0.32g)

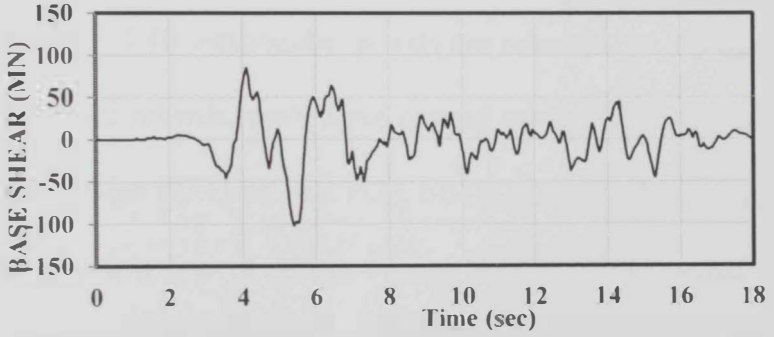

Figure 5.8: Base shear response history of the B1-REG building under a long period earthquake record (RL1) scaled to twice the design earthquake level (0.32g)

5.5 Incremental dynamic analysis

The incremental Dynamic Analysis (IDA) is a powerful computational analysis procedure used to perform a comprehensive assessment of structures under seismic excitation with increasing severity. This analysis procedure was developed for the probabilistic seismic assessment and seismic loss estimation. IDA, also termed dynamic pushover (Mwafy and Elnashai, 2001), is used to estimate the global response of a structure up to collapse (Luco and Cornell, 1998). The IDA approach is now widely recognized in earthquake engineering research. Different assessment methods of structural seismic performance have been developed based on IDA (e.g. Vamvatsikos and Cornell, 2002).

The IDA procedure involves conducting multiple THAs of a structural model under a cluster of ground motion records, which are scaled to several levels of earthquake intensities. The scaling levels should be carefully selected to force the structure throughout the seismic behavior range from elastic to inelastic and finally to the global dynamic instability when the structure collapse. In the current study two earthquake scenarios of 40 earthquake records are selected, as discussed in Chapter 4. For the long period records, each input ground motion is scaled from a PGA of 0.08g (half of the design PGA) up to a PGA of 1.12g to develop the fragility curves of the reference buildings, as shown in Figure 5.9. For short period records, each input ground motion is scaled from a PGA of 0.32g up to a PGA of 4.48g. Figure 5.10 shows a sample of the IDA curves for the B1-REG building. The complete results of the IDAs are presented and discussed in Chapter 6.

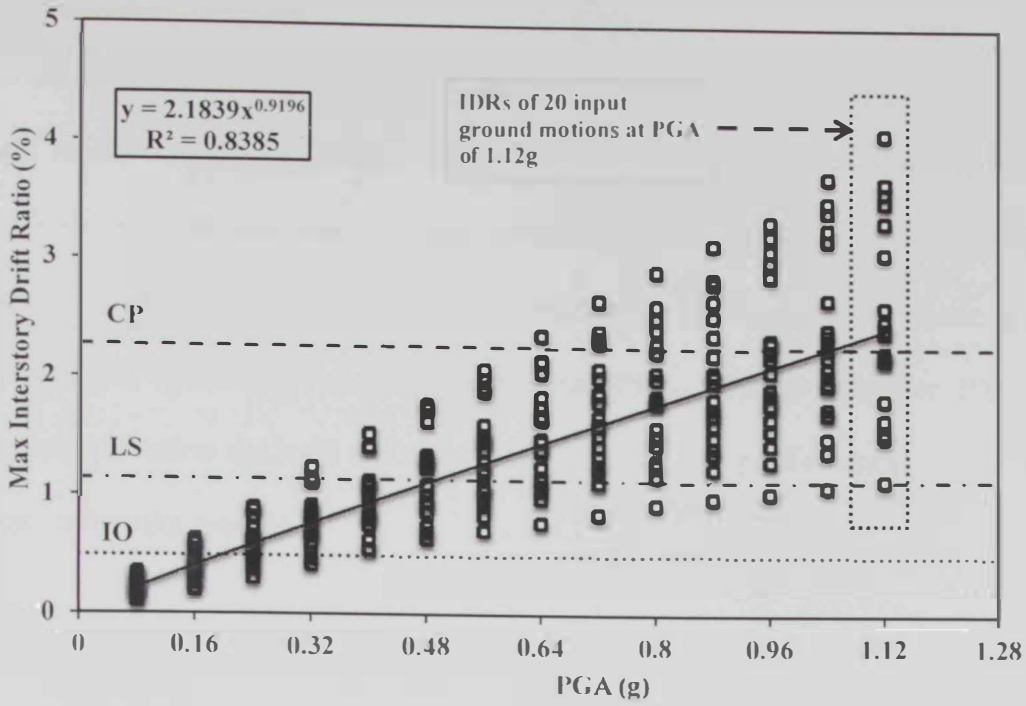

Figure 5.9: IDA results of the B1-REG building obtained from twenty far-field input ground motions along with the power law equations and limit states

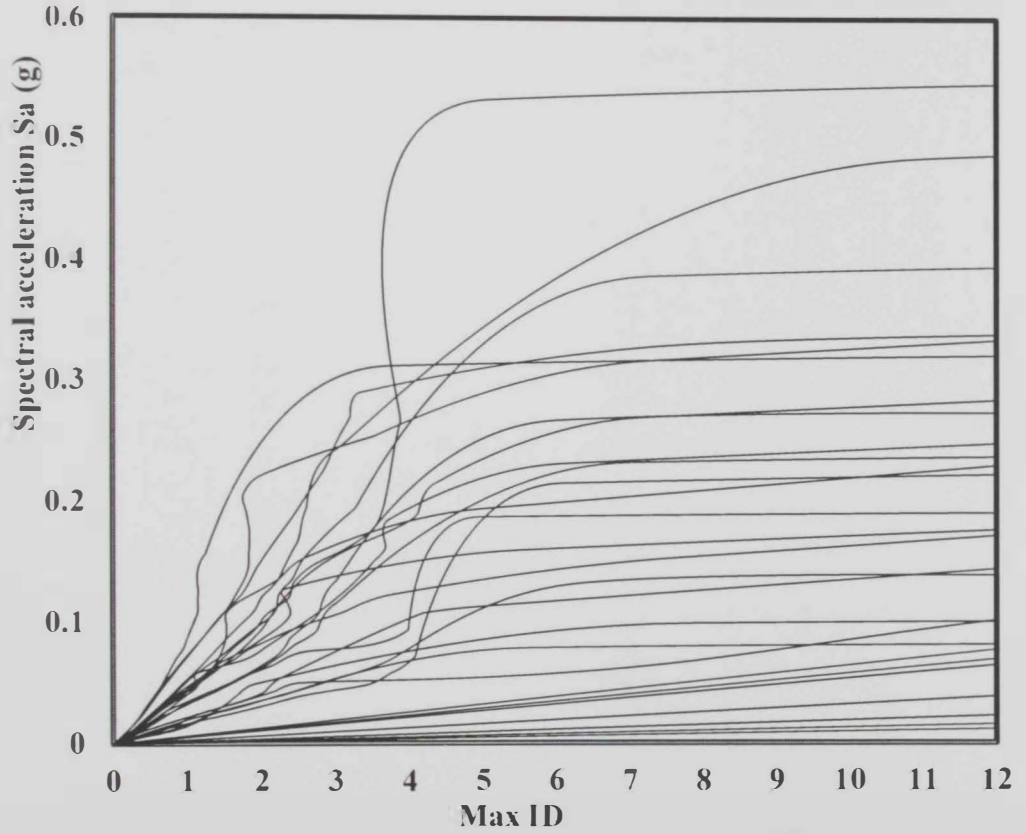

Figure 5.10: IDA curves of the B1-REG building obtained from 20 long period records

5.6 Concluding remarks

Three types of analyses were conducted using the developed Zeus-NL fiber-based models. Firstly, eigenvalue analysis was used to verify the vibration periods and deformed shapes of the reference buildings. Secondly, IPOA was employed to obtain the capacity curves of the reference buildings. The sequence of plastic hinges and concrete crushing were also traced using IPOA. Finally, extensive IDA was conducted to assess the local and overall building inelastic performance under a wide range earthquake records.

Chapter 6: Assessment of Seismic Performance

6.1 Introduction

Inelastic pushover analysis (IPOA) and incremental dynamic analysis (IDA) are employed to assess the seismic response of the five reference regular and irregular buildings. This assessment is based on the local (member) and global (system) structural response, which is compared with the acceptable performance limits that represent different levels of structural damage. The performance criteria include the yielding of tensile reinforcing steel and crushing of confined concrete in structural members. The yielding and crushing are monitored in structural members and mapped with the response at the system level by monitoring the inter-story drift ratios (IDRs) corresponding to the local performance thresholds.

6.2 Evaluation of lateral capacity

Pushover analysis is carried out for the five reference buildings using the uniform lateral load distribution, as discussed in Chapter 5. The capacity curves of the five regular and irregular buildings using a displacement control point selected at the top of each building are presented in Figure 6.1 and Figure 6.2. The capacity curve of the regular building (B1-REG) is shown in Figure 6.1 (a). Comparisons between the capacity curves of the irregular buildings B2-SST, B3-GEO, B4-DIS and B5-WST with B1-REG are presented in Figure 6.1 (b), and Figure 6.2 (a), (b) and (c), respectively. The IDRs corresponding to the first yielding and crushing in structural members as well as the global yielding are mapped on the capacity curves. The maximum base shear obtained from IPOAs represents a conservative estimate of the lateral capacity of a building, as discussed in Chapter 5. The global yielding is evaluated from an elasto-plastic idealization of the real capacity curve. The starting

point of the elasto-plastic branch at a secant stiffness passing through 75% of the ultimate strength is considered as the global yield of a building (Park, 1989).

It is worth noting that, the ultimate strength, initial stiffness and ductility of the building with the extreme soft story irregularity (B2-SST) are slightly lower than those of the regular structure (B1-REG), as shown in Figure 6.1 (b). These minor differences between the characteristic of B2-SST and B1-REG, which are attributed to the stiffness reduction of the extreme soft story, validate the design code approach regarding this type of irregularity. As per ASCE-7 (2010), no special precautions are required in the design of the extreme soft story structures in seismic design category C. In contrast, the above-mentioned characteristics (i.e. strength, stiffness and ductility) of B3-GEO are higher than those of the B1-REG building, as shown in Figure 6.2 (a). Since the foot print of B3-GEO at the lower stories increased, the global building characteristics are enhanced. Again, this observation validates the code approach towards this type of irregularity. For B4-DIS and B5-WST, the ultimate capacity and initial stiffness are much higher than those of B1-REG, while the ductility significantly decreases, as shown in Figure 6.2 (b) and (c). These differences in response are mainly due to the use of the overstrength factor (Ω_o) in the design of buildings B4-DIS and B5-WST at the irregularity levels, as per the recommendation of the design code (ASCE-7, 2010). Although the initial stiffness and ultimate strength of the latter two buildings are improved, the ductility reduction supports the code conservative approach toward the design of these types of vertical irregularity, particularly regarding the use of special load cases in the design.

The IDRs are shown on the capacity curves at the first yield in horizontal and vertical members; global yield; first crushing in vertical members; and at ultimate

strength. Figure 6.3 shows a comparison between the IDRs at different local performance thresholds. It is observed from this comparison that, B2-SST is slightly affected by decreasing the stiffness of the ground floor due to the extreme soft story irregularity. On the other hand, the response of the B3-GEO building is slightly enhanced due to the enlargement of the lower stories dimensions, and hence IDRs are slightly higher than those of B1-REG. Although the initial stiffness and ultimate strength of B4-DIS and B5-WST are increased, the ductility and IDRs are significantly decreased, as shown in Figure 6.2 and Figure 6.3. This is attributed to the discontinuity of the lateral force-resisting-system (LFRS) and the extreme weak story irregularities. In addition to the above, it is observed from Figure 6.1 and Figure 6.2 that the capacity curves of the five reference structures are pressed at the calculated failure due to the crushing of the confined concrete of the shear wall.

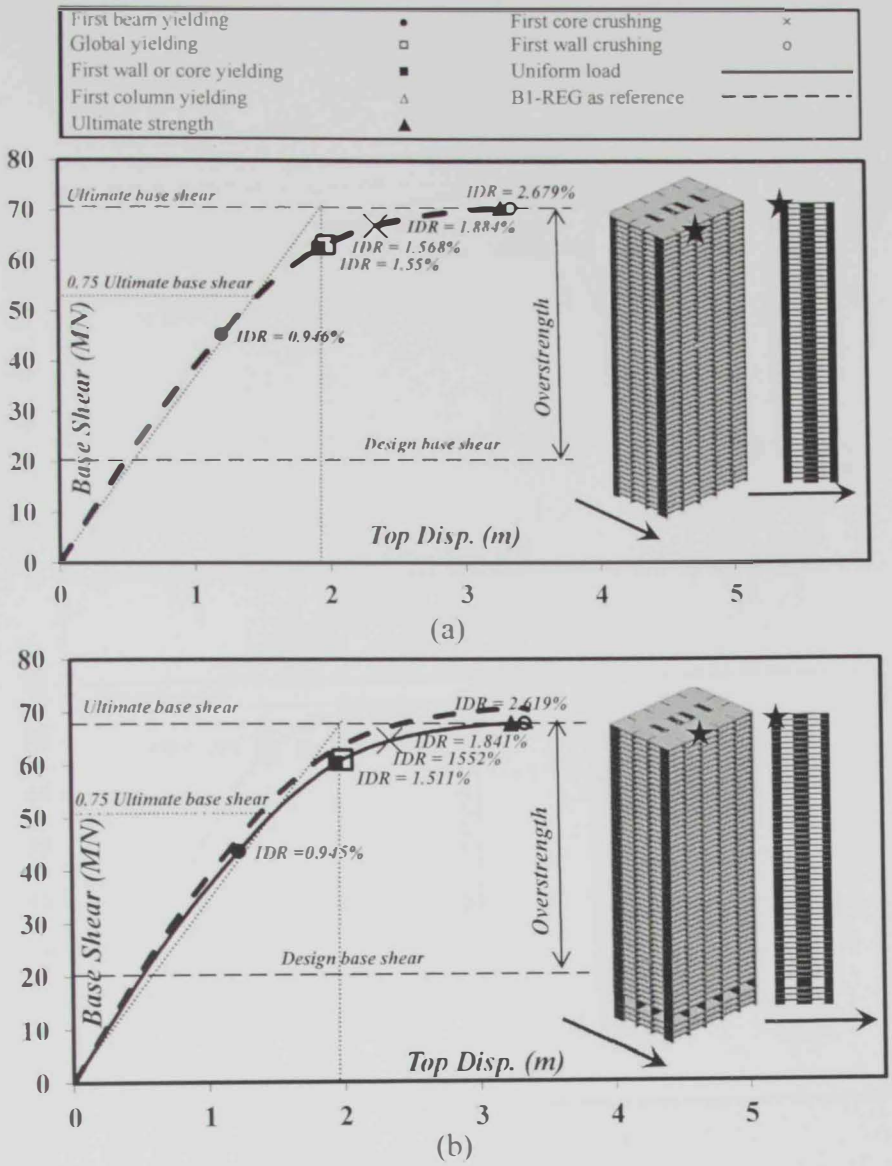

Figure 6.1: Lateral capacity of reference buildings in the transverse direction along with inter-story drift ratios at the first indication of member yielding and crushing: (a) B1-REG and, (b) B2-SST

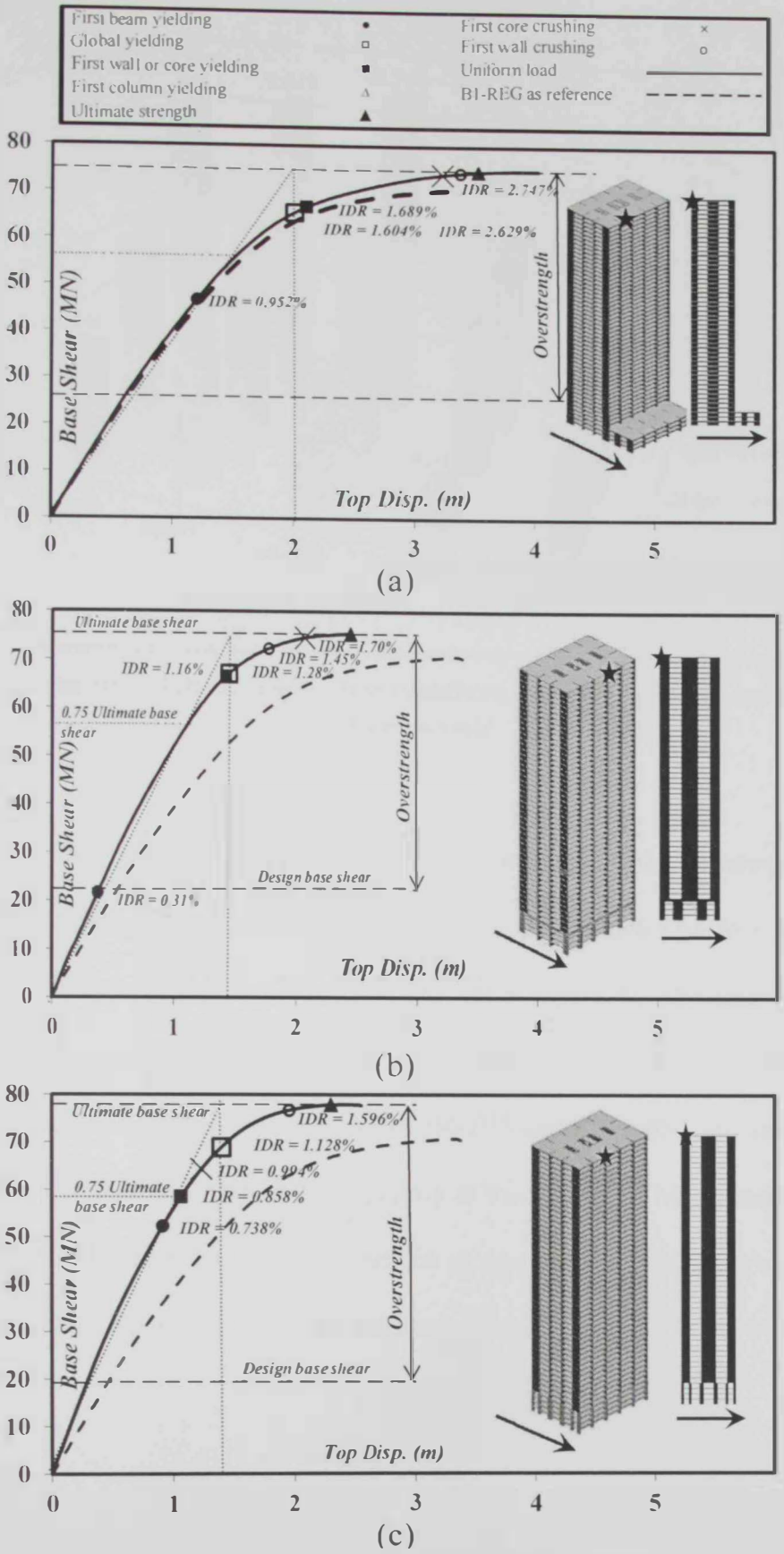

Figure 6.2: Lateral capacity of reference buildings in the transverse direction along with inter-story drift ratios at the first indication of member yielding and crushing: (a) B3-GEO, (b) B4-DIS, and (c) B5- WST

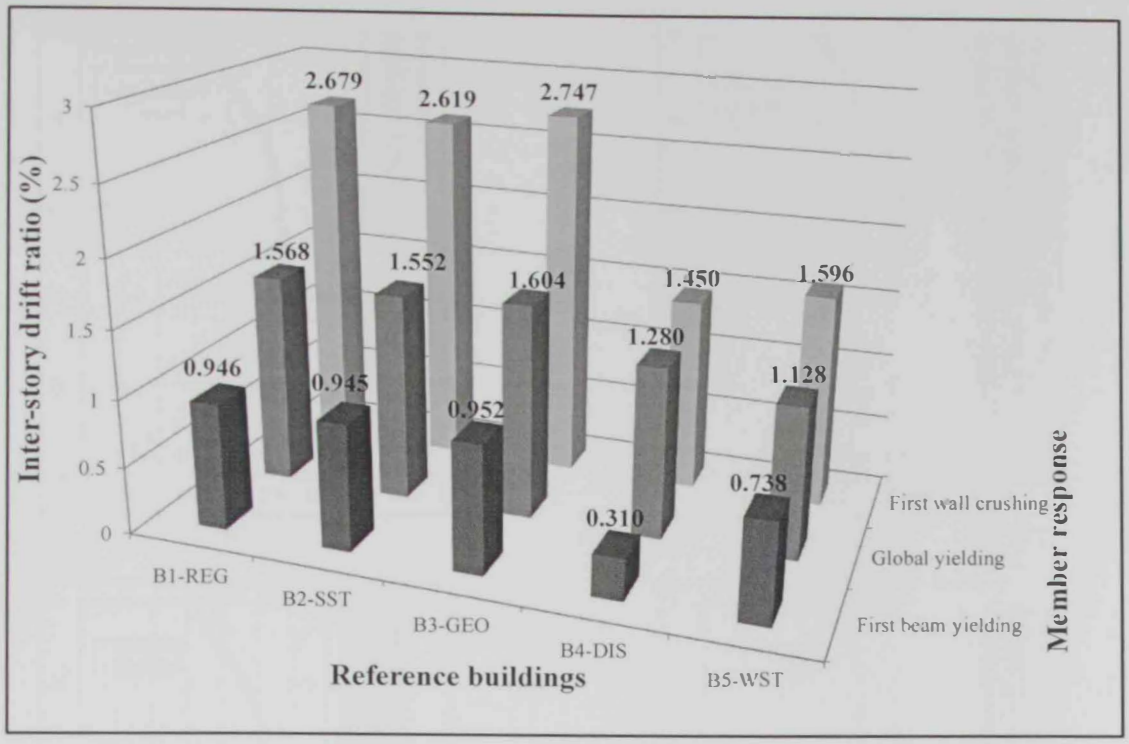

Figure 6.3: Inter-story drift ratios at the first indications of member yielding and crushing, and at global yield

Figure 6.4 depicts the distribution of IDRs throughout the building height at the ultimate strength for the five reference structures. It is shown from this figure that the IDR distributions of the first three building are comparable. The maximum IDR of B3-GEO is slightly higher compared with that of the B1-REG building. The discrepancies of IDRs at the lower stories of B4-DIS and B5-WSST are attributed to the significant change in LFRS and irregularity at these levels. The presented results in Figure 6.1 to Figure 6.4 clearly support the design code provisions related to the design of different types of irregularity, as discussed in Chapter 3.

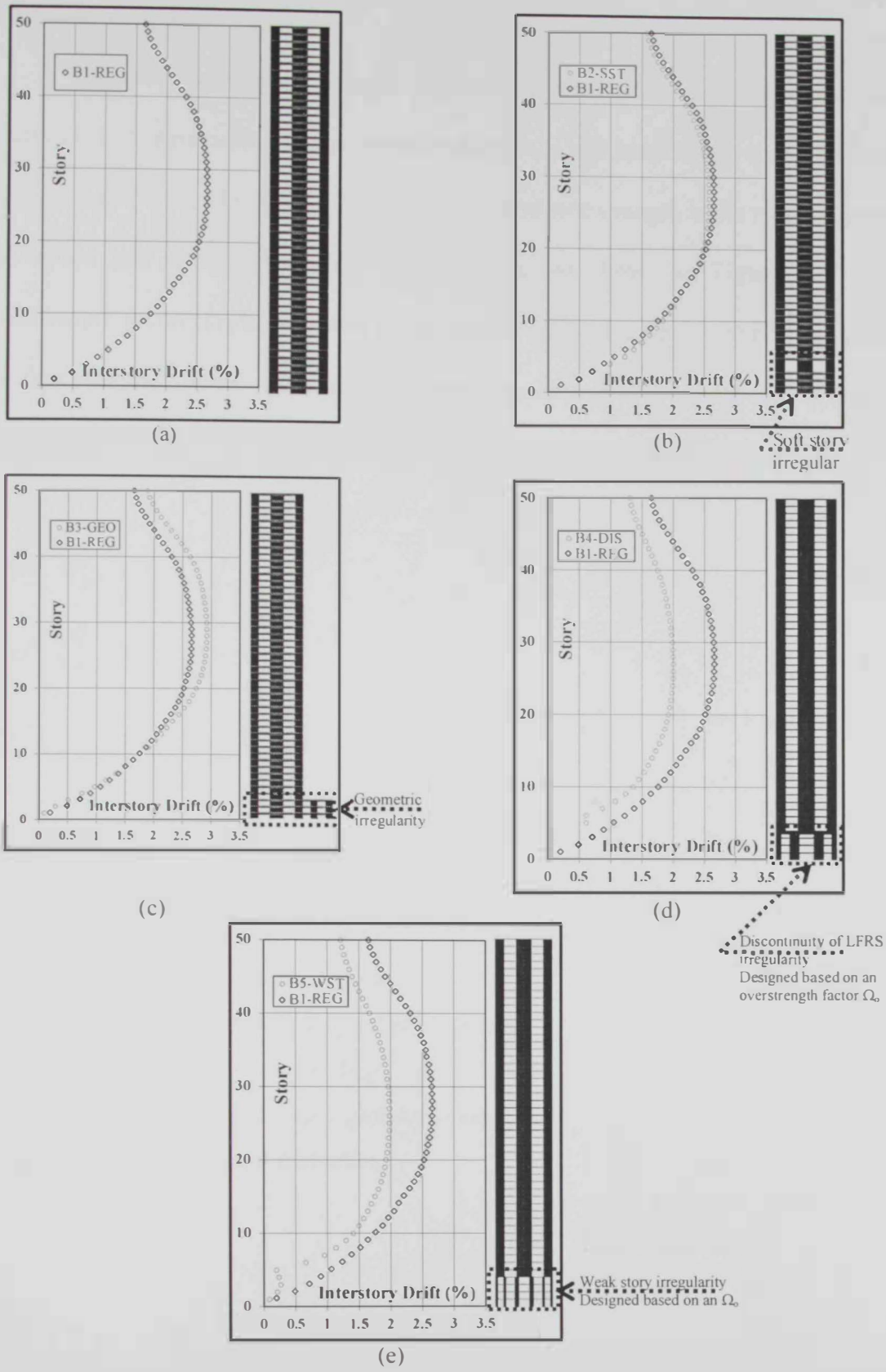

Figure 6.4: Distributions of inter-story drift ratios at ultimate strength: (a) B1-REG, (b) B2-SST, (c) B3-GEO, (d) B4-DIS, and (e) B5- WST

6.3 Assessment of overstrength

The actual strength is influenced by several parameters such as the material characteristics, structural systems, member properties, connection between structural members, and design factor of safety. The structural overstrength is the ratio between the actual and design strength of the building, as shown in Figure 6.5. The overstrength factor (Ω) is measured in the present study at different levels such as at the first yielding, global yielding and ultimate capacity. IPOAs results are employed to estimate various overstrength factors, as shown in Eqns 6.1 to 6.3.

$$\Omega_{1ph}=\frac{V_y}{V_d} \qquad 6.1$$

$$\Omega_{gy}=\frac{V_{gy}}{V_d} \qquad 6.2$$

$$\Omega_u=\frac{V_u}{V_d} \qquad 6.3$$

where:

Ω_{1ph}: overstrength factor at first plastic hinge

Ω_{gy}: overstrength factor at global yielding

Ω_u: overstrength factor at ultimate capacity

V_y: lateral strength of the building at first plastic hinge

V_d: design lateral strength of the building

V_{gy}: lateral strength of the building at global yielding

V_u: ultimate lateral strength of the building

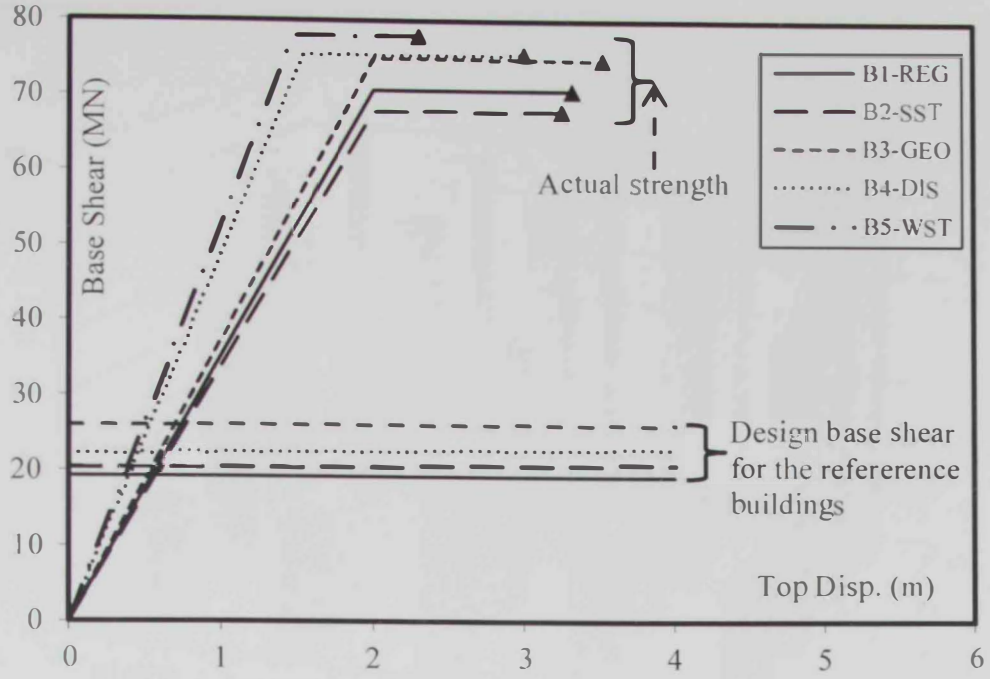

Figure 6.5: Idealize capacity envelopes of the five reference buildings

The base shear values of the reference structures at the formation of first plastic hinge (first yielding), global yielding, and ultimate capacity are compared with the design base shear in Figure 6.6. It is shown that the base shear of the B1-REG and B2-SST buildings are comparable, while the strength value of the B3-GEO building is slightly higher due to the larger footprint at lower stories. Unlike the global yielding and ultimate strength of the B4-DIS building, the lateral strength at the first indication of plastic hinge in horizontal members is much lower than other buildings as a result of the early yielding in the transfer slab. The higher base shear of B4-DIS at global yielding and ultimate capacity is attributed to the use of an Ω_o factor in the design of the irregular part of the building. Similarly, for the B5-WST building, the base shear values are generally higher than other structures due to the use of an Ω_o, as per the design code recommendation for the extreme weak story irregularity.

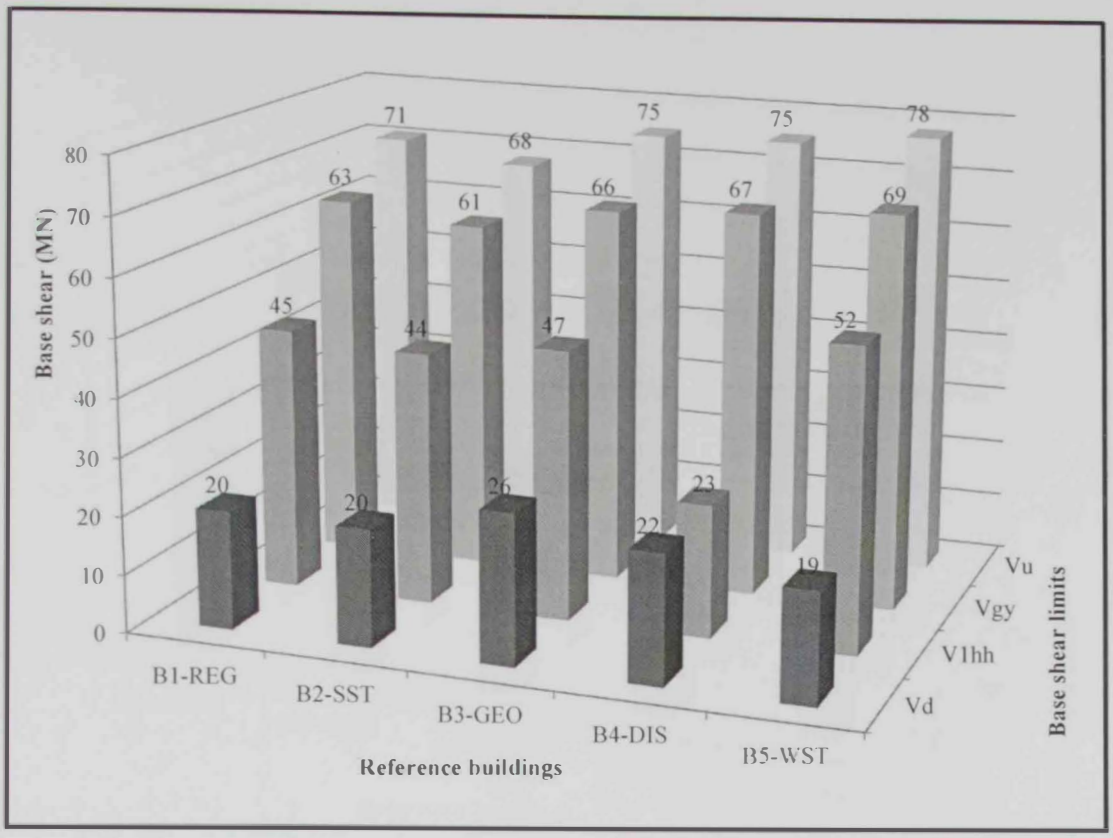

Figure 6.6: Base shear of reference structures at the design, first plastic hinge, global yielding and ultimate capacity

Figure 6.7 depicts the overstrength factors at the first plastic hinge, global yielding and ultimate capacity of the five reference buildings. The overstrength factors of B1-REG and B2-SS buildings are almost comparable, which confirms the marginal effect of the soft story irregularity on lateral capacity. Due to the high design base shear of building B3-GEO, the overstrength factors of this structure are lower than the regular one. The overstrength factor at the first plastic hinge of building B4-DIS is significantly lower than in other buildings due to the early yielding of the transfer slab, which supports the heavy vertical load from typical stories. The overstrength factors of the latter building at global yielding and ultimate capacity are slightly lower than in the regular building. The overstrength factors of the B5-WST building are higher than in other structures due to the use of an Ω_o in design (ASCE-7, 2010).

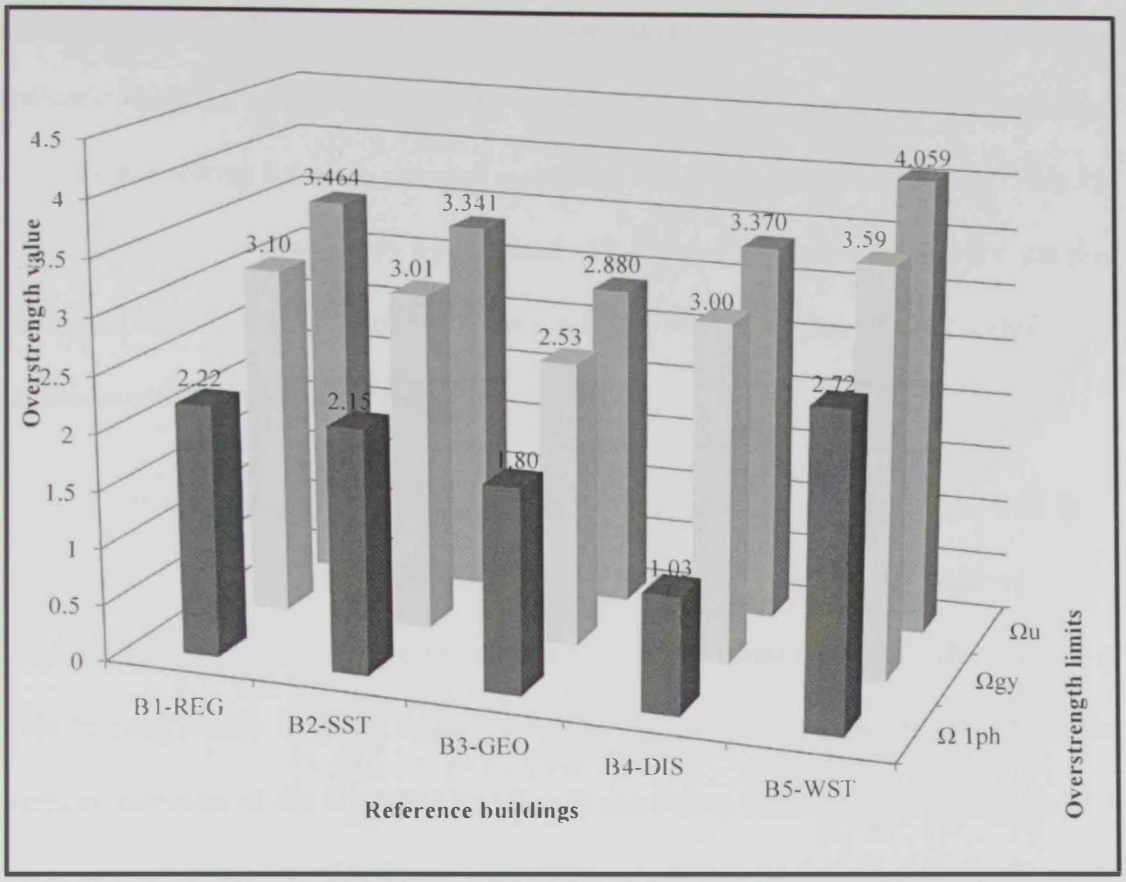

Figure 6.7: Overstrength factors at the first plastic hinge, global yielding and ultimate capacity of the reference buildings

6.4 Assessment of member response

The seismic performance assessment at the member level is significant for accurate evaluation of limit states and the response of regular and irregular structures. The yielding of reinforcing steel and crushing of confined concrete are important indications for the structural failure. Hence, yielding and crushing of the five reference structures are assessed in subsequent sections. Additionally, the shear response of critical members is evaluated to detect any possible brittle shear failure modes.

6.4.1 Plastic hinge distributions

In the current study, a plastic hinge (local yield) forms when the strain of tensile rebar exceeds the steel yield strain (Elnashai and Mwafy, 2002; Mwafy and

Elnashai, 2002). Plastic hinges (PHs) are monitored throughout the multistep inelastic analysis, as shown in Figure 6.8 and Figure 6.9. For the B1-REG building, the PHs are shown for all horizontal members, while for other buildings the first PH in horizontal members is only highlighted. All PHs of vertical members for the five reference buildings are mapped in Figure 6.8 and Figure 6.9 due to their significance on the overall building response.

It is noted that the first PH in horizontal members is recorded at the middle of the building height except for B4-DIS members due to the early yielding in the transfer slab. In the case of the extreme soft story structure (B2-SST), the number of PHs is comparable to those of the B1-REG building. The number of PHs in the vertical members of the B3-GEO building is more than those in other buildings. This observation is due to the increased stiffness of this building, which results in attracting higher lateral forces. The results presented in Figure 6.9 show that increasing the lateral design forces leads to increasing the number of PHs. It is noteworthy that, no PHs are recorded in the vertical members of B4-DIS and B5-WST at the lower stories, which were designed with an overstrength factor (Ω_0) as per ASCE-7 (2010).

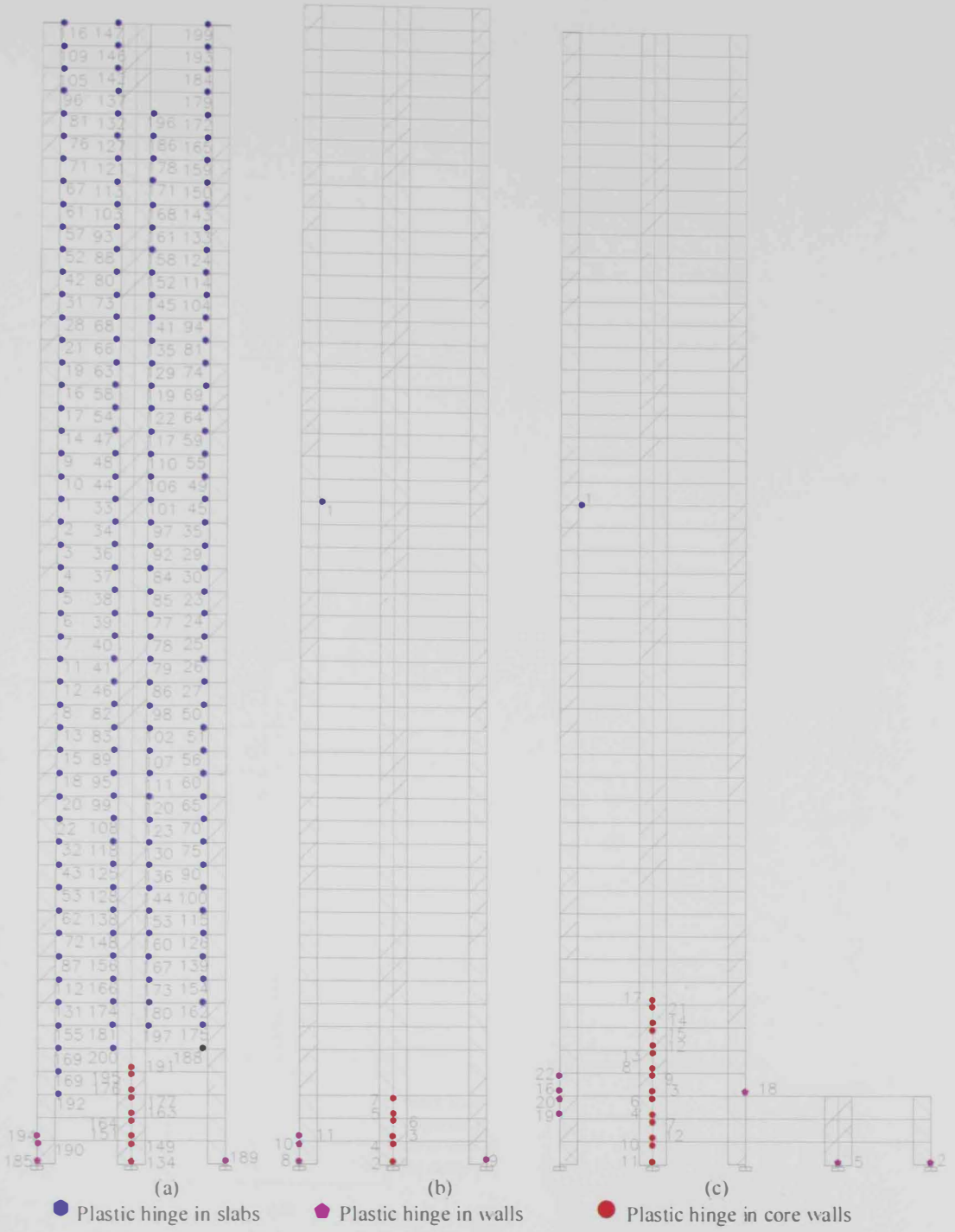

Figure 6.8: Plastic hinge distributions: (a) in horizontal and vertical elements of B1-REG, (b) in the vertical elements and the first PH in horizontal elements of B2-SST, and (c) in the vertical elements and the first PH in horizontal elements of B3-GEO

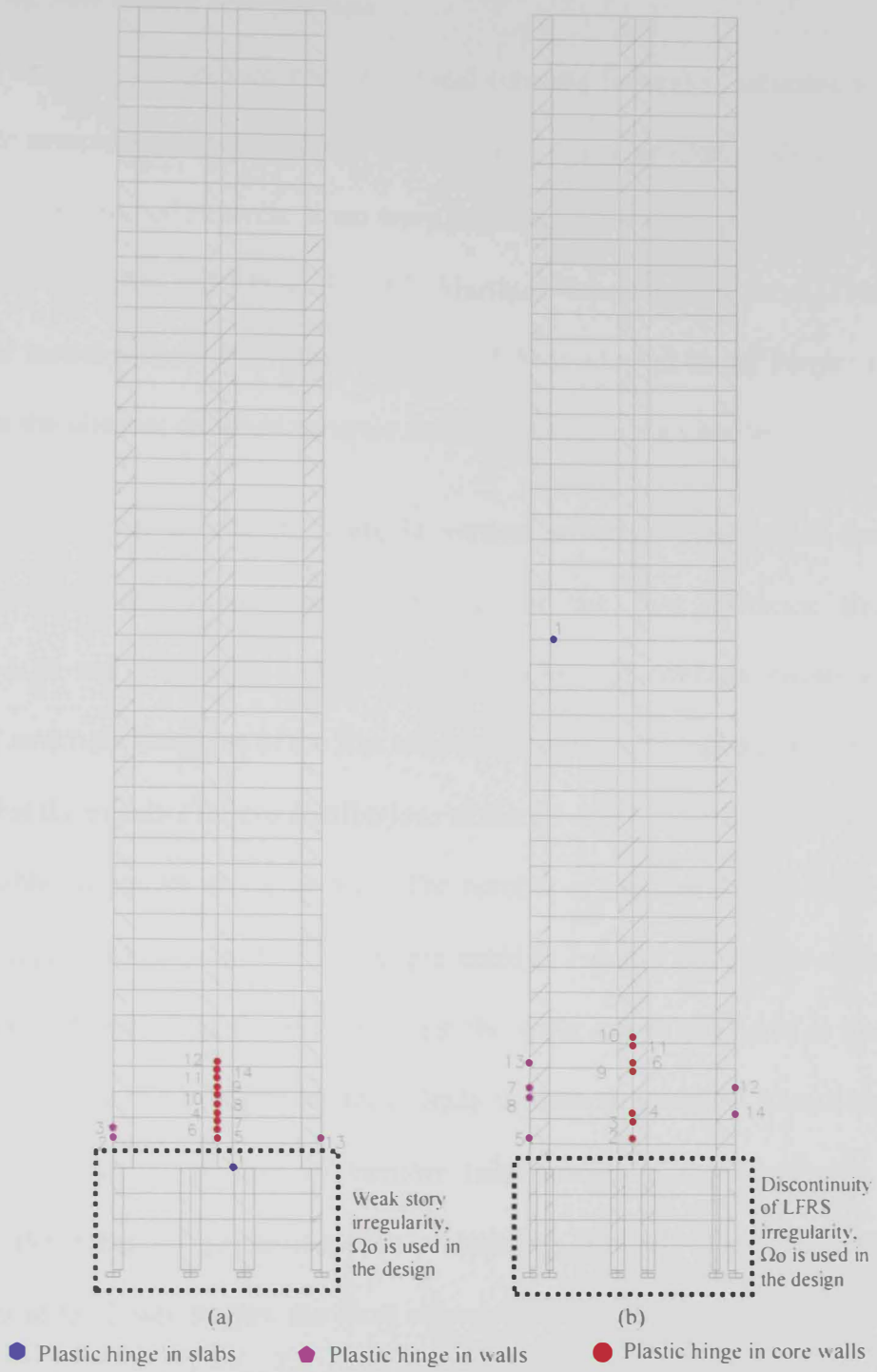

Figure 6.9: Plastic hinge distributions: (a) in the vertical elements and the first PH in horizontal elements of B4-DIS, and (b) in the vertical elements and the first PH in horizontal elements of B5-WST

6.4.2 Concrete failure distributions

Crushing of confined concrete (local concrete failure) is assumed when the concrete compressive strain exceeds the allowable strain. Several concrete models to evaluate the confined concrete strain were proposed in previous studies (e.g. Mander et al., 1988; Madas and Elnashai, 1992; Martínez-Rueda and Elnashai, 1997). The concrete model proposed by Mander et al. (1988) is adopted in the current study to evaluate the ultimate confined concrete strain, as discussed in Chapter 4.

The confined concrete strain in vertical structural members is monitored throughout the multistep inelastic analyses of the five reference structures. Figure 6.10 and Figure 6.11 show the distributions of concrete crushing in the vertical structural members of the five reference buildings throughout the height. It is noted that the member failure distributions of the B1-REG and B2-SST buildings are comparable, as shown in Figure 6.10. The number of member failure cases in B3-GEO is higher than that in B1-REG, as presented in Figure 6.10. This is attributed to the higher stiffness of the former building at the lower stories compared to that of the regular structure. This higher stiffness leads to attracting higher lateral load, and hence increasing the number of member failure cases at the irregularity levels. Despite the enhanced global response of building B3-GEO due to increasing its footprint at the lower stories, the local response clearly shows the disadvantages of the geometric irregularity. No indications of confined concrete crushing are recorded in the vertical members of B4-DIS and B5-WST at the lower stories, which are designed using the Ω_o factor, as per ASCE-7 (2010). This is attributed to the satisfactory design of the reference buildings and the special provisions of the design code for irregular structures.

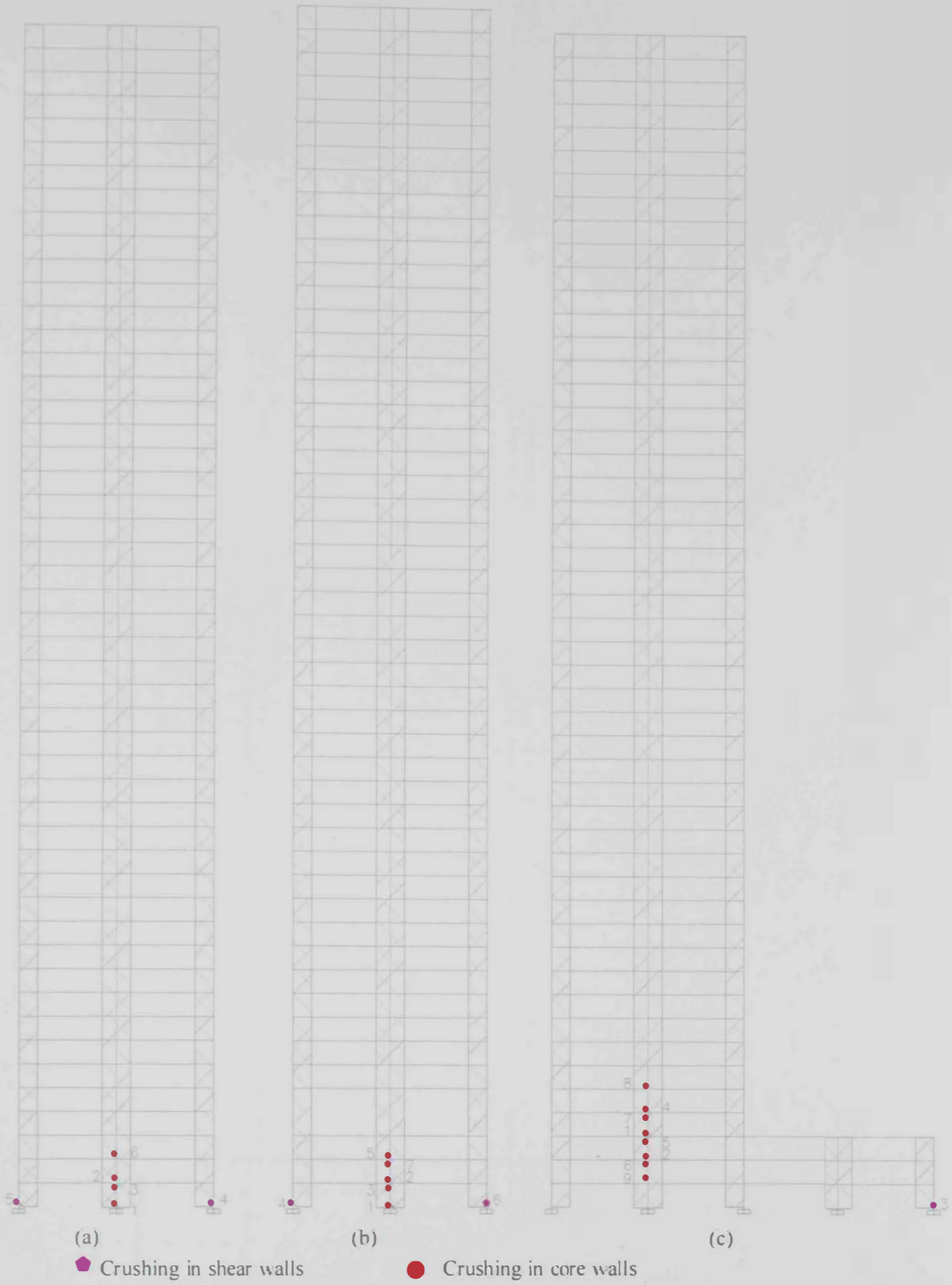

Figure 6.10: Distributions of concrete crushing: (a) in vertical elements of B1-REG, (b) in vertical elements of B2-SST, and (c) in vertical elements of B3-GEO

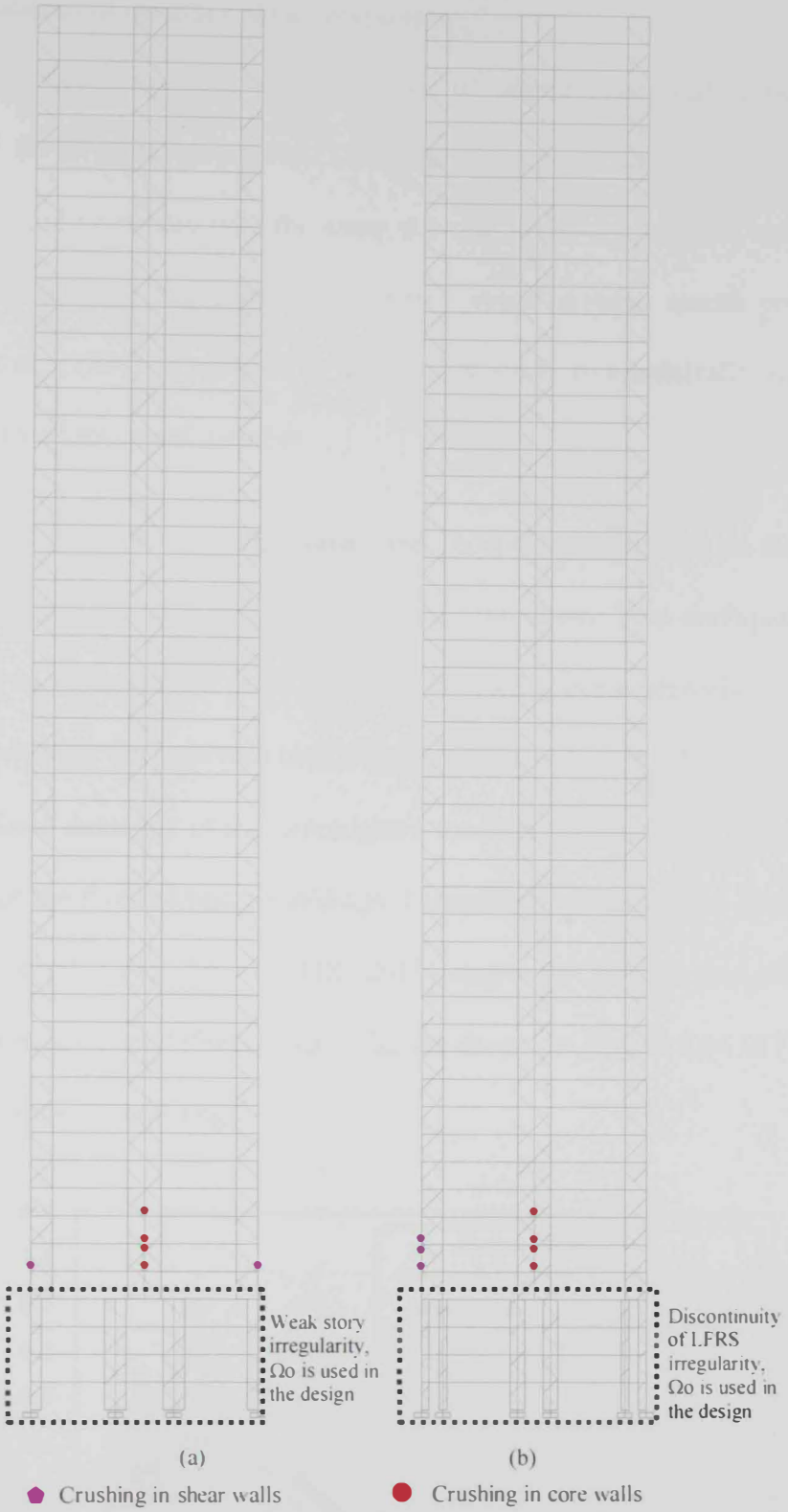

Figure 6.11: Distributions of concrete crushing: (a) in vertical elements of B4-DIS and (b) in vertical elements of B5-WST

6.4.3 Assessment of member shear response

Shear forces may be the main cause of failure under earthquake loading, particularly for irregular structures. The shear demands of key structural members are obtained and compared with the shear strength to provide insights into the shear failure potential. The experimentally verified shear strength model proposed by Priestley et al. (1994) is adopted in the current study to realistically estimate the shear capacity of structural member.

The IDA results of long period and short period records, as discussed in Chapters 4 and 5, are used for shear response assessment. Two earthquake records are selected to represent the mean spectrum of each seismic scenario in the period range of interest for the reference buildings, as shown in Figure 6.12 and Figure 6.13. The shear force demands of the investigated members are obtained from the Zeus-NL results of the five reference buildings. Comparisons between the shear demand, V_d, shear strength using the ACI-318 (2011) approach, V(ACI), and shear supply using the Priestley et al. (1994) model, V_{pr}, are shown in Figure 6.14 to Figure 6.42 for the five reference buildings.

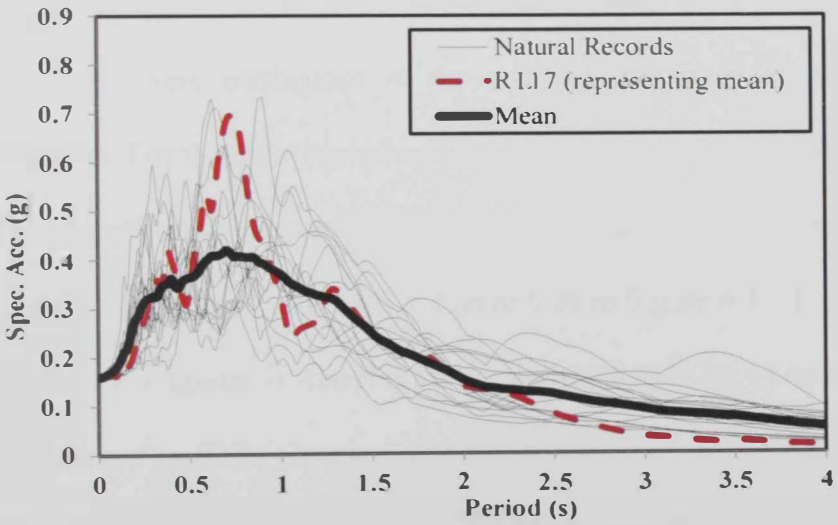

Figure 6.12: Comparison between the response spectrum of the selected record for shear assessment and response spectra of 20 long period records

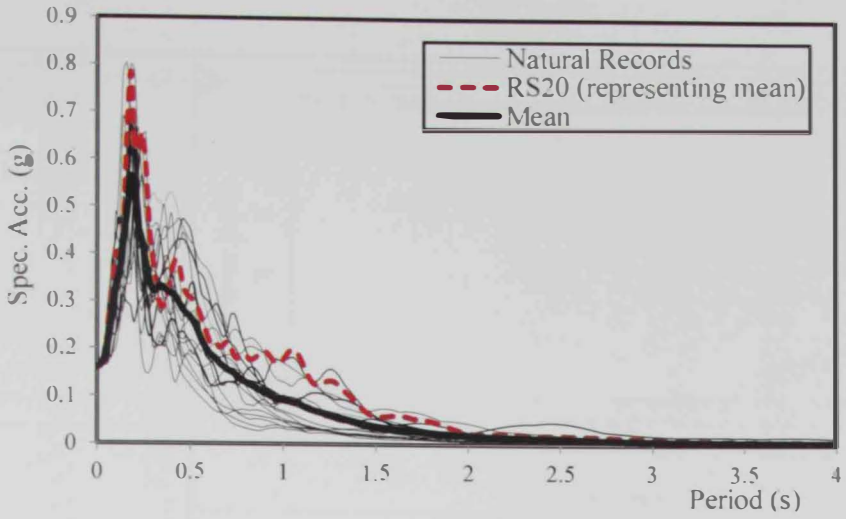

Figure 6.13: Comparison between the response spectrum of the selected record for shear assessment and response spectra of 20 short period records"

It is shown from Figure 6.14 to Figure 6.25, which illustrate the comprehensive shear force assessment results using the long period earthquake record (RL17), that shear failure is not observed in any structural member of the five reference buildings before reaching the preliminary collapse prevention (CP) limit state, as discussed in subsequent sections. These results are attributed to the impact of the long period records on high-rise buildings in which the flexural response is more significant than shear. On the other hand, Figure 6.26 to Figure 6.42 show that the short period earthquake record has a major impact on the shear response and the limit states under severe earthquake of the reference buildings, particularly the irregular structures. For the short period earthquake scenario, the IDR corresponding to shear failure significantly decreases as a result of the detected shear failure before the preliminary CP limit state, as shown in Figure 6.26 to Figure 6.42. It is important to note that the shear failure is detected in Figures 6.14 to 6.42 when the V_{pe}-V_{pr} value exceeds zero. The IDRs observed at the first indication of shear failure of the B1-REG, B2-SST, B3-GEO, B4-DIS, and B5-WST buildings are 1.55%, 1.5%, 1.62%, 0.64%, 0.78%, respectively.

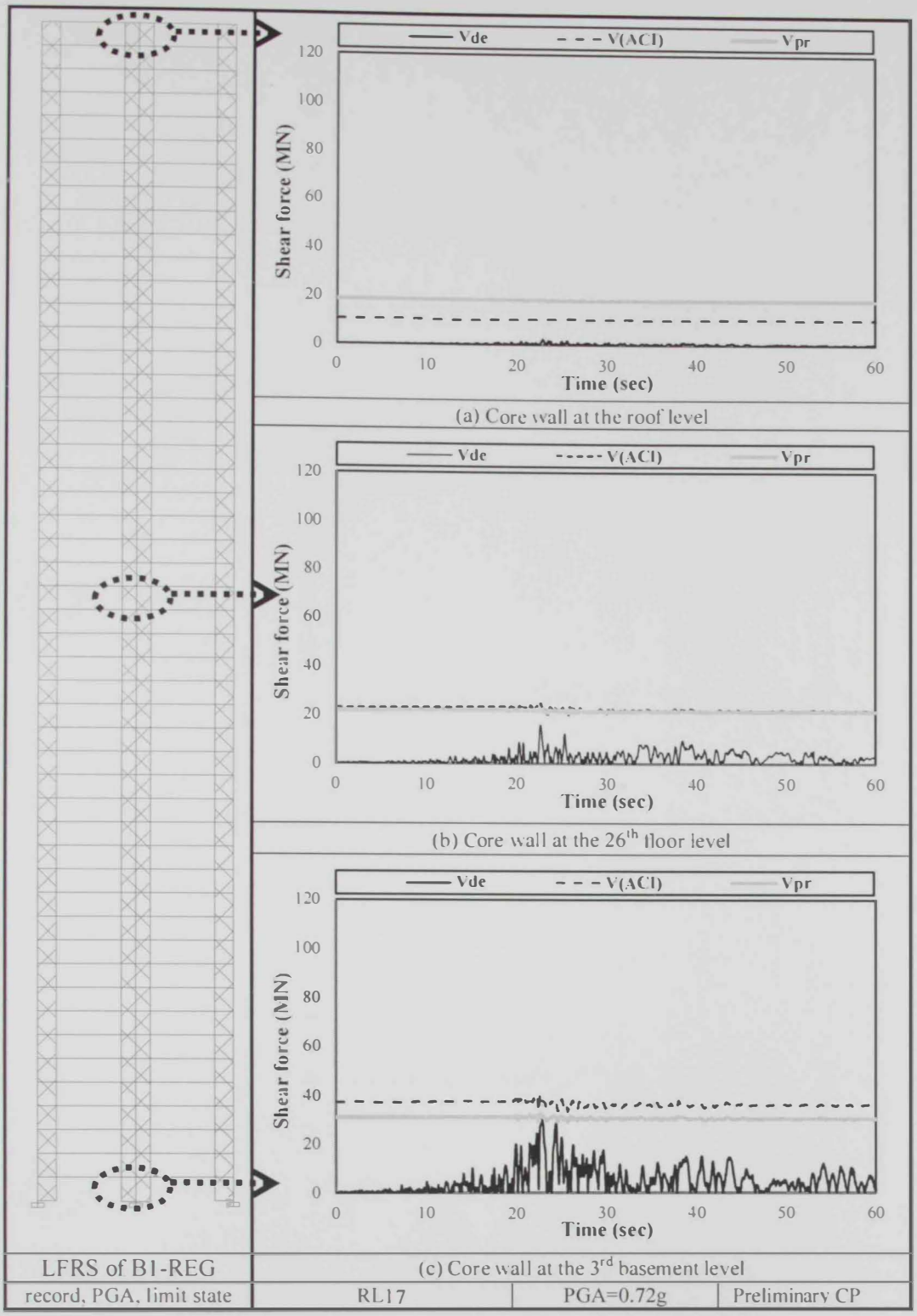

Figure 6.14: Shear demand using RL17 versus shear strength using ACI and Priestley et al. (1994) models for the core walls of B1-REG

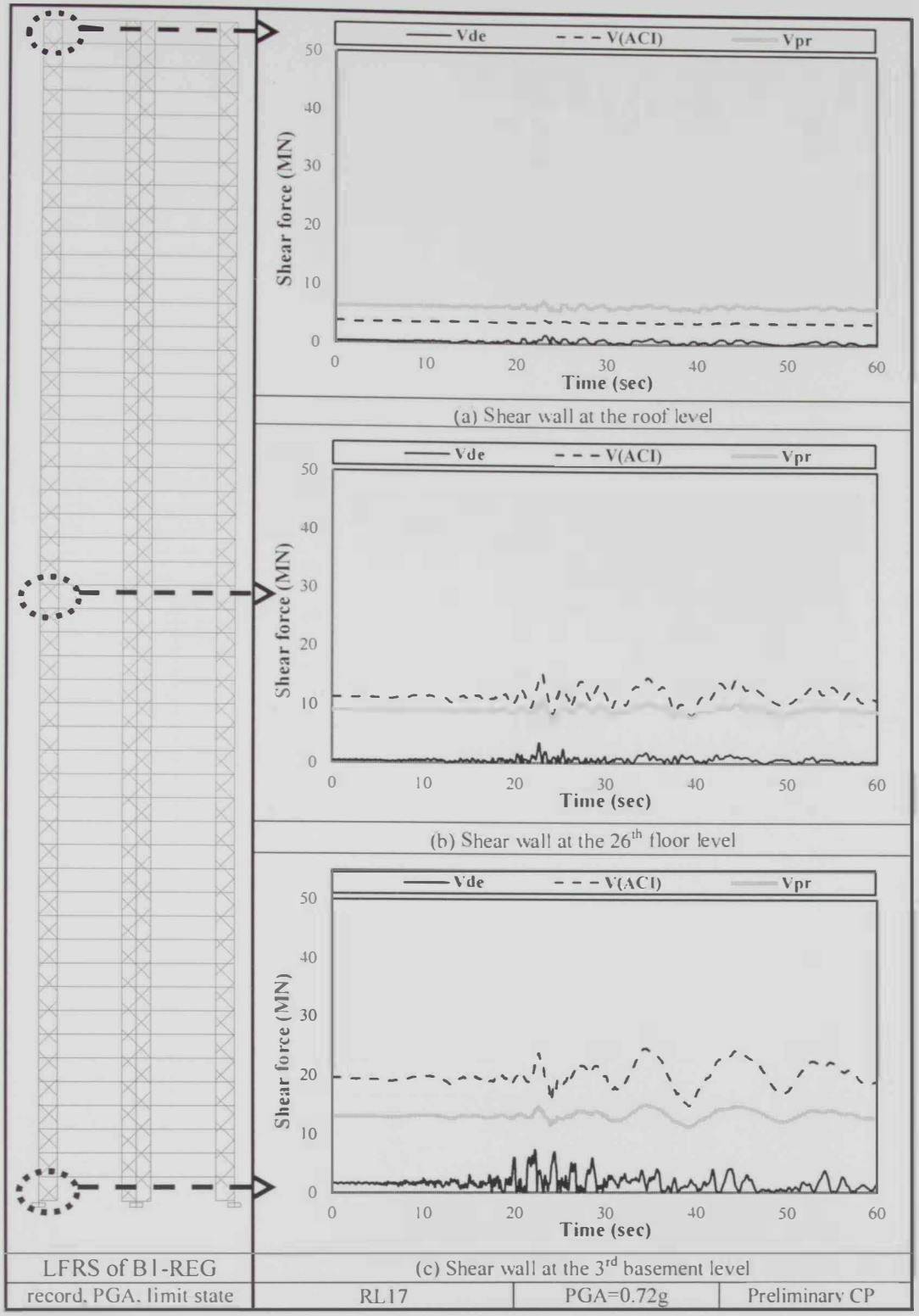

Figure 6.15: Shear demand using RL17 versus shear strength using ACI and Priestley et al. (1994) models for the shear walls of B1-REG

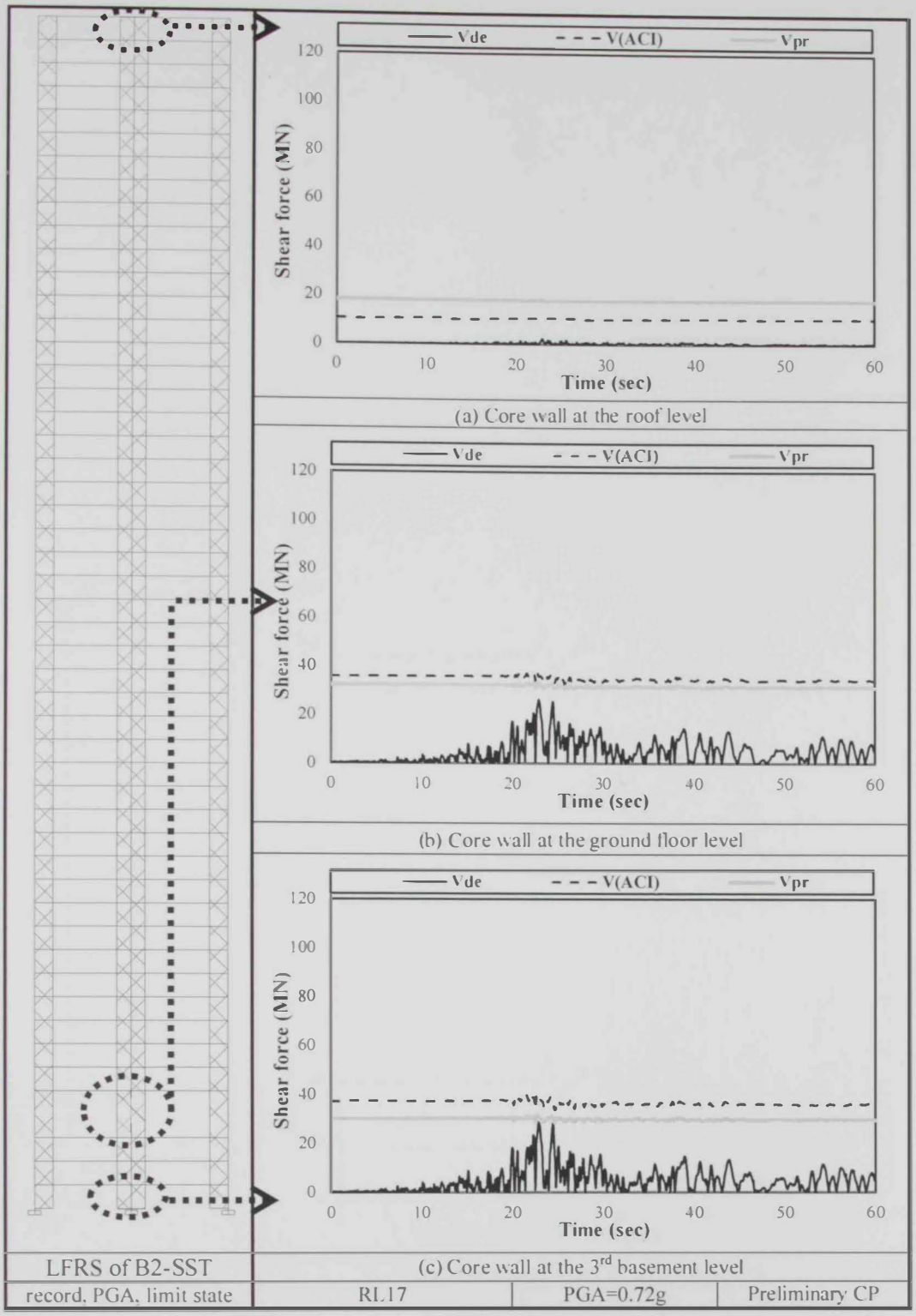

Figure 6.16: Shear demand using RL17 versus shear strength using ACI and Priestley et al. (1994) models for the core walls of B2-SST

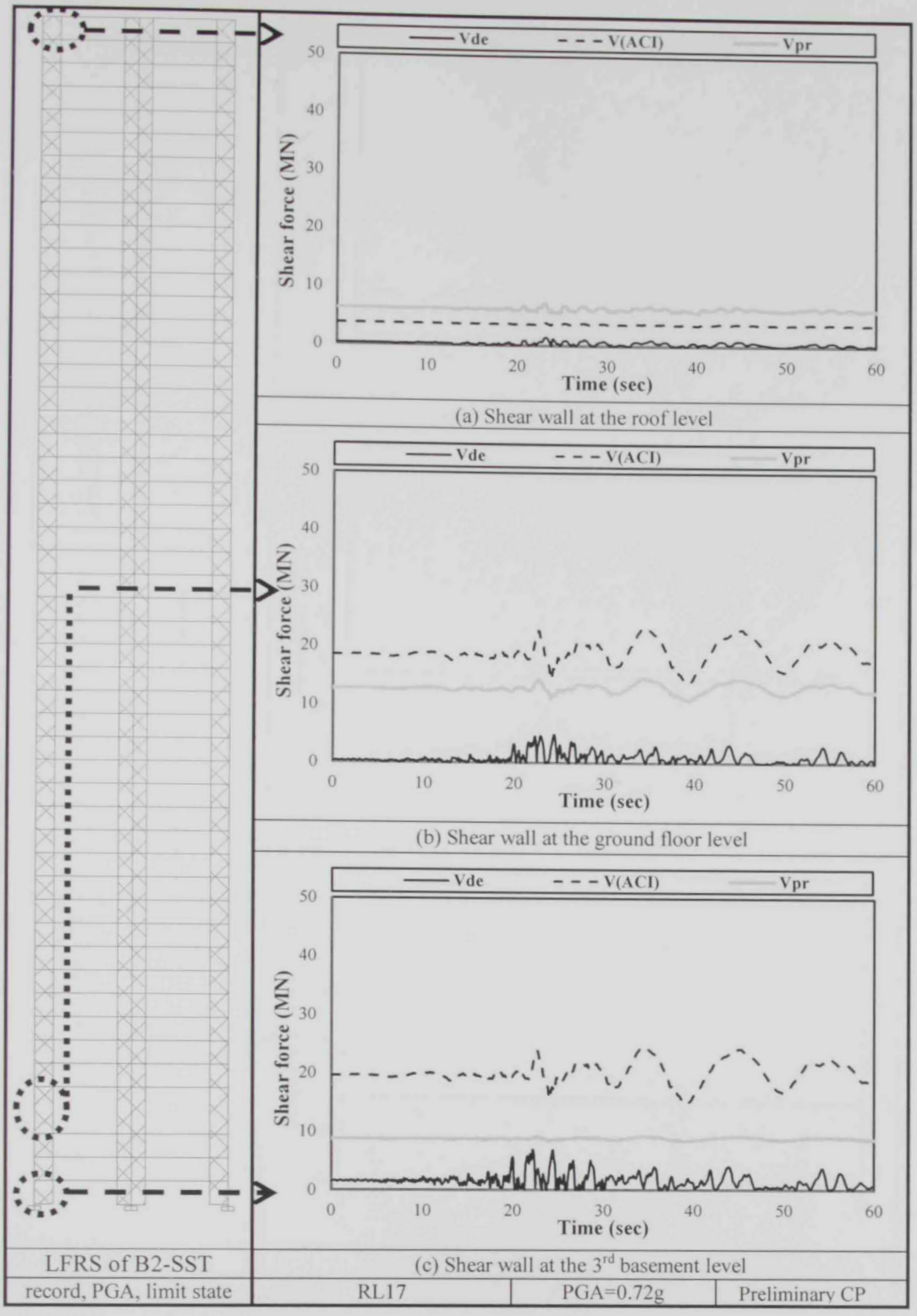

Figure 6.17: Shear demand using RL17 versus shear strength using ACI and Priestley et al. (1994) models for the shear walls of B2-SST

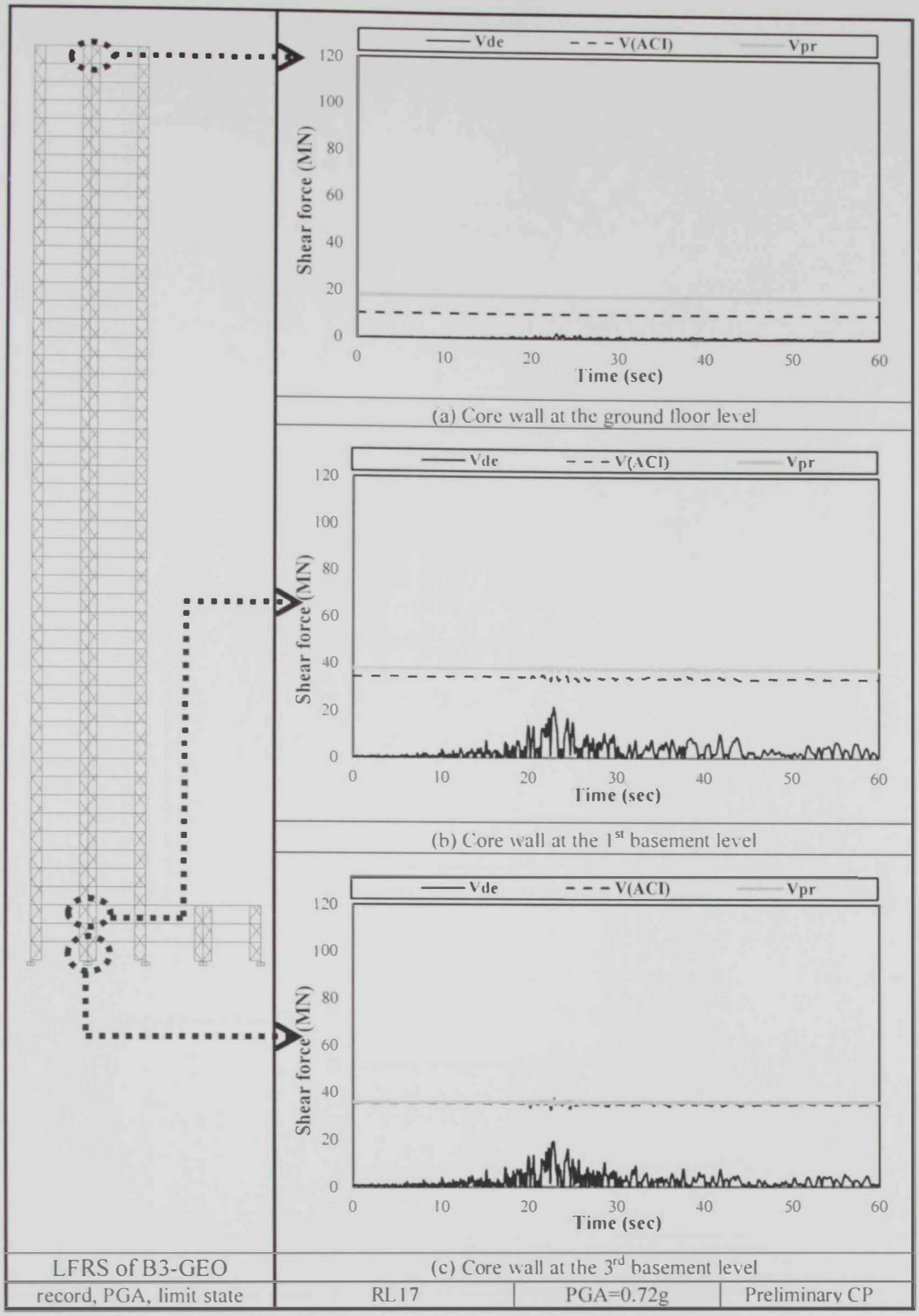

Figure 6.18: Shear demand using RL17 versus shear strength using ACI and Priestley et al. (1994) models for the core walls of B3-GEO

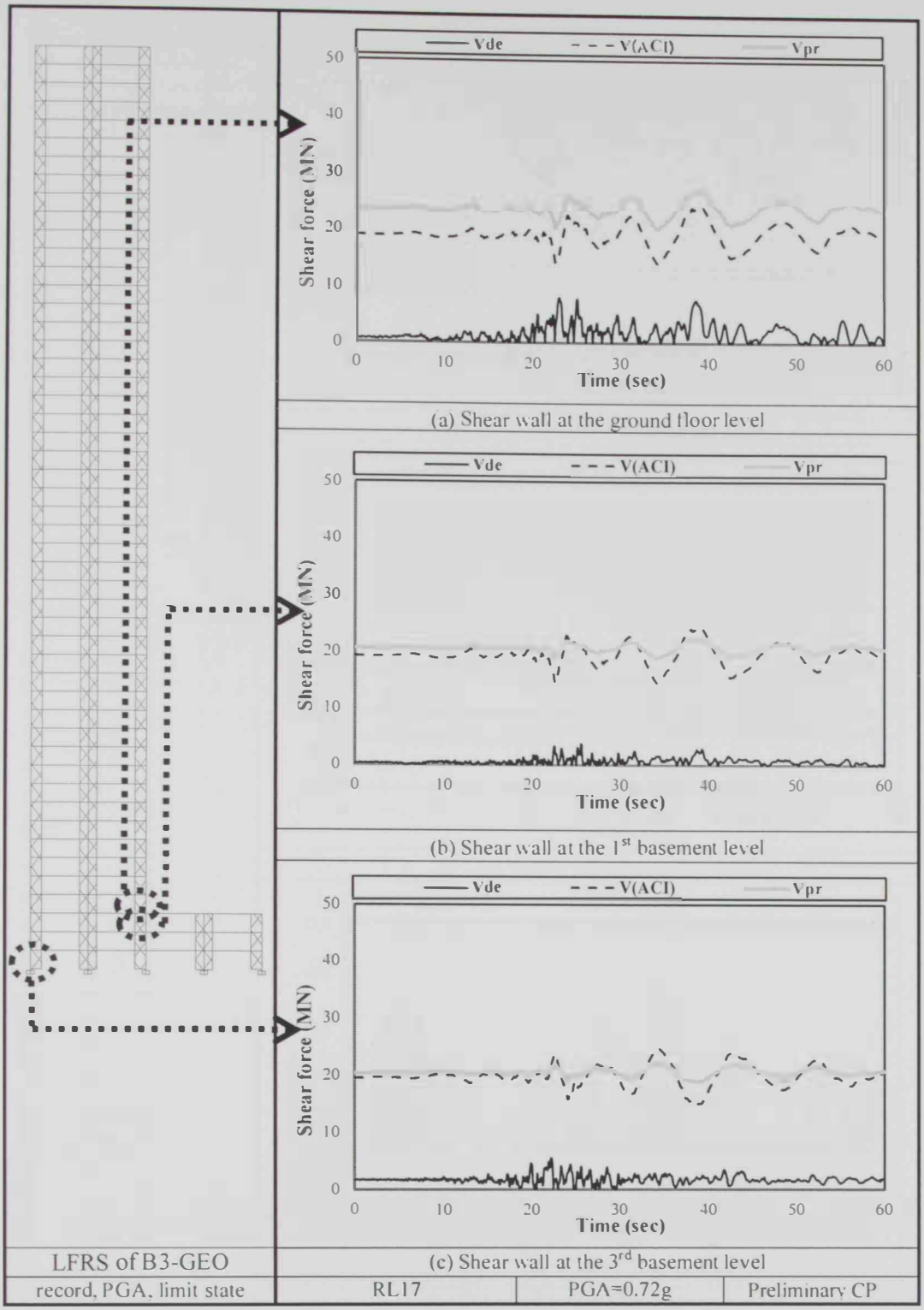

Figure 6.19: Shear demand using RL17 versus shear strength using ACI and Priestley et al. (1994) models for the shear walls of B3-GEO

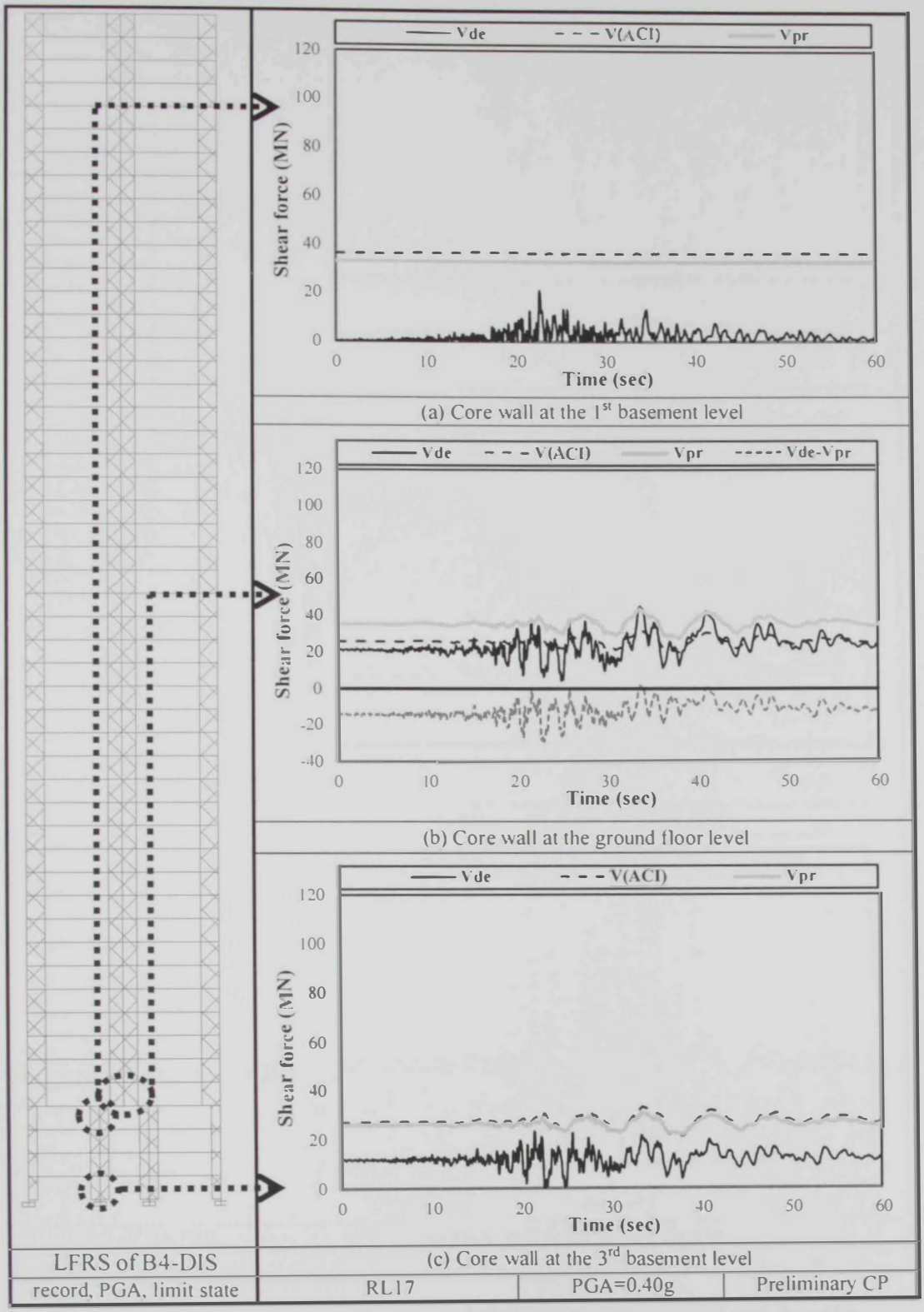

Figure 6.20: Shear demand using RL17 versus shear strength using ACI and Priestley et al. (1994) models for the core walls of B4-DIS

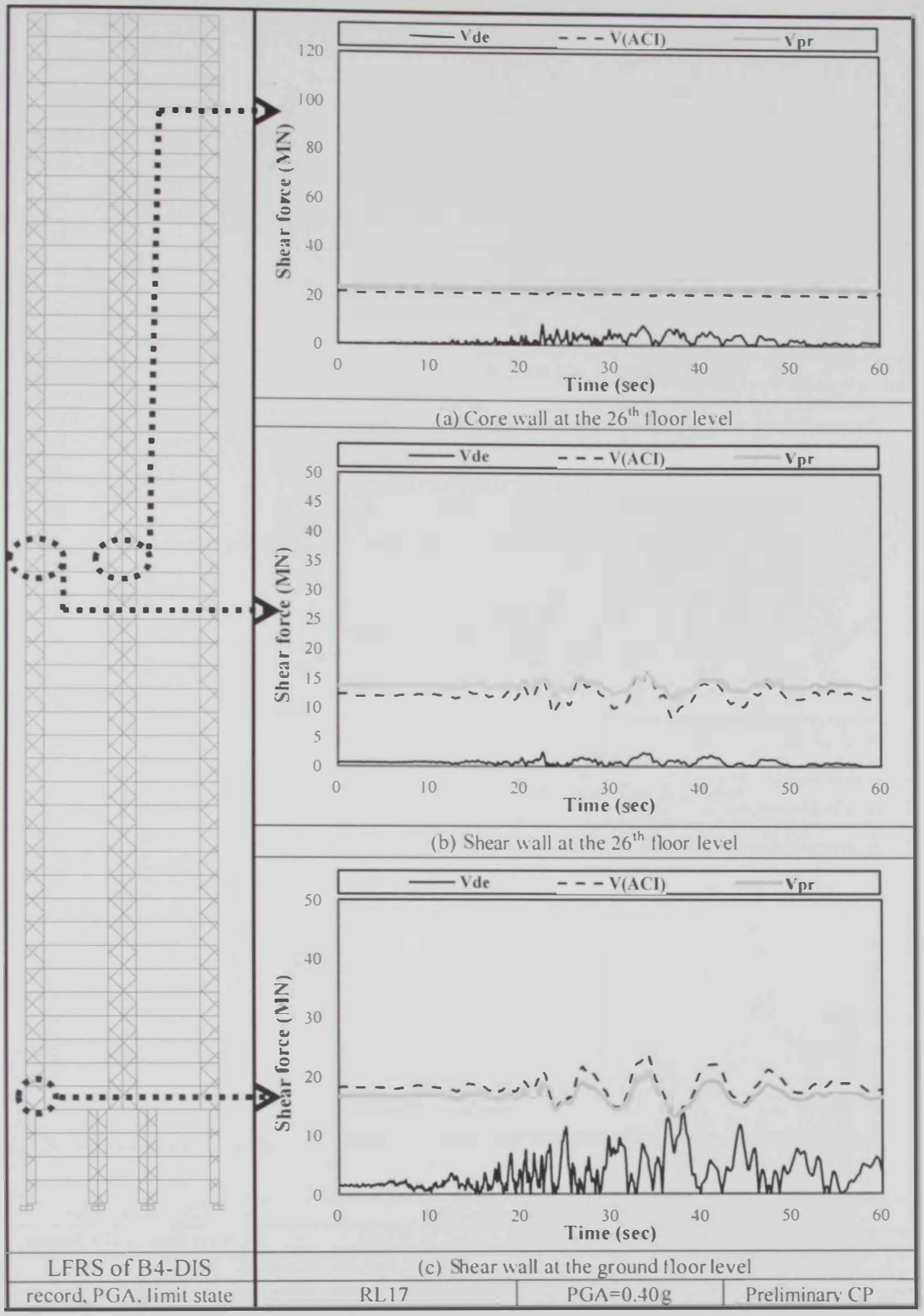

Figure 6.21: Shear demand using RL17 versus shear strength using ACI and Priestley et al. (1994) models for the core and shear walls of B4-DIS

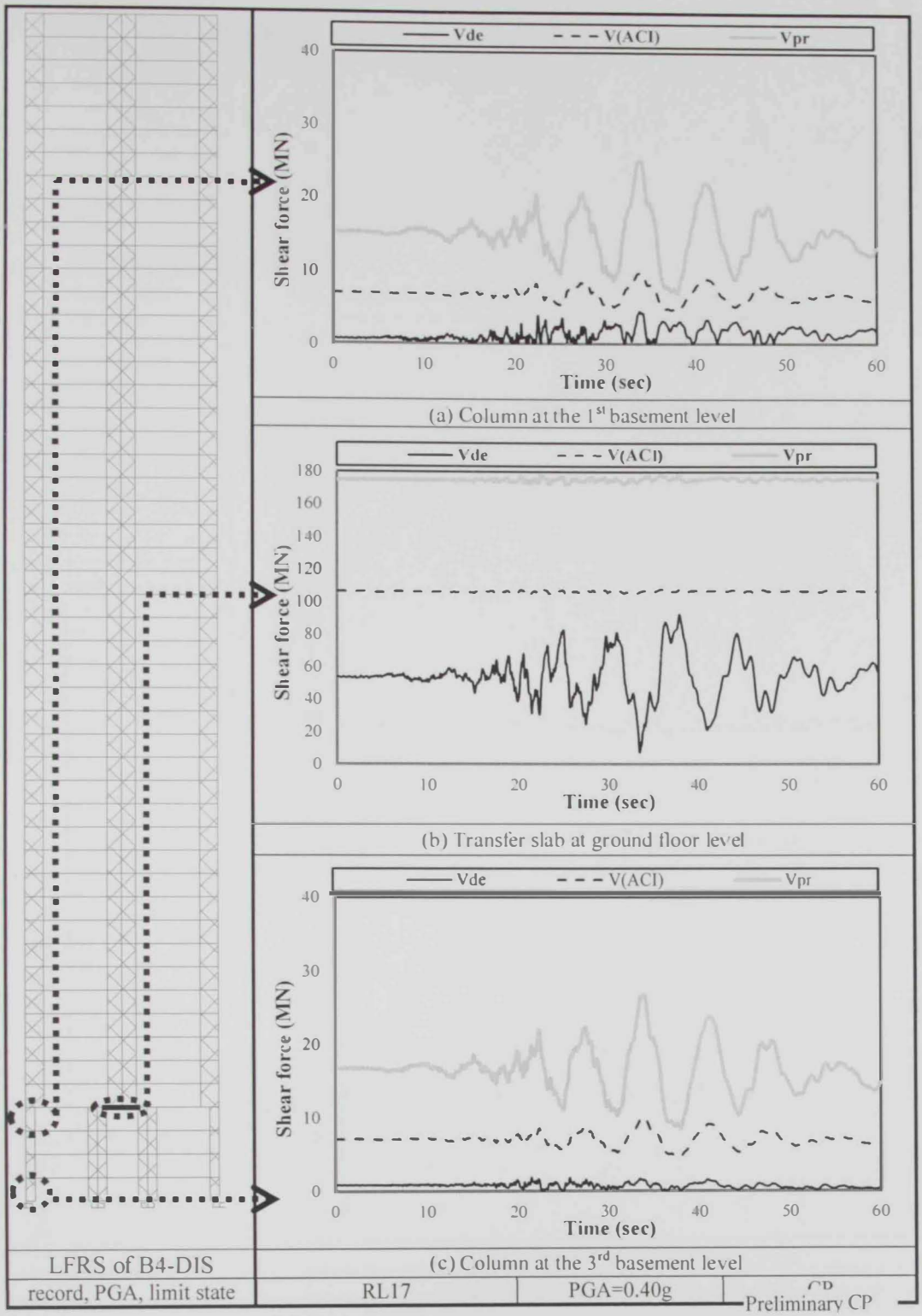

Figure 6.22: Shear demand using RL17 versus shear strength using ACI and Priestley et al. (1994) models for the columns and the transfer slab of B4-DIS

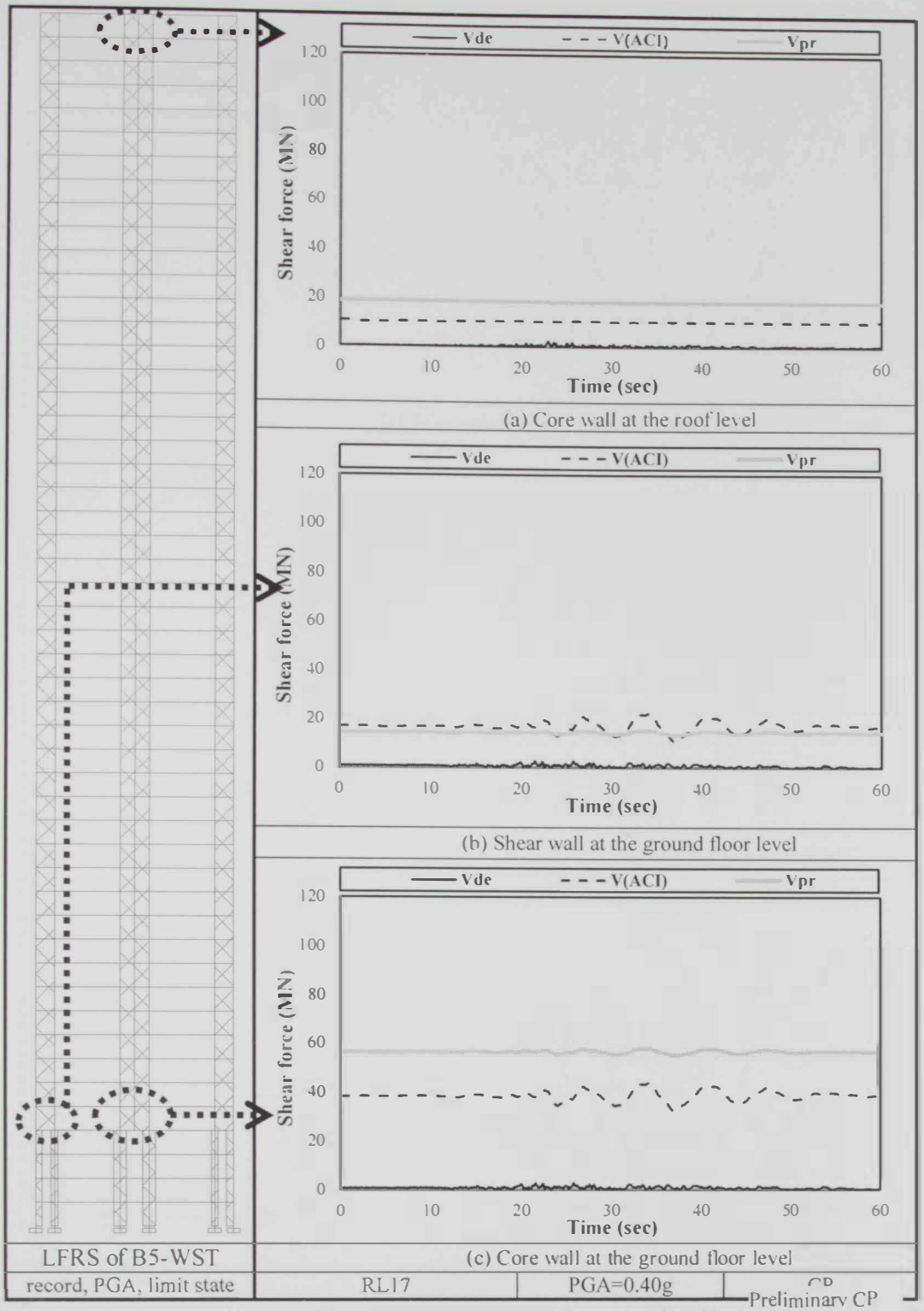

Figure 6.23: Shear demand using RL17 versus shear strength using ACI and Priestley et al. (1994) models for the core and the shear walls of B5-WSST

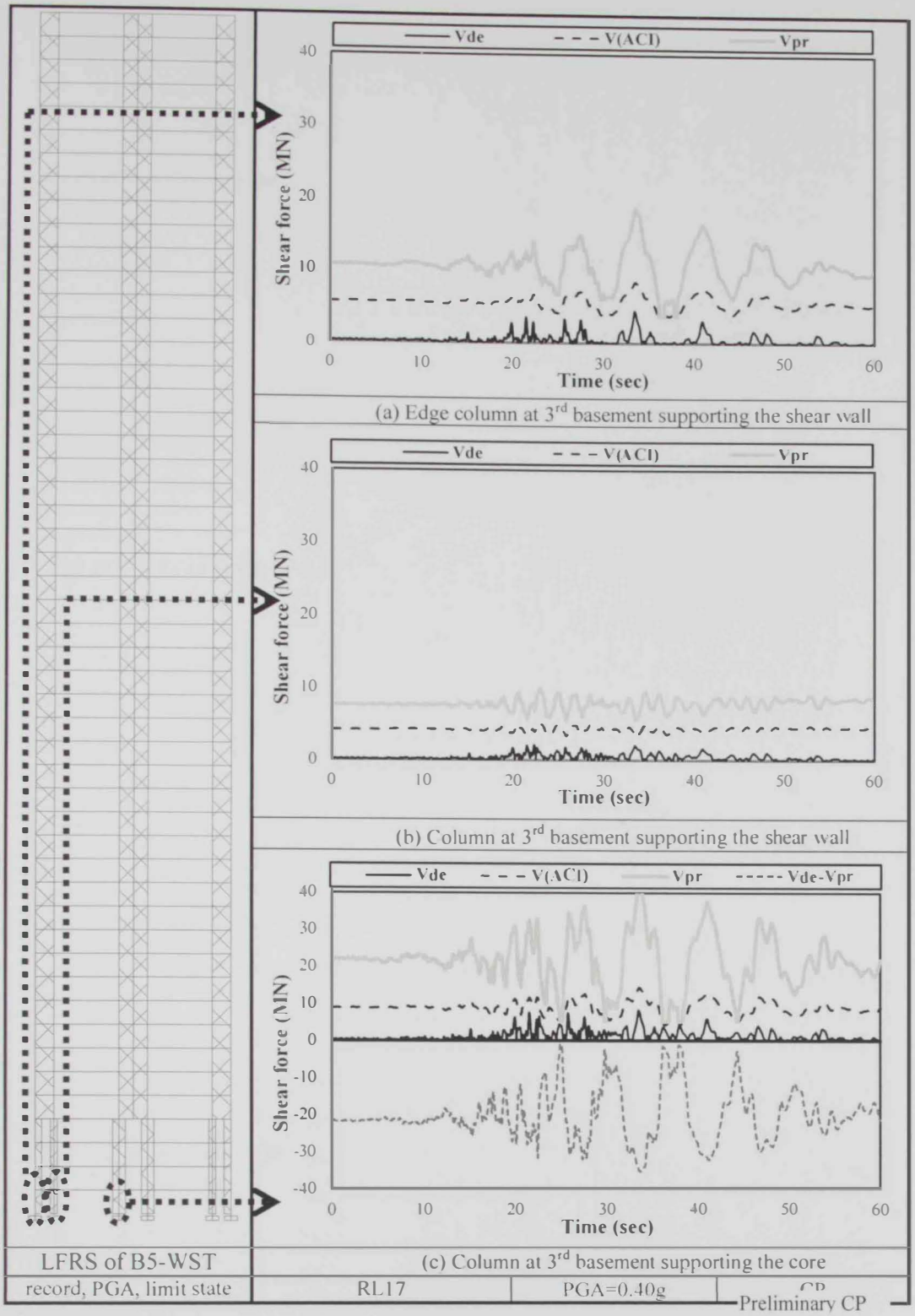

Figure 6.24: Shear demand using RL17 versus shear strength using ACI and Priestley et al. (1994) models for the columns of B5-WST at 3rd basement

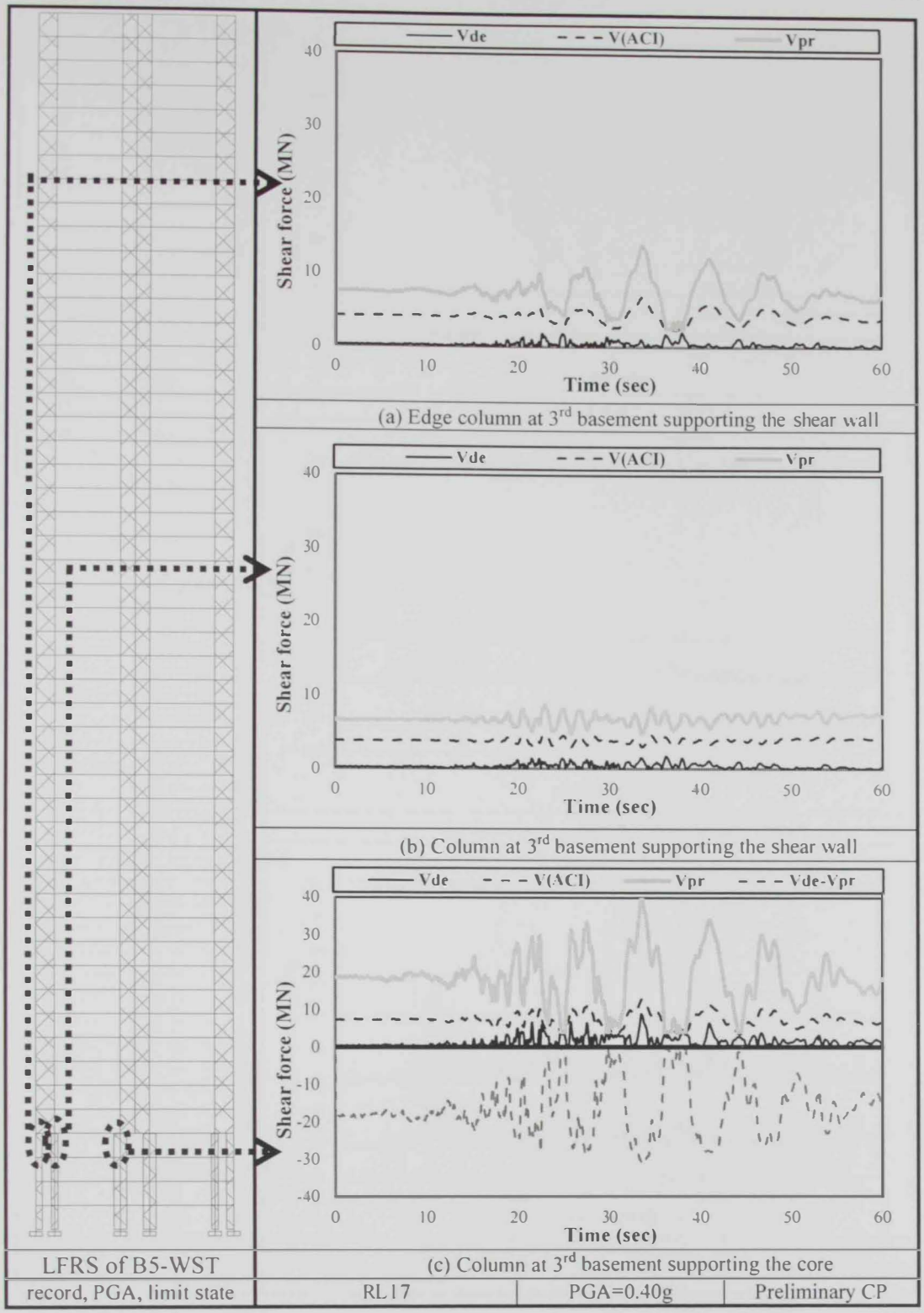

Figure 6.25: Shear demand using RL17 versus shear strength using ACI and Priestley et al. (1994) models for the columns of B5-WST at ground floor

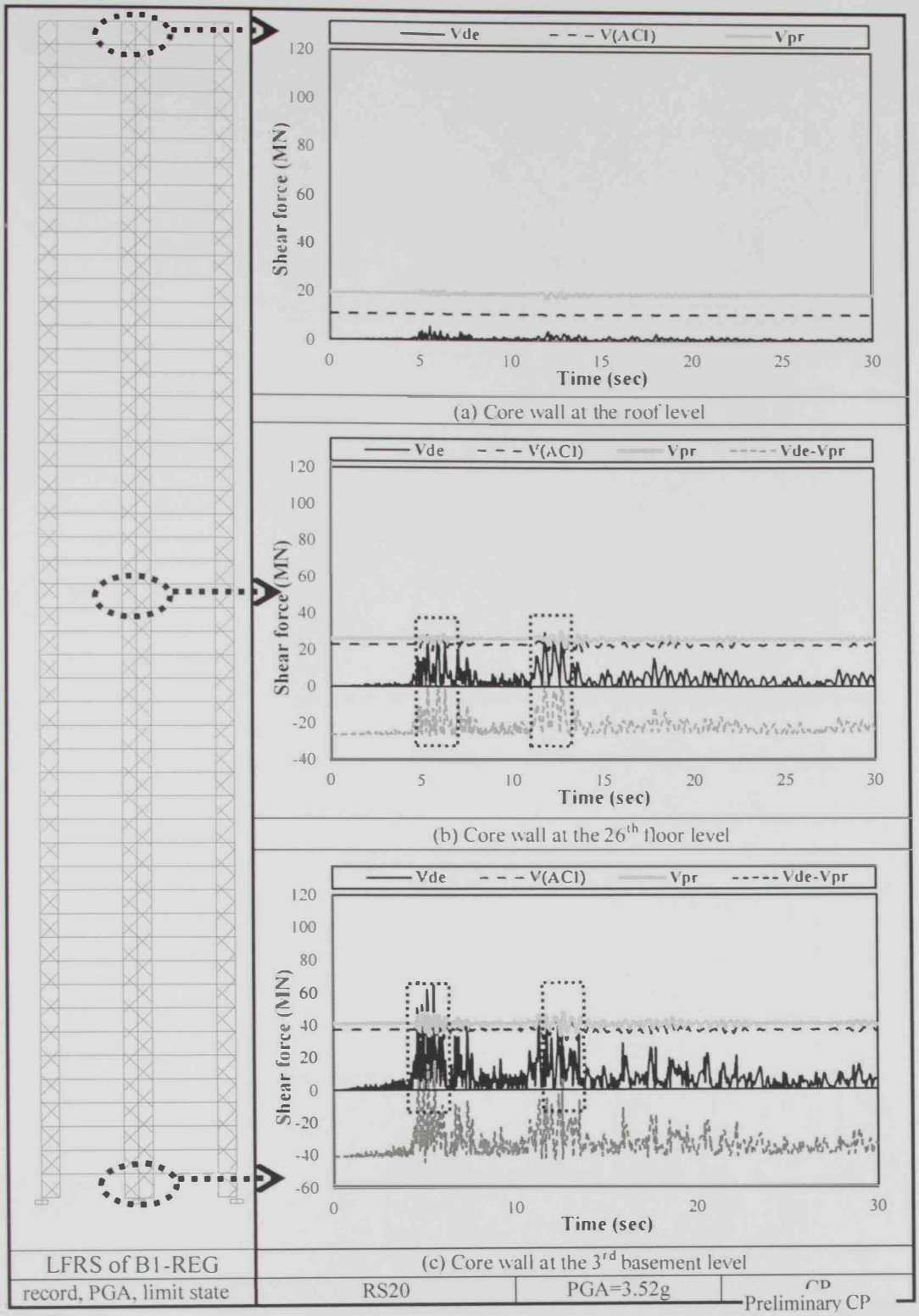

Figure 6.26: Shear demand using RS20 versus shear strength using ACI and Priestley et al. (1994) models for the core walls of B1-REG

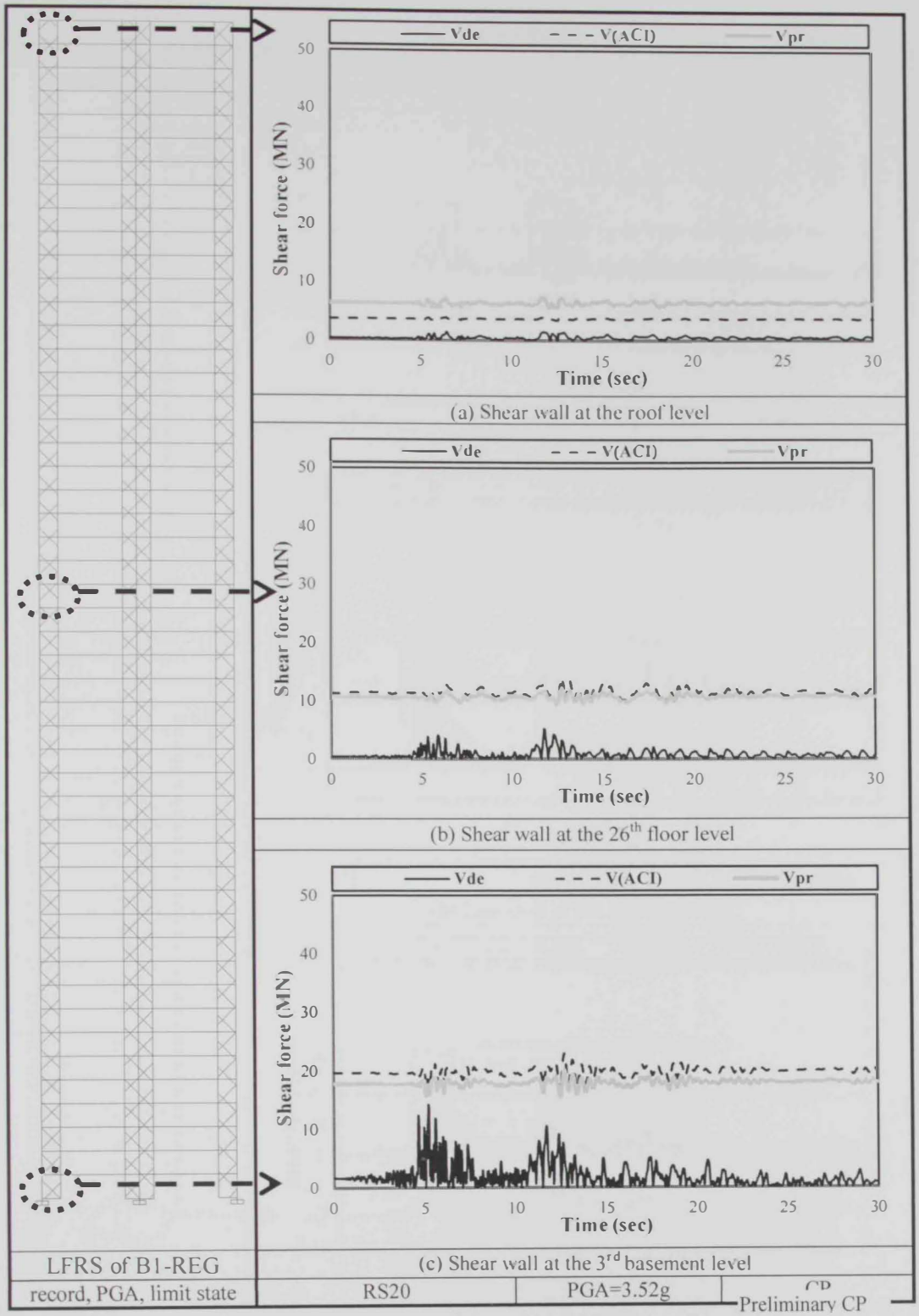

Figure 6.27: Shear demand using RS20 versus shear strength using ACI and Priestley et al. (1994) models for the shear walls of B1-REG

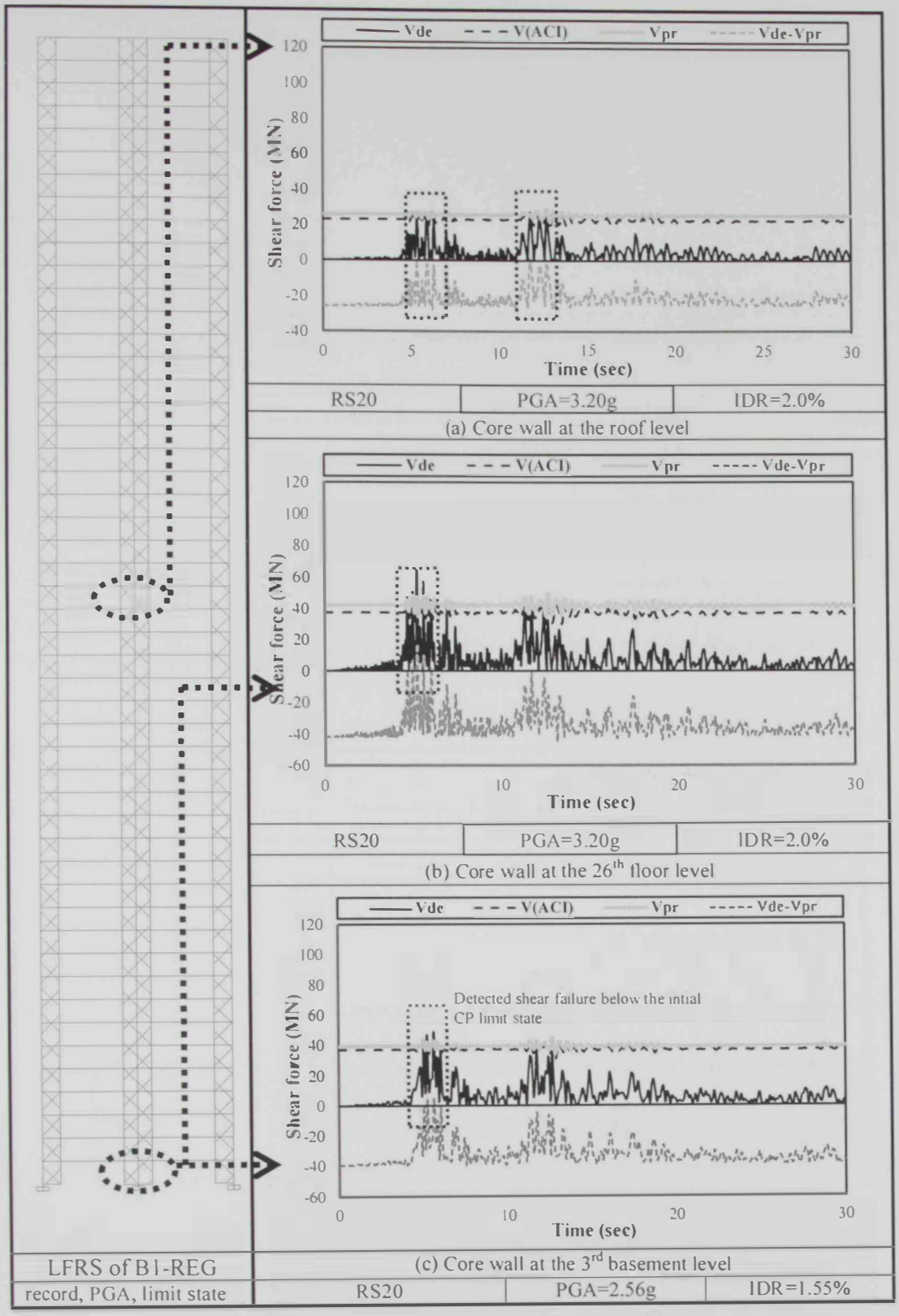

Figure 6.28: Shear demand using RS20 versus shear strength using ACI and Priestley et al. (1994) models for the core walls of B1-REG at a PGA of 3.2g and 2.56g

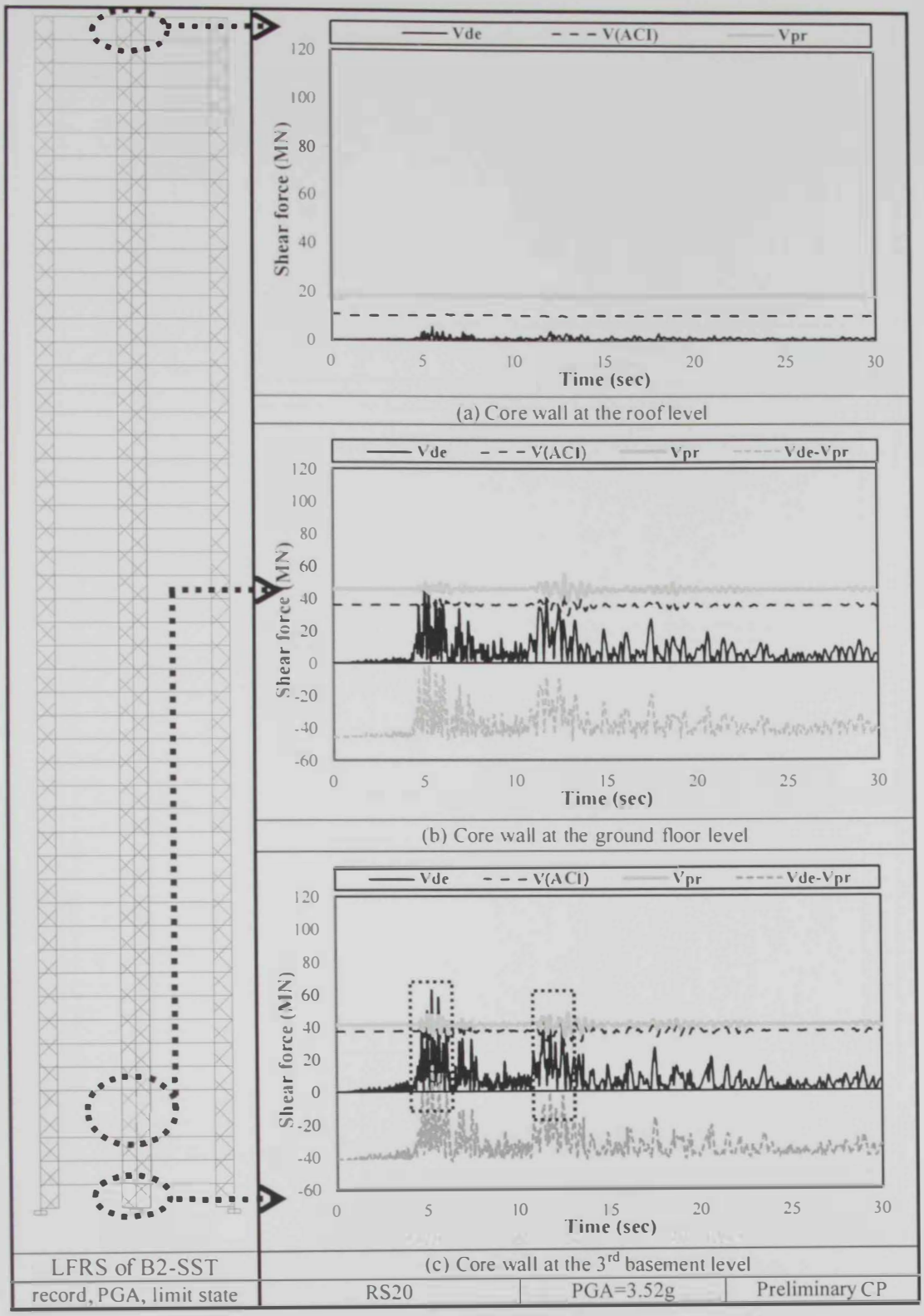

Figure 6.29: Shear demand using RS20 versus shear strength using ACI and Priestley et al. (1994) models for the core walls of B2-SST

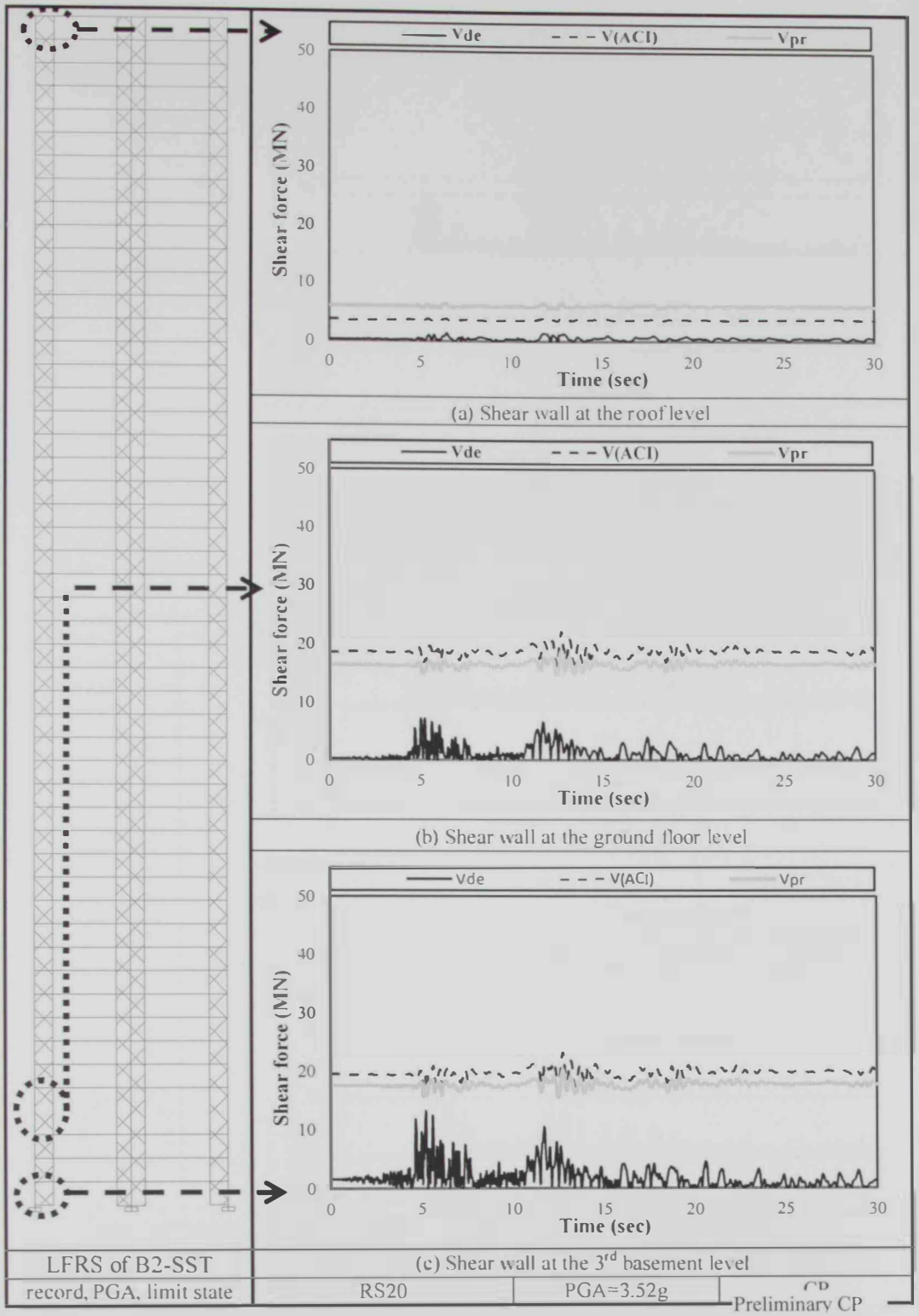

Figure 6.30: Shear demand using RS20 versus shear strength using ACI and Priestley et al. (1994) models for the shear walls of B2-SST building

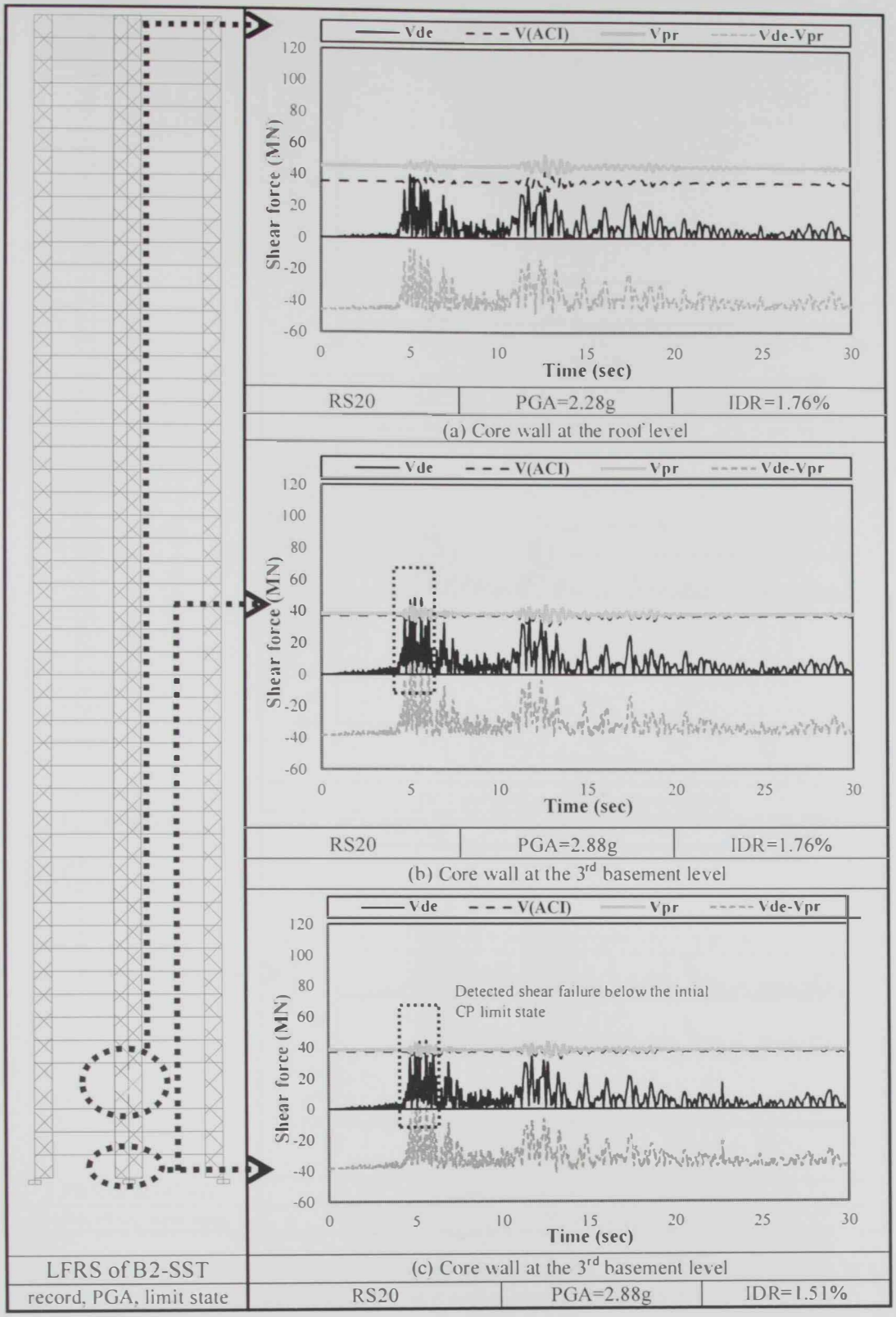

Figure 6.31: Shear demand using RS20 versus shear strength using ACI and Priestley et al. (1994) models for the core walls of B2-SST at a PGA of 2.88g and 2.56g

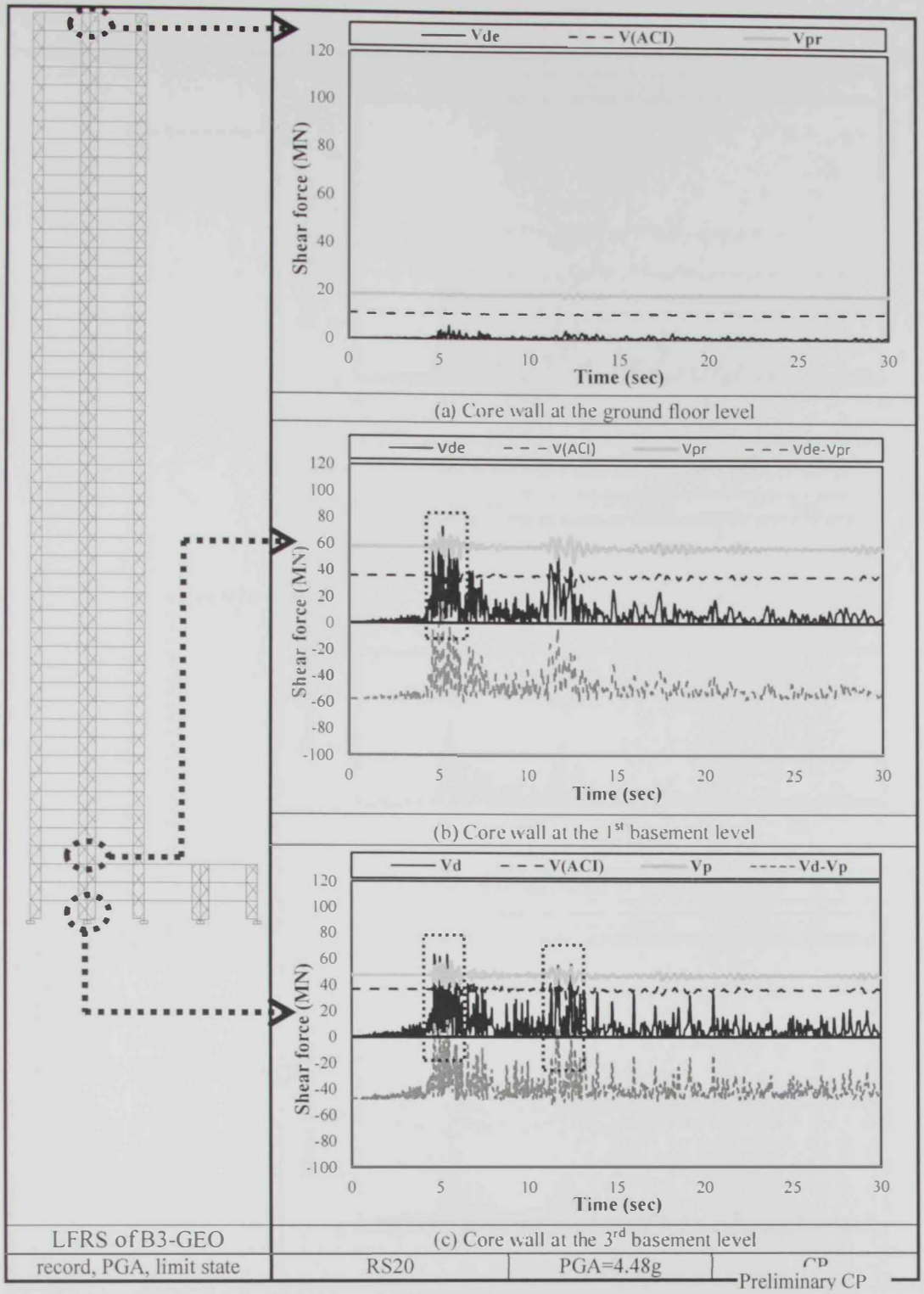

Figure 6.32: Shear demand using RS20 versus shear strength using ACI and Priestley et al. (1994) models for the core walls of B3-GEO

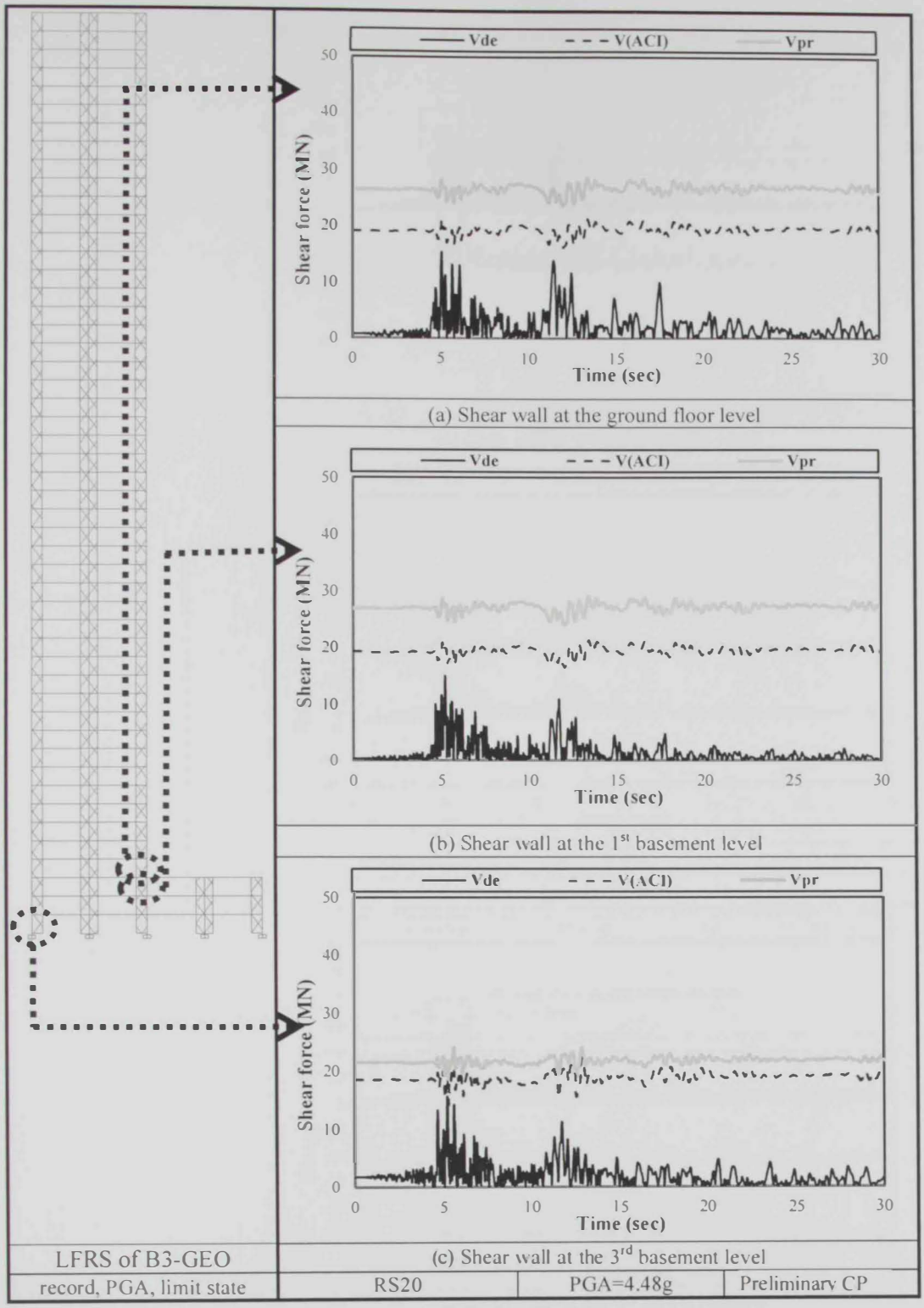

Figure 6.33: Shear demand using RS20 versus shear strength using ACI and Priestley et al. (1994) models for the shear walls of B3-GEO

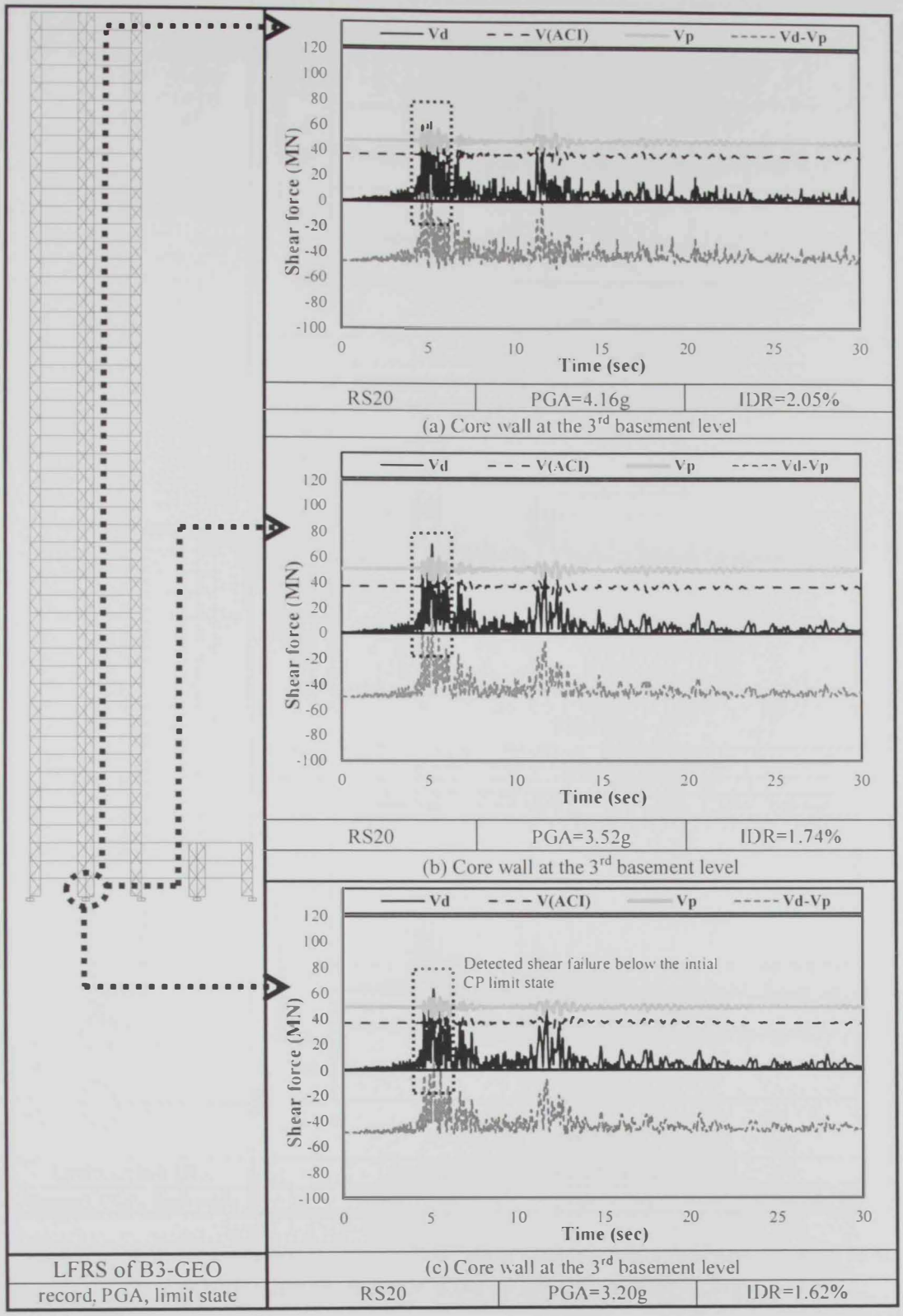

Figure 6.34: Shear demand using RS20 versus shear strength using ACI and Priestley et al. (1994) models for the core walls of B2-SST at a PGA of 4.16g, 3.52g and 3.20g

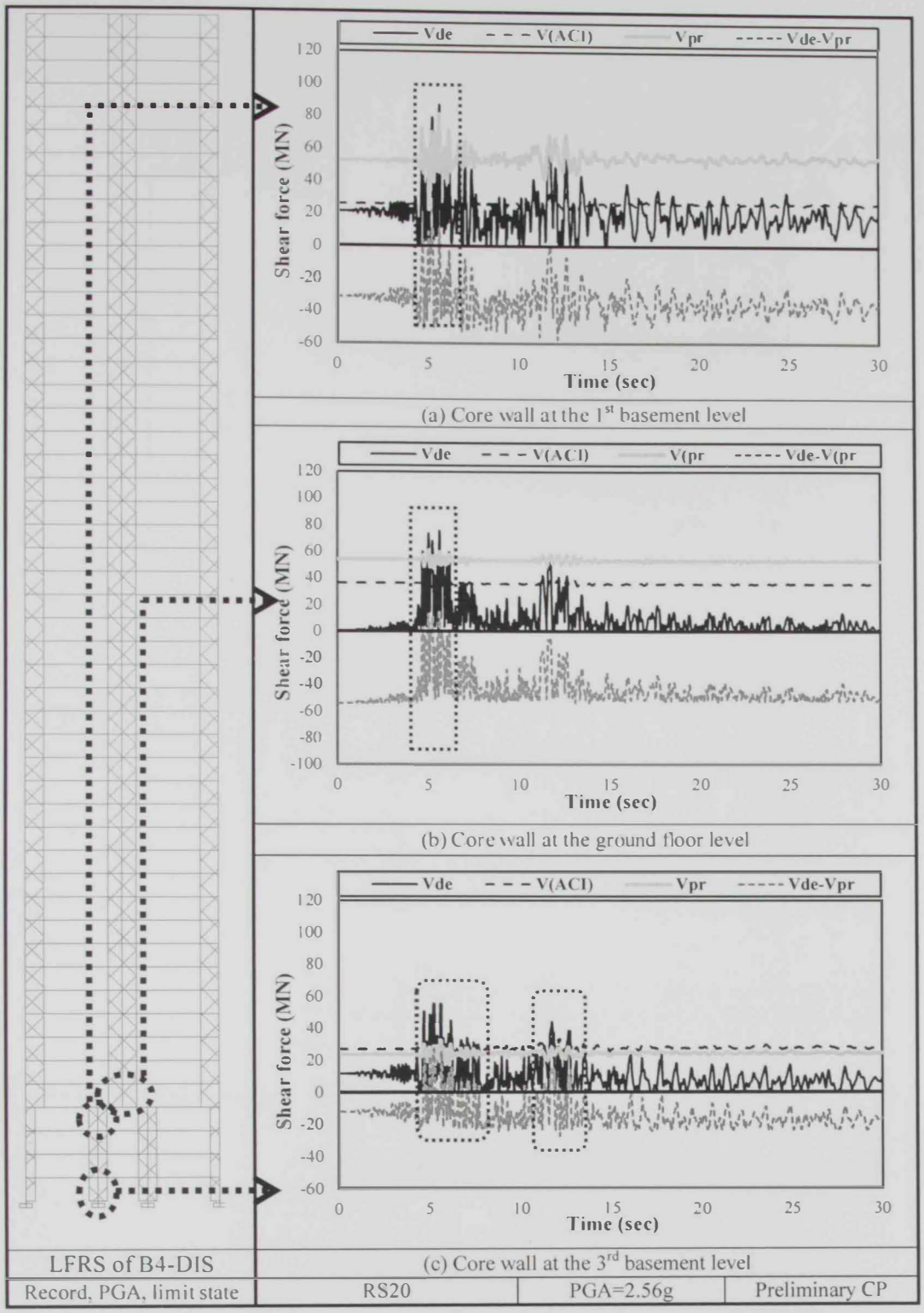

Figure 6.35 Shear demand using RS20 versus shear strength using ACI and Priestley et al. (1994) models for the core walls of B4-DIS at PGA=2.56g

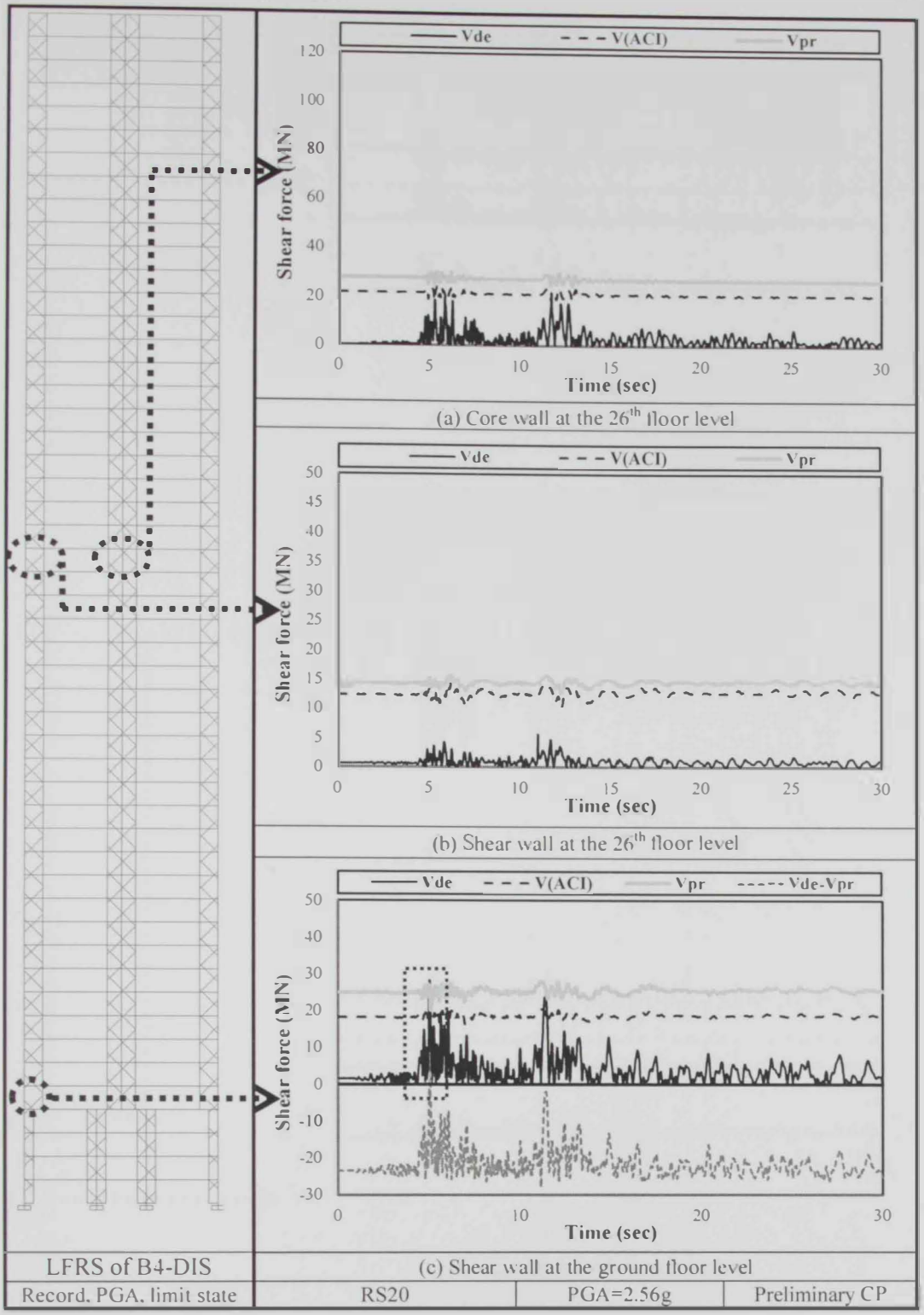

Figure 6.36 Shear demand using RS20 versus shear strength using ACI and Priestley et al. (1994) models for the core and shear walls of B4-DIS at PGA=2.56g

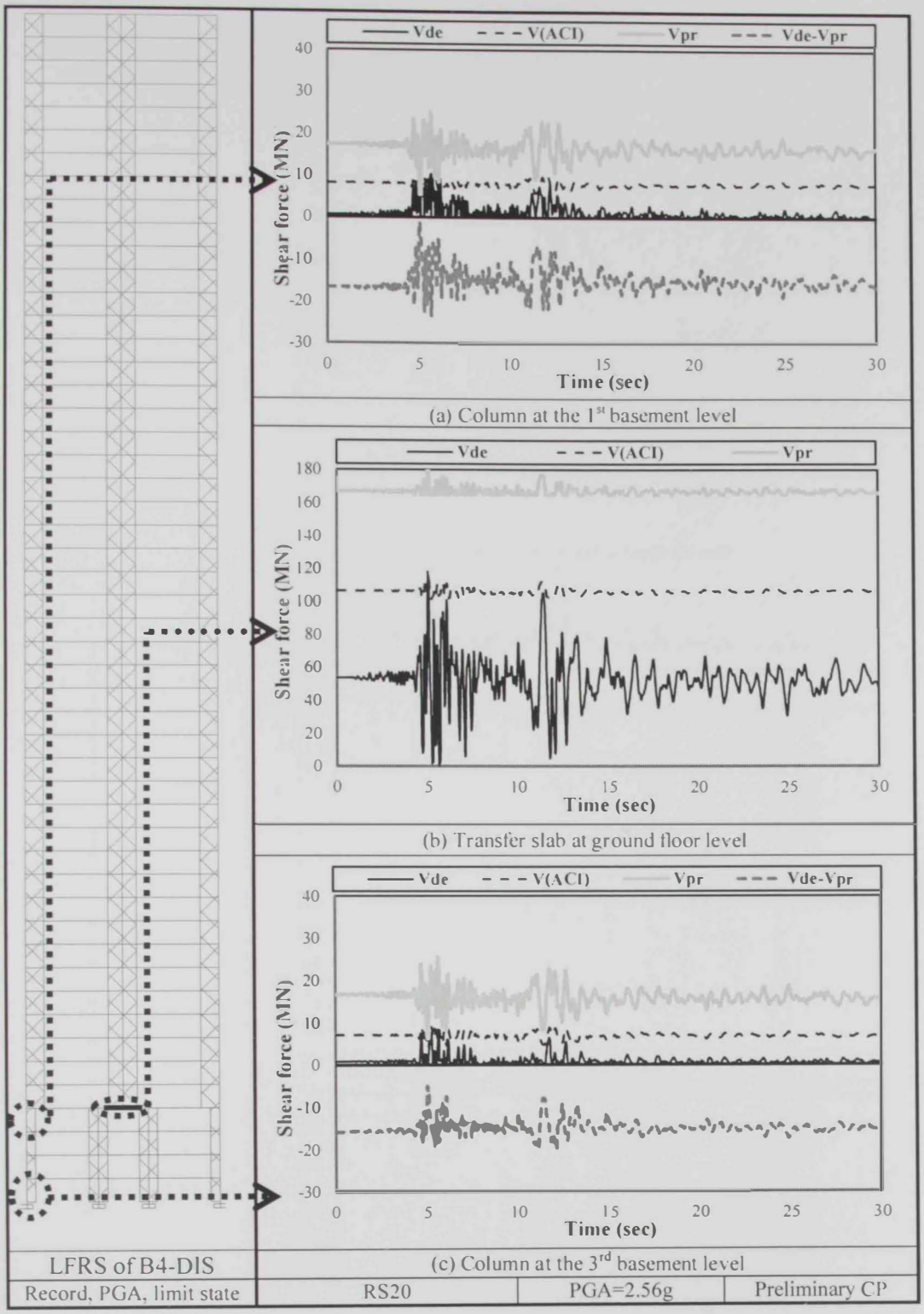

Figure 6.37: Shear demand using RS20 versus shear strength using ACI and Priestley et al. (1994) models for the transfer slab and the shear walls of B4-DIS at PGA=2.56g

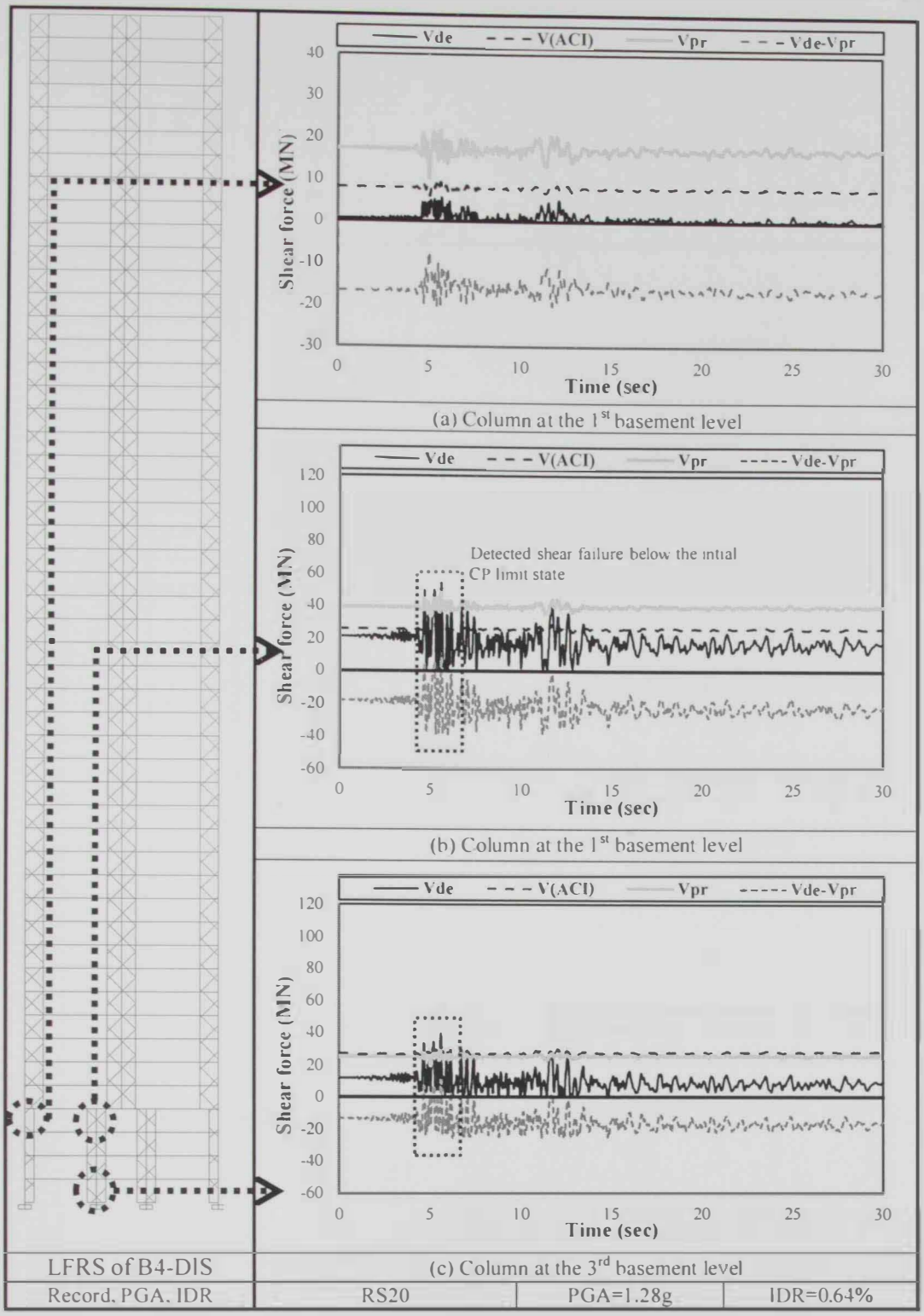

Figure 6.38: Shear demand using RS20 versus shear strength using ACI and Priestley et al. (1994) models for the core and the shear walls of B4-DIS at PGA=1.28g

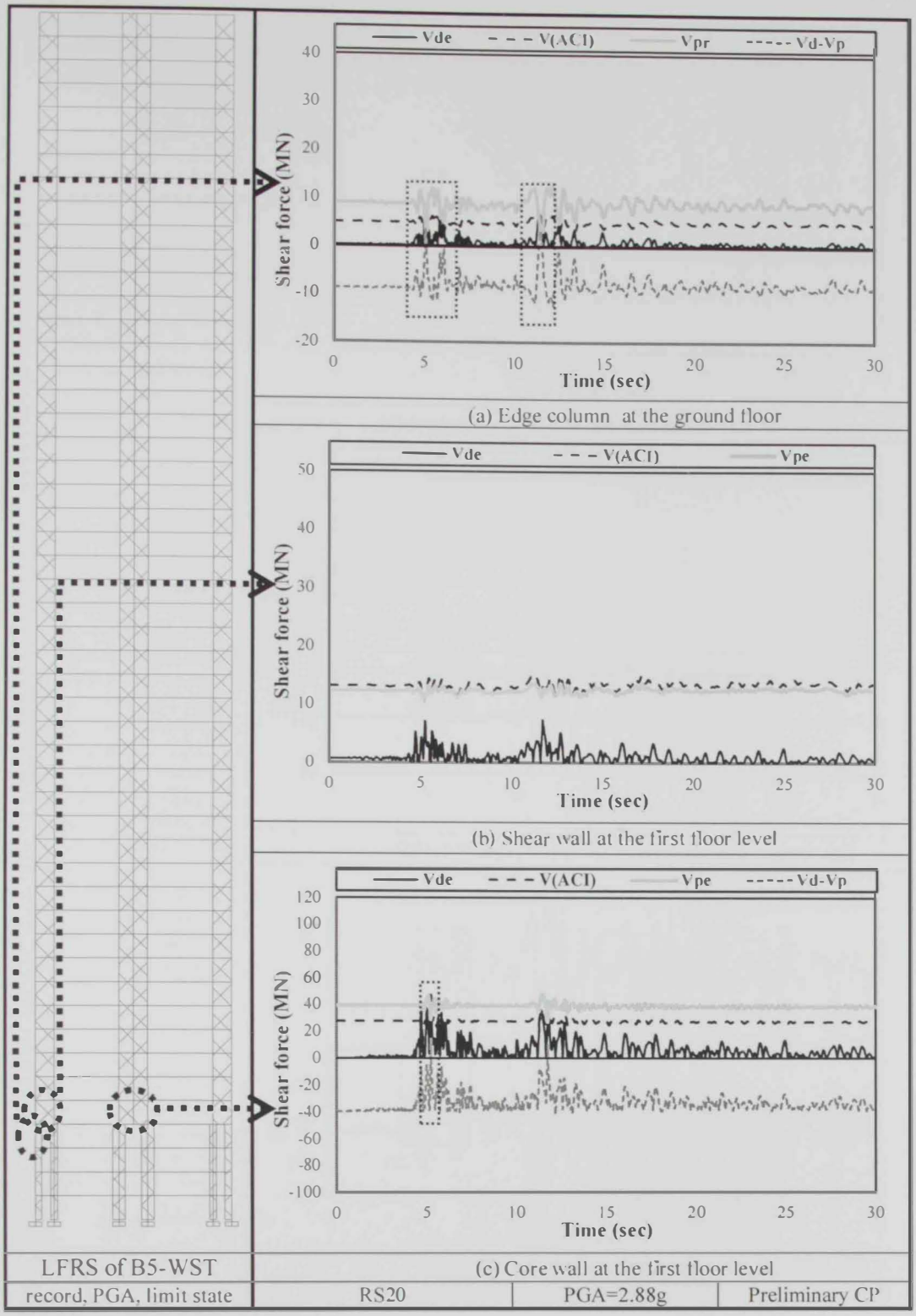

Figure 6.39: Shear demand using RS20 versus shear strength using ACI and Priestley et al. (1994) models for edge column, shear wall and core wall of B5-WST at PGA =2.88g

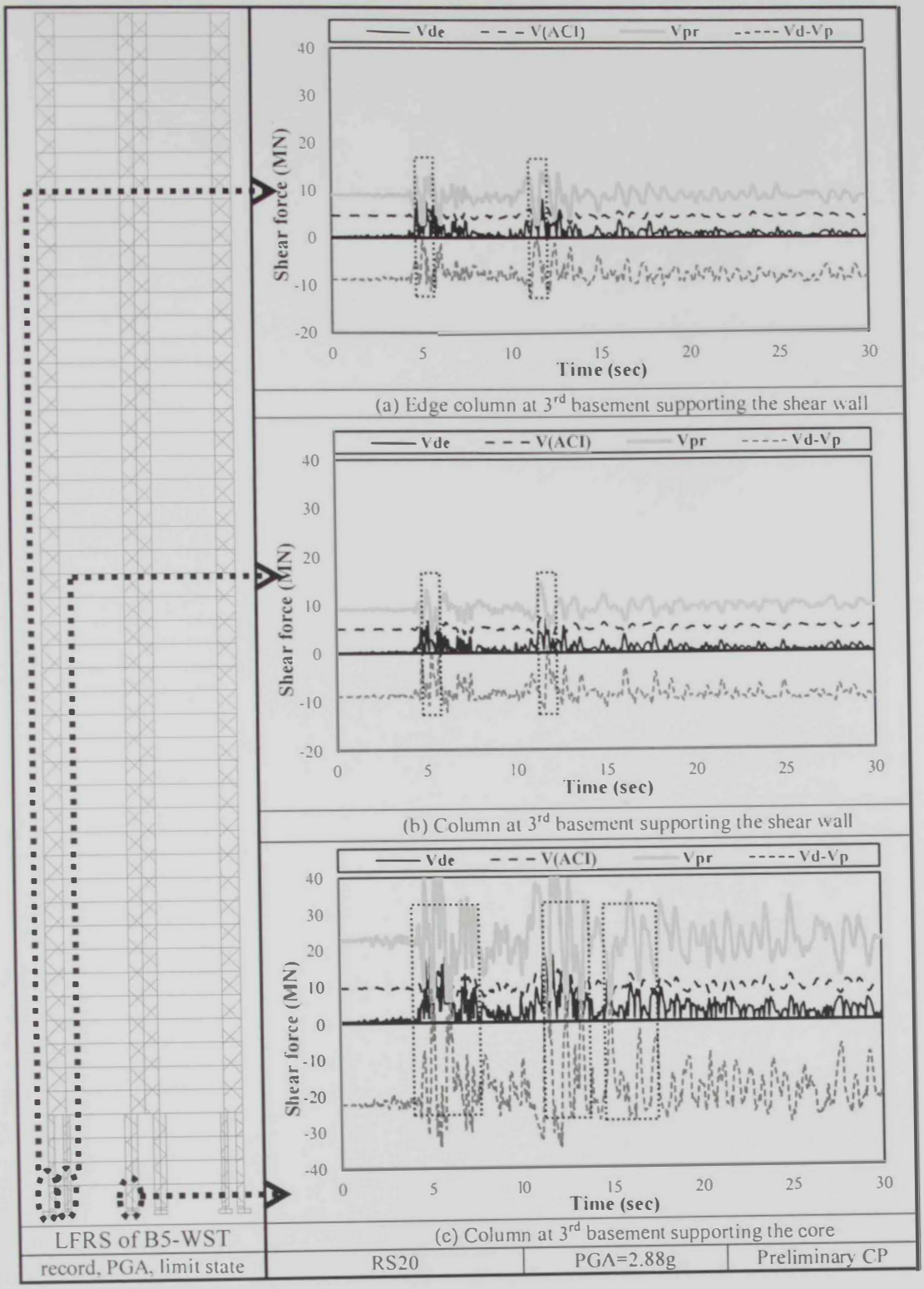

Figure 6.40: Shear demand using RS20 versus shear strength using ACI and Priestley et al. (1994) models for the 3rd basement columns of B5-WST at PGA =2.88g

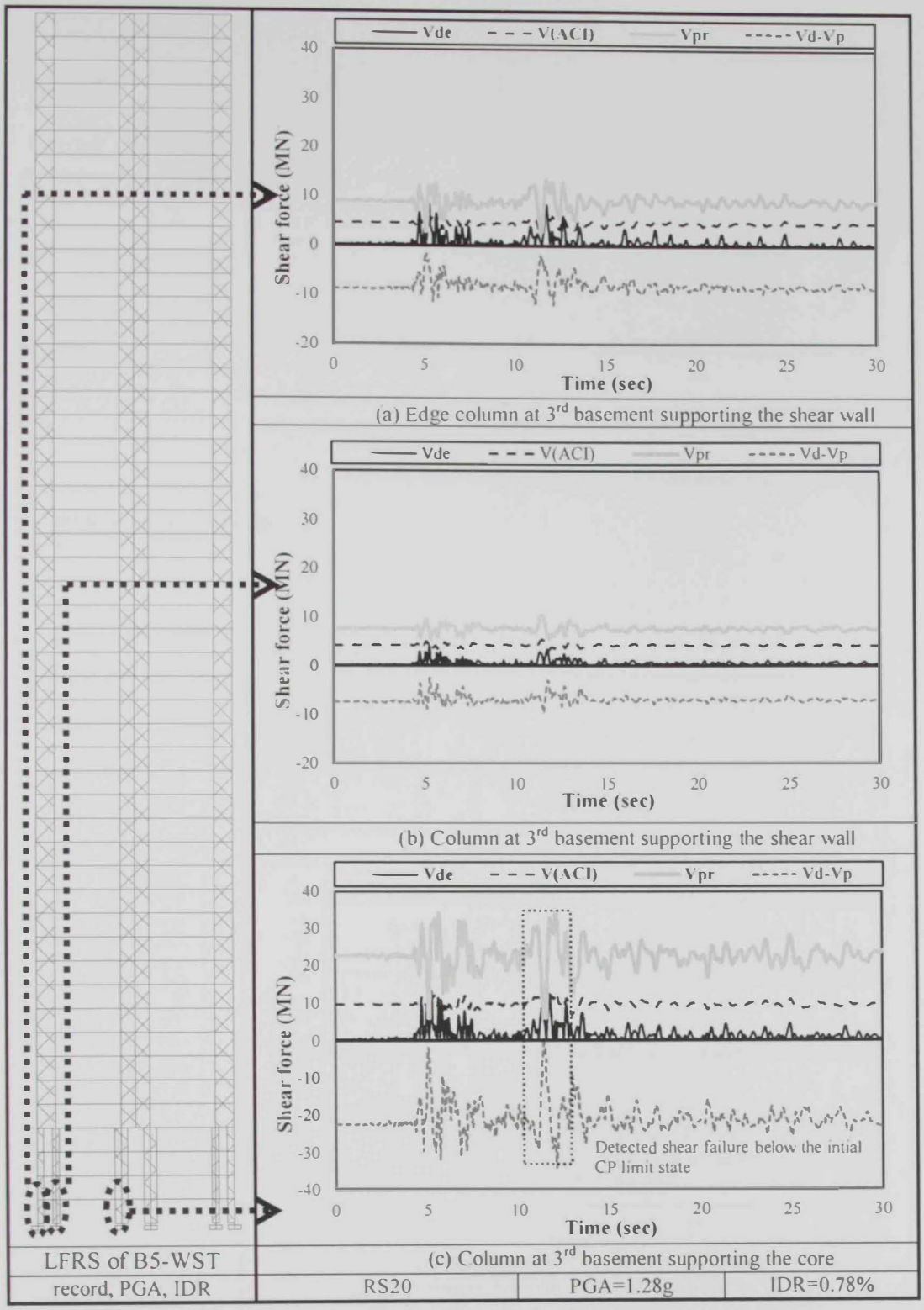

Figure 6.41: Shear demand using RS20 versus shear strength using ACI and Priestley et al. (1994) models for the 3rd basement columns of B5-WST at PGA =1.28g

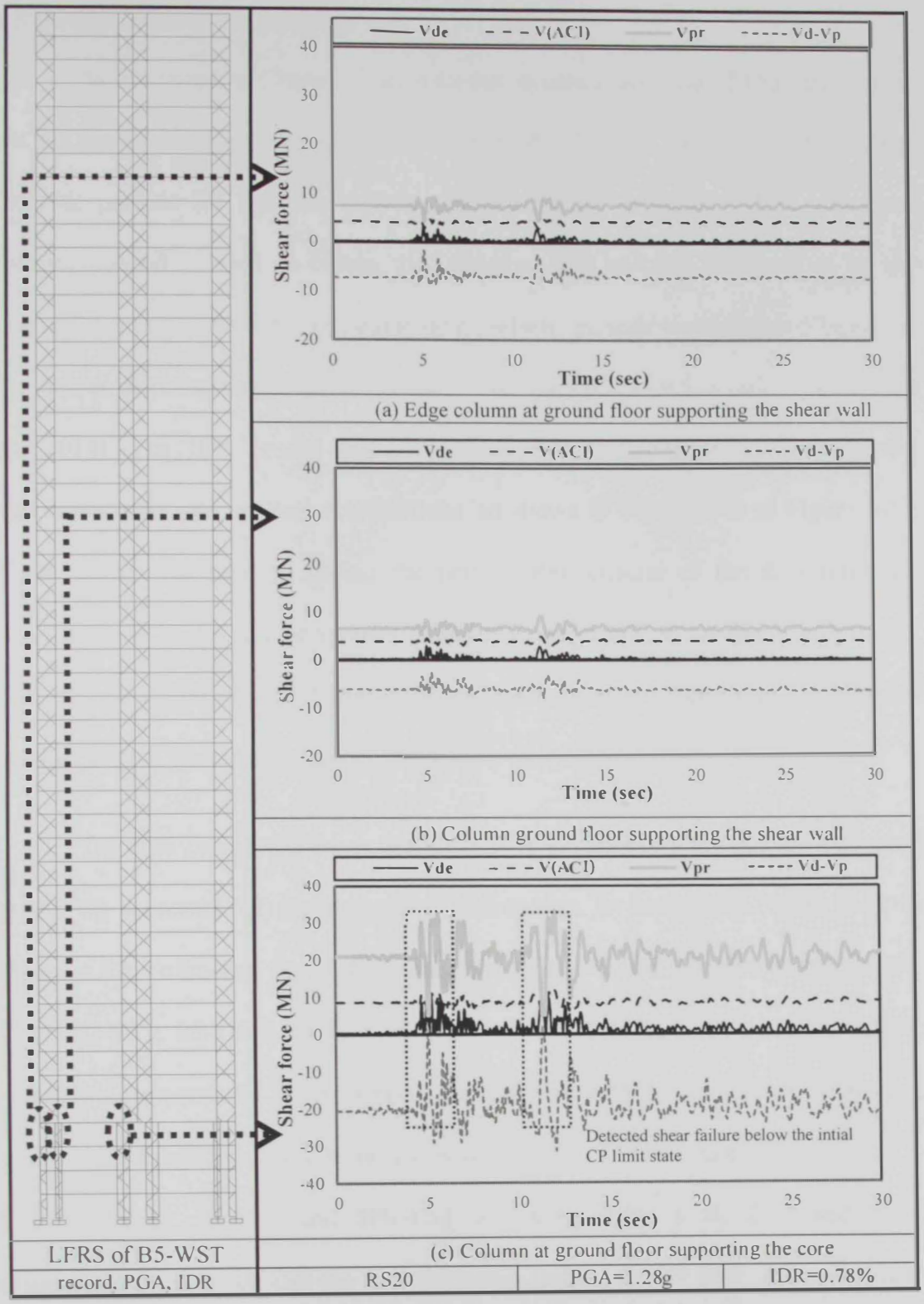

Figure 6.42: Shear demand using RS20 versus shear strength using ACI and Priestley et al. (1994) models for the ground floor columns of B5-WST at PGA =1.28g

6.5 Development of IDA curves

As discussed in Chapter 5, incremental dynamic analyses (IDAs) are carried out for the five reference buildings. In order to develop the IDA curves, equivalent inelastic periods for the five reference structures are calculated. The equivalent inelastic period is used to obtain the corresponding spectral acceleration of the twenty long period records. The equivalent inelastic periods are calculated based on the first three inelastic periods weighted by the mass participation ratios (Alwaile et al., 2014). The IDA results are used to develop the relationship between the maximum IDRs and spectral accelerations, as shown in Figure 6.43 to Figure 6.47. These curves are used to define the performance criteria of the five reference structures. the Immediate occupancy (IO) limit state is defined at the first deviation from the elastic response, while the CP limit state is determined when the stiffness reaches 20% of the elastic value (Vamvatsikos and Cornell, 2002).

The IDR corresponding to the IO and CP performance criteria are estimated at the 16 percentile of the lognormal distribution, as shown in Figure 6.43 to Figure 6.47. Following the above-mentioned approach, the IO limit states of B1-REG, B2-SST, B3-GEO, B4-DIS and B5-WST are 0.49%, 0.48%, 0.51%, 0.27%, and 0.44%, respectively. These limits are consistent with the local response results, as discussed hereafter. The IDR corresponding to the CP limit state of B1-REG, B2-SST, B3-GEO, B4-DIS and B5-WST are 4.97, 4.56, 6.08, 2.17 and 3.61, respectively. It is noted that the IDR corresponding to the CP limit state calculated using the IDA curves are significantly higher than those obtained from THA and previous studies, as discussed hereafter.

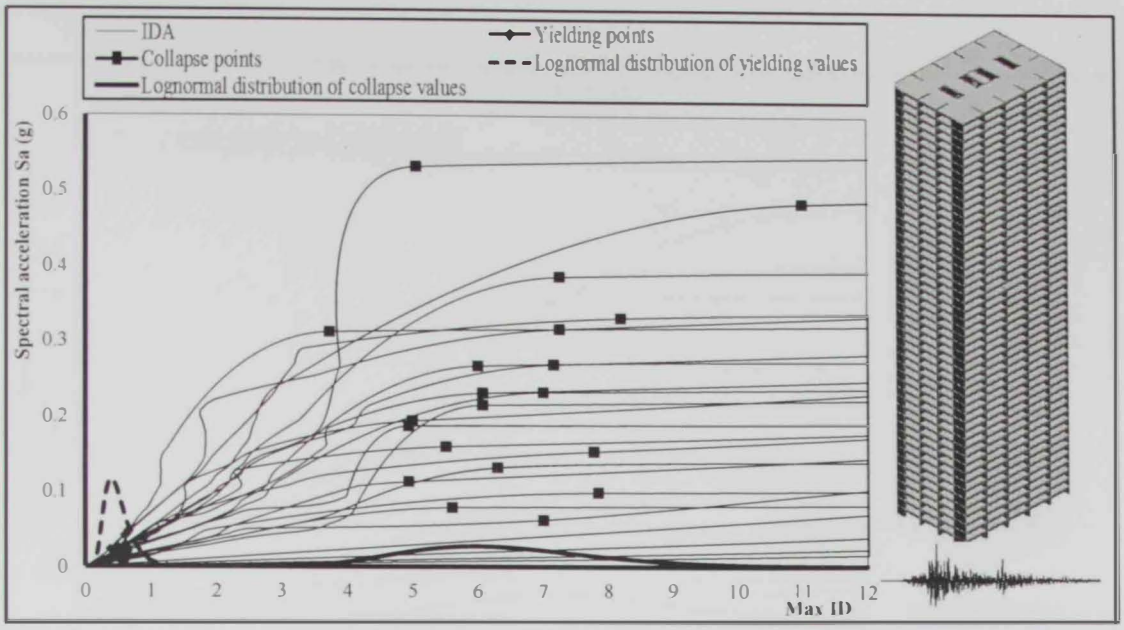

Figure 6.43: IDA curves of B1-REG showing the first yielding and collapse points as well as the lognormal distributions of the yielding and collapse points

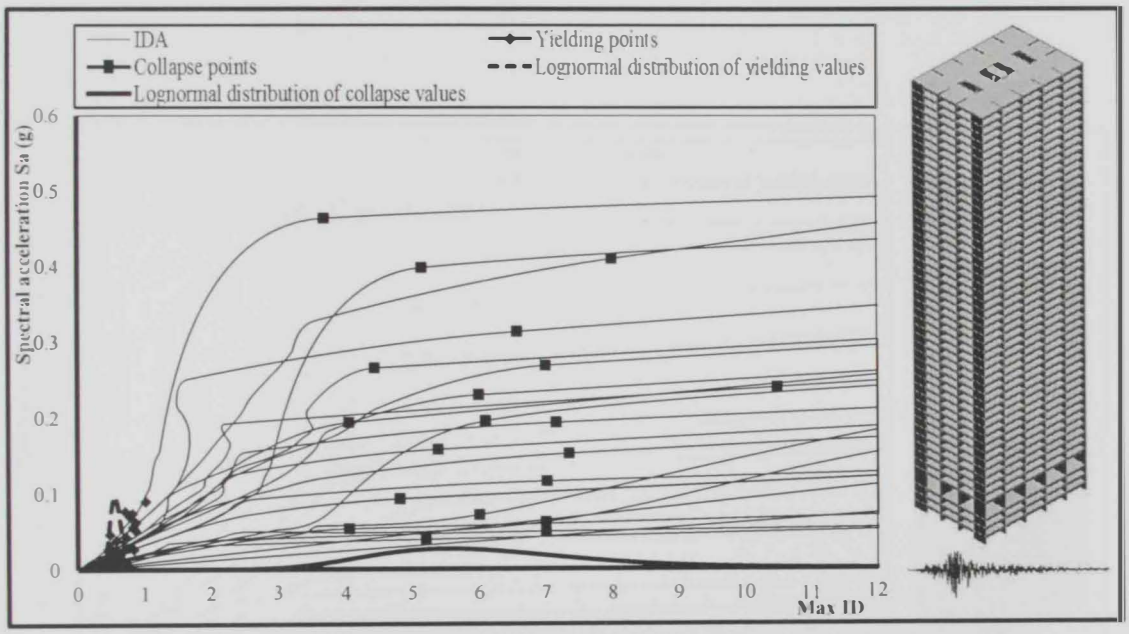

Figure 6.44: IDA curves of B2-SST showing the first yielding and collapse points as well as the lognormal distributions of the yielding and collapse points

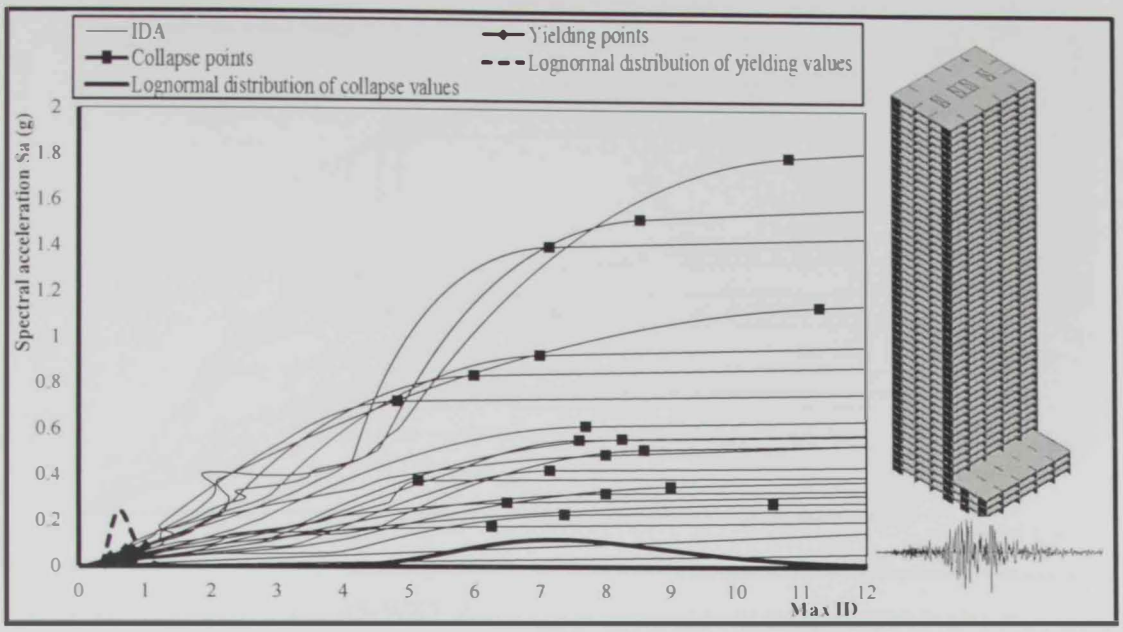

Figure 6.45: IDA curves of B3-GEO showing the first yielding and collapse points as well as the lognormal distributions of the yielding and collapse points

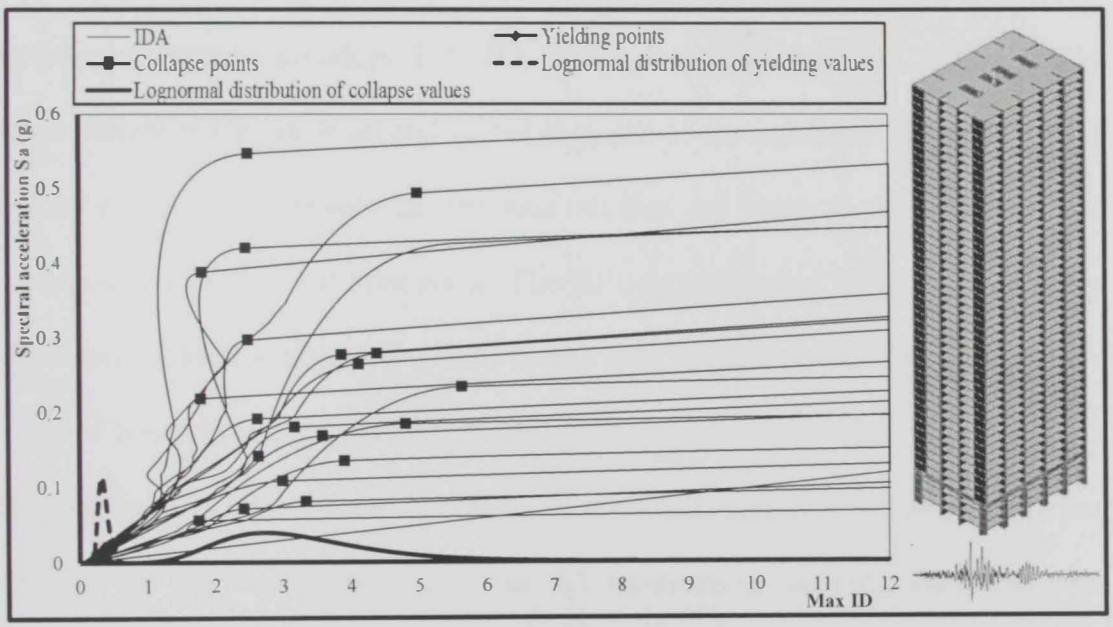

Figure 6.46: IDA curves of B4-DIS showing the first yielding and collapse points as well as the lognormal distributions of the yielding and collapse points

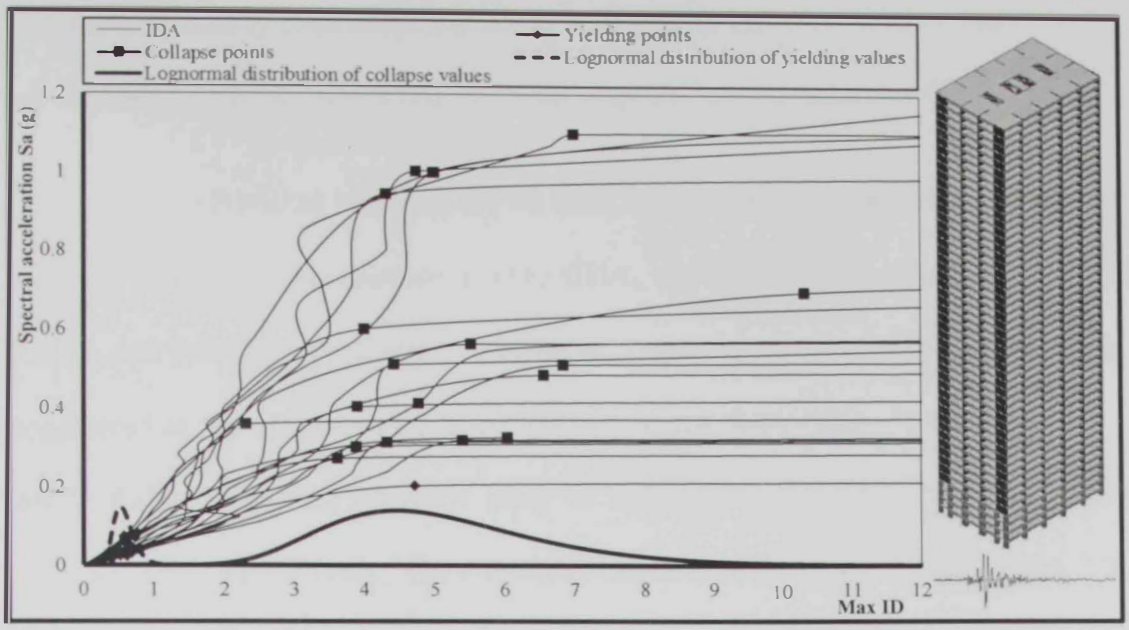

Figure 6.47: IDA curves of B5-WST showing the first yielding and collapse points as well as the lognormal distributions of the yielding and collapse points

6.6 Performance criteria

Based on the literature review presented in Chapter 2, the following three performance criteria are adopted: (i) IO, (ii) LS, and (iii) CP (ASCE/SEI-41, 2007). In the current study, the local and global response of the reference structures as well as the experimental results of previous studies are used to identify the IDR corresponding to different limit states. The IDR corresponding to the first indication of reinforcing steel yielding represents the IO limit state, while the first indication of confined concrete crushing in vertical structural elements indicates the CP limit state. This approach is initially used to estimate the performance criteria from IPOAs and IDAs of the reference structures. Table 6.1 summarizes the limit states from the previous studies undertaken by Ghobarah (2004), Li et al. (2006), Lee and Ko (2007) Beyer et al. (2008), Panagiotou et al. (2010), and Lehman et al. (2013) in addition to the results of different analyses conducted in the present study. It important to note

that, the preliminary limit states presented in this table using the current study results are evaluated without considering the shear response of structural members.

For the B1-REG building, the IO limit states obtained from IPOAs as well as the local and global response from IDAs (IDA_L and IDA_G, respectively) are 0.95%, 0.61%, and 0.49%, respectively. To be on the conservative side, the IDA results are considered at the 16 percentile. It is shown that the IDA_G value is consistent with ASCE-7 (2010) and the previous study of Lehman et al. (2013), and hence it is adopted in the current study. The CP limit state of B1-REG significantly varies. The most conservative value proposed in the experimental study of Lehman et al. (2013) is adopted in this study. The selected IDR corresponding to the CP limit state is 2.27%, which is slightly higher than that proposed by ASCE/SEI-41 (2007).

For the irregular structures, the IO limit state is obtained from the most conservative value of the conducted analyses (i.e. IDA_G). For B2-SST, B3-GEO, B4-DIS and B5-WST, the IO limit state is 0.48%, 0.51%, 0.27% and 0.44%, respectively. Due to the insufficient experimental studies and the lack of code recommendations for the CP limit state of irregular high-rise buildings as well as the dispersion of the results observed from the present study, the most conservative CP limit state (i.e. from IDA_L) are adjusted using the regular building CP value (i.e. 2.27). The aforementioned approach results in CP limit states of 2.26%, 2.39%, 1.18% and 1.38% for B2-SST, B3-GEO, B4-DIS and B5-WST, respectively. It is important to note that the selected CP performance criteria of B4-DIS and B5-WST are conservative and in line with those recommended in the previous experimental studies by Li et al. (2006) and Lee and Ko (2007), as shown in Table 6.1. Finally, the LS limit state represents a significant damage sustained by the structure and accounts

for a reasonable margin of safety against collapse. This margin is considered 50% of the CP performance criteria (ASCE/SEI-41, 2007).

Table 6.1: Preliminary limit states of reference buildings without shear assessment

Selection approach		Reference structure														
		B1-REG			B2-SST			B3-GEO			B4-DIS			B5-WST		
		Limit state – interstory drift (%)														
		IO	LS*	CP	IO	LS*	CP	IO	LS*	CP	IO	LS*	CP	IO	LS*	CP
ASCE 41-07		0.50	1.00	2.00												
Previous studies	Ghobarah (2004)	0.40	1.50	2.50												
	Li et al. (2006)												1.25			
	Lee and Ko (2007)															1.57
	Beyer et al. (2008)	0.30		2.40												
	Panagiotou et al. (2010)	0.35	0.89	2.36												
	Lehman et al. (2013)	0.50	1.00	2.27												
Current study	IPOA	0.95		2.68	0.95		2.62	0.95		2.75	0.31		1.45	0.74		1.60
	IDA_L - 16%	0.61		3.07	0.61		3.06	0.79		3.23	0.39		1.60	0.55		1.86
	IDA_L - 50%	0.70		3.46	0.71		3.44	0.92		3.66	0.47		1.95	0.64		2.23
	IDA_L - 84%	0.81		3.89	0.82		3.86	1.08		4.16	0.55		2.38	0.74		2.69
	IDA_G - 16%	0.49		4.97	0.48		4.56	0.51		6.08	0.27		2.17	0.44		3.61
	IDA_G - 50%	0.60		6.31	0.56		5.93	0.66		7.61	0.34		3.08	0.56		4.90
	IDA_G - 84%	0.74		8.02	0.65		7.71	0.86		9.52	0.41		4.36	0.72		6.67
Preliminary selected limit state		0.49	1.14	2.27	0.48	1.13	2.26	0.51	1.20	2.39	0.27	0.59	1.18	0.44	0.69	1.38

IO: Immediate Occupancy, LS: Life Safety, CP: Collapse Prevention,
IPOA: Inelastic Pushover Analysis at first indication of yield and confined concrete crushing,
IDA_L: Limit states are based on the local response (first indication of reinforcing steel yield and confined concrete crushing) obtained from Incremental Dynamic Analysis,
IDA_G: Limit states are based on the global response (first indication of global yield and collapse) obtained from Incremental Dynamic Analysis (Vamvatsikos and Cornell, 2002),
* LS limit state is considered 50% of the CP counterpart

The preliminary limit states shown in Table 6.1 are re-evaluated based on the shear response assessment, as discussed in Section 6.4.3. The CP limit states of the benchmark buildings are not influenced under the effect of long period earthquake records, as shown in Table 6.2. In contrast, the shear response assessment results using the short period records have a significant effect on the CP limit states of the five reference buildings, as shown in Table 6.2. Accordingly, it is decided to select two groups of limit states depending on the earthquake scenario, as shown in Table 6.3. Since the LS and CP limit states of B5-WST are close to each other, the LS limit

state is eliminated for the near-field earthquake scenario. Table 6.3 depicts the final limit states of the five reference structures.

Table 6.2: Impact of shear response on limit states from different earthquake scenarios

Record scenario	Reference structure														
	B1-REG			B2-SST			B3-GEO			B4-DIS			B5-WST		
	Limit state – interstory drift (%)														
	IO	LS	CP	IO	LS	CP	IO	LS	CP	IO	LS	CP	IO	LS	CP
Long period records	-	-	-	-	-	-	-	-	-	-	-	-	-	-	-
Short period records	-	-	1.55	-	-	1.50	-	-	1.62	-	-	0.64	-	-	0.78

[-] Not affected

Table 6.3: Final limit states of reference buildings for different earthquake scenarios considering shear assessment

Record scenario	Reference structure														
	B1-REG			B2-SST			B3-GEO			B4-DIS			B5-WST		
	Limit state – interstory drift (%)														
	IO	LS	CP	IO	LS	CP	IO	LS	CP	IO	LS	CP	IO	LS	CP
Long period records	0.49	1.14	2.27	0.48	1.13	2.26	0.51	1.20	2.39	0.27	0.59	1.18	0.44	0.69	1.38
Short period records	0.49	0.78	1.55	0.48	0.75	1.50	0.51	0.81	1.62	0.27	0.32	0.64	0.44	*	0.78

*: LS limit state is close to the CP performance criterion, and hence it is eliminated

6.7 Assessment of structural response

The overall structural response of the five reference structures is assessed in the current study using two sets of earthquake records, as discussed in Chapter 4. The lateral capacity of the reference buildings is evaluated in section 6.2 using IPOAs, while the vulnerability assessment of the reference structures using IDA is discussed in subsequent sections.

6.7.1 Development of fragility relationships

Seismic vulnerability refers to the likelihood of damage in structural members or in the entire structural system. The seismic vulnerability assessment is an essential component in loss assessment systems. Therefore, in the last few decades, several studies were focused on the seismic vulnerability of structures (e.g. Singhal and Kiremidjian, 1997; Rossetto and Elnashai, 2003; Ji et al., 2007b;

Colangelo, 2008; Mwafy, 2010; Rajeev and Tesfamariam, 2012; Kaynia et al., 2013; Cunha et al., 2014). The probability of exceeding different limit states is estimated based on the seismic vulnerability results. Lack of information, particularly related to seismic hazard and exposed systems, is the main source of uncertainty in vulnerability assessment.

In the current study, a large numbers of IDAs (2800 analyses) are undertaken for the reference high-rise buildings using two earthquake scenarios, as discussed in Chapter 4 and Chapter 5. The IDAs results, which are obtained from the long period earthquake records, are shown in Figure 6.48 to Figure 6.52, while the results obtained from the short period records are shown in Figure 6.53 to Figure 6.57. These figures illustrate the relationships between the input ground motion intensities (PGAs) and the structural damage indicators (IDRs). The regression analysis results are also shown in the presented figures. The equations presented in Figure 6.48 to Figure 6.57 are in the following power-law form: $y=ax^b$, where y is the structural demand (IDR), x is the earthquake record intensity (PGA), while a and b are the regression coefficients. Additionally, the coefficient of determination (R^2), which represents the correlation between IDR and PGA, is shown in the presented figures. The results shown in Figure 6.48 to Figure 6.57 are used to develop the fragility curves of the five reference structures at different limit states, as discussed hereafter.

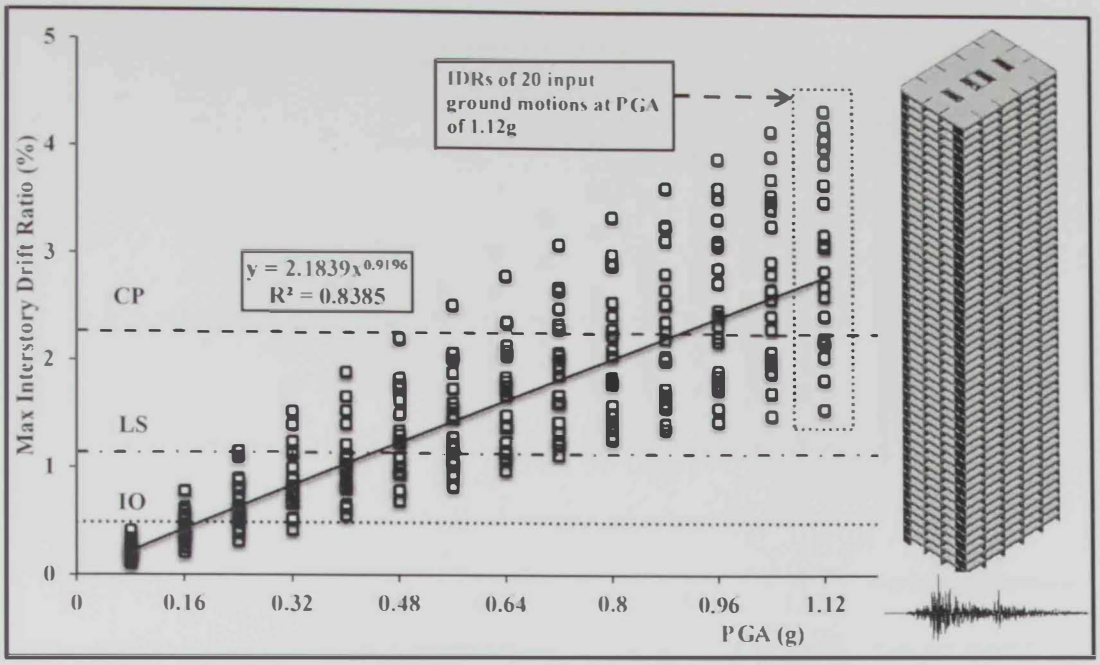

Figure 6.48: IDA results of B1-REG obtained from twenty long period input ground motions along with the power law equations and limit states

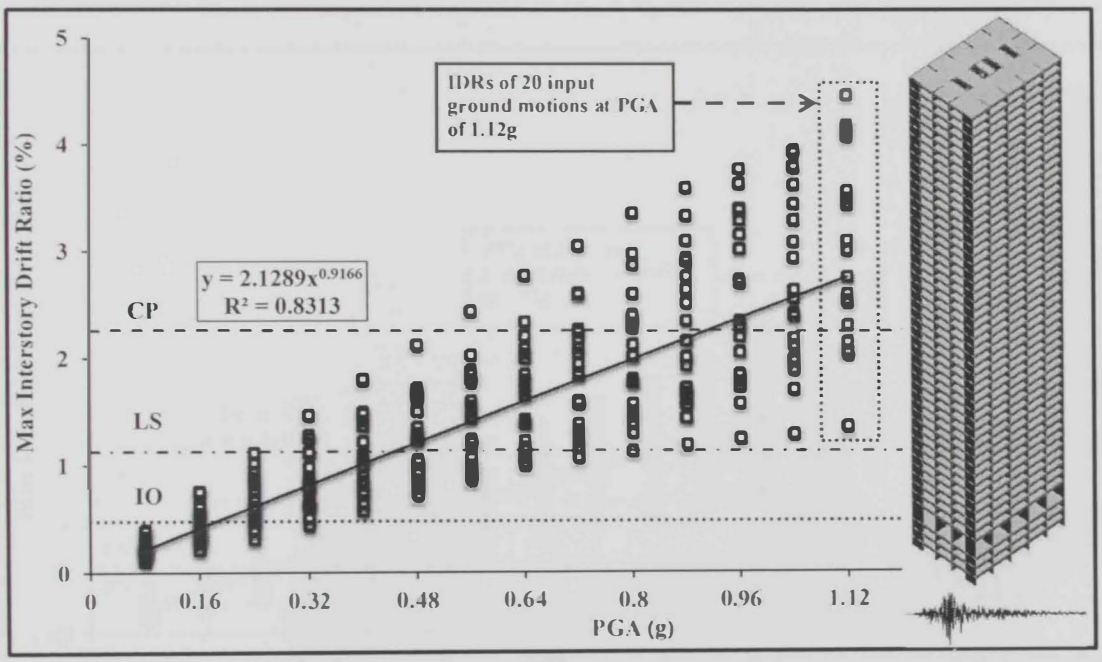

Figure 6.49: IDA results of B2-SST obtained from twenty long period input ground motions along with the power law equations and limit states

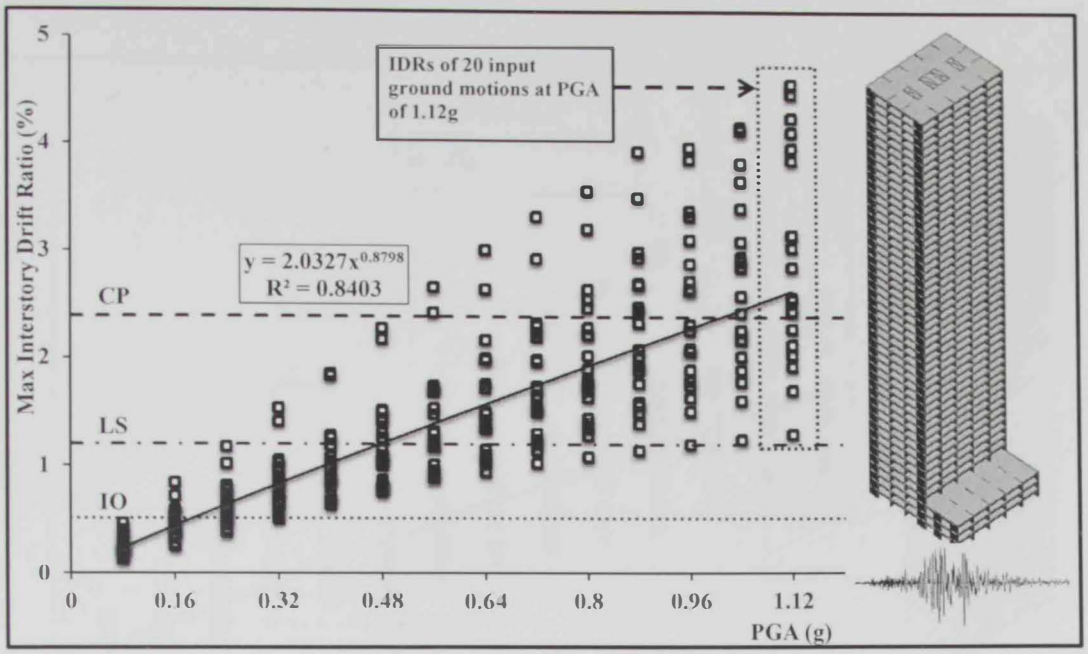

Figure 6.50: IDA results of B3-GEO obtained from twenty long period input ground motions along with the power law equations and limit states

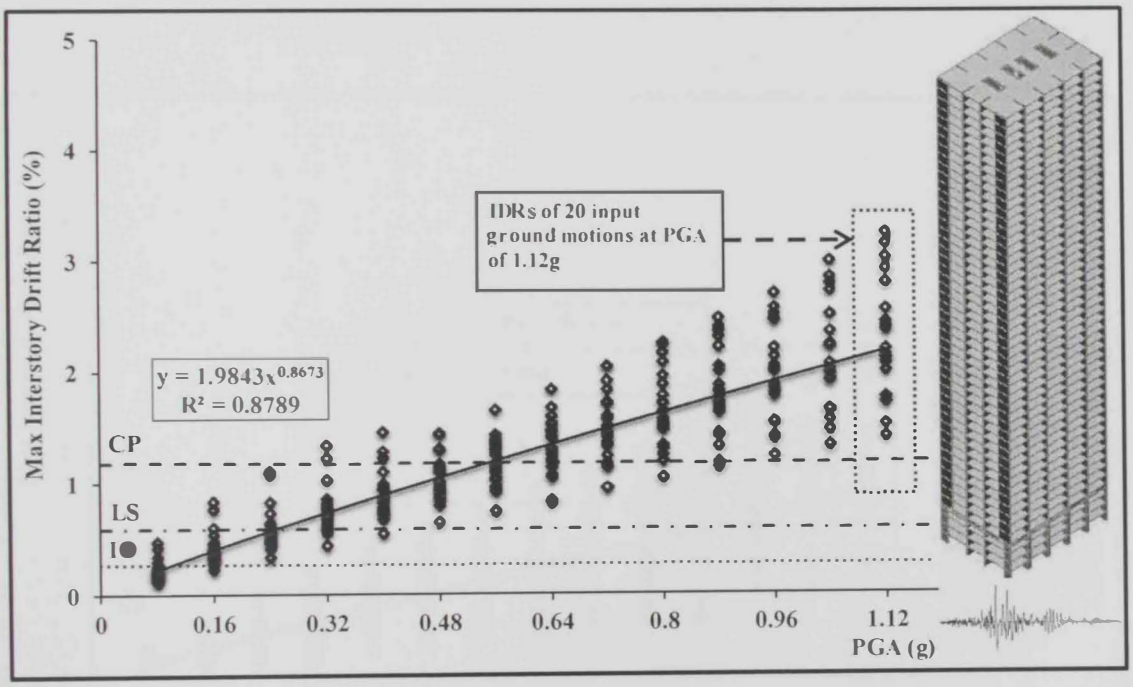

Figure 6.51: IDA results of B4-DIS obtained from twenty long period input ground motions along with the power law equations and limit states

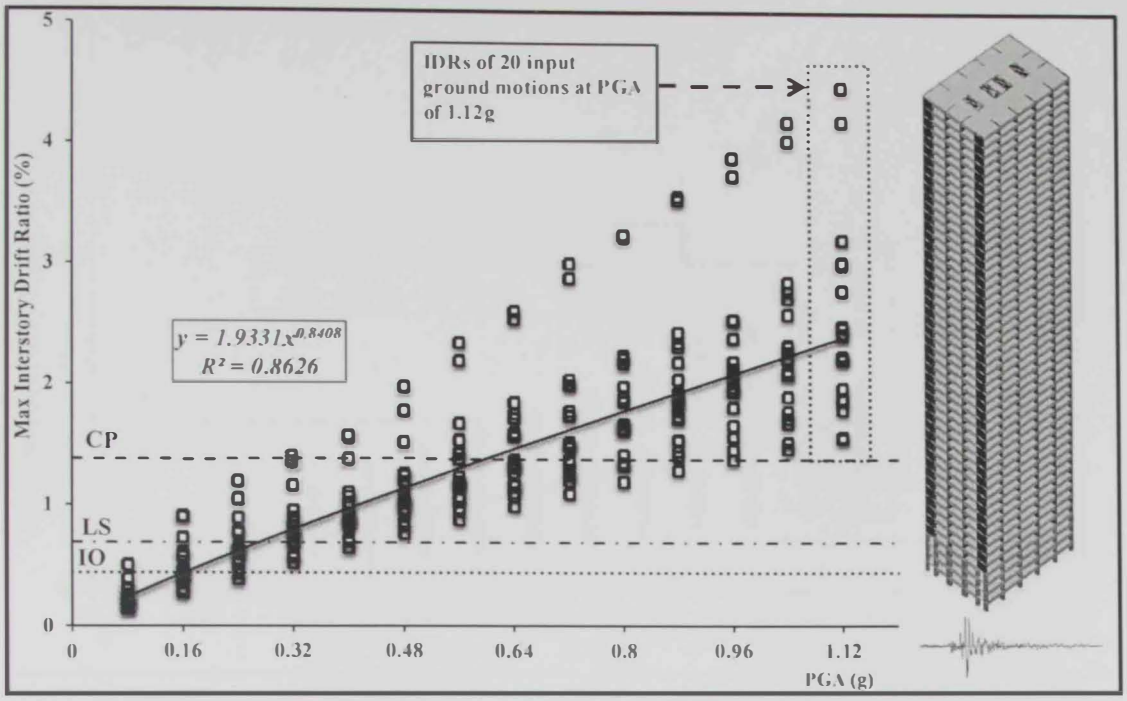

Figure 6.52: IDA results of B5-WST obtained from twenty long period input ground motions along with the power law equations and limit states.

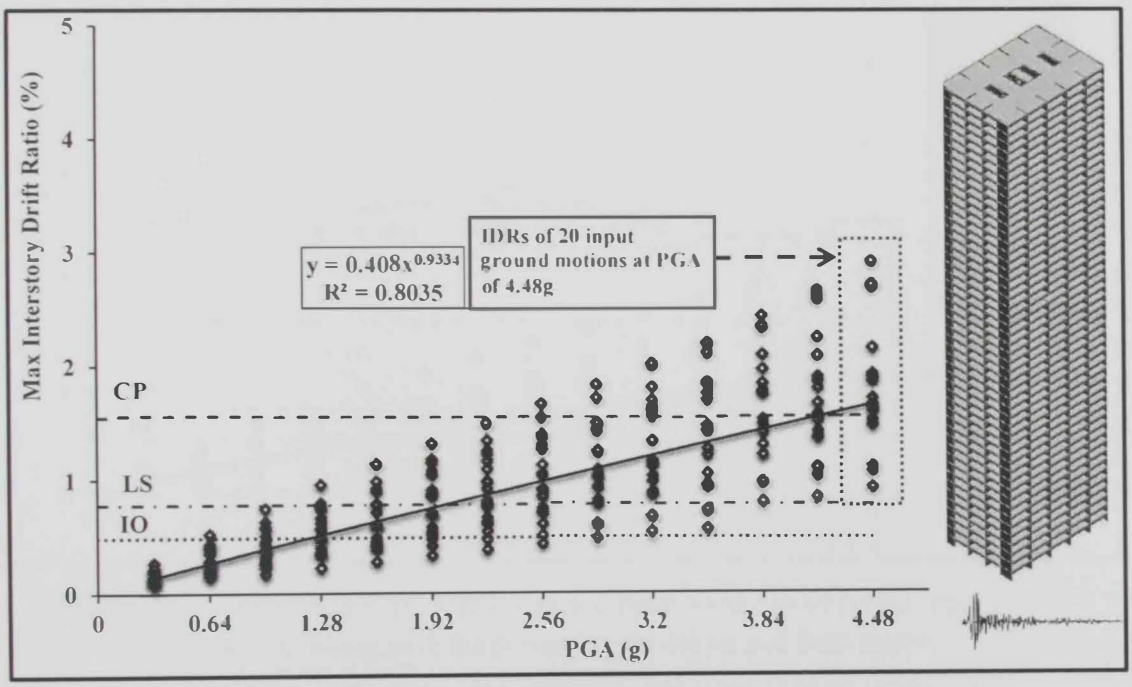

Figure 6.53: IDA results of B1-REG obtained from twenty short period input ground motions along with the power law equations and limit states.

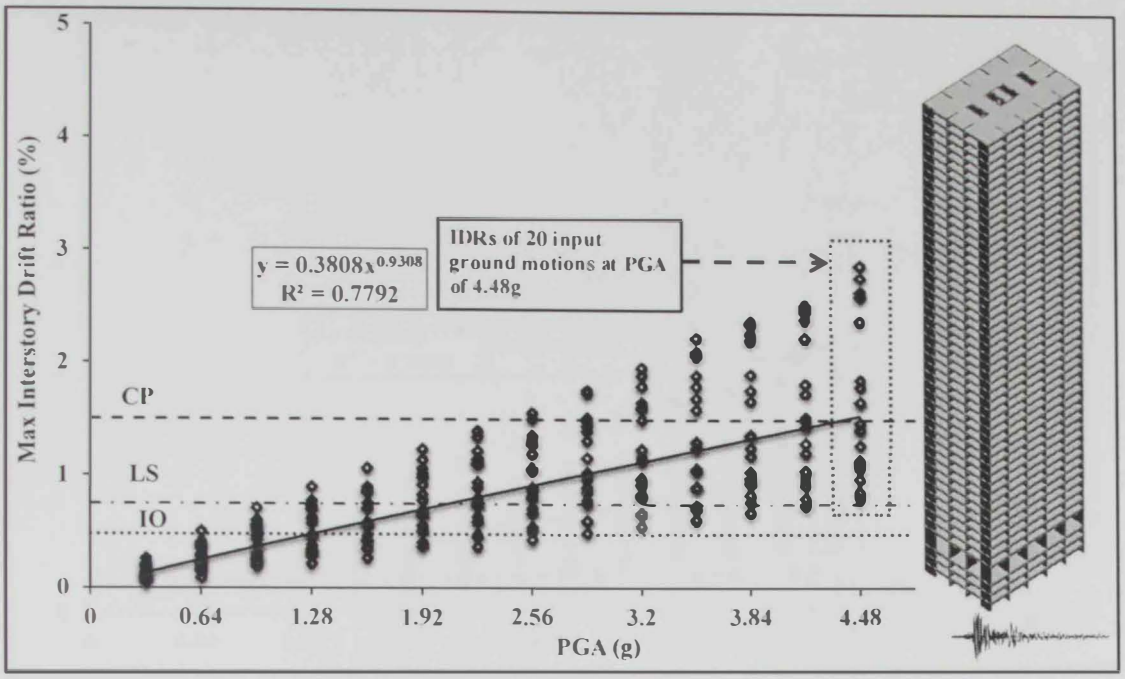

Figure 6.54: IDA results of B2-SST obtained from twenty short period input ground motions along with the power law equations and limit states

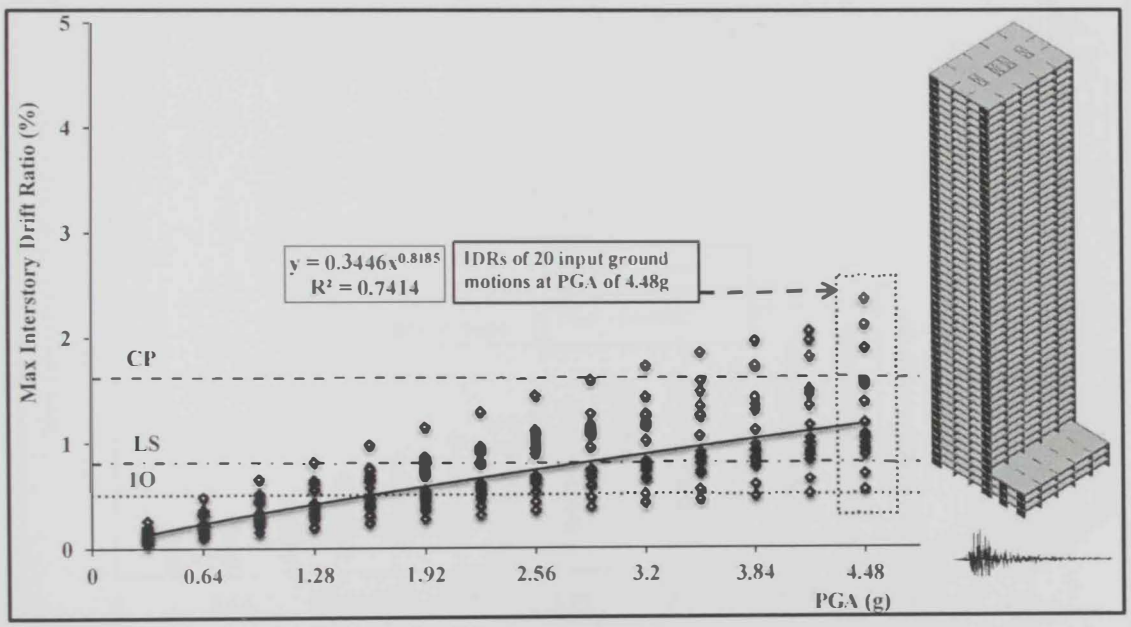

Figure 6.55: IDA results of B3-GEO obtained from twenty short period input ground motions along with the power law equations and limit states

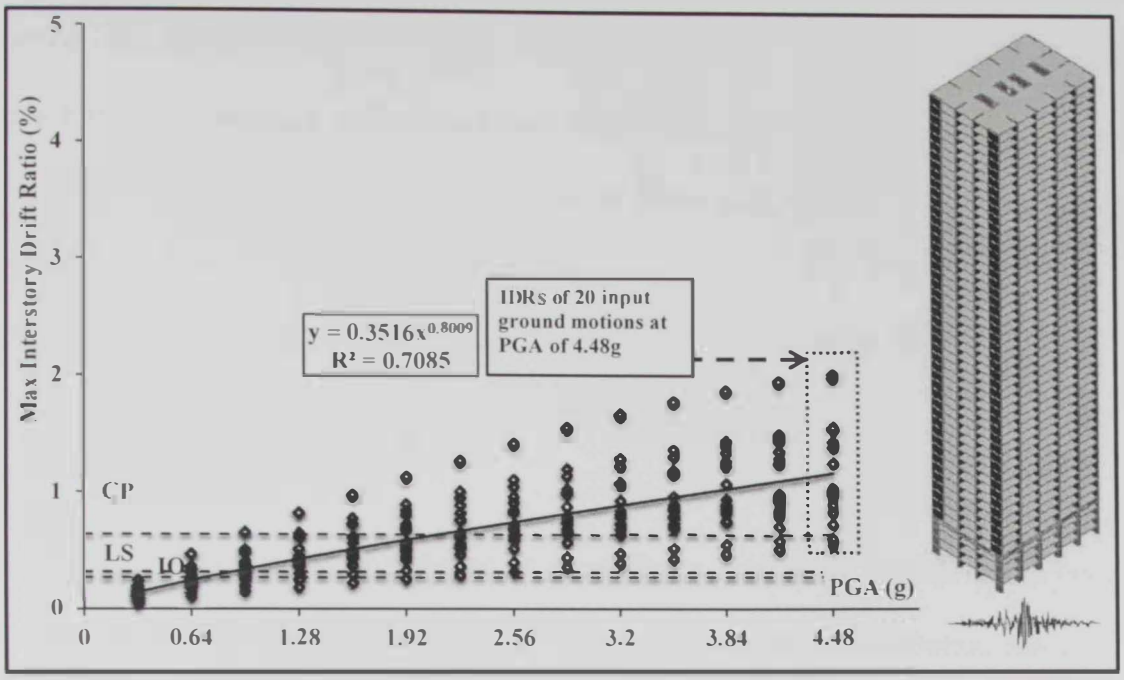

Figure 6.56: IDA results of B4-DIS obtained from twenty short period input ground motions along with the power law equations and limit states

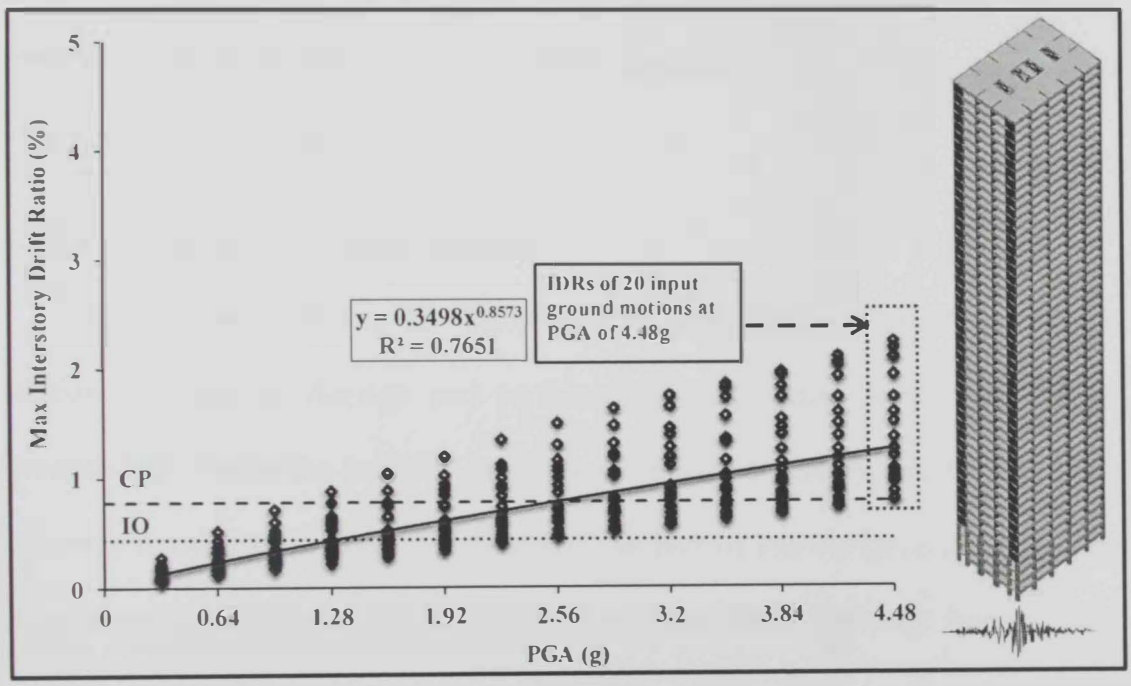

Figure 6.57: IDA results of B5-WST obtained from twenty short period input ground motions along with the power law equations and limit states

A simple mathematical definition of the fragility curves is shown in Eqn 6.4, where the fragility function F(x) is the probability of the system demand (D) reaching or exceeding a pre-selected limit state. The expression in Eqn 6.5 is used to develop the fragility curves in the current study (Wen et al., 2004).

$$F(x)= (P(LS \mid D = IDR) \quad 6.4$$

$$P(LS \mid GMI)= 1-\Phi*(\frac{(\lambda_{CL}-\lambda_{D|GMI}}{\beta}) \quad 6.5$$

where P(LS|GMI) is the probability of exceeding a limit state at different ground motion intensities (GMI), Φ is the standard normal cumulative distribution function, λ_{CL} = In (median of maximum IDR for a certain limit state), $\lambda_{D|GMI}$ = In (calculated median PGA intensity from the fitted power law equation, as discussed above, and β is the total uncertainty. The flowchart shown in Figure 6.58 summarizes different phases adopted in the present study to derive the fragility curves of the regular and irregular reference buildings.

6.7.2 Uncertainties in fragility analysis

Several uncertainties are introduced in the fragility parameters and the relation between the damage and performance limit states. Two categories of uncertainties exist in the fragility, namely epistemic and aleatory uncertainties. The epistemic uncertainty is generally caused by the lack of knowledge, and it could be reduced using more information. The aleatory uncertainty randomly happens and cannot be reduced (e.g. Kiureghian and Ditlevsen, 2009).

There are many sources of uncertainty in the derivation of the fragility curves such as material characteristics, structural system properties, modeling approach, system capacity and seismic demand. To decrease the uncertainty due to the

analytical idealization, the fiber-based modeling approach is adopted in the current study, as discussed in Chapter 4. Moreover, the IDAs conducted to derive the fragility curves using a large number of input ground motions significantly reduce the uncertainty. Previous studies concluded that other sources of the uncertainty such as the uncertainty due to the inherent variability of the material properties have a minor impact on the structural seismic performance (e.g. Kwon and Elnashai, 2006; Mwafy et al., 2014). The variability in the material characteristics is therefore considered as a deterministic uncertainty in the present study.

The following uncertainty sources are considered in the current study: (i) seismic demand due to the variability in the input ground motions, (ii) modeling, and (iii) capacity uncertainty. The above-mentioned sources of uncertainty were also considered in several previous studies (e.g. Taylor, 2007; Mwafy, 2010; Kaynia et al., 2013). The total uncertainty β, which accounts for the aforementioned uncertainty sources, is considered as follows:

$$\beta = \sqrt{\beta_{D|GMI}^2 + \beta_{CL}^2 + \beta_{M}^2} \qquad 6.6$$

where $\beta_{D|GMI}$ is the demand uncertainty = $\ln \sqrt{(1+ S^2)}$ and S^2 is the standard error of demand data, which is treated probabilistically. β_{CL} is the capacity uncertainty, and β_M is modeling uncertainty. The β_{CL} and β_M are considered deterministic in this study and their values are 0.3 and 0.2, respectively (Wen et al., 2004; Jeong et al., 2012).

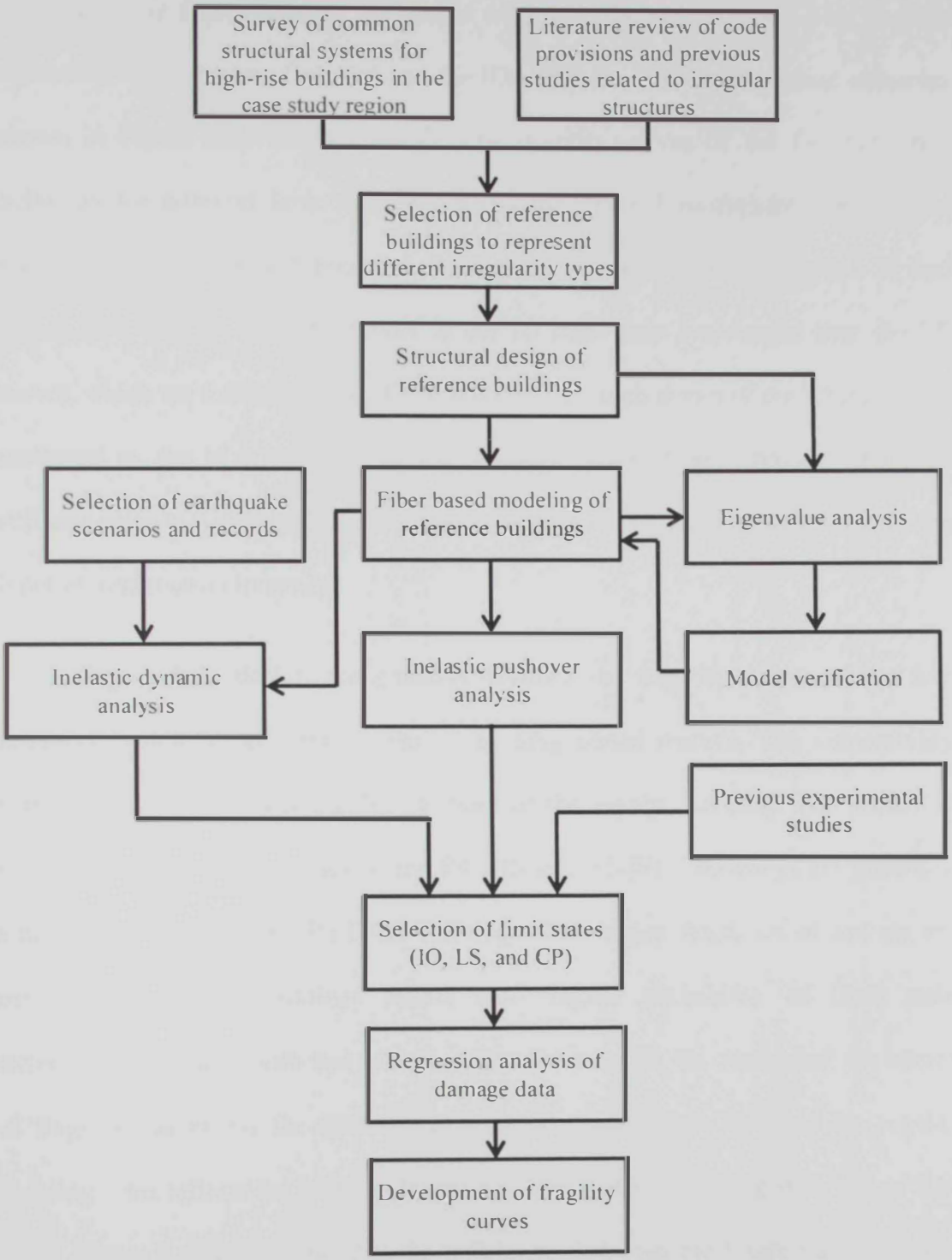

Figure 6.58: Summary of the adopted procedure for the derivation of fragility curves

6.7.3 Vulnerability assessment of reference structures

The analytical procedure for deriving the fragility curves of the benchmark buildings using a large number of IDAs is adopted in the present study. The fragility curves are derived using Eqn. 6.5 and the IDAs results of the two seismic scenarios shown in Figure 6.48 to Figure 6.57. The fragility curves of the five reference buildings for different limit states using the long period earthquake scenario are shown in Figure 6.59 and Figure 6.60. Generally, it is shown in Figure 6.59 and Figure 6.60 that the fragility curves of the IO limit state are steeper than the LS curves, which are followed by the CP fragilities. The high slopes of the IO curves are attributed to the high stiffness of the structure before first yielding. This high stiffness prior to yielding decreases the variability of the IDRs with respect to the input ground motion intensity.

Figure 6.61 depicts comparisons between the fragility curves of the five reference buildings using the results of the long period records. The vulnerability curves of B2-SST are comparable to those of the regular building. The presented results show that the fragilities of the B4-DIS and B5-WST buildings are generally steeper than those of the B1-REG building. The steeper fragilities of the above-mentioned irregular buildings reflect their higher probability of limit state exceedance compared with that of the regular structure. On the other hand, the slopes of fragility curves for the B3-GEO building are lower than those of the regular building. This reflects the lower vulnerability of B3-GEO compared with that of B1-REG. Figure 6.61 also shows that the differences between the fragilities of the five reference structures at the CP limit state are much higher than those at the IO performance level. This is attributable to the higher seismic demands in the inelastic range, particularly near collapse, as shown in Figure 6.61.

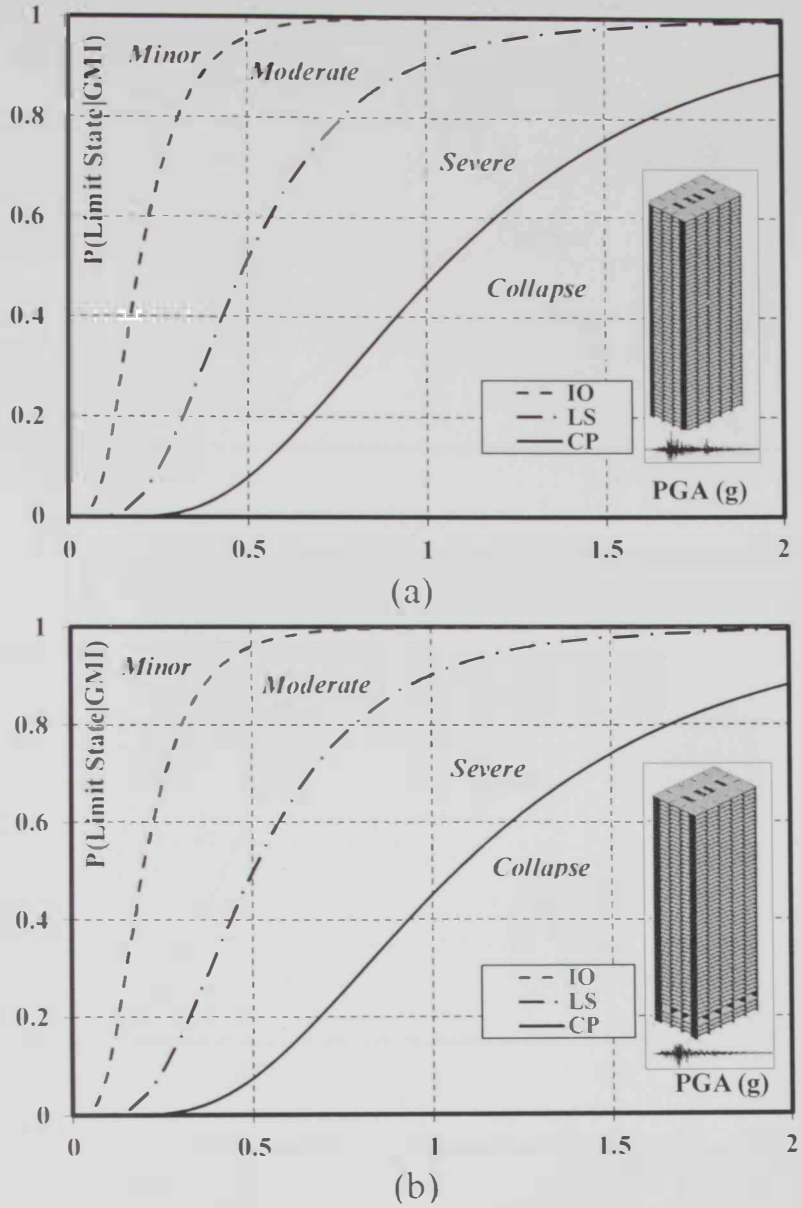

Figure 6.59: Fragility relationships of buildings obtained from IDAs using twenty long period records: (a) B1-REG and (b) B2-SST

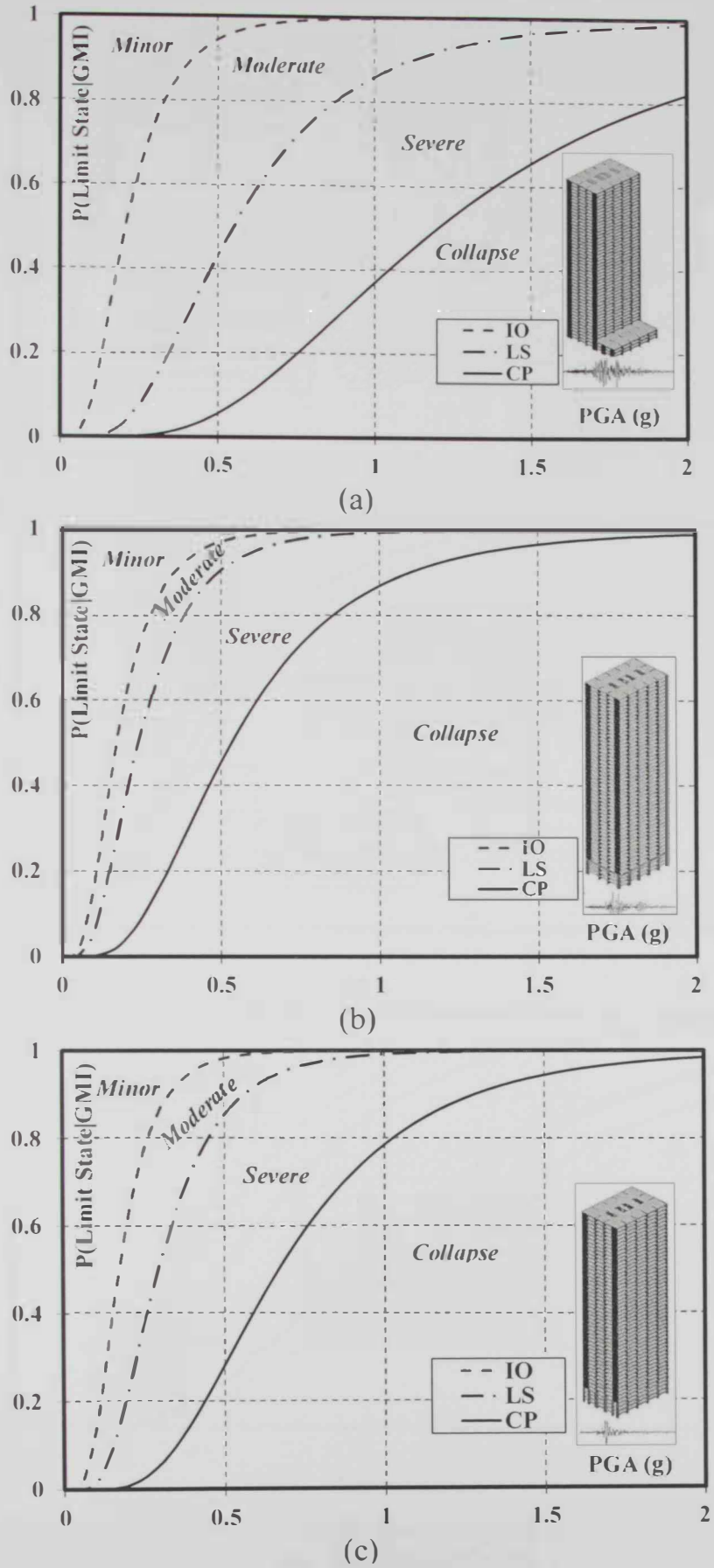

Figure 6.60: Fragility relationships of buildings obtained from IDAs using twenty long period records: (a) B3-GEO, (b) B4-DIS and (c) B5-WST

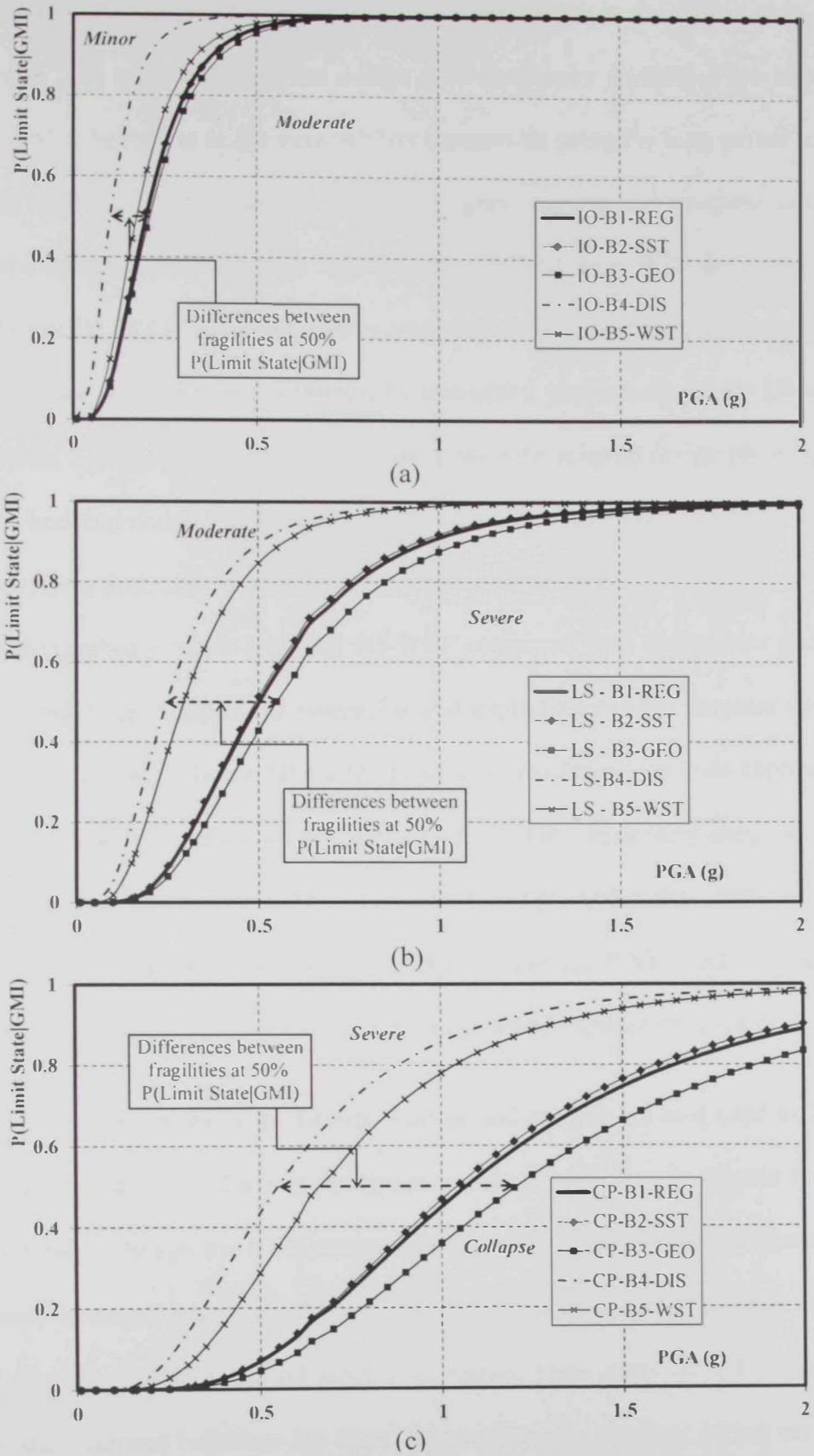

Figure 6.61: Comparisons between the fragility relationships of the five reference structures at three limit states: (a) IO, (b) LS, and (c) CP

The probabilities of exceeding different limit states at the design (1d), twice the design (2d) and four times the design (4d) earthquake intensities are shown in Figure 6.62. The results of the vulnerability assessment using the long period records confirm the satisfactory response of well-designed regular and irregular buildings under the design earthquake with regard to the CP limit state. With the exception of B4-DIS and B5-WST, the limit state exceedance probabilities are also acceptable at the design and twice the design earthquake intensities, particularly for the LS and CP limit states. These observations are consistent with the seismic design philosophy of modern building codes. On the other hand, the LS and CP fragilities as well as the corresponding limit state exceedance probabilities at different intensities confirm the higher vulnerability of B4-DIS and B5-WST compared with the regular and other irregular buildings. Despite the assigned overstrength factor to the irregular stories of B4-DIS and B5-WST during the design process, as per the design code approach, the deficiencies due to the discontinuity of the LFRS and the weak story irregularities are confirmed. The results highlight the expected higher earthquake losses in certain categories of irregular structures (i.e. B4-DIS and B5-WST) and the need for mitigation strategies to reduce these losses for new and existing irregular buildings.

The IDA results of the twenty short period records are also used to develop the fragility curves of the five reference building, as shown in Figure 6.63 and Figure 6.64. Although the IDRs corresponding to the CP performance criteria of the reference structures significantly decrease as a result of considering shear response under the effect of short period earthquake record, particularly for B4-DIS and B5-WST, the reference buildings are more vulnerable under the long period earthquake scenario as shown from the stepper fragilities in Figure 6.59 and Figure 6.60.

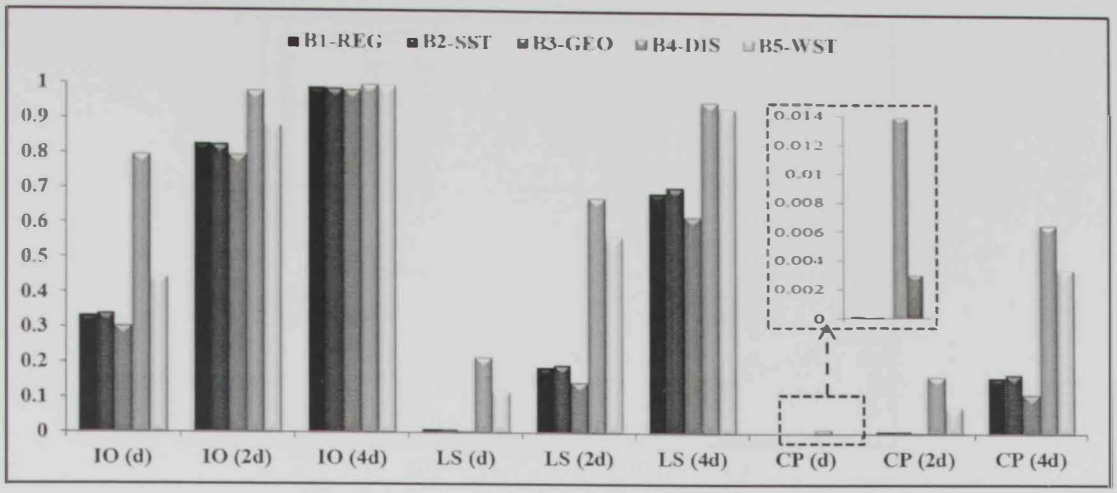

Figure 6.62: Comparison of limit state exceedance probabilities of the reference buildings at different PGAs intensities

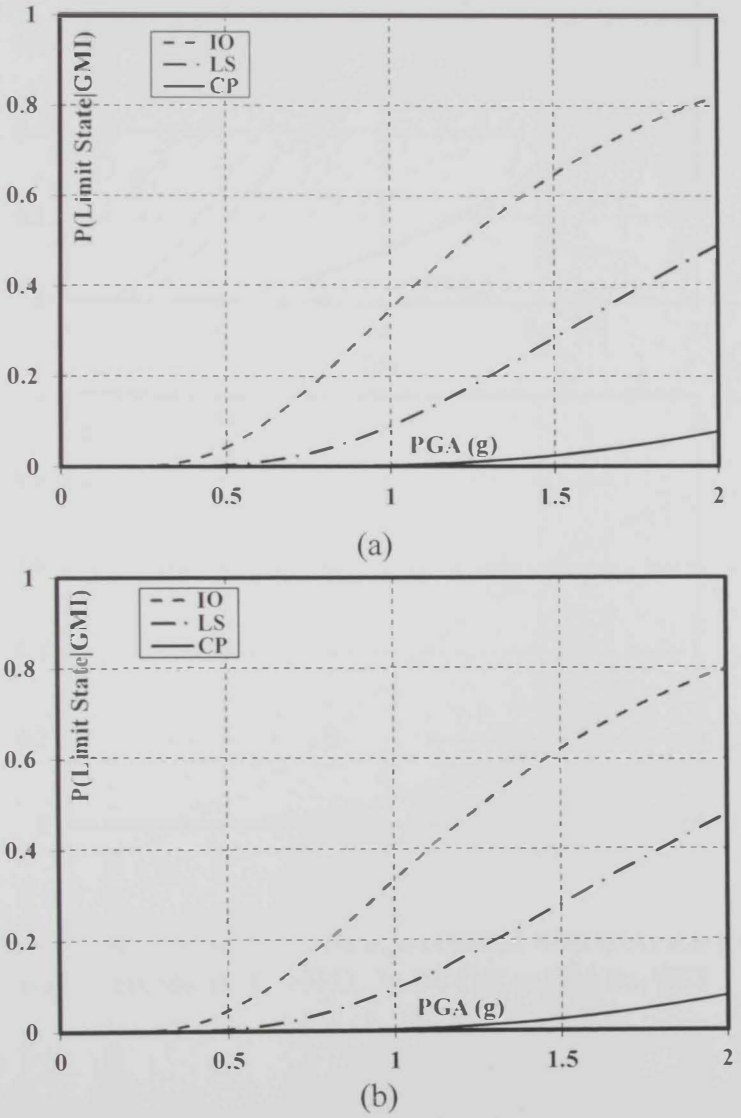

Figure 6.63: Fragility relationships of buildings obtained from IDAs using twenty short period records: (a) B1-REG and (b) B2-SST

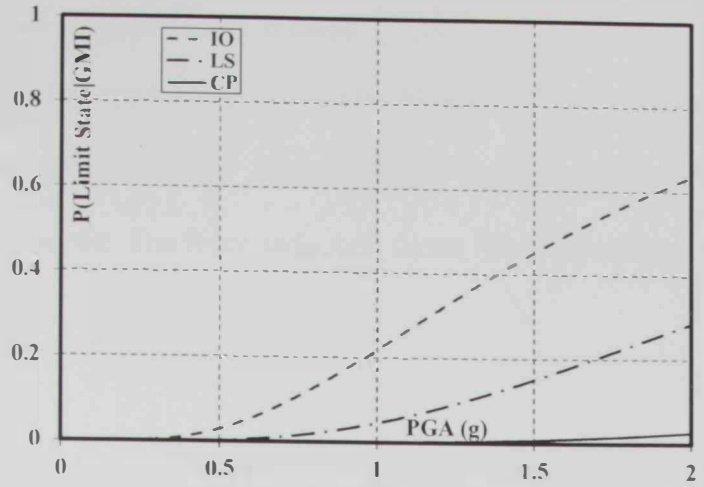

(a)

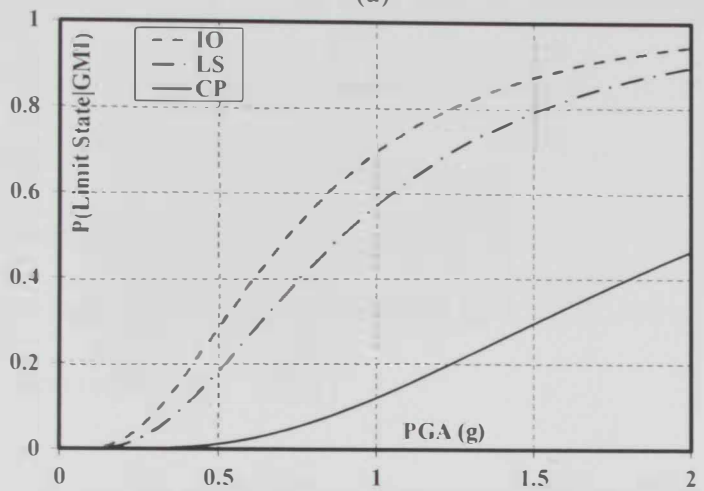

(b)

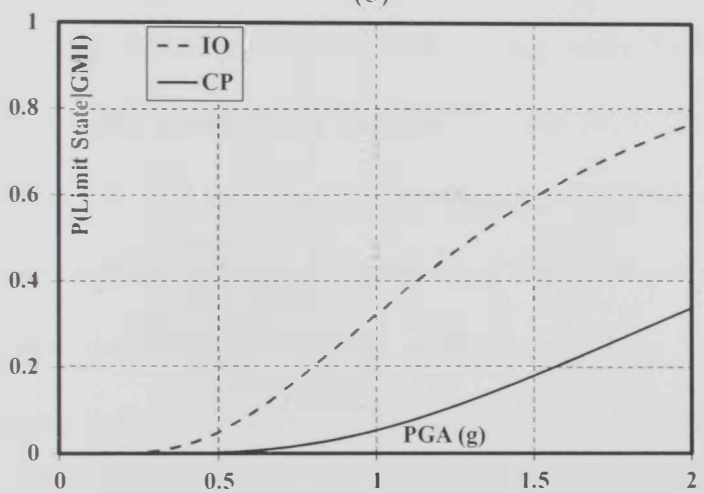

(c)

Figure 6.64: Fragility relationships of buildings obtained from IDAs using twenty short period records: (a) B3-GEO, (b) B4-DIS and (c) B5-WST

6.8 Assessment of seismic design factors

Following the approach proposed by Mwafy (2011), which was discussed in Chapter 2, the seismic design factors of the regular and irregular benchmark structures are estimated. The force reduction factor (R) is calculated as follows:

$$R = \frac{a_c}{a_y} x\Omega_{1ph} \qquad 6.7$$

where a_c is the PGA at the first indication of collapse, a_y is the PGA at first indication of yielding in structural members and Ω_{1ph} is the overstrength factor at the first indication of yielding. The deflection amplification factor (C_d) is considered equal to the IDR at collapse to the IDR at first yielding (Mwafy, 2011). The IDA results using the selected 20 long period records discussed in Chapter 4 are employed to evaluate the seismic design response factors, as a result of their higher impact on the response of the reference structures.

Table 6.4 shows the maximum, minimum and median PGA and IDR of the five reference buildings at the first indication of yielding, while Table 6.5 depicts the results at collapse. The definition of collapse for the reference structures was discussed in section 6.6. The overstrength factors at the first indication of yielding for the five reference buildings are calculated using IPOAs and IDAs, as shown in Figure 6.65. Since the IPOA results are unreliable for long period structures, particularly irregular buildings, it is decided to use the overstrength factors calculated using IDA to evaluate the seismic design factors.

The IDRs and PGAs ratios at yield and collapse are depicted in Figure 6.66 to Figure 6.70, while Figure 6.71 summaries these ratios. It is shown in Figure 6.71 that $PGA_{c/y}$ is larger than $IDR_{c/y}$ for the five reference structure, where $PGA_{c/y}$ is the ratio between PGA at collapse (a_c) to PGA at yield (a_y) and $IDR_{c/y}$ is the ratio between

IDR at collapse (IDR_c) to IDR at yield (IDR_y). The difference between $PGA_{c,y}$ and $IDR_{c/y}$ is significant for B4-DIS compared with the other reference structures. These differences reflect the margin of safety when C_d is considered equal to R, as per the design code (FEMA-P695, 2009).

Table 6.4: Summary of IDAs at the first indication of the plastic hinge

Buildings	B1-REG		B2-SST		B3-GEO		B4-DIS		B5-WST	
	PGA	IDR	PGA	IDR	PGA	IDR	PGA	IDR	PGA	IDR
Max.	0.48	1.10	0.48	1.02	0.64	1.11	0.40	0.72	0.56	0.94
Min.	0.16	0.64	0.16	0.62	0.18	0.60	0.08	0.37	0.16	0.70
Median	0.32	0.78	0.32	0.76	0.41	0.93	0.16	0.48	0.36	0.86

Table 6.5: Summary of IDAs at the first indication of collapse

Buildings	B1-REG		B2-SST		B3-GEO		B4-DIS		PGA	
	PGA	IDR	PGA	IDR	PGA	IDR	PGA	IDR	PGA	IDR
Max.	1.68	2.34	1.28	2.60	1.84	2.67	0.96	1.35	0.96	1.54
Min.	0.56	2.04	0.56	2.03	0.56	2.19	0.32	1.00	0.32	1.33
Median	0.96	2.20	0.96	2.26	1.08	2.40	0.52	1.18	0.68	1.38

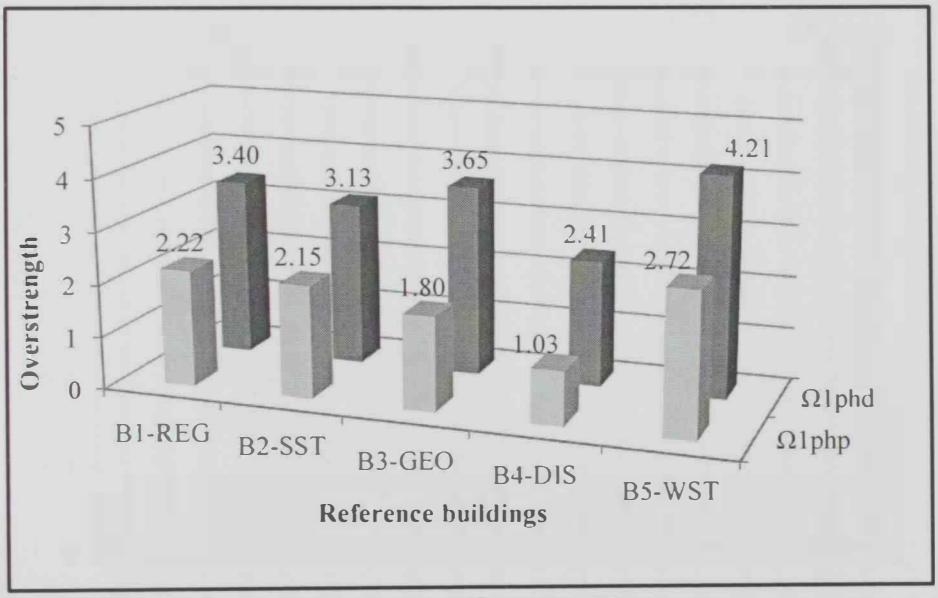

Ω1php. Overstrength factor at the first indication of yielding from IPOAs
Ω1phd Overstrength factor at the first indication of yielding from IDAs

Figure 6.65: Estimated overstrength factors using IPOAs and IDAs results

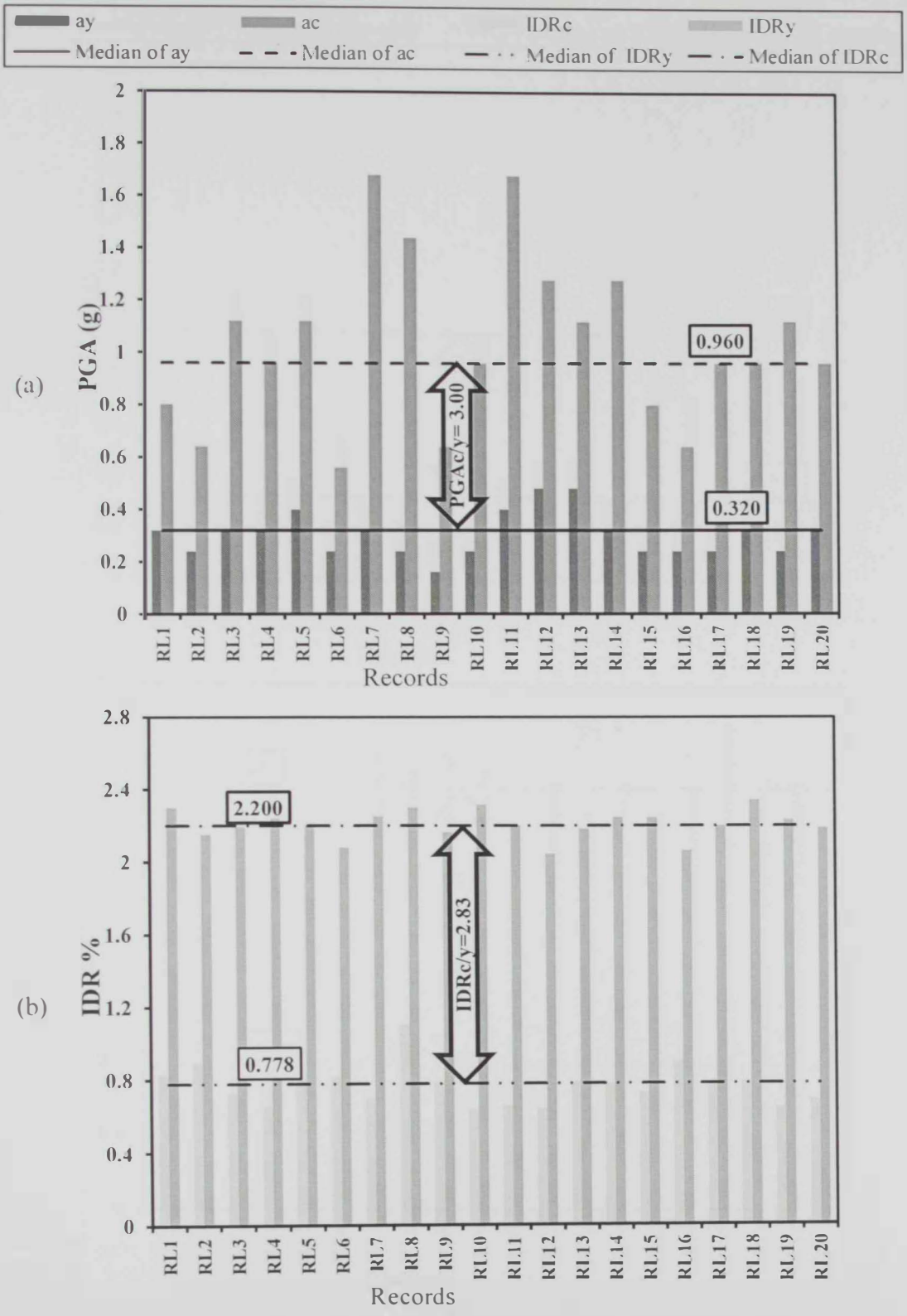

Figure 6.66: IDA results of the B1-REG building: (a) Collapse-to-yield peak ground acceleration ratio ($PGA_{c/y}$), and (b) Collapse-to-yield inter story drift ratio ($IDR_{c/y}$)

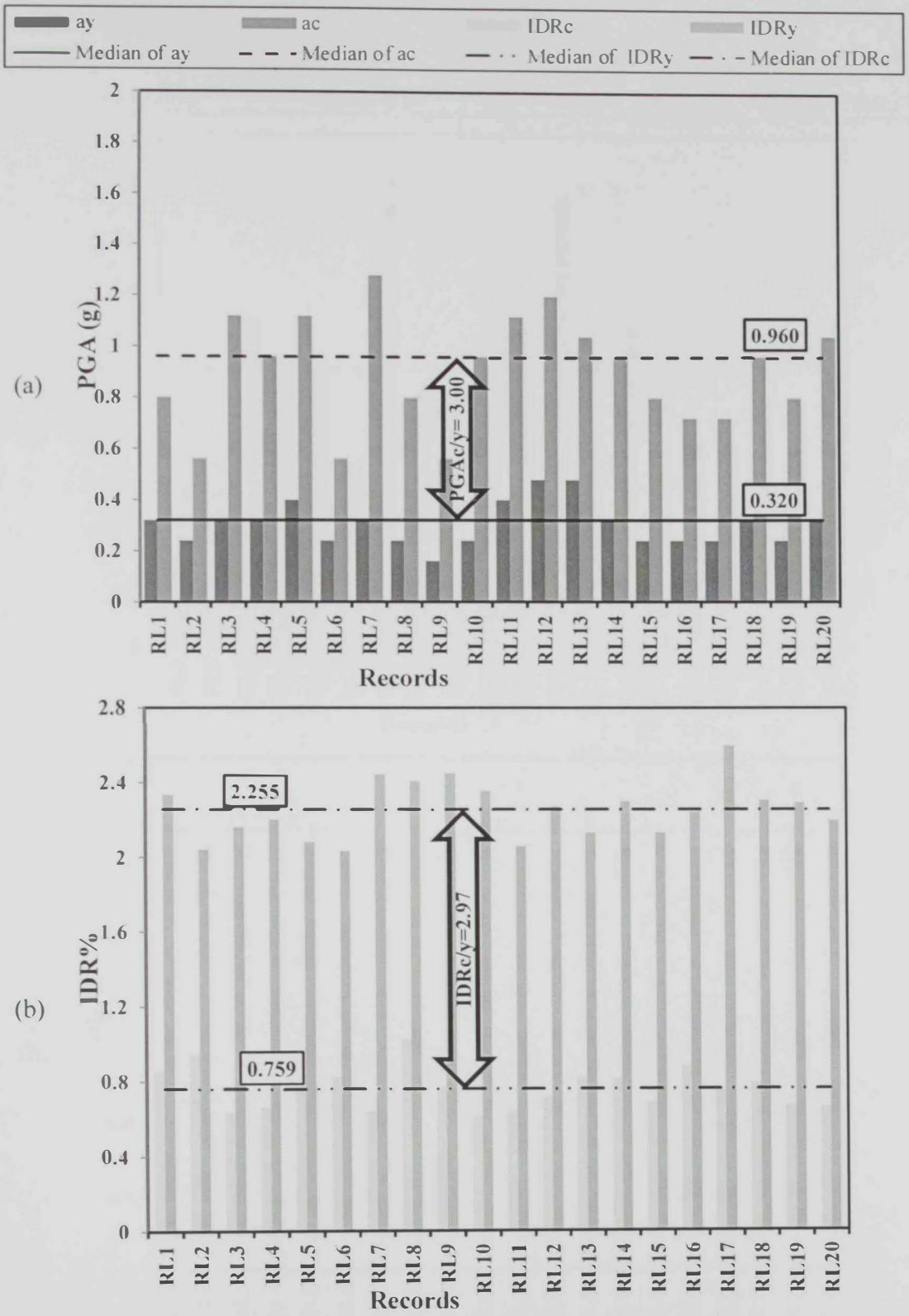

Figure 6.67: IDA results of the B2-SST building: (a) Collapse-to-yield peak ground acceleration ratio ($PGA_{c/y}$), and (b) Collapse-to-yield inter story drift ratio ($IDR_{c/y}$)

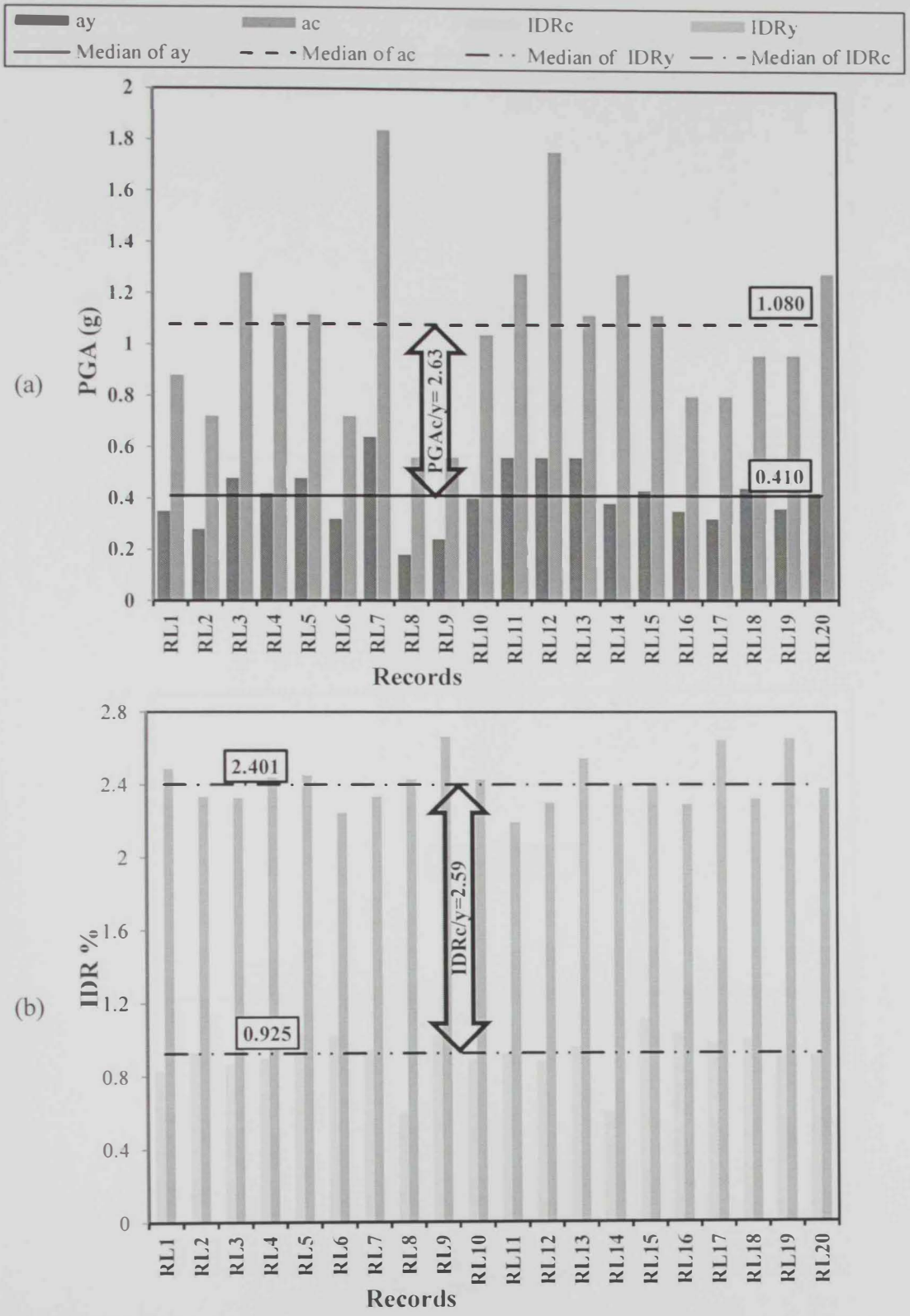

Figure 6.68: IDA results of the B3-GEO building: (a) Collapse-to-yield peak ground acceleration ratio ($PGA_{c/y}$), and (b) Collapse-to-yield inter story drift ratio ($IDR_{c/y}$)

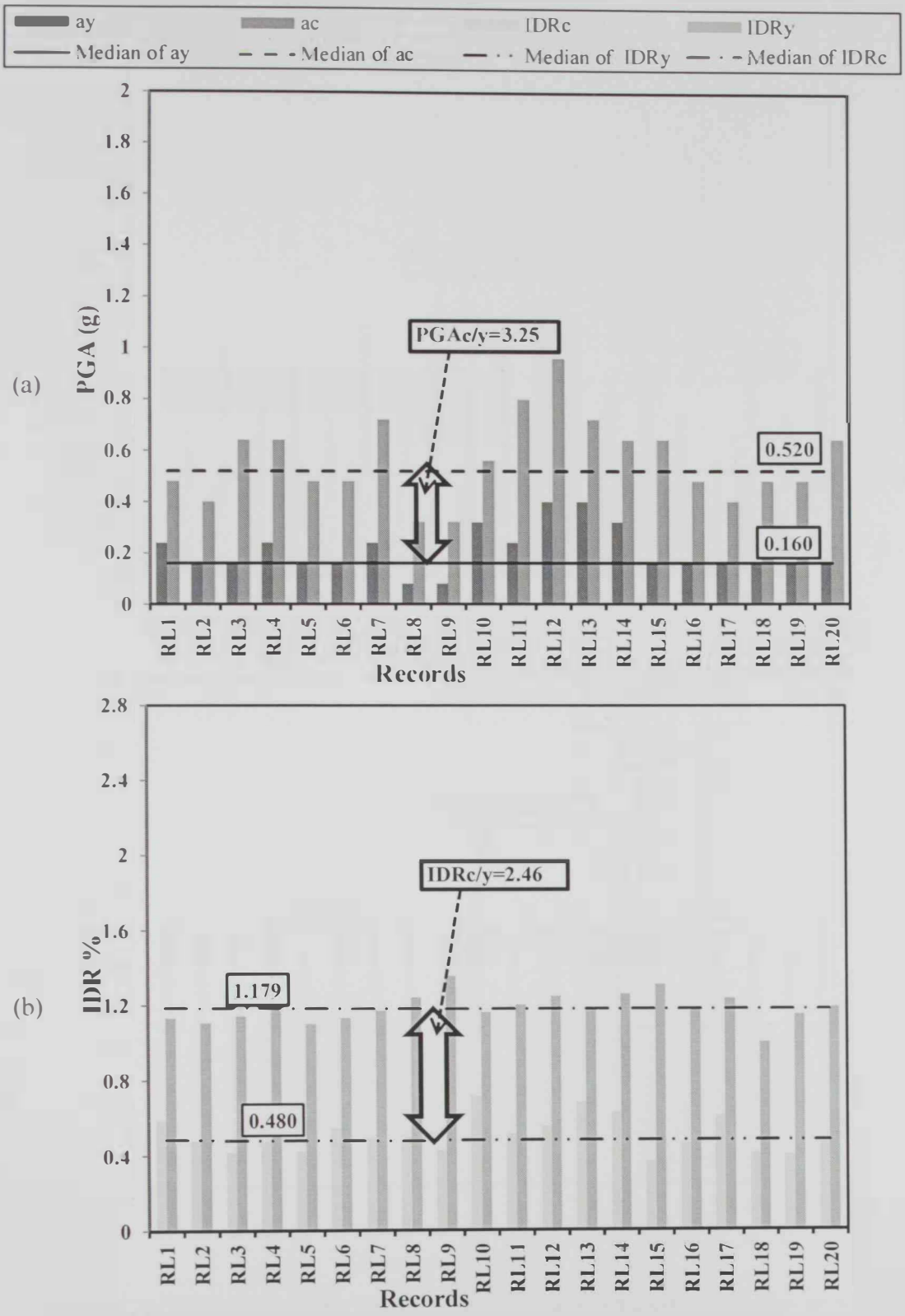

Figure 6.69: IDA results of the B4-DIS building: (a) Collapse-to-yield peak ground acceleration ratio ($PGA_{c/y}$), and (b) Collapse-to-yield inter story drift ratio ($IDR_{c/y}$)

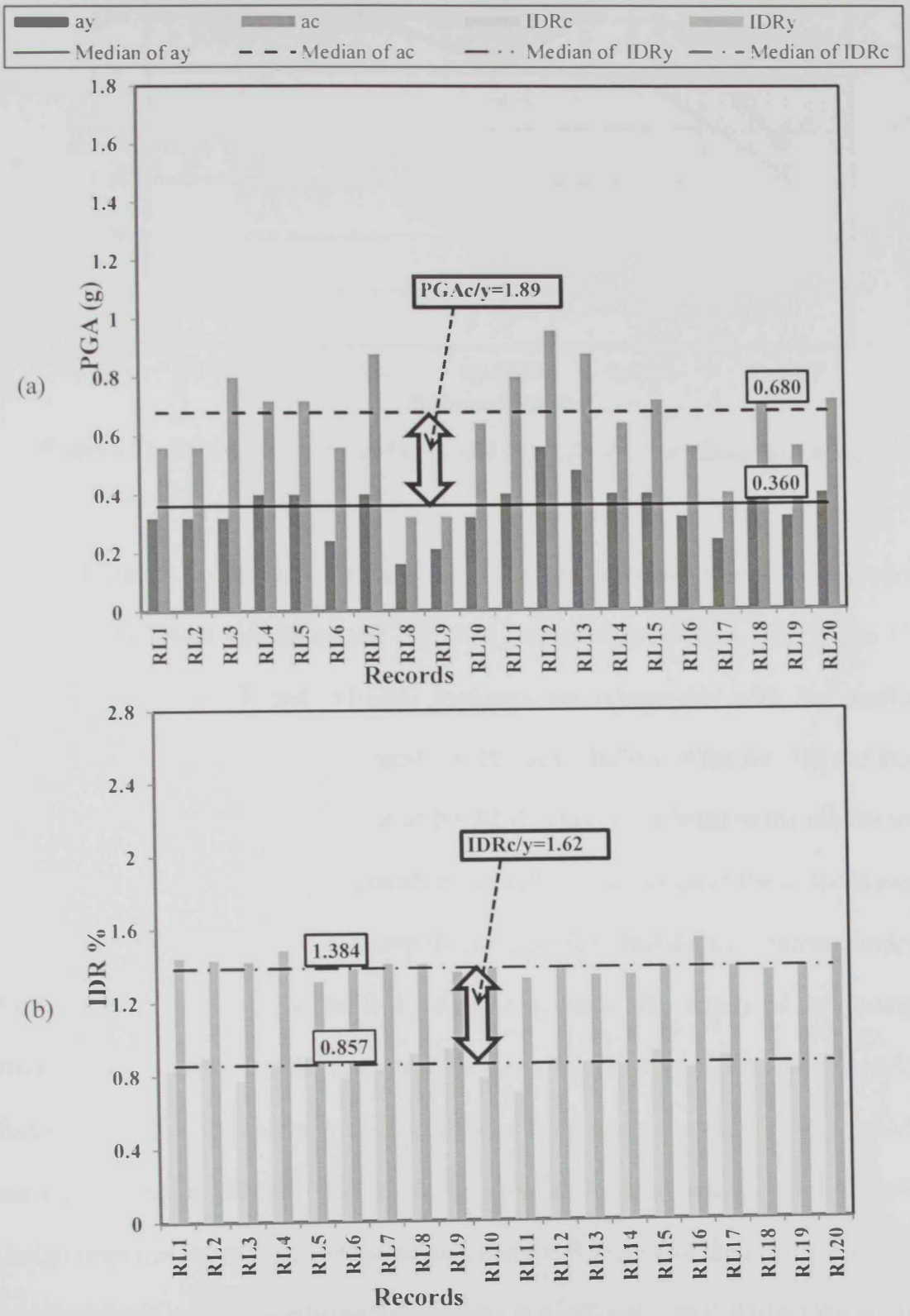

Figure 6.70: IDA results of the B5-WST building: (a) Collapse-to-yield peak ground acceleration ratio ($PGA_{c/y}$), and (b) Collapse-to-yield inter story drift ratio ($IDR_{c/y}$)

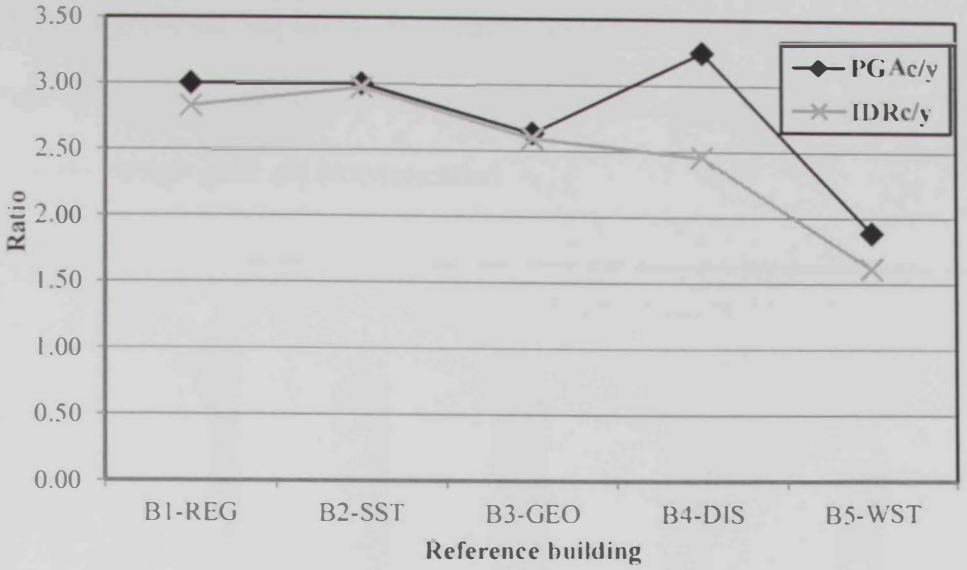

Figure 6.71: Relationship between $PGA_{c/y}$ and $IDR_{c/y}$ for the five reference buildings

Figure 6.72 depicts a comparison between the calculated R and C_d factors for the five benchmark buildings with the code recommended values. The R and C_d factors of the B2-SST and B3-GEO buildings are comparable with the regular structure (B1-REG). On the other hand, the R and C_d factors of the B4-DIS and B5-WST buildings are lower than those of B1-REG. This is attributed to the significant irregularity and the use of overstrength factor (Ω_o) in the design of the lower stories of the latter two buildings. It is shown from Figure 6.72 that the code recommended factors are conservative for the five reference systems. The results of the present study clearly confirm that the impacts of different irregularity types on the R and C_d factors vary. The discontinuity of the LFRS and the weak story irregularity, which are represented by B4-DIS and B5-WST, have the highest impact on the seismic design response factor. The results indicate that the R factors of the regular structure and buildings with insignificant irregularity (i.e. B2-SST and B3-GEO) can be initially increased by 10-20%. Further increase is possible after a carful assessment of the structures designed using the suggested reduction in seismic design forces.

impact of irregularity on the local and global response of tinuity in LFRS and weak story, the conservative R and C_d e are recommended.

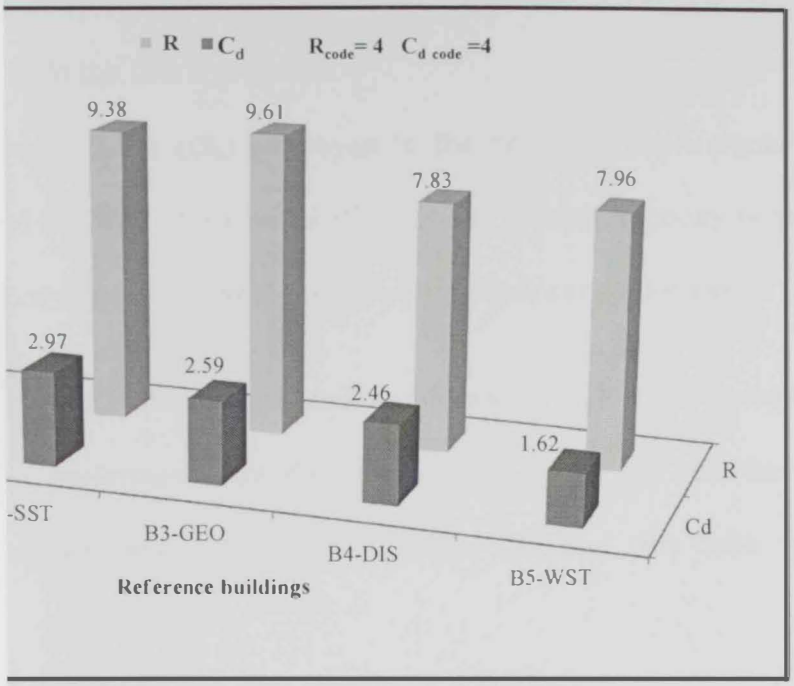

ors of the five reference buildings obtained from IDAs using long period input ground motions

s

assessment of the local and global response of the five ings investigated in this study was discussed in this chapter. at the member level included monitoring of: (i) plastic crete crushing, and (iii) shear response. The assessment at : (i) lateral capacity evaluation, and (ii) fragility assessment. DAs and IDAs were performed using a wide range of senting two earthquake scenarios to account for the input y. The IPOAs results indicated that:

Due to the significant impact of irregularity on the local and global response of buildings with a discontinuity in LFRS and weak story, the conservative R and C_d factors of the design code are recommended.

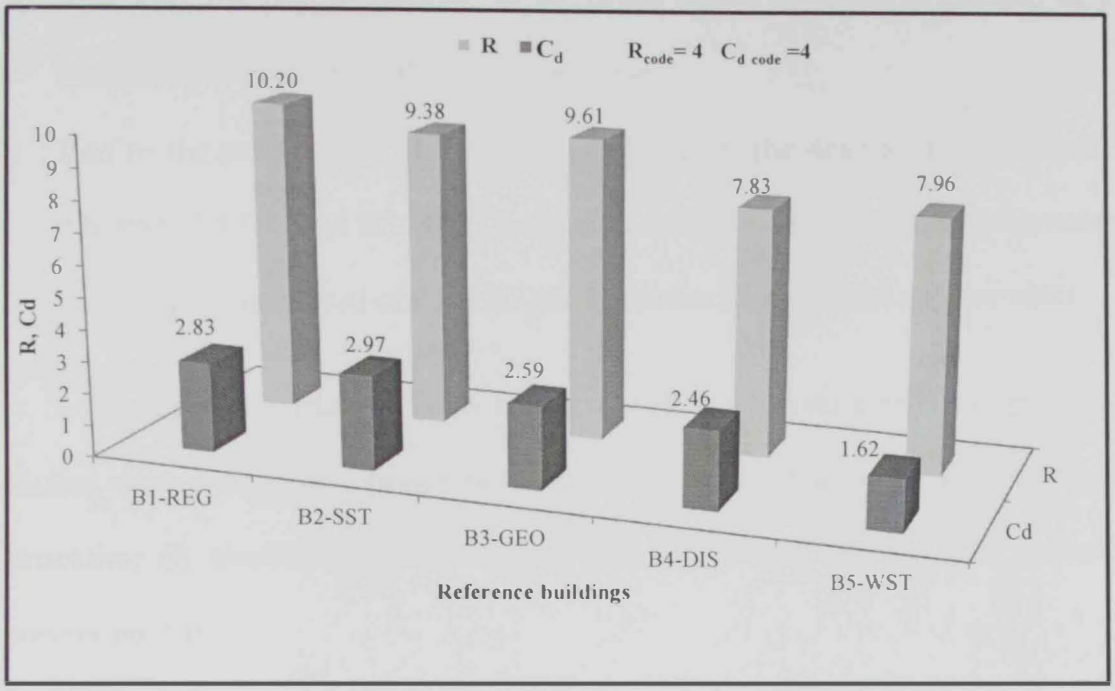

Figure 6.72: R and C_d factors of the five reference buildings obtained from IDAs using long period input ground motions

6.9 Concluding remarks

The vulnerability assessment of the local and global response of the five reference high-rise buildings investigated in this study was discussed in this chapter. The seismic assessment at the member level included monitoring of: (i) plastic hinges, (ii) confined concrete crushing, and (iii) shear response. The assessment at the global level involves: (i) lateral capacity evaluation, and (ii) fragility assessment. A large number of IPOAs and IDAs were performed using a wide range of earthquake records representing two earthquake scenarios to account for the input ground motion uncertainty. The IPOAs results indicated that:

- The initial stiffness, ultimate strength and ductility of the building with extreme soft story irregularity (B2-SST) were marginally lower than those of the regular structure (B1-REG).
- Increasing the plan dimensions at the lower stories of B3-GEO resulted in a marginal enhancement in the lateral response.
- Due to the overstrength factor (Ω_o) employed in the design of the irregular buildings B4-DIS and B5-WST, their initial stiffness and ultimate capacity were much higher than those of B1-REG, while the ductility significantly decreased.

Based on the IPOA and IDA results as well as a literature review of previous studies, three conservative performance criteria were selected for the five reference structures: (i) immediate occupancy, IO; (ii) life safety, LS; and (iii) collapse prevention, CP.

The shear assessment results of the reference structures indicated that:

- For long period earthquake records, no shear failure was observed in structural members before reaching the flexural-based collapse prevention limit state.
- The flexural-based limit states were substantially decreased due to the early detection of shear failure under short period earthquake records, particularly for the irregular structures.

The fragility curves of the regular and irregular reference high-rise buildings were derived using 2800 IDAs considering the most important uncertainties. The comparison between the fragility curves of the five reference buildings indicated that:

- Satisfactory performance was observed for the well-designed regular and irregular buildings under the design earthquake.
- The fragility curves of B2-SST and B3-GEO reflected their marginal lower vulnerability compared with that of B1-REG.
- With the exception of B4-DIS and B5-WST, the probabilities of exceeding different limit states were also acceptable at twice the design earthquake intensity.
- The vulnerability assessment highlighted the expected higher earthquake losses for buildings B4-DIS and B5-WST, and the need for mitigation strategies to reduce these losses for new and existing irregular buildings.

Finally, the seismic design factors of the reference buildings were assessed and compared with the code recommended factors. The results indicated that:

- The code recommended factors were conservative for the five reference structures but with different margins of safety.
- The R and C_d factors of the B2-SST and B3-GEO buildings were comparable with the regular structure. The R factors of the regular structure and buildings with insignificant irregularity (B2-SST and B3-GEO) can be safely increased by 10-20%.
- The R factor of the B4-DIS and B5-WST buildings was much lower than that of the regular structure, and hence the conservative code R factors were recommended for these irregularity categories.

Chapter 7: Summary and Conclusions

7.1 Synopsis

The aim of this study was to assess the inelastic seismic behavior and verify the seismic design factors of regular and vertically irregular high-rise structures. Reference buildings were selected and designed for the purpose of this study. Fiber-based simulation models were developed for the reference structures in order to assess their vulnerability and seismic design factors using IPOAs, IDAs and a wide range of input ground motions. This study included the following tasks:

7.1.1 Selection and design of reference structures

Five 50-story RC buildings denoted B1-REG, B2-SST, B3-GEO, B4-DIS and B5-WST were selected to represent well-designed regular and irregular high-rise buildings and the common construction practice in the case study area (Dubai, UAE). With the exception of the lower stories of structures with a discontinuity in LFRS and extreme weak story (i.e. B4-DIS and B5-WST, respectively), the structural system of the five references buildings comprised of RC shear walls and core walls connected with RC flat slabs. The LFRS at the lower stories of B4-DIS involved RC columns and core walls, while it only consisted of RC columns in building B5-WST. The five reference buildings were fully designed and detailed using 3D finite element models according to the international building codes adopted in the study region.

7.1.2 Analytical modeling and selection of input ground motions

Inelastic fiber-based simulation models were developed for the five 50-story reference structures. The simulation models were verified using the dynamic characteristics obtained from both the 3D design models and the fiber-based simulation models. The ground motion uncertainty was accounted for using 40

earthquake records. Two earthquake scenarios were selected to represent the seismicity of the study region: (i) far-field earthquakes with a medium-to-high magnitude and long distant from the epicenter, and (ii) near-field events with a low-to-medium magnitude and a short site-to-source distance.

7.1.3 Vulnerability assessment and seismic design factors

A large number of IDAs were performed to develop the fragility relationships of the five reference structures at different performance levels. The adopted performance limit states were selected based on the comprehensive results of the current study and a literature review of previous experimental and analytical studies related to shear wall structures and irregular buildings. IPOAs and IDAs results were also employed to assess the seismic design response factors of the reference regular and irregular buildings.

7.2 Conclusions

The following conclusions were drawn based on the findings of this study:

7.2.1 Design of reference buildings

- The overstrength factor (Ω_o) employed in the design of highly irregular buildings substantially increased the concrete cross-sections and reinforcing steel of structural member.
- Although the seismic design code recommends the use of Ω_o as an additional safety factor for certain irregular structures, the design process of the buildings with a discontinuity in LFRS (B4-DIS) and extreme weak story (B5-WST) confirmed the need for imposing reduction limits on the cross-sections and steel ratios of the stories above the irregularity levels to avoid any sudden changes in stiffness and strength.

7.2.2 Selection of performance criteria

- The limit states of the reference tall buildings were significantly influenced by the characteristics of the selected earthquake records and the irregularity type.
- For the far-field earthquake scenario, the limit states were controlled by flexure. The IDRs corresponding to the IO limit state of the B1-REG, B2-SST, B3-GEO, B4-DIS and B5-WST buildings were 0.49%, 0.48%, 0.51%, 0.27% and 0.44%, respectively. The IDRs corresponding to the CP limit state of the B1-REG, B2-SST, B3-GEO, B4-DIS and B5-WST buildings were 2.27%, 2.26%, 2.39%, 1.18% and 1.38%, respectively.
- For the near-field earthquake scenario, the CP limit state was significantly influenced by the member shear response. Accordingly, the IDRs corresponding to the CP limit state of the B1-REG, B2-SST, B3-GEO, B4-DIS and B5-WST buildings were 1.55%, 1.5%, 1.62%, 0.64% and 0.78%, respectively.

7.2.3 Vulnerability assessment of irregular high-rise buildings

- The negative impacts of the extreme soft story irregularity, which was represented by the B2-SST building, on the seismic response were marginal at both the local and global levels.
- The global seismic response of the B3-GOE structure was generally enhanced compared with that of the regular building due to the increased dimensions of lower stories. However, the deficiency in the local response of this irregular building was confirmed from the large number of plastic hinges and cases of concrete crushing, particularly at the setback level.
- Although a suitable Ω_0 factor was employed in the design of the B4-DIS and B5-WST irregular buildings, the two buildings were more vulnerable than the regular and other irregular structures. The first indications of member yielding

and failure were observed directly above the irregularity level. This confirmed the need to carefully design the structural elements directly above the irregularity level and to assess the seismic response using inelastic time-history analysis as a final verification of the design.

- Shear failure had significant impacts on the seismic response of both the regular and irregular reference buildings under the near-field earthquake scenario.
- The study confirmed the satisfactory performance of well-designed regular and irregular high-rise buildings under the design earthquake. With the exception of B4-DIS and B5-WST, the seismic response of the reference buildings was also acceptable under severe events representing twice the design earthquake. The alarming seismic response of B4-DIS and B5-WST at twice the design earthquake was shown from the observed probability of exceeding the CP limit state (20% and 10%, respectively).

7.2.4 Assessment of seismic design response factors

- With the exception of the B4-DIS building, the calculated overstrength factors using IDAs were more than those recommended by the design code. The unsatisfactory response of the B4-DIS building was confirmed from the observed minimal overstrength factor.
- For the regular structure and buildings with insignificant irregularity (i.e. B2-SST and B3-GEO), the R factors could be safely increased by 10-20%. A further increase in the R factors is possible after a careful assessment of the structures designed using the suggested reduction in the seismic design forces. Due to the significant impacts of the irregularities related to discontinuities in LFRS and weak story on the local and global seismic response of high-rise buildings, the conservative code R factors are recommended.

- The calculated C_d factors for the reference regular and irregular structures were significantly lower than those recommended by the design code. This amplification factor could be decreased by 10-20%. A more reduction in the C_d factor is possible after a carful assessment of the structures designed using the proposed reduction.

7.3 Recommendations for future work

- A systematic loss estimation and mitigation study for the UAE and the surrounding region using the developed fragility relationships in the current study and in other recent seismic vulnerability assessment studies is highly needed.
- Future studies are needed to analytically and experimentally investigate the seismic response of irregular structures with different structural systems and building heights.
- Vulnerability assessment of regular and irregular structures designed using the proposed modifications in the existing seismic design factors is needed.
- Future studies should address the impacts of irregularity on the seismic response of pre-code and substandard buildings.
- The IPOA procedure needs to be developed further to account for higher modes and the dynamic characteristics of irregular structures, and hence provides an easy tool for seismic design and assessment.
- Assessment of different irregularity features using a reliable 3D modeling approach of high-rise buildings is highly needed in order to account for the torsional effect.
- In future studies, multi-axial input ground motions need to be considered in the seismic assessment of irregular tall buildings.

Bibliography

Abdallh, J. A., & Al-homoud, A. S. (2004). Seismic hazard assessment of United Arab Emirates and its surroundings. *Journal of Earthquake Engineering, 8*(6), 817-837.

ACI-318. (2011). *Building Code Requirements for Structural Concrete (ACI 318-11 Metric) and Commentary.*

AD-IBC. (2013). " Abu Dhabi International building code."

Al-Haddad, M., Siddiqi, G., Al-Zaid, R., Arafah, A., Necioglu, A., & Turkelli, N. (1994). A basis for evaluation of seismic hazard and design criteria for Saudi Arabia. *Earthquake Spectra, 10*(2), 231-258.

Al Khatibi, E., Abou Elenean, K., Megahed, A., & El-Hussain, I. (2014). Improved characterization of local seismicity using the Dubai Seismic Network, United Arab Emirates. *Journal of Asian Earth Sciences, 90*, 34-44.

Aldama-Bustos, G., Bommer, J., Fenton, C., & Stafford, P. (2009). Probabilistic seismic hazard analysis for rock sites in the cities of Abu Dhabi, Dubai and Ra's Al Khaymah, United Arab Emirates. *Georisk, 3*(1), 1-29.

Ali, M., & Moon, K. S. (2007). Structural developments in tall buildings: current trends and future prospects. *Architectural Science Review, 50*(3), 205-223.

Almazán, J. L., & de la Llera, J. C. (2003). Accidental torsion due to overturning in nominally symmetric structures isolated with the FPS. *Earthquake engineering & structural dynamics, 32*(6), 919-948.

Alwaile, W., M., M. A., Pilakoutas, K., & Guadagnini, M. (2014). *Framework for Developing Fragility Relations of High-Rise RC Wall buildings based on verified Modelling Approach.* Paper presented at the European Conference on Earthquake Engineering and Seismology (2ECEES), Istanbul, Turkey, 24-28 Augest 2014.

Ambraseys, N., & Melville, C. (1982). A History of Persian Earthquakes Cambridge Univ. *Press, New York.*

Ambraseys, N., Melville, C., & Adams, R. (1994). The seismicity of Egypt, Arabia and the Red Sea. *The Seismicity of Egypt, Arabia and the Red Sea, by NN Ambraseys and CP Melville and RD Adams, pp. 201. ISBN 0521391202. Cambridge, UK: Cambridge University Press, January 1995., 1.*

Ambraseys, N. N., Simpson, K. u., & Bommer, J. J. (1996). Prediction of horizontal response spectra in Europe. *Earthquake engineering & structural dynamics, 25*(4), 371-400.

ASCE-7. (2010). "Minimum design loads for buildings and other structures, ASCE Standard ASCE/SEI 7-10." American Society of Civil Engineers, Reston, VA, .

ASCE/SEI-41. (2007). Seismic Rehabilitation of Existing Buildings (ASCE/SEI 41-06). *American Society of Civil Engineers, Reston, VA, US.*

ATC-13. (1985). *Earthquake damage evaluation data for California*: Applied Technology Council.

Athanassiadou, C. (2008). Seismic performance of R/C plane frames irregular in elevation. *Engineering Structures, 30*(5), 1250-1261.

Aziminejad, A., & Moghadam, A. (2005). *Performance of asymmetric single story buildings based on different configuration of center of mass, rigidity and resistance.* Paper presented at the Proceedings of the 4th European workshop on the seismic behaviour of irregular and complex structures, CD ROM. Thessaloniki.

Baker, W. F., Korista, D. S., & Novak, L. C. (2007). Burj Dubai: Engineering the world's tallest building. *The Structural Design of Tall and Special Buildings, 16*(4), 361-375.

Beyer, K., Dazio, A., & Priestley, M. (2008). Quasi-static cyclic tests of two U-shaped reinforced concrete walls. *Journal of Earthquake Engineering, 12*(7), 1023-1053.

Borzi, B., Pinho, R., & Crowley, H. (2008). Simplified pushover-based vulnerability analysis for large-scale assessment of RC buildings. *Engineering Structures, 30*(3), 804-820.

Bracci, J. M., Kunnath, S. K., & Reinhorn, A. M. (1997). Seismic performance and retrofit evaluation of reinforced concrete structures. *Journal of Structural Engineering, 123*(1), 3-10.

Bracci, J. M., Reinhorn, A. M., & Mander, J. B. (1992). Seismic resistance of reinforced concrete frame structures designed only for gravity loads: part I-design and properties of a one-third scale model structure. *Technical Rep. No. NCEER-92, 27.*

Calvi, G., Pinho, R., Magenes, G., Bommer, J., Restrepo-Vélez, L., & Crowley, H. (2006). Development of seismic vulnerability assessment methodologies over the past 30 years. *ISET journal of Earthquake Technology, 43*(3), 75-104.

Campbell, K. W. (1985). Strong motion attenuation relations: a ten-year perspective. *Earthquake Spectra, 1*(4), 759-804.

CEN. (2004). *Eurocode-8: Design of structures for earthquake resistance, Part 1: General rules, seismic actions, and rules for buildings, EN 1998–1:2004." CEN, European Committee for Standardization, Brussels.*

Chintanapakdee, C., & Chopra, A. K. (2003). *Evaluation of the modal pushover analysis procedure using vertically" regular" and irregular generic frames*: Earthquake Engineering Research Center, College of Engineering, University of California.

Chintanapakdee, C., & Chopra, A. K. (2004). *Evaluation of modal pushover analysis using vertically irregular frames.* Paper presented at the Proceedings of the 13th World conference on earthquake engineering, CD ROM. Vancouver.

Chopra, A. K. (2012). *Dynamics of structures* (4 ed. Vol. 3): Prentice Hall New Jersey.

Chopra, A. K., & Goel, R. K. (2002). A modal pushover analysis procedure for estimating seismic demands for buildings. *Earthquake engineering & structural dynamics, 31*(3), 561-582.

Cohen, B. (2006). Urbanization in developing countries: Current trends, future projections, and key challenges for sustainability. *Technology in society, 28*(1), 63-80.

Colangelo, F. (2008). *On the Computation of Seismic Fragility Curves.* Paper presented at the The 14th World Conference on Earthquake Engineering, Beijing, China.

CSI. (2011a). ETABS - Integrated building design software, Computers and Structures, Inc., Berkeley, California *Journal of Structural Engineering, , 125(9):*, 1038-1047.

CSI. (2011b). SAFE - Slab Analysis by the Finite Element Method." Computers and Structures, Inc., Berkeley, California.

CSI. (2011c). Computer program SAP2000 v15. 1.0. *Computers and Structures Inc., Berkeley, California.*

Cunha, A., Caetano, E., Ribeiro, P., & Müller, G. (2014). A comparative study on fragility analyses in earthquake engineering.

Das, S., & Nau, J. M. (2003). Seismic design aspects of vertically irregular reinforced concrete buildings. *Earthquake Spectra, 19*(3), 455-477.

De-la-Colina, J. (2003). Assessment of design recommendations for torsionally unbalanced multistory buildings. *Earthquake Spectra, 19*(1), 47-66.

De la Llera, J. C., Almazan, J. L., & Vial, I. J. (2005). Torsional balance of plan-asymmetric structures with frictional dampers: analytical results. *Earthquake engineering & structural dynamics, 34*(9), 1089-1108.

De Stefano, M., & Pintucchi, B. (2002). *A model for analyzing inelastic seismic response of plan-irregular building structures.* Paper presented at the Proceedings of the 15th ASCE engineering mechanics conference, CD ROM. New York.

De Stefano, M., & Pintucchi, B. (2008). A review of research on seismic behaviour of irregular building structures since 2002. *Bulletin of Earthquake Engineering, 6*(2), 285-308.

Elnashai, A., & Mwafy, A. (2002). Overstrength and force reduction factors of multistorey reinforced-concrete buildings. *The structural design of tall buildings, 11*(5), 329-351.

Elnashai, A., Papanikolaou, V., & Lee, D. (2012). ZEUS-NL user manual. *Civil and Environmental Engineering Department, University of Illinois at Urbana–Champaign.*

Elnashai, A. S., & Di Sarno, L. (2008). *Fundamentals of earthquake engineering*: Wiley Chichester.

EMSC. (2014). http://www.emsc-csem.org/

ESD. (2012). Internet site for European strong-motion data (http://www.isesd.hi.is/ESD_Local/frameset.htm).

FEMA-450. (2004). *NEHRP Recommended Provisions for Seismic Regulations for New Buildings and Other Structures (FEMA 450): Provisions/Prepared by the Building Seismic Safety Council*: Building Seismic Safety Council, National Institute of Building Sciences.

FEMA-P695. (2009). Quantification of Building Seismic Performance Factors: FEMA P695, Washington, DC.

FEMA-P750. (2009). NEHRP recommended seismic provisions for new buildings and other structures. Washington, DC (USA): Building Seismic Safety Council.

FEMA-P795. (2011). Quantification of Building System Performance and Response Factors: FEMA P795, prepared by Applied Technology Council, prepared for the Federal Emergency Management Agency, Washington, D.C.

fib. (2014). Tall buildings: Structural design of concrete buildings up to 300m tall, fib Bulletin No. 73. Lausanne, Switzerland: The International Federation for Structural Concrete.

Ghobarah, A. (2004). *On drift limits associated with different damage levels.* Paper presented at the International workshop on performance-based seismic design.

Grünthal, G., Bosse, C., Sellami, S., Mayer-Rosa, D., & Giardini, D. (1999). Compilation of the GSHAP regional seismic hazard for Europe, Africa and the Middle East.

GSHAP. (2004). Global Seismic Hazard Assessment Program

Halis, G., M, & Emre, I., H. (2007). A proposal for the classification of structural systems of tall buildings. *Building and environment, 42*(7), 2667-2675.

Haselton, C., Whittaker, A., Hortacsu, A., Baker, J., Bray, J., & Grant, D. (2012). *Selecting and Scaling Earthquake Ground Motions for Performing Response-History Analyses.* Paper presented at the Proceedings of the 15th World Conference on Earthquake Engineering.

Heidari, A., Rahgozar, R., & Kamgar, R. (2014). Free vibration analysis of tall bulinding with geometrical discontinuites. *asian journal of civil engineering (BHRC), 15*(1), 107-122.

ICC. (2012). "International building code." International Code Council, Country Club Hills, IL, .

Iervolino, I., & Cornell, C. A. (2005). Record selection for nonlinear seismic analysis of structures. *Earthquake Spectra, 21*(3), 685-713.

Izzuddin, B. (2012). ADAPTIC User Manual.

Jeong, S.-H., & Elnashai, A. S. (2005). Analytical assessment of an irregular RC frame for full-scale 3D Pseudo-dynamic testing part I: analytical model verification. *Journal of Earthquake Engineering, 9*(1), 95-128.

Jeong, S.-H., Mwafy, A. M., & Elnashai, A. S. (2012). Probabilistic seismic performance assessment of code-compliant multi-story RC buildings. *Engineering Structures, 34*, 527-537.

Ji, J., Elnashai, A. S., & Kuchma, D. A. (2007a). An analytical framework for seismic fragility analysis of RC high-rise buildings. *Engineering Structures, 29*(12), 3197-3209.

Ji, J., Elnashai, A. S., & Kuchma, D. A. (2007b). Seismic fragility assessment for reinforced concrete high-rise buildings. Mid-America Earthquake Center: University of Illinois at Urbana-Champaign.

Kalkan, E., & Kunnath, S. K. (2006). Adaptive modal combination procedure for nonlinear static analysis of building structures. *Journal of Structural Engineering, 132*(11), 1721-1731.

Kappos, A. J., Panagopoulos, G., Panagiotopoulos, C., & Penelis, G. (2006). A hybrid method for the vulnerability assessment of R/C and URM buildings. *Bulletin of Earthquake Engineering, 4*(4), 391-413.

Kaviani, A., Paul, A., Bourova, E., Hatzfeld, D., Pedersen, H., & Mokhtari, M. (2007). A strong seismic velocity contrast in the shallow mantle across the Zagros collision zone (Iran). *Geophysical Journal International, 171*(1), 399-410.

Kaynia, A. M., Taucer, F., Hancilar, U., & Iervolino, I. (2013). Guidelines for deriving seismic fragility functions of elements at risk: Buildings, lifelines, transportation networks and critical facilities. Ispra (Va) - Italy Publications Office of the European Union.

Khan, Z., El-Emam, M., Irfan, M., & Abdalla, J. (2013). Probabilistic seismic hazard analysis and spectral accelerations for United Arab Emirates. *Natural hazards, 67*(2), 569-589.

Kim, J., & Choi, H. (2005). Response modification factors of chevron-braced frames. *Engineering Structures, 27*(2), 285-300.

Kiureghian, A. D., & Ditlevsen, O. (2009). Aleatory or epistemic? Does it matter? *Structural Safety, 31*(2), 105-112.

Konert, G., Afifi, A., Al-Hajri, S., De Groot, K., Al Naim, A., & Droste, H. (2001). AAPG Memoir 74, Chapter 24: Paleozoic Stratigraphy and Hydrocarbon Habitat of the Arabian Plate.

Kossobokov, V., & Nekrasova, A. (2012). Global seismic hazard assessment program maps are erroneous. *Seismic instruments, 48*(2), 162-170.

Krawinkler, H., & Seneviratna, G. (1998). Pros and cons of a pushover analysis of seismic performance evaluation. *Engineering Structures, 20*(4), 452-464.

Kwon, O.-S., & Elnashai, A. (2006). The effect of material and ground motion uncertainty on the seismic vulnerability curves of RC structure. *Engineering Structures, 28*(2), 289-303.

Lee, H.-S., & Ko, D.-W. (2007). Seismic response characteristics of high-rise RC wall buildings having different irregularities in lower stories. *Engineering Structures, 29*(11), 3149-3167.

Lehman, D. E., Turgeon, J. A., Birely, A. C., Hart, C. R., Marley, K. P., Kuchma, D. A., & Lowes, L. N. (2013). Seismic Behavior of a Modern Concrete Coupled Wall. *Journal of Structural Engineering, 139*(8), 1371-1381.

Li, C., Lam, S., Zhang, M., & Wong, Y. (2006). Shaking table test of a 1: 20 scale high-rise building with a transfer plate system. *Journal of Structural Engineering, 132*(11), 1732-1744.

Li, Q., Fang, J., & Jeary, A. (2000). Free vibration analysis of cantilevered tall structures under various axial loads. *Engineering Structures, 22*(5), 525-534.

Lu, X., Su, N., & Zhou, Y. (2013). Nonlinear time history analysis of a super-tall building with setbacks in elevation. *The Structural Design of Tall and Special Buildings, 22*(7), 593-614.

Luco, N., & Cornell, C. A. (1998). *Effects of random connection fractures on the demands and reliability for a 3-story pre-Northridge SMRF structure.* Paper presented at the Proceedings of the 6th US national conference on earthquake engineering.

Madas, P., & Elnashai, A. (1992). A new passive confinement model for the analysis of concrete structures subjected to cyclic and transient dynamic loading. *Earthquake engineering & structural dynamics, 21*(5), 409-431.

Mander, J. B., Priestley, M. J., & Park, R. (1988). Theoretical stress-strain model for confined concrete. *Journal of Structural Engineering, 114*(8), 1804-1826.

Martínez-Rueda, J. E., & Elnashai, A. (1997). Confined concrete model under cyclic load. *Materials and Structures, 30*(3), 139-147.

Michalis, F., Dimitrios, V., & Manolis, P. (2006). Evaluation of the influence of vertical irregularities on the seismic performance of a nine-storey steel frame. *Earthquake engineering & structural dynamics, 35*(12), 1489-1509.

Moehle, J. P. (1984). Seismic response of vertically irregular structures. *Journal of Structural Engineering, 110*(9), 2002-2014.

Moehle, J. P., & Alarcon, L. F. (1986). Seismic analysis methods for irregular buildings. *Journal of Structural Engineering, 112*(1), 35-52.

Moehle, J. P., Ghodsi, T., Hooper, J. D., Fields, D. C., & Gedhada, R. (2011). Seismic Design of Cast-in-Place Concrete Special Structural Walls and Coupling Beams: NEHRP Seismic Design Technical Brief.

Moon, K. S., Connor, J. J., & Fernandez, J. E. (2007). Diagrid structural systems for tall buildings: characteristics and methodology for preliminary design. *The Structural Design of Tall and Special Buildings, 16*(2), 205-230.

Mwafy, A. (2010). Analytically derived fragility relationships for the modern high-rise buildings in the UAE. *The Structural Design of Tall and Special Buildings, 21*(11), 824-843.

Mwafy, A. (2011). Assessment of seismic design response factors of concrete wall buildings. *Earthquake Engineering and Engineering Vibration, 10*(1), 115-127.

Mwafy, A., & Elnashai, A. (2001). Static pushover versus dynamic collapse analysis of RC buildings. *Engineering Structures, 23*(5), 407-424.

Mwafy, A., & Elnashai, A. (2002). Calibration of force reduction factors of RC buildings. *Journal of Earthquake Engineering, 6*(2), 239-273.

Mwafy, A., Elnashai, A., Sigbjörnsson, R., & Salama, A. (2006). Significance of severe distant and moderate close earthquakes on design and behavior of tall buildings. *The Structural Design of Tall and Special Buildings, 15*(4), 391-416.

Mwafy, A., Hussain, N., & El-Sawy, K. (2014). Seismic performance and cost-effectiveness of high-rise buildings with increasing concrete strength. *The Structural Design of Tall and Special Buildings*.

Naeim, F., Alimoradi, A., & Pezeshk, S. (2004). Selection and scaling of ground motion time histories for structural design using genetic algorithms. *Earthquake Spectra, 20*(2), 413-426.

NASA. (2014). Gateway to Astronaut Photography of Earth http://eol.jsc.nasa.gov/

NBCC. (2005). National Building Code of Canada 2005. Institute for Research in Construction, National Research Council of Canada, Ottawa, Ont.

NEHRP. (2010a). Evaluation of the FEMA P-695 Methodology for Quantification of Building Seismic Performance Factors. *NaTional InsTiTuTe of sTandards and TeChnology, UsA*.

NEHRP. (2010b). Nonlinear structural analysis for seismic design. *NEHRP Seismic Design Technical Brief No. 4.*

NEHRP. (2011). Selecting and Scaling Earthquake Ground Motions for Performing Response-History Analyses. *National Institute of Standards and Technology: Redwood City, California.*

NIST. (2010). GCR 10-917-8,(2010)"Evaluation of the FEMA P-695 Methodology for Quantification of Building Seismic Performance Factors,". *National Institute of Standards and Technology, Gaithersburg, MD.*

Panagiotou, M., Restrepo, J. I., & Conte, J. P. (2010). Shake-table test of a full-scale 7-story building slice. Phase I: Rectangular wall. *Journal of Structural Engineering, 137*(6), 691-704.

Park, R. (1989). Evaluation of ductility of structures and structural assemblages from laboratory testing. *Bulletin of the New Zealand National Society for Earthquake Engineering, 22*(3), 155-166.

PEER. (2012). NGA Database, Pacific Earthquake Engineering Research Center. *University of California, Berkeley, USA, (http://peer.berkeley.edu/peer_ground_motion_database), berkeley. edu/nga.*

Priestley, M., & Grant, D. (2005). Viscous damping in seismic design and analysis. *Journal of Earthquake Engineering, 9*(sup2), 229-255.

Priestley, M. N., Verma, R., & Xiao, Y. (1994). Seismic shear strength of reinforced concrete columns. *Journal of Structural Engineering, 120*(8), 2310-2329.

Rajeev, P., & Tesfamariam, S. (2012). Seismic fragilities for reinforced concrete buildings with consideration of irregularities. *Structural Safety, 39*, 1-13.

Rajendran, C., Rajendran, K., Shah-Hosseini, M., Beni, A. N., Nautiyal, C., & Andrews, R. (2013). The hazard potential of the western segment of the Makran subduction zone, northern Arabian Sea. *Natural hazards, 65*(1), 219-239.

Rossetto, T., & Elnashai, A. (2003). Derivation of vulnerability functions for European-type RC structures based on observational data. *Engineering Structures, 25*(10), 1241-1263.

Rossetto, T., & Elnashai, A. (2005). A new analytical procedure for the derivation of displacement-based vulnerability curves for populations of RC structures. *Engineering Structures, 27*(3), 397-409.

Rota, M., Penna, A., & Strobbia, C. (2006). *Typological fragility curves from Italian earthquake damage data.* Paper presented at the Proceedings 1st European

conference on earthquake engineering and seismology. Geneva, Switzerland, 3-8 September 2006.

Saiidi, M., & Sozen, M. A. (1981). Simple nonlinear seismic analysis of R/C structures. *Journal of the Structural Division, 107*(5), 937-953.

Shabbir, F., & Omenzetter, P. (2008). *Forced vibration testing of a thirteen storey concrete building.* Paper presented at the 2008 NZSEE Conference, Taupo, New Zealand.

Shahrooz, B. M., & Moehle, J. P. (1990a). Evaluation of seismic performance of reinforced concrete frames. *Journal of Structural Engineering, 116*(5), 1403-1422.

Shahrooz, B. M., & Moehle, J. P. (1990b). Seismic response and design of setback buildings. *Journal of Structural Engineering, 116*(5), 1423-1439.

Shama, A. A. (2011). Site specific probabilistic seismic hazard analysis at Dubai Creek on the west coast of UAE. *Earthquake Engineering and Engineering Vibration, 10*(1), 143-152.

Sigbjornsson, R., & Elnashai, A. (2005). Hazard assessment of Dubai, UAE, for close and distant earthquakes. *Journal of Earthquake Engineering.*

Sigbjornsson, R., & Elnashai, A. (2006). Hazard assessment of Dubai, United Arab Emirates, for close and distant earthquakes. *Journal of Earthquake Engineering, 10*(5), 749-773.

Simpson, K. A. (1996). *Attenuation of strong ground-motion incorporating near-surface foundation conditions.* PhD, Imperial College, University of London, London, UK.

Singhal, A., & Kiremidjian, A. (1997). A method for earthquake motion-damage relationships with application to reinforced concrete frames, Technical report NCEER -97-0008, September 10, 1997.

Spence, S. M., & Kareem, A. (2013). Tall Buildings and Damping: A Concept-Based Data-Driven Model. *Journal of Structural Engineering.*

Stern, R. J., & Johnson, P. (2010). Continental lithosphere of the Arabian Plate: a geologic, petrologic, and geophysical synthesis. *Earth-Science Reviews, 101*(1), 29-67.

Taylor, E. D. (2007). *The development of fragility relationships for controlled structures.* Washington University, 2007. Department of Civil Engineering.

TBI. (2010). Guidelines for performance-based seismic design of tall buildings. *Berkeley: University of California (PEER Report No. 2010/05)*.

USGS. (2014). http://earthquake.usgs.gov

Valmundsson, E. V., & Nau, J. M. (1997). Seismic response of building frames with vertical structural irregularities. *Journal of Structural Engineering, 123*(1), 30-41.

Vamvatsikos, D., & Cornell, C. A. (2002). Incremental dynamic analysis. *Earthquake Engineering & Structural Dynamics, 31*(3), 491-514.

Varadharajan, S., Sehgal, V., & Saini, B. (2013). Seismic behavior of multistory RC building frames with vertical setback irregularity. *The Structural Design of Tall and Special Buildings*.

Wen, Y., Ellingwood, B., & Bracci, J. M. (2004). Vulnerability function framework for consequence-based engineering.

Wong, R. (2013). *Construction of Transfer Plate - from various case studies*.

Yu, E., Whang, D. H., Conte, J. P., Stewart, J. P., & Wallace, J. W. (2005). Forced vibration testing of buildings using the linear shaker seismic simulation (LSSS) testing method. *Earthquake engineering & structural dynamics, 34*(7), 737-761.

Yun, S.-Y., Hamburger, R. O., Cornell, C. A., & Foutch, D. A. (2002). Seismic performance evaluation for steel moment frames. *Journal of Structural Engineering, 128*(4), 534-545.

Appendix A: Survey of Irregularity Structures

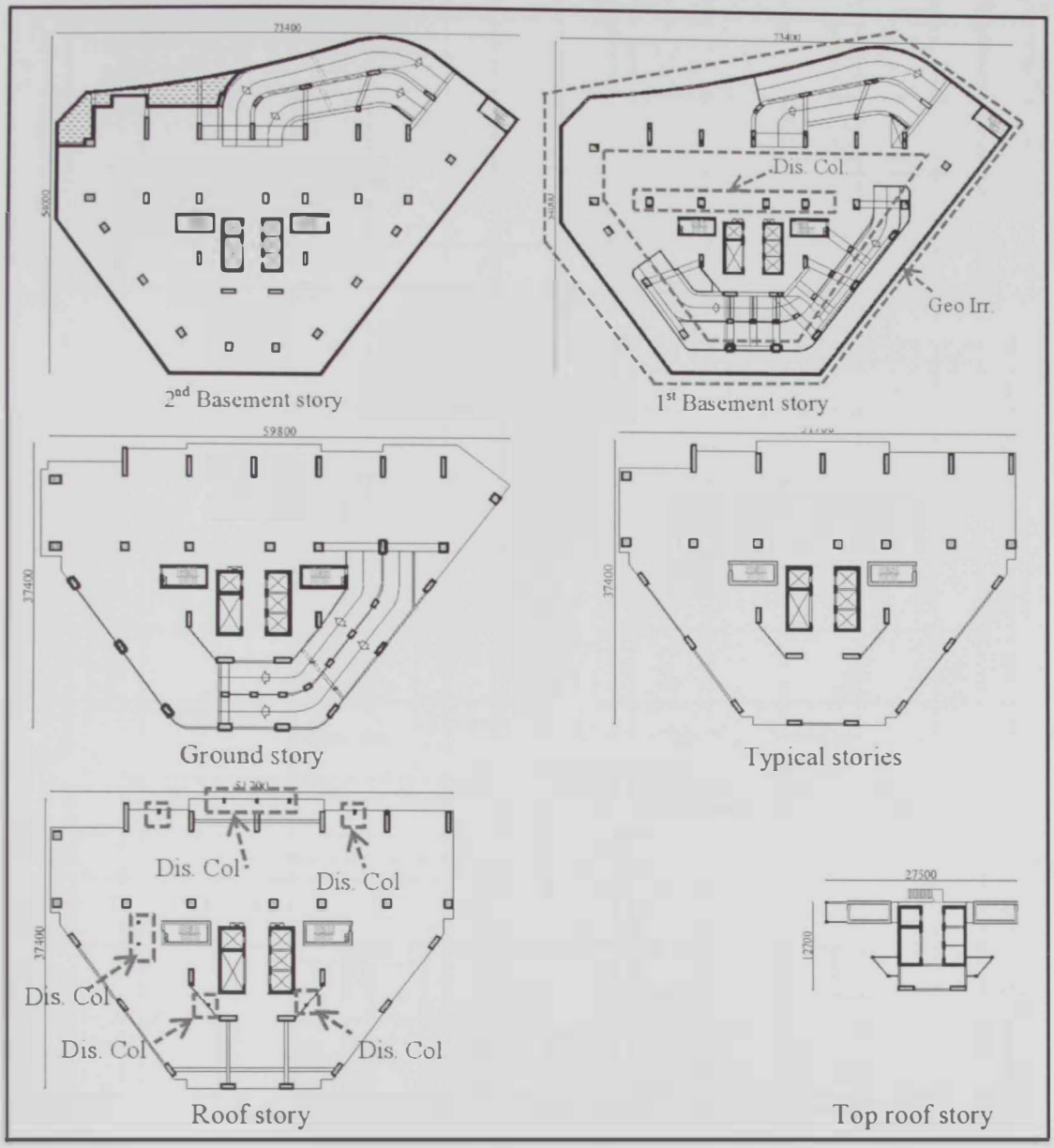

Figure A.1: Surveyed buildings – layouts of building 2 showing its irregularity features

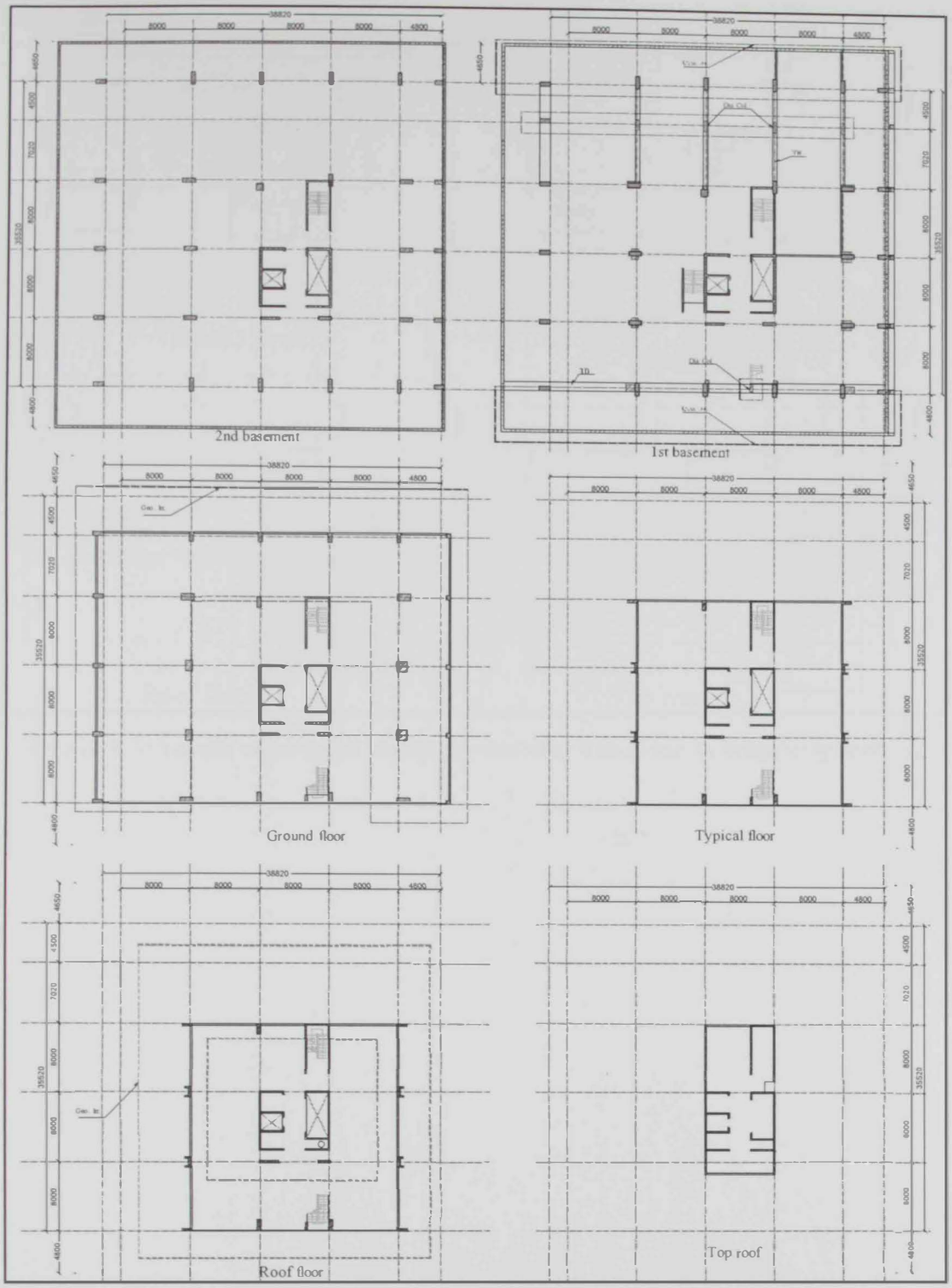

Figure A.2: Sample of surveyed buildings – building 3 showing its irregularity features

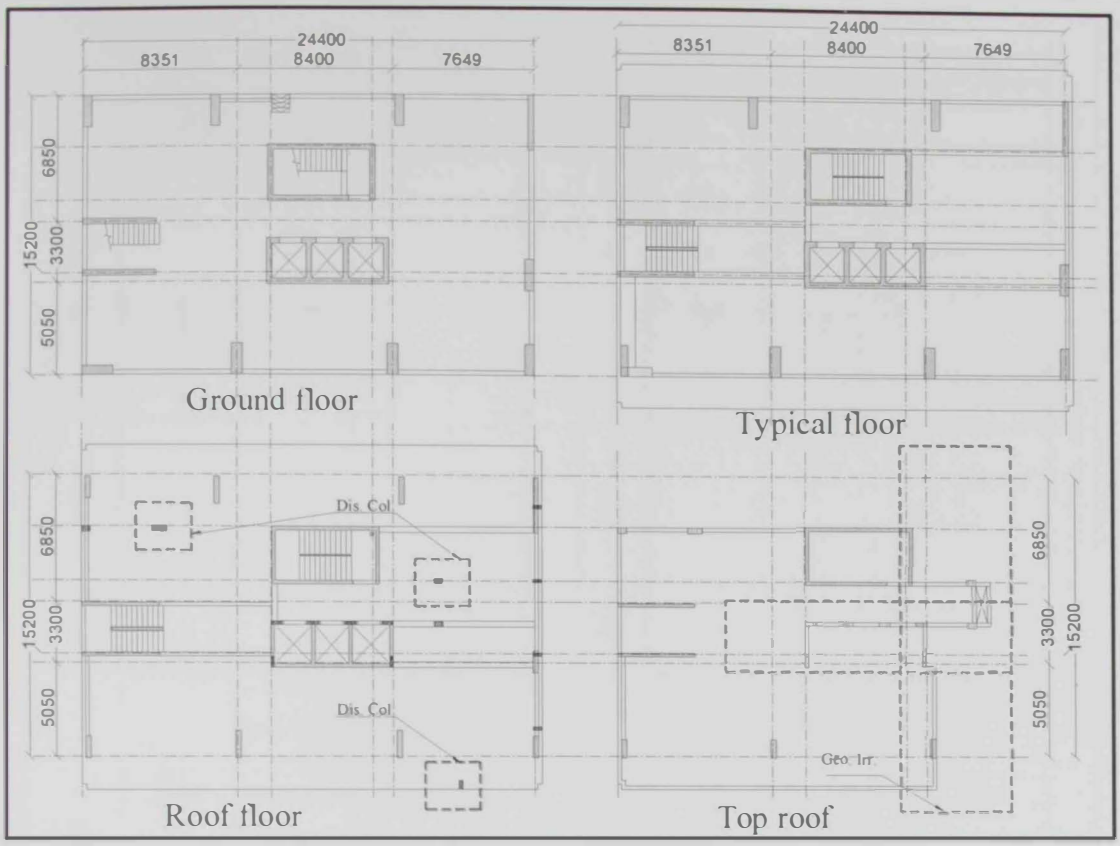

Figure A.3: Sample of surveyed buildings – building 4 showing its irregularity features

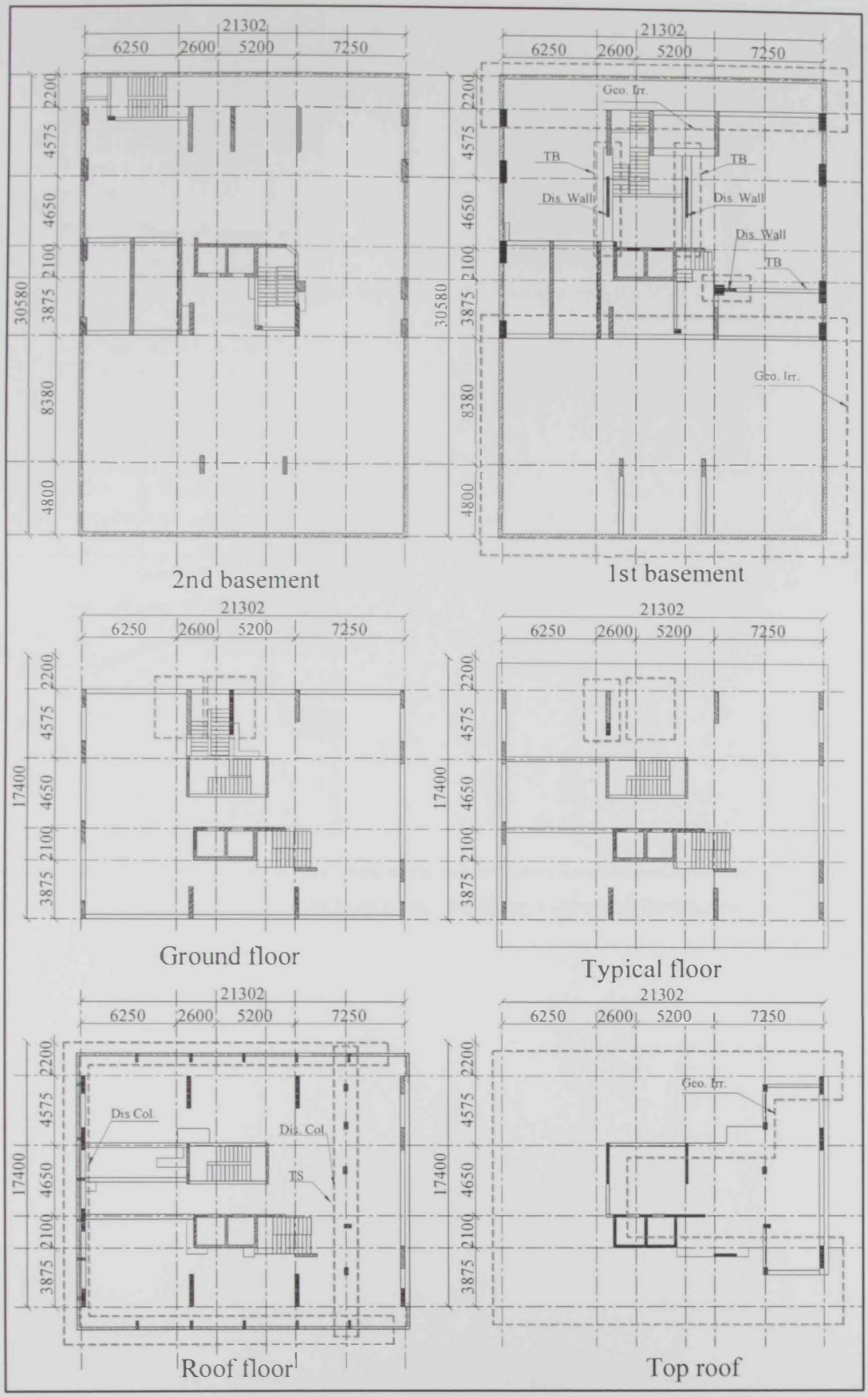

Figure A.4: Sample of surveyed buildings – building 5 showing its irregularity features

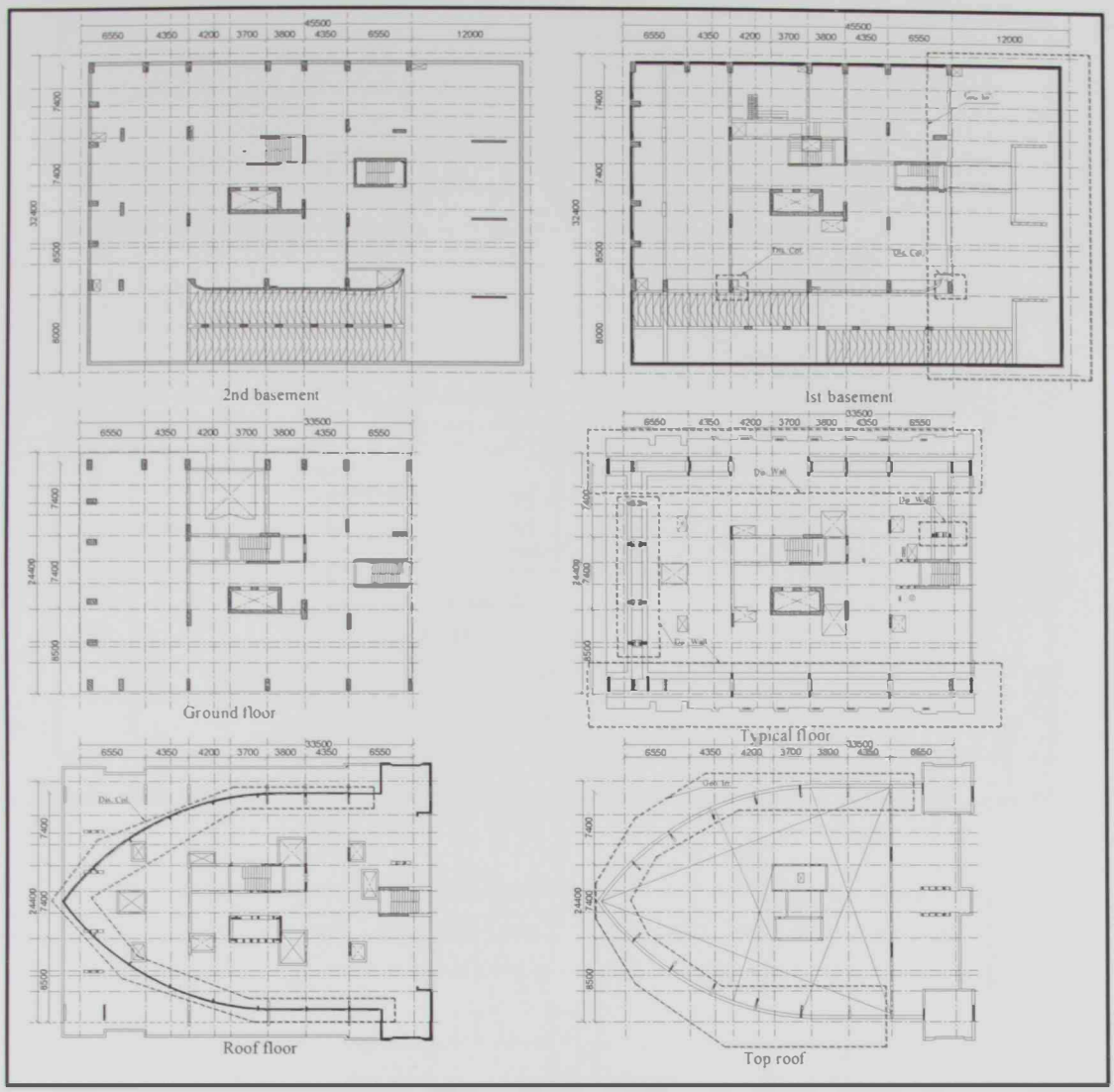

Figure A.5: Sample of surveyed buildings – building 6 showing its irregularity features

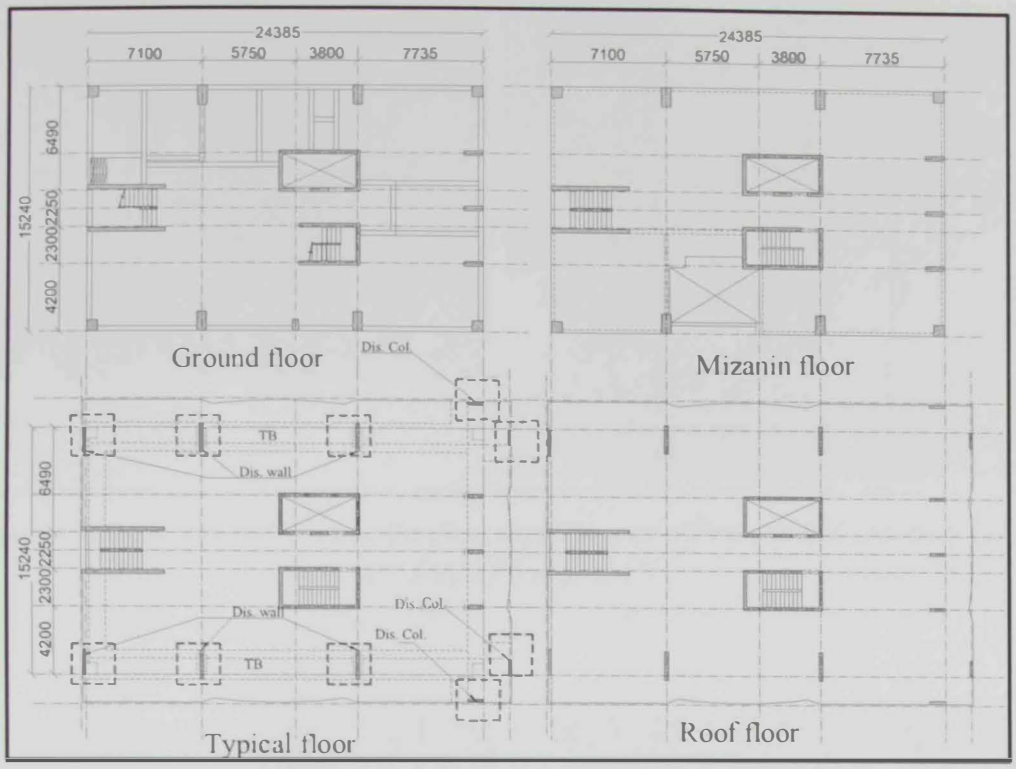

Figure A.6: Sample of surveyed buildings – building 7 showing its irregularity features

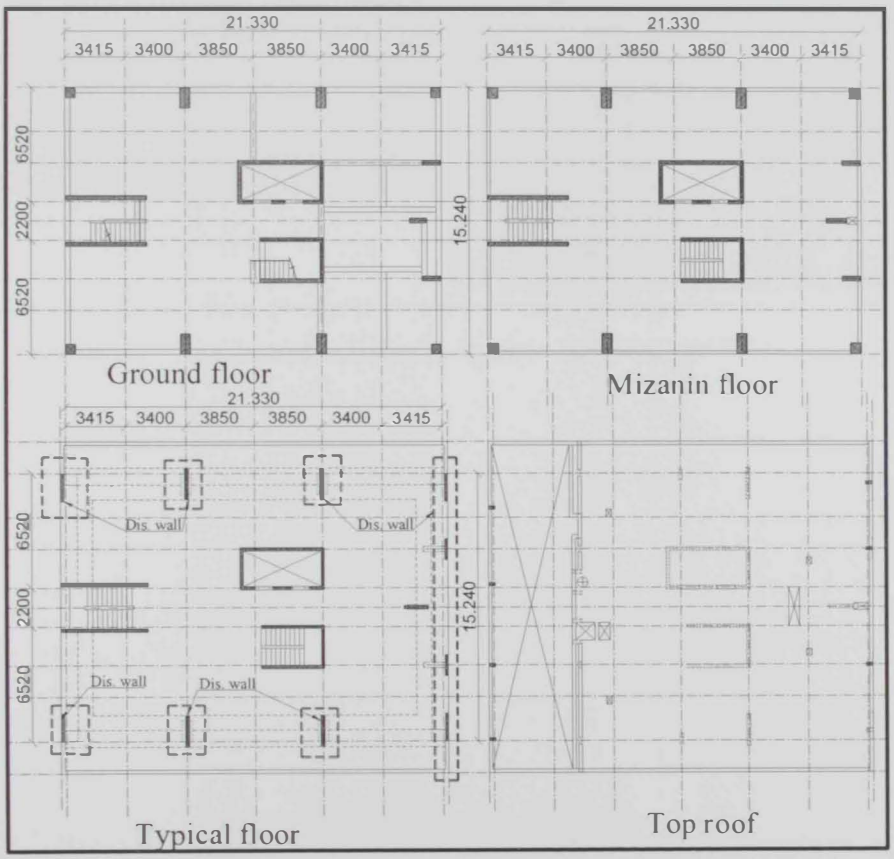

Figure A.7: Sample of surveyed buildings – building 8 showing its irregularity features

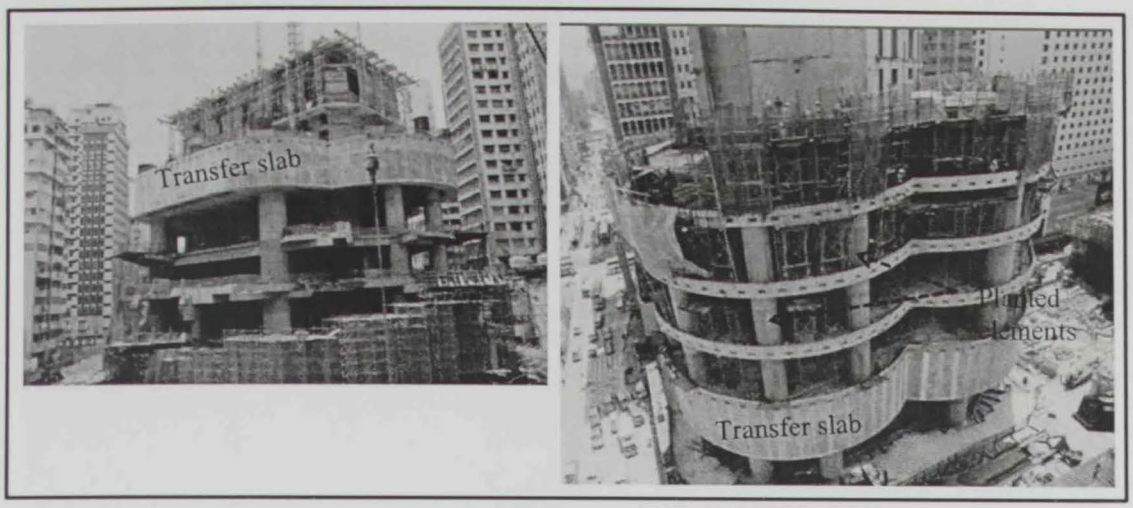

Figure A.8: Four meters thick transfer plate supporting an office tower of Langham Place - building 9 (Wong, 2013)

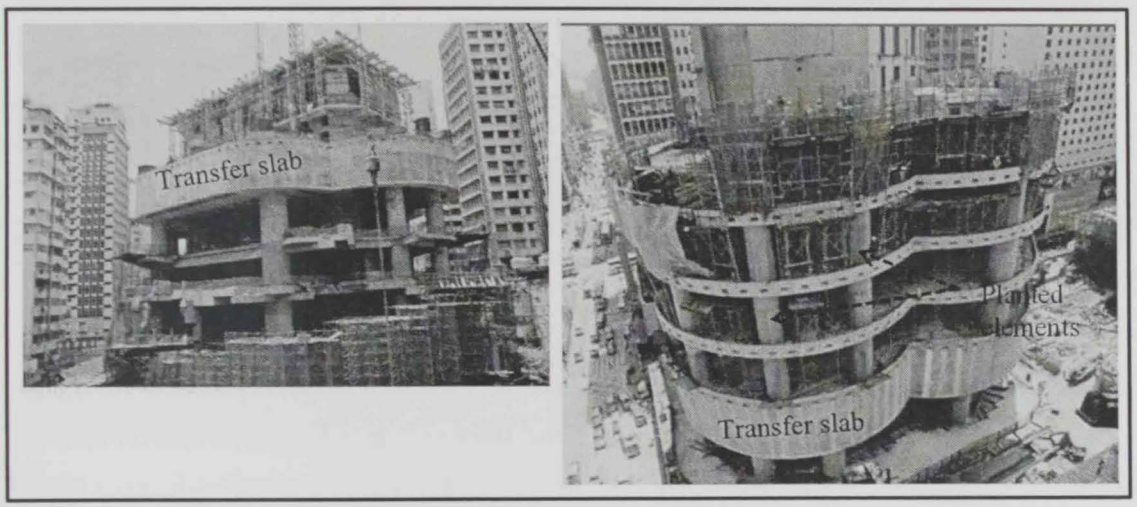

Figure A.9: Residential building in Jordan - building 10 (Wong, 2013)

Figure A.10: Residential development in Tiu Keng Leng, Metro Town - building 11 (Wong, 2013)

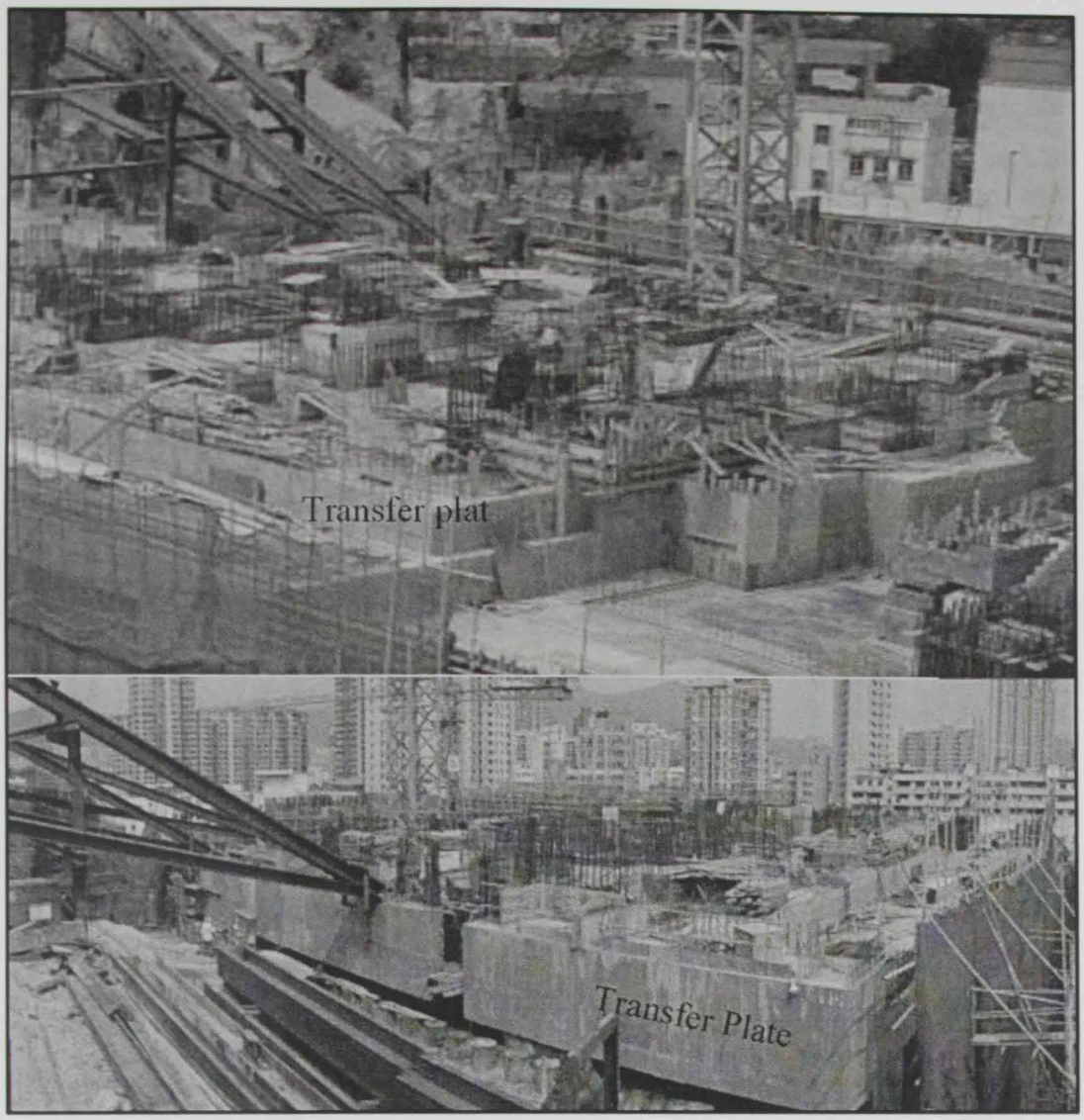

Figure A.11: Residential Development in To Kwa Wan - building 12 (Wong, 2013)

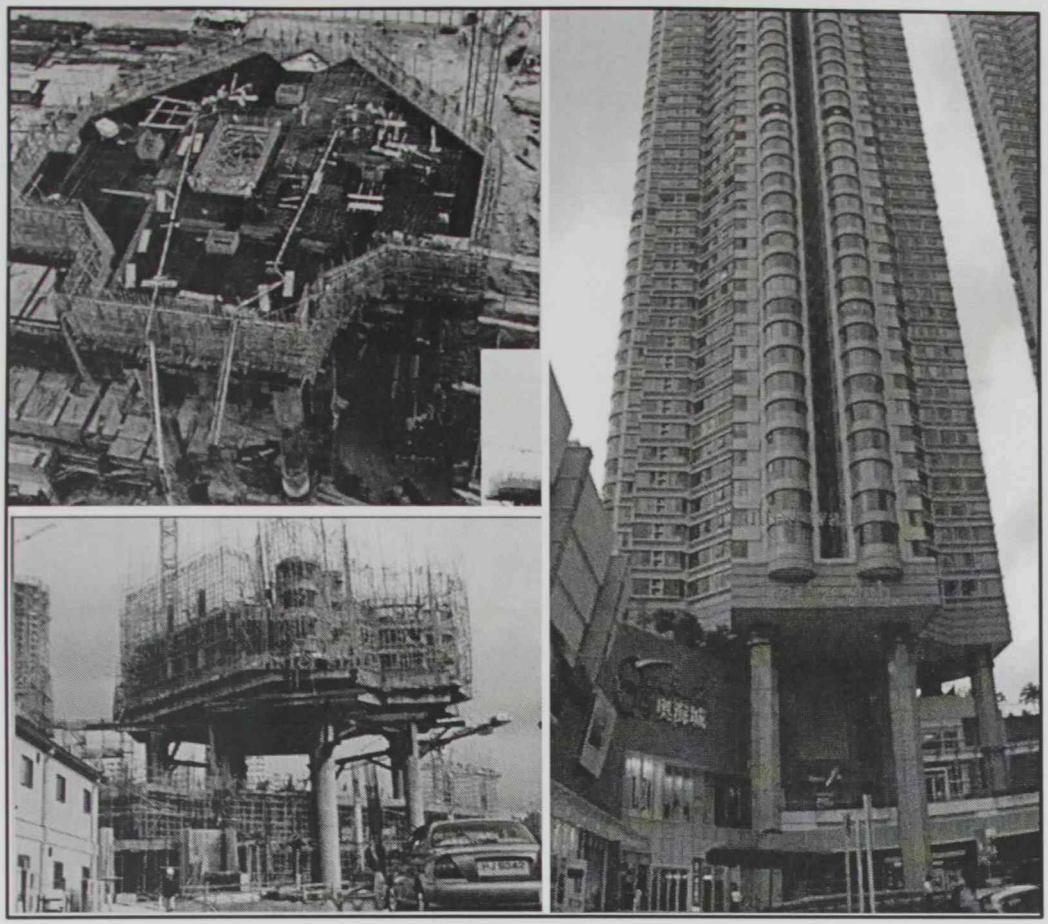

Figure A.12: Olympian City in Tai Kwok Tsui - building 13 (Wong, 2013)

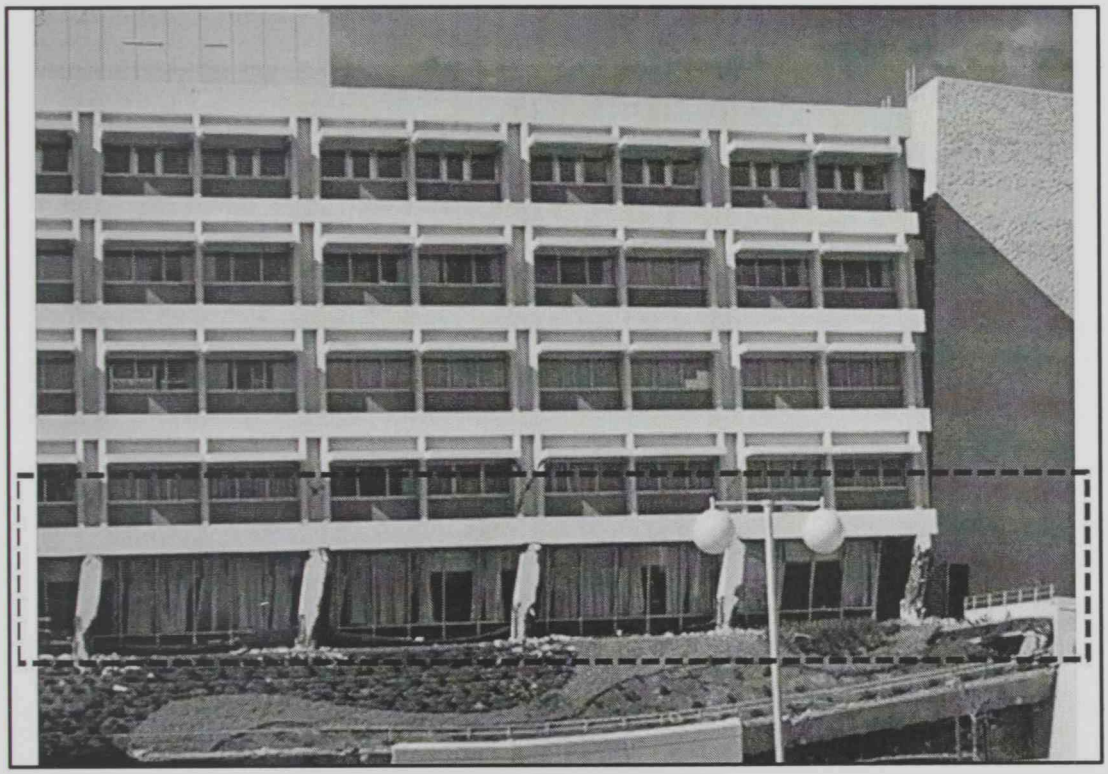

Figure A.13: Weak story damage, 1971 San Fernando earthquake - building 14 (Moehle et al., 2011)

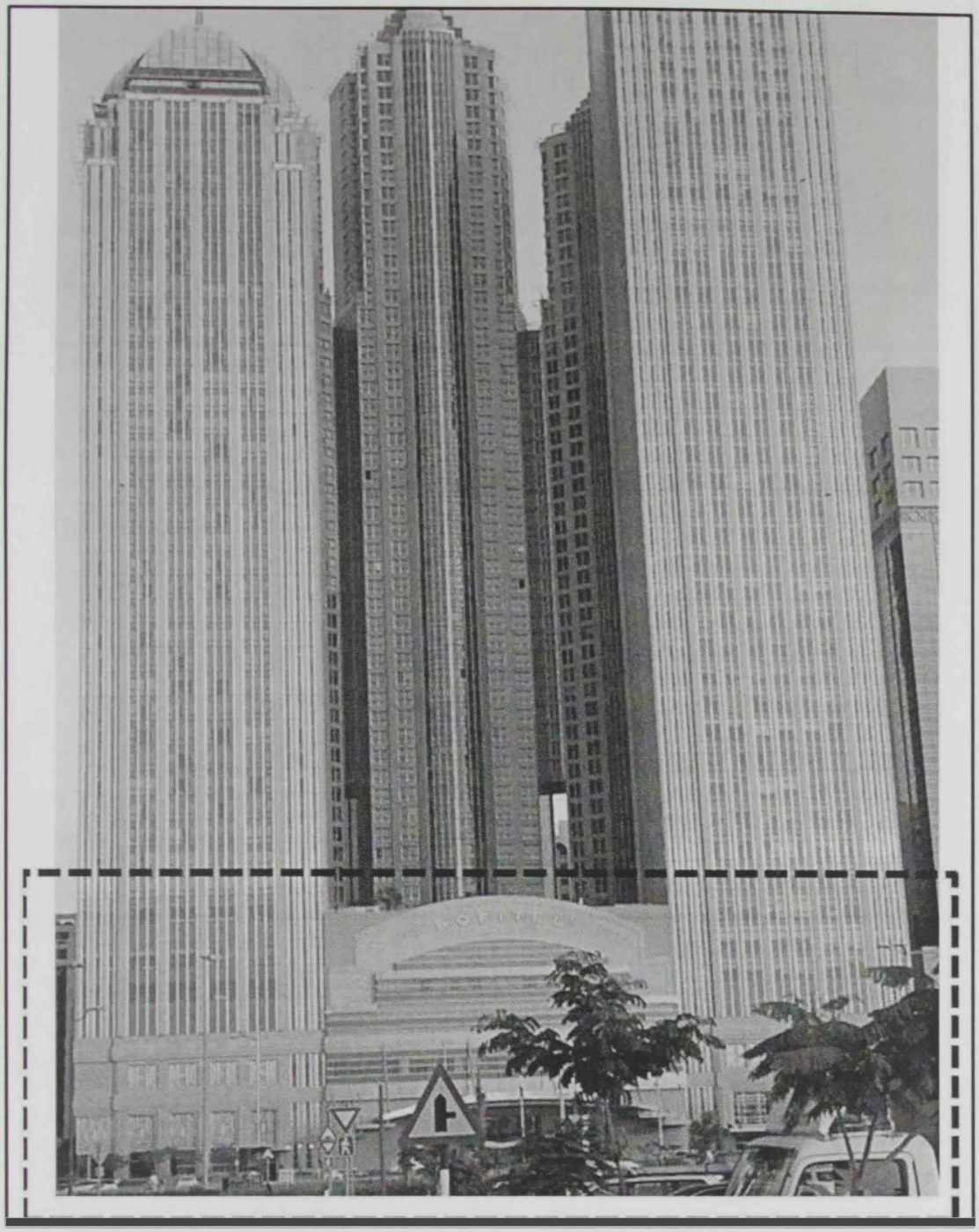

Figure A.14: Possible geometric irregularity of a sample high-rise building in Abu Dhabi - building 15

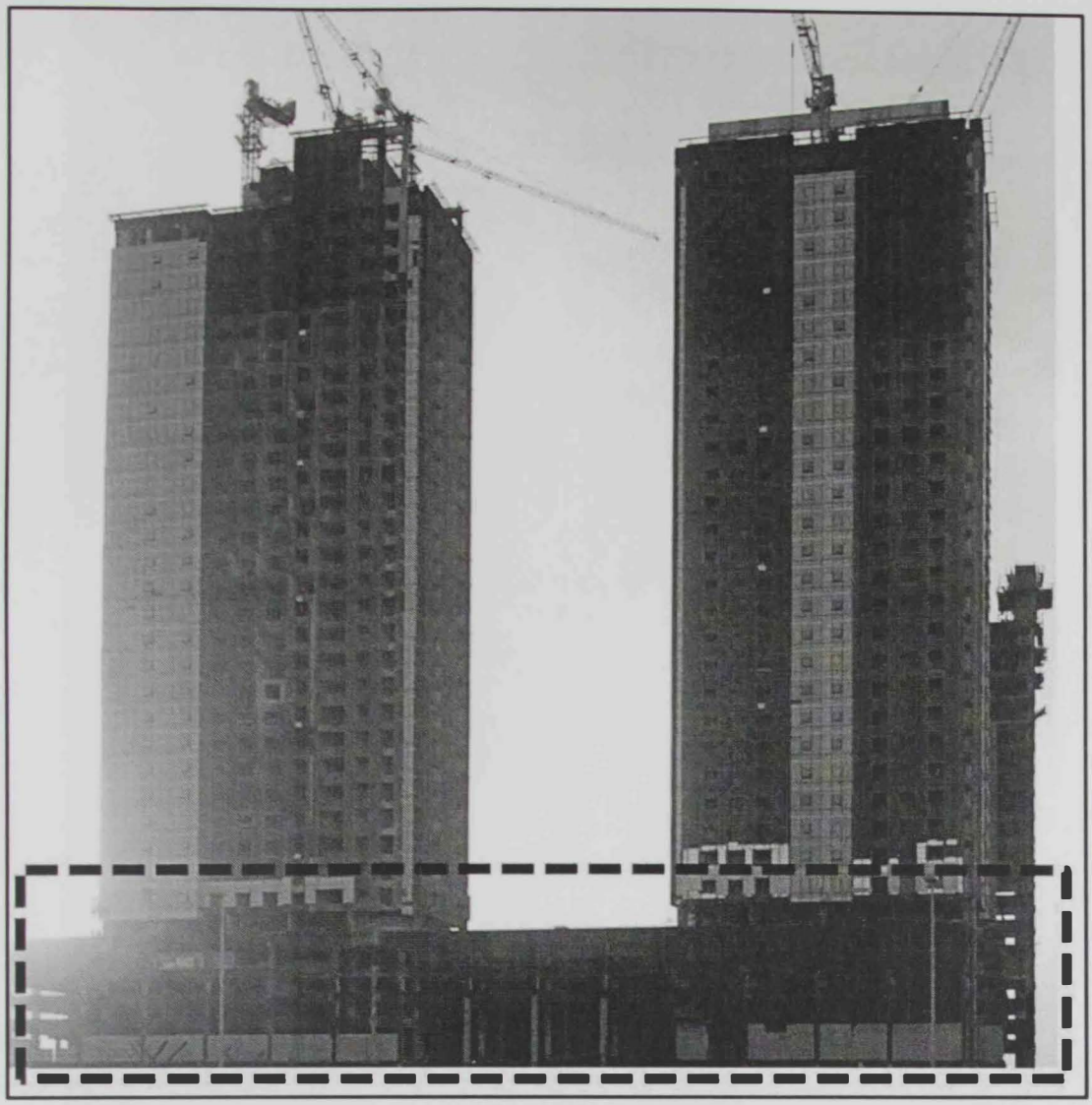

Figure A.15: Possible geometric irregularity in an office in Abu Dhabi- building 16

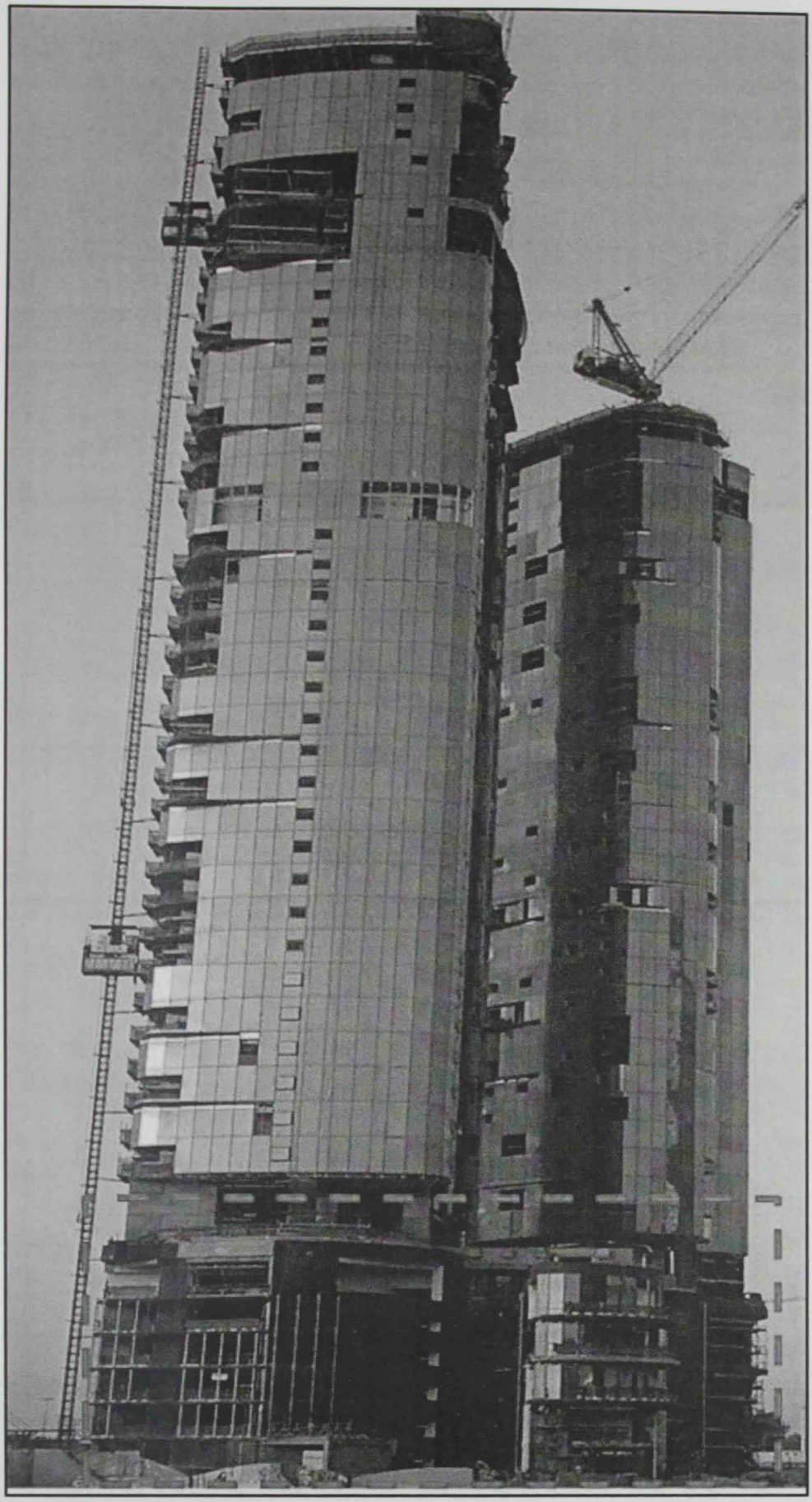

Figure A.16: Possible geometric irregularity of an office building in Abu Dhabi- building 17

Appendix B: Sample of IDA Results

B.1 Sample of top displacement histories

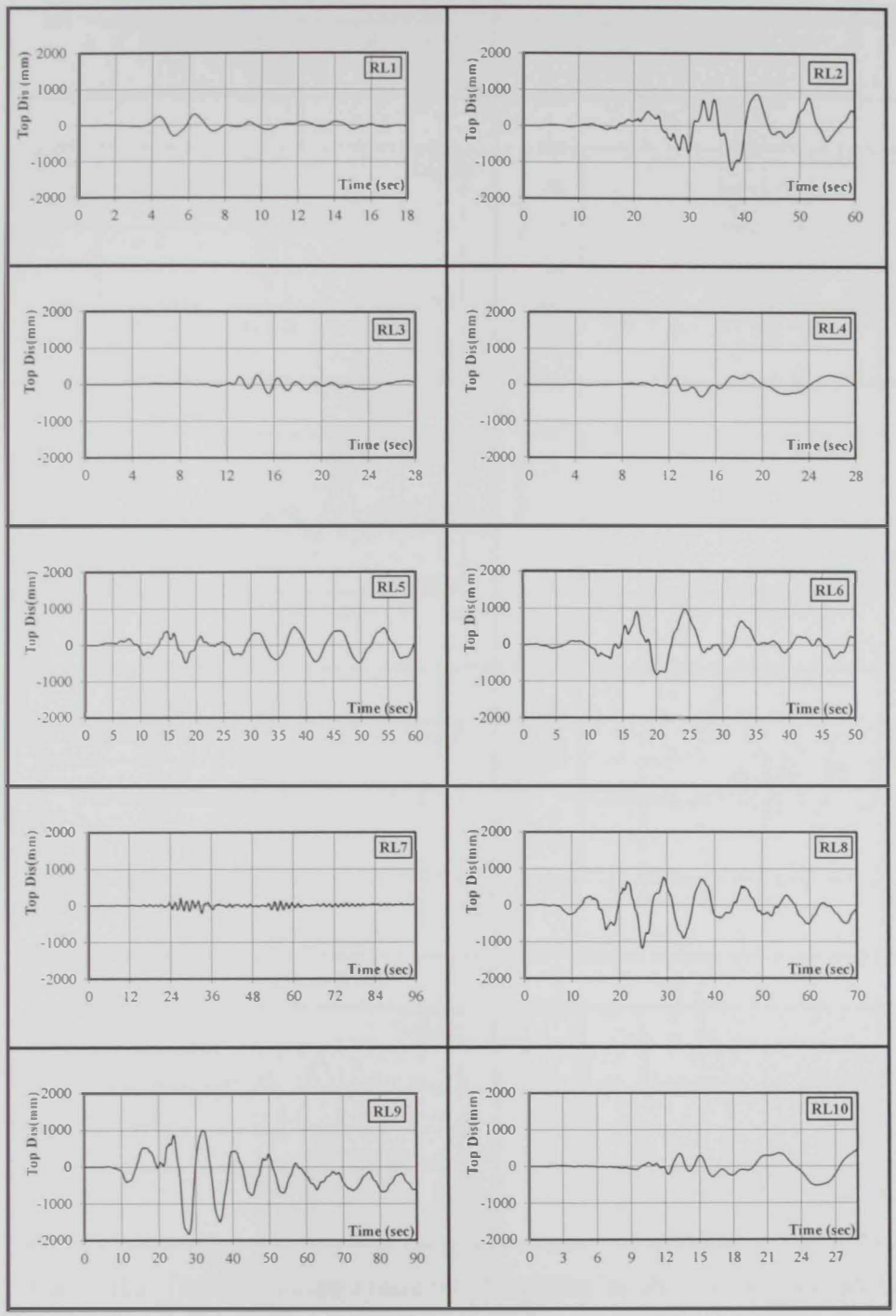

Figure B.1: Top displacement histories of building B1-REG for ten selected records representing far-field earthquakes (RL1 to RL10) at twice the design earthquake (0.32g)

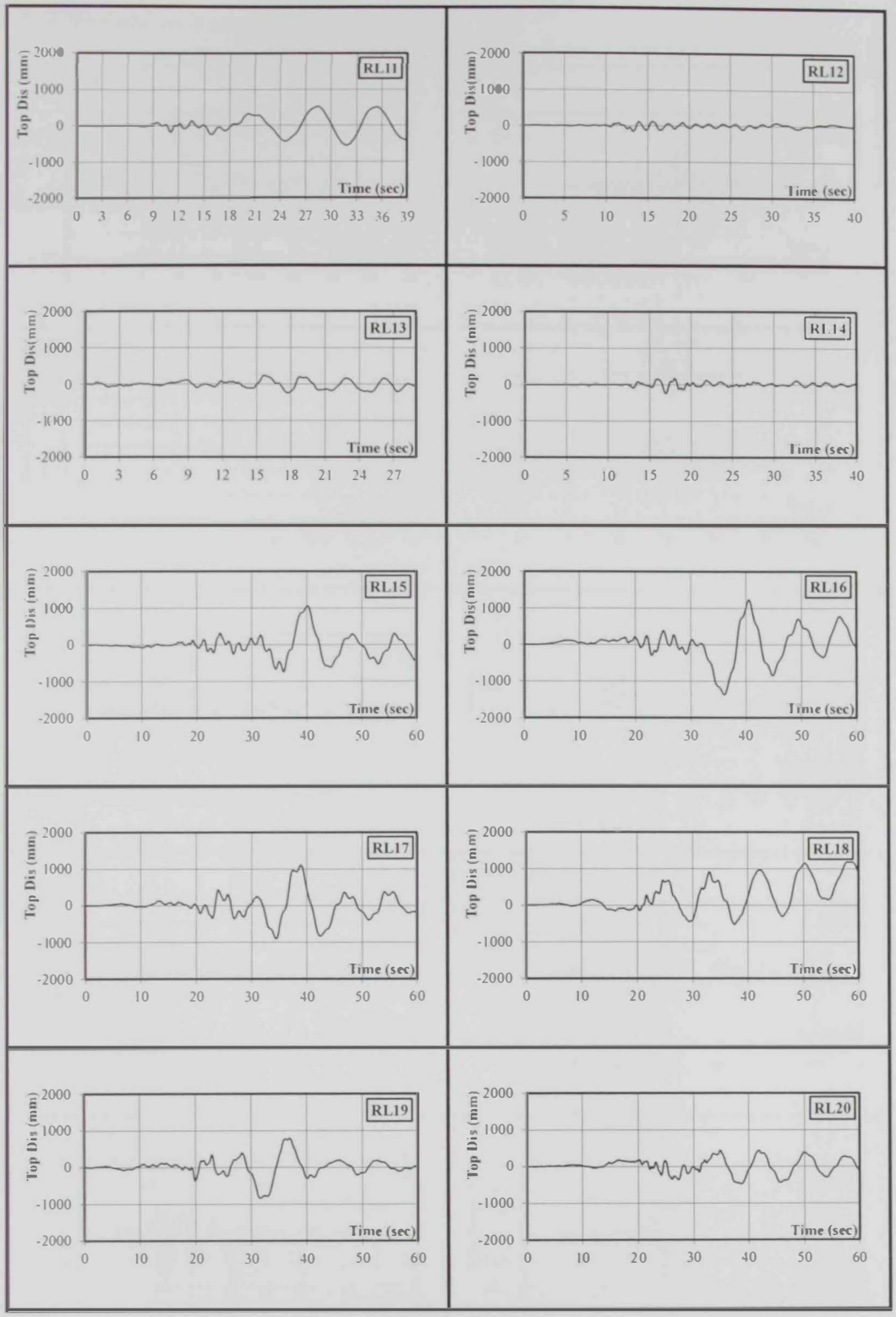

Figure B.2: Top displacement histories of building B1-REG for ten selected records representing far-field earthquakes (RL11 to RL20) at twice the design earthquake (0.32g)

B.2 Sample of base shear histories

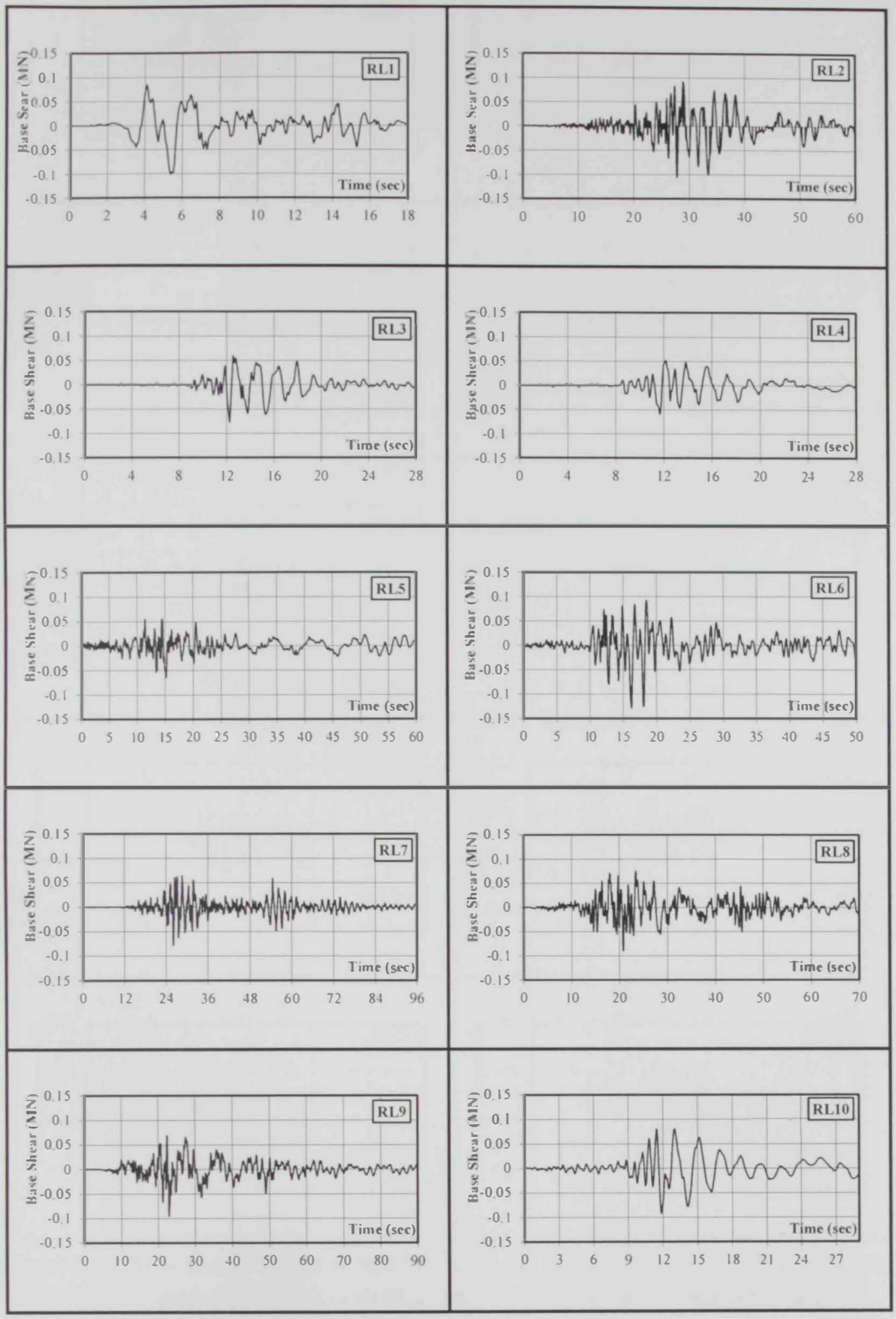

Figure B.3: Base shear histories of building B1-REG for ten selected records representing far-field earthquakes (RL1 to RL10) at twice the design earthquake (0.32g)

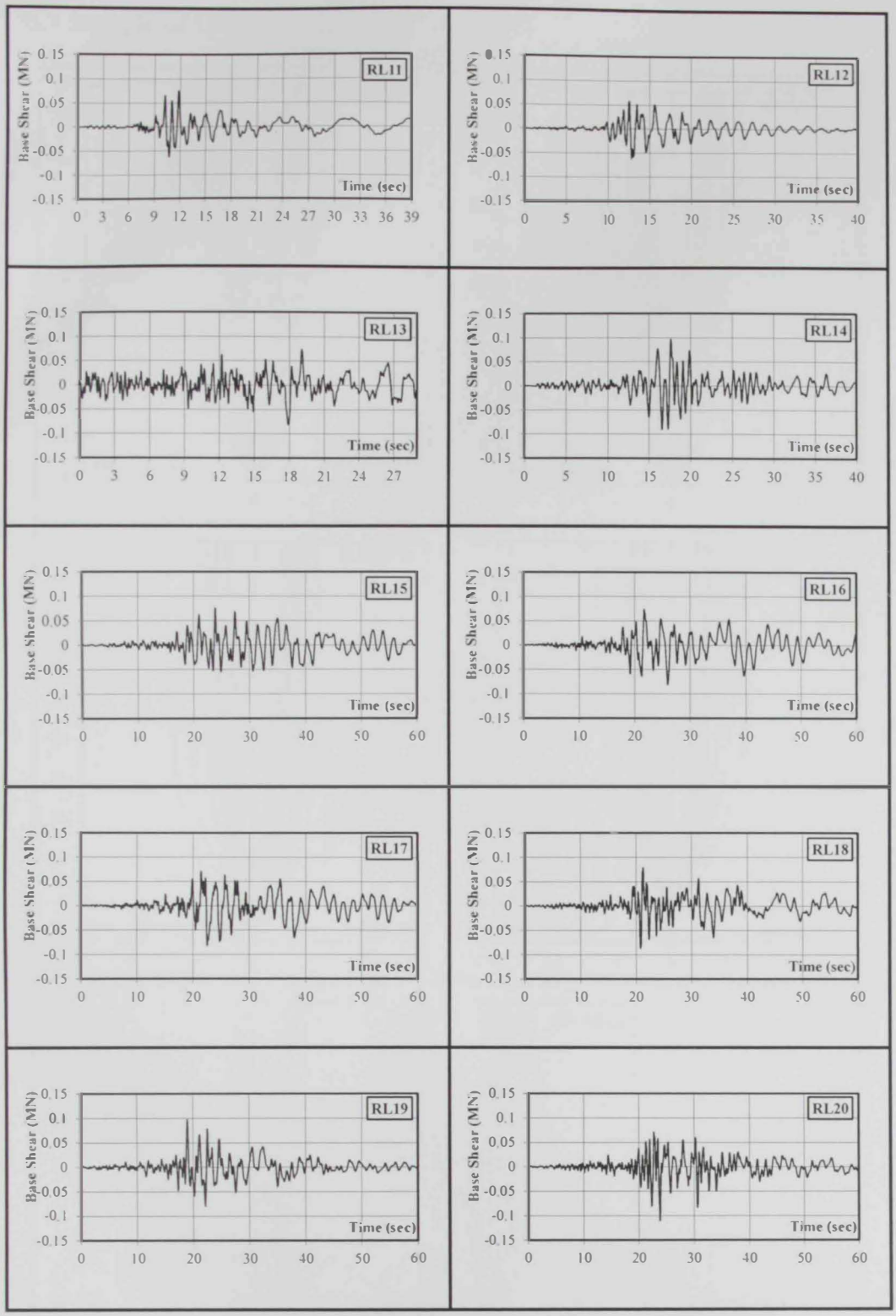

Figure B.4: Base shear histories of building B1-REG for ten selected records representing far-field earthquakes (RL11 to RL20) at twice the design earthquake (0.32g)

B.3 Sample of IDRs

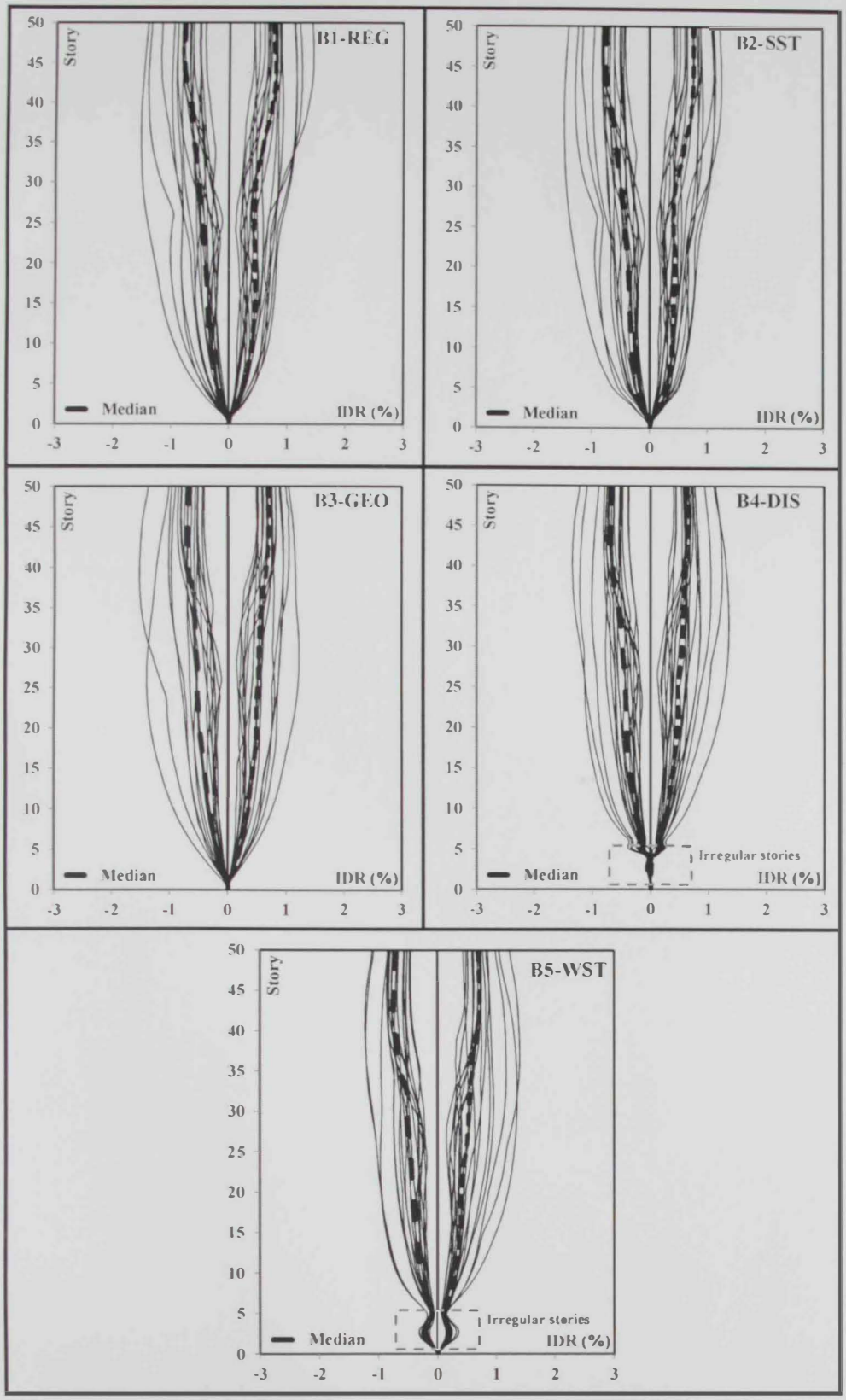

Figure B.5: IDRs of five reference buildings for twenty far-field earthquake records at twice the design earthquake (0.32g)